APPLICATIONS OF SELF-ORGANIZING MAPS TO STATISTICAL DOWNSCALING OF MAJOR REGIONAL CLIMATE VARIABLES

A thesis submitted in fulfillment
of the requirements for the degree of

Doctor of Philosophy

in

Environmental Science

at

The University of Waikato

by

Chonghua Yin

THE UNIVERSITY OF
WAIKATO
Te Whare Wānanga o Waikato

2011

ABSTRACT

This research developed a practical methodological framework, which integrated most of the important aspects related to statistical downscaling. The framework showed high skills when applied to downscale daily precipitation, minimum and maximum temperatures over southeast Australia.

Within the framework, self-organizing maps (SOM) algorithm was incorporated as the core technique for interpreting the relationship between the predictor and predictand under consideration following the latest advances in synoptic climatology. The SOM classified large-scale predictors into a small number of synoptic patterns on a physically meaningful basis. By mapping the observed local climate variable (predictand) to these patterns, a downscaling model structure, SOM-SD, was constructed based on the NCAR/NCEP reanalysis data. Moreover, for a new atmospheric state, an ensemble of predictand values was generated by a stochastic re-sampling technique inside the SOM-SD. To improve seasonality of downscaled results, a simple seasonal predictand pool (SPP) scheme was introduced, which can acquire similar skills as the traditional solutions of dividing a year into four seasons.

The framework identified and applied a broad suite of statistical indices, including mean, variance, cumulative distribution function (CDF), extreme events to assess the performance of the SOM-SD. In addition, some non-parametric methods were also employed to evaluate the uncertainty of the downscaling approach, which improved its robustness in practice. The quality control of the input data consists of another important component of the framework, which assessed GCM predictors from three aspects: (a) replicate reliably synoptic patterns depicted by the reanalysis data; (b) remain relatively stable in the future; and (c) produce similar downscaling skills as the reanalysis data.

Finally, the framework provided an equal-distance CDF mapping method to adjust the discrepancies between the downscaled values and the corresponding observations. This method adjusted the downscaled CDF for the projection period on the difference between the CDFs of the downscaled GCM baseline and observed values. Thus the framework combines the advantages of statistical downscaling model and bias correction method. Moreover, the framework puts a

strong emphasis on its flexibility, which underpins its application to other regions, as well as to support impact assessment studies.

ACKNOWLEDGEMENTS

It is my pleasure to acknowledge those who have assisted me in the production of this thesis. A research of this size involves the invaluable contributions of many different people so as that it would not have been possible without the support of many people. Your kindness, generosity and support made this 3½ year study an enjoyable and team-building experience.

To begin with, I would like to thank my wonderful supervisors, Dr Wei Ye, Dr Yinpeng Li, and Prof Janet F. Bornman at the International Global Change Centre for your encouragement, support, and numerous helpful discussions during the development of this study. Your ideas, comments and suggestions are invaluable for me and this study. Special acknowledgment is due to Dr Yinpeng Li who provided me with the huge volume of climate model data and Australian observation data.

I would like to say thank you to the whole of IGCC staff for their support and help. They are Dr Peter Urich, Dr Lisa Storey, Dr. Peter Kouwenhoven, Prof Richard Warrick, Matthew Dooley and Marian Holdaway. Special thanks to Prof Neil Ericksen and Glennis Ericksen for accommodating me and my wife at their place. We lived there since we came to New Zealand. In addition, many thanks to my fellow PhD students, Meng Wang, Saleem Sarwar and Electra Kalaugher for their support, encouragement and assistance with my topic. My sincere thanks also go to my family for their love, patience, and care. My special thanks go to my loving wife, Xiuqin Zhang, to whom this thesis is dedicated. She is a fantastic artist, who designed and produced numerous maps appearing throughout this thesis.

This research was made possible through the support from the Asia Pacific Network for Global Change Research (APN) CAPaBLE project, CRP2008-02CMY. It was carried out in collaboration with the key laboratory of regional climate-environment research for temperate East Asia (RCE-TEA), Chinese Academy of Sciences. I wish to say a big thank you to my colleagues and friends over there, especially to my Master supervisor Prof Xiaodong Yan.

This PhD thesis is dedicated to my dear wife, Xiuqin

for your support and love.

Table of Contents

ACRONYMS AND ABBREVIATIONS

AM	analog model
ANN	artificial neural network
AOGCM	atmosphere ocean global circulation model
CA	constructed analog
CCA	canonical correlation analysis
CDF	cumulative distribution function
CMIP3	phase 3 of the coupled model inter-comparison project
CSI	critical successful index
DDSM	dynamic downscaling
DJF	December-January-February
DSSAT	decision support system for agro-technology transfer
EOF	empirical orthogonal function
ERA-40	ECMWF 40 Year Re-analysis Data
GCM	general circulation model
HMM	hidden Markov model
IPCC	Intergovernmental Panel on Climate Change
JJA	June-July-August
JRA-25	Japanese 25-year Reanalysis data
LARS-WG	Long Ashton Research Station Weather Generator
LULC	land use and land cover types
MAM	March-April-May
MARS	multivariate non-linear non-parametric regression based on wavelet analyses or spline interpolation method
MOS	Model Output Statistics
MR	multiple regression
NCAR	National Center for Atmospheric Research
NCEP	National Centers for Environmental Prediction
NNR	NCEP/NCAR reanalysis data
PC	principal component (also: Personal Computer)
PCA	principal component analysis
PCR	principal component regression
PDF	Probability Density Function
PLSR	partial least square regression
RCM	Regional Climate Model
RMSE	Root Mean Squared Error
SDSM	Statistical Downscaling Model
SOM	Self-Organizing Maps
SOM-SD	Statistical downscaling based on Self-Organizing Maps

SOM-BCSD	SOM-SD in combination with Bias Correction
SON	September-October-November
SVM/RVM	support/relevance vector machine
SWAT	Soil and Water Assessment Tool
WG	weather generators

LIST OF FIGURES

Figure

LIST OF TABLES

Table

CHAPTER ONE

BACKGROUND AND INTRODUCTION

1.1 Climate change and downscaling background

1.1.1 Observed climate change

Since the beginning of the Industrial Revolution, the energy balance of the Earth's climate system has been altered greatly, partly due to human-induced increasing emissions of greenhouse gases and aerosols and extensive changes in land use and land cover. The atmospheric concentration levels of carbon dioxide are now higher than at any time over the last 800,000 years (Lüthi et al., 2008). Direct observations of recent climate show that there is a clear warming trend in the climate system evident from increases in global average air and ocean temperatures, widespread melting of snow and ice, and rising global average sea level. Global mean temperature has rise 0.8±0.2°C since the late 19th century (IPCC, 2007a). The temperature increases are also significant but variable at regional scales. From 1910 to 2005, Australia's average temperature increased by 0.89ºC (0.09℃ per decade). The rate of increase has accelerated since 1950 - average temperature increased by 0.95ºC (0.17ºC per decade) (Suppiah et al., 2006). Moreover, trends in the frequency and intensity of extreme temperature and rainfall events are rising faster than the means (Alexander et al., 2007). South-east Australian snow depths at the start of October have declined 40% in the past 40 years (Nicholls, 2005). Based on a series of evidences around the world, the Intergovernmental Panel on Climate Change (IPCC) has concluded that it is very likely that most of the globally-averaged warming observed over the last fifty years is the result of greenhouse gases emissions from human activities (IPCC, 2007a).

1.1.2 Climate change SRES scenarios

To estimate future climate change, the IPCC developed a series of greenhouse gas emission scenarios – Special Report Emission Scenarios (SRES) – to reflect the current understanding of the likely trends in future emission and the uncertainties that surround these trends. The scenarios allow analysis of "what if?" questions

based on various assumptions about population growth, economic development and technological change for a long time horizon that covers periods of a century. There are four basic SRESs to reflect different storylines: A1, A2, B1 and B2. Accordingly, several different scenarios were developed for each storyline (IPCC, 2007c).

- The A1 storyline and scenario family describes a future world of very rapid economic growth, global population peaks around 2050 and declines thereafter, and there is rapid introduction of new and more efficient technologies. The A1 scenario family includes three sub-groups – fossil fuel intensive (A1FI), non-fossil energy sources (A1T), or a balance across all sources (A1B).
- The A2 storyline and scenario family depicts a future world of regional self-reliance and preservation of local culture. Fertility patterns across regions converge very slowly, which leads to a continuously increasing population. Economic development is primarily regionally oriented, and per capita economic growth and technological change are more fragmented and slower than in other storylines.
- The B1 storyline and scenario family describes a convergent world of economic, social, and environmental sustainable development, but with the same global population as in the A1 storyline.
- The B2 storyline and scenario family describes a world in which the emphasis is on local solutions to economic, social, and environmental sustainability. Global population will steadily increase at a rate lower than A2. Economic development lies between the B1 and A1 storylines, and is less rapid, while technological change is more diverse.

Fig. 1.1 shows the envelope for the anthropogenic (human-induced) greenhouse gases emission and the projections of global annual mean temperature rise under the different SRES. All greenhouse gases including carbon dioxide, methane, nitrous oxide and sulphur dioxide are converted into equivalent carbon dioxide. By the end of this century, the scenario A1F generates the largest increases in global GHG emission and temperature (4.0°C, likely range is 2.4°C to 6.4°C), and B1 produces the smallest increase (temperature increase of 1.8°C with likely range between 1.1°C to 2.9°C). Moreover, the IPCC projections indicate that warming over many land areas is greater than global annual mean warming but

varies by region accompanied by even larger inter-annual variations. For precipitation, its spatial variability will generally increase, contributing to a reduction in rainfall in the subtropics and an increase at high latitudes and in parts of the tropics. The intensity and frequency of extreme weather events are also expected to increase (IPCC 2007a).

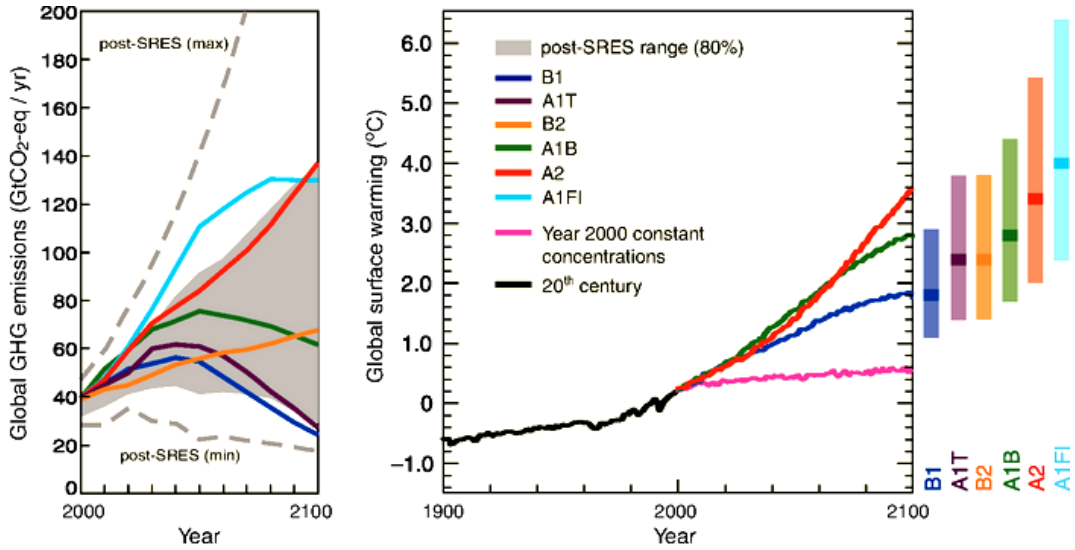

Fig. 1.1. Left Panel: Global GHG emissions (in $GtCO_2$-eq) in the absence of climate policies: six illustrative SRES marker scenarios (colored lines). Right Panel: Solid lines are multi-model global averages of surface warming for scenarios A2, A1B and B1, shown as continuations of the 20Th-century simulations. The bars at the right of the figure indicate the best estimate (solid line within each bar) and the likely range assessed for the six SRES marker scenarios for 2090-2099. All temperatures are relative to the period 1980-1999 (IPCC, 2007c).

1.1.3 Downscaling background

Climate change has been exerting important implications for natural environments and human society: from energy supply and infrastructure, to agriculture and ecosystems, at both global and regional scales. The demand for assessments of climate change impacts has grown significantly since the release of the IPCC Third Assessment Report (TAR), particularly for regions which are vulnerable to changes in climate, including the associated changes in frequency and intensity of extreme conditions. Reliable information regarding the rate at which climate changes are occurring and the magnitude of future changes is essential for the development of robust, multi-decadal planning and management strategies. At present, *general circulation models* (GCMs) are widely recognized as the most

appropriate tools for providing the transient global climate simulations and exploring future climate change scenarios.

GCMs are physically based on the principle of fluid dynamics and describe the entire globe using 3-dimensional grids, on which the prognostic equations of the atmosphere are solved to obtain a trajectory of the global climate compatible with the external forcings under given initial conditions. To reduce the enormous calculating requirements, they usually have to use coarse spatial horizontal resolution (in the order of a few hundreds of kilometers) and a set of numerical and parameterization schemes to simplify sub-grid-scale processes and characteristics such as clouds and *land use and land cover types* (LULC). Although these relative coarse resolutions are generally sufficient to reproduce the main large-scale features of the current climate, they present one of the primary challenges for regional/local climate change impact assessments that typically require high resolution climate change information (in some cases, down to a few kilometers, or even finer)(Robinson and Finkelstein, 1991). Regional climate change impact assessments evaluate the potential impacts of climate change on a specific region to provide key input for the development of adaptation strategies to reduce the vulnerability of human and natural systems to the coming changes.

There is a mismatching in spatial scale between GCM outputs and regional assessments (Robinson and Finkelstein, 1991; Fuhrer et al., 2006; IPCC, 2007a). Thus, it has been an active research field on how to translate projected changes in climate at the semi-continental scale into local conditions relevant to regional impacts assessment. Generally, downscaling techniques are employed to complete such a task (i.e., to derive finer resolution regional-scale or site climate change scenarios from coarser resolution GCM output). They have been widely applied in e.g., hydrological and ecological impact studies.

1.2 Downscaling Methods

In the last couple of decades, a large number of downscaling techniques have been proposed, which can be divided into two main categories: *dynamical downscaling* (DDSM) and *statistical downscaling* (SDSM). DDSM nests a *regional climate model* (RCM) into the GCM to represent the atmospheric physics with a higher horizontal grid box resolution within a limited area of interest. SDSM establishes statistical links between large(r)-scale weather and observed local-scale weather.

There are many comprehensive reviews of downscaling methods and their applications, such as Hewitson and Crane (1996), Wilby and Wigley (1997), Hanssen-Bauer et al., (2005), Christensen et al. (2007) and Fowler et al. (2007). A recent review can be found in Maraun et al. (2010). The following gives a brief summary of both approaches based on the above reviews. Emphasis is put on SDSM as it is the method used in this thesis. DDSM is introduced for the purpose of comparison.

1.2.1 Statistical downscaling

Traditionally, *statistical downscaling* (SDSM) has been seen as an alternative to *dynamical downscaling* (DDSM). SDSM essentially consists of employing statistical techniques to establish *strong* empirical relationships between the GCM simulated large-scale circulation variables (predictors) and the required regional or local scale climate variables (predictands) (Bronstert et al., 2002; Fowler et al. 2007). In other words, it refers to methods in which sub-grid scale changes in climate are calculated as a function of larger-scale climate. The relationship is then exploited to obtain information on the local variable out of the large-scale predictors. The central framework of SDSM can be expressed as:

$$p = F(X) + \epsilon \qquad (1.1)$$

where p is the local climate variable (predictand), and X is the large-scale state (single or multiple predictors), and F is the function that relates the two and is typically established through a trial-and-error method based on site observations or gridded reanalysis data, and ε is the uncertainty (error) term (van Storch et al. 2000; Fowler et al. 2007). Simple SDSMs disregard any residual noise term ε; whereas state-of-the-art SDSMs explicitly provide a noise model to represent variability and extremes. The former are often called deterministic, and the latter stochastic SDSM (van Storch, 1999a).

Typically, regression expressions (simple or multiple), stochastic processes (*Hidden Markov Mode*-HMM) and machine learning (*artificial neural network*-ANN) methods are employed to construct the function F. A wide variety of combinations also exist, for instance, merging neural networks and clustering as proposed in this thesis, or merging analog methods and canonical correlation (e.g. Fernández and Sáenz, 2003). The SDSM downscaling methods are generally

grouped into three categories (Wilby and Wigley, 1997; Wilby et al., 2004):

- *Regression models* - statistical relationships are calculated between large-area and site-specific surface climate, or between large-scale upper air data and local surface climate (e.g., Li and Smith, 2009; Bergant and Kajfez-Bogataj, 2005).

- *Weather typing schemes* - statistical relationships are determined between particular atmospheric circulation types and local weather (e.g., Hidalgo et al., 2008; Timbal et al., 2009).

- *Stochastic weather generators* - these statistical models may be conditioned on the large-scale state in order to derive site-specific weather (e.g., Richardson and Wright, 1984; Semenov and Barrow, 1997).

Applying the transfer function *F* (Eq. 1.1) to predictors from numerical models in a weather forecasting context is justified if the predictors are realistically simulated, and thus, these methods are also known as perfect prognosis downscaling (e.g., Klein et al., 1959; Kalnay, 2003; Wilks, 2006). Even though SDSM does not incorporate any physical knowledge about the underlying relationship between the large- and regional-scale variables under consideration, the physical principles behind the relationship often can be identified from the statistical results by means of the spatial signatures of the anomalies. In this way, if the identified physical mechanism is plausible to remain unchanged in an altered climate, the SDSM will likely perform correctly under such altered conditions.

The development of an actual downscaling scheme generally involves two steps: 1) the selection of informative large-scale predictors and 2) the development of a statistical relationship between large-scale predictors and local-scale predictand (i.e., Eq. 1.1). The first step is almost equally important for SDSM as the second step, but few studies have systematically studied and included this step (e.g., Brinkmann, 2002; Cavazos and Hewitson, 2005; Hofer et al., 2010). In general, SDSM is based on the following three assumptions for suitable predictors (e.g., Benestad et al., 2008). The predictors must (1) have a physical relationship to the predictand, (2) be reliably represented by the reanalysis data or GCM, and (3) reflect climate change.

Often, the first step also requires transformation of the original predictors into a useful or interpretable form. This is because predictors are generally high-dimensional fields of grid-based values. It is thus common to reduce the dimensionality of the predictor field and to decompose it into modes of variability. Possibly the most widely used multivariate statistical technique for dimensionality reduction in the atmospheric sciences is *principal component analysis* (PCA) (Preisendorfer, 1988; Jolliffe, 2002; Hannachi et al., 2007). The technique became popular for analysis of atmospheric data following the research by Lorenz (1956), who called the technique *empirical orthogonal function* (EOF) analysis. Both names are commonly used, and refer to the same set of procedures (Wilks, 2006). PCA provides a set of orthogonally-based vectors (empirical orthogonal functions) to convert a data set containing a large number of variables into a data set containing fewer new variables. These new variables are linear combinations of the original ones, which are chosen to represent a large fraction of the variability contained in the original data (Huth, 1999). PCA, however, does not account for any information about the predictands, so that the predictor/predictand correlation might thus not be optimal. Different in this respect is *canonical correlation analysis* (CCA) or *partial least square* (PLS) analysis. This method identifies new variables that maximize the interrelationships between the predictor and the predictand field (e.g., Fernández and Sáenz, 2003; Bergant and Kajfez-Bogataj, 2005).

Another important aspect in selecting predictors is to determine an appropriate size of the spatial domain surrounding/near the downscaling target site (i.e., a grid or a station, even an area-averaged basin) (Wilby and Wigley, 2000; Timbal et al., 2009). This is because GCM outputs should not be seen as a true representation for a smaller-scale climate. The local processes represented as parameterization schemes in GCMs are important for the formation of the global climate only through their overall statistics, but not in terms of their details (von Storch, 1999b). Therefore, SDSM often is carried out at a certain spatial scope. There is no consensus on the choice of the most appropriate spatial domain. For example, Chu et al. (2010) carried out their downscaling at a domain with a single grid, while Hidalgo et al. (2008) took the whole USA continent as a downscaling domain. Based on previous studies, it can conclude that the optimum domain size highly depends on seasons, regions, selected predictors and downscaling methods under

consideration (Wilby and Wigley, 2000; Hewiston and Crane, 2006; Hidalgo et al., 2008; Timbal et al., 2009; Chu et al., 2010).

As for the second step (i.e., to establish Eq. 1.1), several studies provide comprehensive reviews (e.g., Wilby and Wigley, 1997; Zorita and von Storch 1999; Trigo and Palutikof, 2001; Fowler et al., 2007; Maraun et al., 2010). This field still remains the cutting edge in the climate change research with novel SDSMs continuing to emerge from each of the three categories. A brief description for each category is given below, while Table 1.1 provides a summary of their relative strengths and weaknesses (Wilby et al., 2004).

1.2.1.1 Regression models

Regression models are conceptually simple and most often used for representing linear or nonlinear relationships between predictands and the large-scale atmospheric predictors. The regression techniques commonly include *multiple regression* (MR) (Murphy, 1999; Hofer et al., 2010), *principal component regression* (PCR) (Li and Smith, 2009), *canonical correlation analysis* (CCA) (Busuioc et al., 2008), *partial least square regression* (PLSR) (Bergant and Kajfez-Bogataj, 2005; Goyal and Ojha, 2010), *multivariate non-linear non-parametric regression* based on wavelet analyses or spline interpolation method (MARS) (Corte-Real et al., 1995; Fischer et al., 2004; Steinacker et al. 2006), *artificial neural network* (ANN) (Crane and Hewitson, 1998) and *support/relevance vector machine* (SVM/RVM) (Tripathi et al., 2006; Ghosh and Mujumdar, 2007). Comparatively speaking, the relationship between predictand and predictors attained from linear regression methods is more straightforward and easier to understand than the non-linear regression approaches, because it is difficult for the latter to interpret its regression parameters.

1.2.1.2 Weather classification scheme

Weather classification methods have a long history of synoptic climatology background. The synoptic climatology provides a powerful tool for the purpose of studying regional climatic conditions by classifying large-scale atmospheric circulation variables into a small number of categories (synoptic patterns) on a physically meaningful basis (Barry and Perry, 2001; Cassano et al., 2006). Typically, synoptic patterns are defined either by applying a cluster analysis

technique, e.g., *fuzzy classification method* (Wetterhall et al., 2009), *self-organizing maps* (Hewitson and Crane, 2002) and *the K-nearest neighbor algorithm* (Opitz-Stapleton and Gangopadhyay, 2010), or using subjective circulation classification schemes (Lamb 1972; Jones et al., 1993). In both cases, synoptic patterns are grouped according to their similarity with 'nearest' neighbors or a reference set. The predictand is then assigned to the prevailing synoptic pattern, and replicated under changed climate conditions by resampling or regression functions (Saunders and Byrne, 1996, 1999; Enke et al., 2005; Hewitson and Crane, 2006; Wetterhall et al., 2009).

Analogue model (AM) is a typical example of a weather classification method in which the large-scale weather situation is compared with the observational record. According to Euclidean distance between the two, the most similar large-scale weather situation in the past is identified, and the corresponding local scale observations (predictand) are selected as prediction for the desired local-scale weather (Zorita and von Storch, 1999; Wetterhall et al., 2005; Timbal et al., 2009). Recently, AM has been expanded to combine with the linear regression technique to form the so-called *constructed analogue* (CA) method (Hidalgo et al., 2008). The CA displays high downscaling skill, especially for precipitation in the USA continent.

Another approach is to combine synoptic classification methods with the non-hidden or hidden Markov model to downscale precipitation. Generally, a first order Markov chain is applied to characterize rainfall occurrence pattern evolutions, in which the transitions between synoptic patterns depend only on the current pattern. Then, conditional on the current pattern, precipitation is stochastically modeled through an auto-logistic regression method or a Gamma distribution (Hughes et al., 1999; Bellone et al., 2000; Vrac et al., 2007). As stochastically influenced by large-scale atmospheric variables, the local rainfall occurrence probabilities are not held constant and vary in time (Charles et al., 2004; Vrac et al., 2007).

1.2.1.3 Weather generator

Weather generators (WGs) are a type of particular SDSM, as they are used to model a full precipitation field in continuous space as their original purpose. Only recently, they have been extended to the downscaling field (Wilks, 1992; Katz,

1996; Katz and Parlange, 1996).

Table 1.1. A summary of the strengths and weaknesses of the main SDSM methods (from Wilby et al., 2004).

Method	Strengths	Weaknesses
Regression models (e.g., linear regression, neural networks, canonical correlation analysis, kriging).	• Relatively straightforward to apply • Employs full range of available predictor variables • 'Off-the-shelf' solution and software available	• Poor representation of observed variance • May assume linearity and/or normality of data • Poor representation of extreme events
Weather typing (e.g., analogue method, hybrid approaches, fuzzy classification, self organizing, Monte Carlo methods)	• Yields physically interpretable linkages to surface climate • Versatile (e.g., can be applied to surface, air quality, flooding, erosion, etc) • Compositing for analysis of extreme events	• Requires additional task of weather classification • Circulation-based schemes can be insensitive to future climate forcing • May not capture intra-type variations in surface climate
Weather generator (e.g., Markov chains, stochastic models, spell length methods, storm arrival times, mixture modeling)	• Production of large ensembles for uncertainty analysis or long simulations for extremes • Spatial interpolation of model parameters using landscape • Can generate sub-daily information	• Arbitrary adjustment of parameters for future climate • Unanticipated effects to secondary variables of changing precipitation parameters

Early versions of WGs, such as *WGEN* (Richardson, 1981; Richardson and Wright, 1984), *SIMMETEO* (Geng et al., 1986, 1988), *MARKSIM* (Jones and Thornton, 2000) and *EARWIG* (Kilsby et al., 2007), are mainly used to stochastically generate climate time series of (usually several) local weather variables for agricultural (e.g., DASST, see Thornton et al., 1994) and hydrological (e.g., SWAT, see Neitsch et al., 1999) modeling studies when weather observations are too short or have missing records (Yang et al., 2005). However, they are only based on the statistical attributes of long-term observed weather data such as the mean, variance, and wet/dry and/or spell transitions, and

do not involve so-called predictors commonly used in SDSMs. The core of most weather generators is a precipitation generator, while secondary variables such as temperature and solar radiation are often modeled conditional on precipitation occurrence (Richardson and Wright, 1984).

Due to their advantages of computational efficiency and ability to simultaneously generate several local variables, WGs has recently extended into the SDSM family. There are two evolution directions. The first is to condition their parameters on large-scale predictors or synoptic patterns as classical SDSMs do (Wilks, 1999; Vrac et al., 2007), while the second is not to directly use large-scale predictors, rather to proportionately adjust local variables to represent climate change based on the relative rainfall and temperature property changes between current and future periods predicted by GCMs. For the latter, a typical example is the stochastic weather generator called *Long Ashton Research Station Weather Generator* (LARS-WG) (Semenov and Barrow, 1997, 2002).

1.2.1.4 Model performance

An important aspect in constructing a good SDSM is how to prevent it from *overfitting.* In statistics, overfitting means that a statistical model describes random error or noise instead of the underlying relationship between predictor and predictand. Overfitting generally occurs when a model is excessively complex, such as having too many model parameters related to predictors. The overfitting also depends on the conformability of the model structure with the data shape, and the magnitude of model error compared to the expected level of noise or error in the data (Everitt, 2002). As most of SDSMs use multivariate data as predictors, they potentially all have the overfitting problem. An overfit SDSM generally has poor predictive performance. To avoid overfitting, one of the most often used method is to split an entire data set into 2 parts: training data and validating data. The model's ability can be evaluated by its performance on the validation data (not used for training), which is assumed to approximate the typical unseen data that a model will encounter. Another option is to use statistical dimensionality reduction techniques such as PCA, CCA and PLS to reduce the predictors so as to explicitly simplify overly complex models (e.g., Li and Smith, 2009). In fact, some additional techniques also have been gradually introduced to prevent SDSMs from overfitting (e.g. cross-validation, regularization, early stopping and

model comparison). For instance, Hofer et al. (2010) applied a moving blocks cross validation procedure to build their SDSM.

A wide variety of methods exist to validate SDSM's performance in simulating specific characteristics of predictand. These are often called metrics or indices, and all involve measures of the relationship between a simulation or set of simulations, and the corresponding observation(s) of the predictand. How to use these different metrics generally depends on the specific application of the impact study. As the inter-comparison studies between SDSMs and between SDSMs and DDSMs is becoming more profound and widely used than before, there have been several attempts to standardize indices, such as STARDEX project (Goodess et al., 2010) and the ENSEMBLES project (van der Linden and Mitchell, 2009). Some good verification indices can also be found in Wilks (2006). As Maraun et al. (2010) pointed out, these verification indices mainly involve (1) general performance measures (e.g., bias and correlation), (2) measures to validate distributions (e.g., Kolmogorov-Smirnov test (Bachner et al., 2008)), (3) measures to validate time series (e.g., *critical successful index* (CSI; Wilks, 2006).

For impact studies, selecting an appropriate model must depend on the objective of the impact studies, as well as other factors such as data availability and the location of regions. However, it should be kept in mind that normally no single SDSM can perform well upon all of the verification indices.

1.2.2 Dynamical downscaling

Dynamical downscaling consists of increasing the spatial resolution of a GCM by means of a physical model which solves the governing equations on a grid with higher resolution (down to 5-50 km) than those used by GCMs (in the order of a few hundreds of kilometers). Initial attempts to improve regional simulation focused on "nesting" a higher-resolution regional model within a global modeling framework (Dickinson et al., 1989; Giorgi et al., 1990; Giorgi and Mearns, 1991; Wang et al., 2004). This dynamical simulation of physical climate processes at a higher spatial resolution is known as *regional climate modeling* (RCM) - the most popular DDSM at present. Sometimes, DDSM is also referred to as 'numerical downscaling' or 'nested modeling' (Fig. 1.2). The well-known RCMs include MM5 (e.g., Liang et al. 2004a, b, 2007; Zhu and Liang 2005, 2007) and RegCM

(e.g., Giorgi et al. 2004), PRECIS (e.g., Jones et al., 2004) and RIEMS (e.g., Xiong et al, 2009).

These nested models allow a much finer description of orographic effects, land-sea contrast and LULC characteristics (Jones et al., 1995; Christensen and Christensen, 2007; Gao et al., 2008). Moreover, the physical and dynamical process parameterizations used by these models are also adapted to the smaller scales they resolve (Zangl 2004; Leung and Wigmosta 1999), and thus they are able to generate realistic mesoscale circulation patterns which are absent from GCMs (Buonomo et al., 2007). Some higher-resolution models are dynamically nested, that is, information is exchanged in both directions between the global and the regional climate model on a regular basis throughout the simulation, allowing higher-resolution regional processes to feedback directly to global climate (Lorenz and Jacob, 2005), but most high-resolution models just use one-way nesting approaches without feedback from the RCM to the driving GCM (Jones et al., 1995).

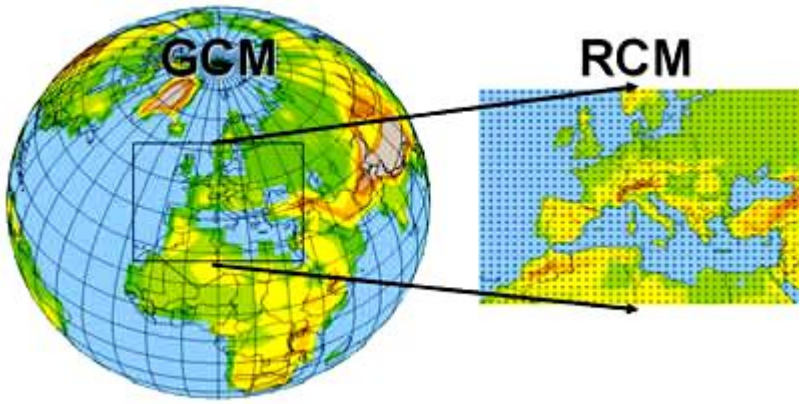

Fig. 1.2. Schematic depiction of the Regional Climate Model nesting approach (from Giorgi, 2008).

In addition, there are two other kinds of approaches widely used by DDSM. The first are the *Variable resolution AOGCMs* (VarGCMs), which enhance resolution over the region of interest while keep a coarse resolution for the rest of the globe (e.g. Déqué and Piedelievre, 1995). For VarGCMs, studies were carried out for the North America (e.g., Fox-Rabinovitz et al., 2001, 2006), North Europe (Barstad et al., 2009), the Mediterranean (Gibelin and Déqué, 2003; Goubanova and Li, 2007), Australia (e.g., McGregor, 2005) and East Asia (e.g., Zou et al., 2010). The other approach known as *High-resolution "time-slice" Atmosphere General Circulation Models* (AGCMs) (e.g., Cubasch et al. 1995) only uses an

AGCM with high resolution globally, but for a short period ("time slices") of a transient AOGCM simulation, say one for present-day (e.g. 1960-1990) and one for future (e.g. 2071-2100) climate conditions. They use the lower boundary conditions provided by a coarse resolution coupled atmosphere-ocean GCM (AOGCM). Because an atmosphere-only model is run for a period of limited duration, the AGCM can attain relatively high resolutions.

The performance of DDSM has been shown to be region-dependent, and thus for various regions there are many different DDSM developed around the world. Currently, there has been considerable international effort to quantify uncertainty in regional climate change through the inter-comparison of multiple RCMs. For example, ENSEMBLES projects in Europe (van der Linden and Mitchell, 2009), Regional Climate Model Inter-comparison Project for Asia (RMIP) (Fu et al., 2005), and the North American Regional Climate Change Assessment Program project for North America (Mearns et al., 2009).

1.2.3 Statistical vs. dynamical downscaling

1.2.3.1 Respective strengths and weaknesses

There are several comparisons of the dynamical and empirical approaches (Hellström et al., 2001; Hellström and Chen, 2003; Fernández, 2004; Díez et al., 2005; Haylock et al., 2006; Lim et al., 2007; Wang et al., 2010). Generally, these studies agree that both approaches have similar skill when validated under present-day conditions. However, large differences may exist between SDSMs and DDSMS (especially in precipitation estimates) when they are applied to climate change scenarios derived from GCMs.

DDSM is able to simulate a host of surface and upper-air variables that are coherent both spatially and temporally, consistent with the passage of weather systems around the world (Christensen et al., 2007). Moreover, nested RCMs are also based on fundamental physical principles and thus are presumed to be at least somewhat transferable from one region to another. That is particularly important for regions where no long-term observations are available or no observations at all, but effects of climate change may impact on regional agriculture, ecosystems, air quality, and many other sectors. However, DDSM has its own inherent limitations.

RCMs are centered over a relatively small region, where boundary conditions must be supplied at each time step. Because of their higher resolution, RCMs typically require a reduced model time step (5 min or less) compared to GCMs (typically 30 min time step) to maintain numerical stability. It should be kept in mind that it is not possible to enhance the RCM resolution without solving additional governing equations. Thus, DDSM is to date extremely expensive to run, so that only a few downscaling scenarios can be afforded. This significantly inhibits the use of dynamical models for long integrations and extensive hypothesis testing. Moreover, DDSM tends to inherit systematic biases from the driving GCM models, and these may be exacerbated in DDSM thus resulting in a poor simulation of the regional climate (Wood et al. 2004; Benestad et al., 2008). Moreover, RCMs are faced with the ***Stationarity*** issue, i.e. RCM parameterizations are assumed to be valid in a perturbed climate. This may be a significant issue for RCMs that have been developed for a specific region. In addition, the dynamical downscaling output is only acquired on a defined high-resolution grid. Additional techniques are needed to disaggregate the output into finer spatial scales, such as the *statistical bias-correction* (BC) procedure (e.g., Ines and Hansen 2006; Sharma, et al., 2007; Piani et al., 2009).

In contrast to DDSM, the main advantages of SDSM are: (1) it is computationally fast and inexpensive; (2) it can be applied easily to GCM outputs; (3) its statistical relationships can be explained rather easily; (4) it can be used for any consistently observed variable, and (5) it can provide site-specific estimations. Such advantageous features make a validated SDSM can be easily applied to multiple GCM outputs with multiple climate change scenarios, to create a rather large sample size of localized climate change projections. Given the climate change projections involve large uncertainty, this sample is essential for an ensemble based approach to evaluate and quantify of uncertainty, as well as making inferences and forecasts in the face of uncertainty, which is critical for many climate change impact assessments.

Table 1.2. A summary of the primary strengths and weaknesses of statistical and dynamical downscaling, or regional climate modeling (modified after Hayhoe, 2010).

Statistical Downscaling	**Dynamic Downscaling**
Strengths	
Computationally efficient	Explicitly consists both large-scale and small-scale physical process, up to the resolution of the model
Requires only monthly or daily GCM output	
Can relate GCM output directly to impact-relevant variables not simulated by climate models	Regional climate response are consistent with global forcing
Can be applied to any consistently- observed variable	They provide data that are coherent both spatially and temporally and across multiple climate variables
Can provide site-specific estimations	
Can be used to generate a large number of realizations in order to quantify uncertainty	They can be used in regions where no observations available
Weakness	
Base on essentially unverifiable assumption that statistical relationship between predictors and predictands remains stationary under future change	Assume that sub-grid parameterization schemes remain stationary in the altered climate
Sensitive to choice of predictors and GCM ability to simulate these predictors	Sensitive to initial boundary conditions from GCMs
Tend to underestimate temporal variance	Highly computation demanding
Require long-term observed data	Difficult to generate multiple scenarios

However, SDSM also has drawbacks that need to be taken into account in its practical applications. First of all, an ideal SDSM needs a strong statistical relationship explaining completely the variability of the local-scale variable. This is never the case since the predictors never explain all of the variability of the local variable which is also affected by local factors not accounted for by the large-scale fields (Wilby et al., 2004; Hewitson and Crane, 2006; Fowler et al., 2007). Furthermore, these relationships are assumed to remain valid under future climate conditions (i.e., ***Stationarity***) that may not always be justified, particularly

for precipitation (Fowler et al., 2007). If climate change dynamically alters these physical processes relative to their present-day observed behavior, the statistical method will not be able to simulate these changes. On the other hand, it indicates that SDSM generally requires long-term observed historical time series to construct and validate the statistical relationship (Eq. 1.1). Besides, the possible lack of reliability of the large-scale data generated by a GCM may affect the skill of SDSM, as it does to the dynamical approaches.

Both statistical and dynamical downscaling techniques are widely employed to estimate the possible impacts of climate change at present, while each approach carries with it its own inherent benefits and limitations. The primary benefits and limitations to statistical and dynamical downscaling methods are summarized in Table 1.2.

1.2.3.2 Miscellaneous

There is no particular type of downscaling method that is absolutely superior to all others. However, with the increasing reliability and availability of RCM scenarios, recent work on statistical downscaling has aimed to combine the benefits of these two approaches (e.g., Schneider et al., 2009; Pinto et al., 2010). That is to say, under the name *model output statistics* (MOS), gridded RCM simulations are statistically corrected and downscaled to point scales. Accordingly, an alternative classification for downscaling techniques was proposed by Rummukainen (1997) and was adapted by Maraun et al. (2010), who suggested to classify statistical downscaling approaches into *perfect prognosis* (PP; also referred to as "perfect prog"), MOS, and WGs. Generally, the PP consists of classical regression-based and weather-typing-based SDSMs, while MOS is also called statistical-dynamical downscaling approach (e.g., Schneider et al., 2009; Pinto et al., 2010).

MOS can be seen as a two-step procedure. It firstly uses the dynamical downscaling method to get regional climate information from GCM outputs. Next, these regional results are statistically downscaled to or are used to *statistical bias-correction* (BC) procedure to attain grid-scale results (e.g., Ines and Hansen 2006; Sharma, et al., 2007; Piani et al., 2009). Moreover, with more RCM scenarios available, the first step will be omitted and SDSMs will be directly applied to RCM outputs rather than GCM simulations in the future. Therefore, the core of

MOS still belongs to the DDSM and SDSM family. The BC procedure mostly resembles a post-process procedure to fix the downscaling biases between downscaled and observed data. Certainly, it also can be directly used to GCM outputs termed as *Bias Correction Spatial Downscaling* (BCSD) (Wood et al., 2004; Maurer, 2007).

A further comparison between BCSD and other downscaling methods is beyond the scope of this thesis; but can be found in Wood et al. (2004), Maurer (2007) and Maurer and Hidalgo (2008).

1.3 Research objectives and framework

1.3.1 Problem statement

It is a systematic procedure to select and construct a downscaling model for generating a set of climate change scenarios for regional climate impact assessments from the large-scale GCM outputs. DDSM can give a more accurate description of mesoscale atmospheric circulation than its original driving GCM, but it is not suitable for constructing long-term or multiple regional scenarios to depict the huge uncertainties of climate change due to its expensive computational requirements. Therefore, SDSM will still be a good alternative for regional climate change impact studies at present and for the foreseeable future. However, SDSMs are faced with some practical issues for their extensive applications in regional impact studies.

Firstly, few studies have systematically researched how to select informative large-scale predictors (e.g., Brinkmann, 2002; Cavazos and Hewitson, 2005; Hofer et al., 2010), although it is essential for a successful SDSM (Wilby et al., 2004). Generally, the selection of the optimum combination of predictors is solely based on past observed data or reanalysis data, such as NNR and ERA40. When applied to GCMs, the SDSMs rely on the hypothesis that the chosen predictors will capture the essence of the large-scale changes in a warmer future climate that drive the local climate (Timbal et al., 2009), but the hypothesis is usually investigated outside the scope of downscaling studies rather than in the perspective of statistical downscaling.

Secondly, climate change projections involve large uncertainty. Although it is the

uncertainty in atmospheric behavior that makes the atmosphere interesting (Wilks, 2006), the evaluation and quantification of uncertainty, as well as making inferences and forecasts in the face of uncertainty are a key challenge for many deterministic SDSMs as well as DDSMs (Maraun et al., 2010). What is required is a probabilistic climate projection that can reflect the uncertainties involved. The stochastic SDSMs have the ability to generate complete distributions and thus better represent local variability and extremes. Future work on statistical downscaling should incorporate stochastic approaches. In fact, these stochastic techniques should be used by default, in particular when downscaling of extremes is required. This is a development trend for SDSMs (Christensen and Hewitson 2007; Maraun et al., 2010).

Thirdly, there is a lack of consistency in evaluating the performance of downscaling methods for their applications to impact analyses (Hayhoe, 2010). Downscaling methods are mainly used to diagnose climate regimes rather than intentionally link to regional climate impact analyses (while they are also evaluated according to some statistical metrics of interest). Therefore, the current vast majority of impact studies still simply use the most readily available downscaling method, although there are a plethora of downscaling approaches. For instance, many hydrological or ecological studies still use a *simple delta approach*, where the difference in mean climate between today and a future time period is simply added or subtracted to current conditions or a so-called *Bias Correction Spatial Downscaling* (BCSD) (Hay et al., 2000; Wood et al., 2004; Maurer, 2007; Wolfe et al., 2008).

Fourthly, some studies have shown that GCMs are rarely able to reproduce very well the observed climate at regional scales, even though the quality of GCM climate projections is constantly improving (e.g., Mullan et al., 2001; Harvey and Wigley, 2003; Nieto et al., 2004). The GCM restrictions in regional scales can be explained partly by their limited horizontal resolution, model uncertainties and the over-simplified sub-grid parameterization schemes (von Storch et al., 1993). As a result, even using the optimum combination of predictors, SDSMs is still unable o eliminate model biases between the downscaled results and observer data (e.g., Timbal et al., 2009l; Chu et al., 2010). Of course, some uncertainties may also result from poor quality of input data, the estimated model parameters, or simplifying assumptions used in the model. On the one hand, these biases will

continue to propagate when downscaling GCM outputs under the SRES scenarios. On the other hand, they will propagate into and may finally degrade impact analysis quality. Thus, biases limit the SDSM use in impact studies for decision-making; biases need to be removed before the downscaling results are used as input to a decision support model.

Lastly, SDSMs need the strong statistical relationships between large-scale predictors and local variables to remain valid under future climate conditions (i.e., ***Stationarity***). However, these relationships are essentially unverifiable before they really take place in the future. While this should not necessarily be interpreted as a weakness of the SDSMs, since RCMs also make use of unverifiable parameterizations adjusted to present-day climate (Fernández, 2004; Maraun et al., 2010), it is possible that the downscaling will mislead impact analysis if climate change dynamically alters these statistical relationships relative to their present-day observed behavior.

1.3.2 Research objectives and framework

Water and food security are the fundamental issues in relation to socio-economical development, both nationally and internationally. The seemingly accelerating climate change and intensified variability, such as aridification and enhanced extreme weather events, has made the issues more serious but with increased complication. How to mitigate and/or adapt such changes has been becoming a strategically important question for policy makers at various levels. However, there is a lack of models and tools that can be used to support the analysis of the potential of mitigation measures and their associated cost-benefit assessment.

The objective of this research is to construct a robust downscaling scheme to provide reliable regional climate change scenarios to support regional integrated climate impact assessment, with the tasks to address the following particular issues and presents relevant solutions to overcome them.

- **Systematically assess the performance of GCMs involved in this study** based on the available reanalysis data (e.g., NNR or ERA-40), not only from the traditional assessment purpose (e.g., Mullan et al., 2001), but also from the statistical downscaling perspective. The latter was carried out by taking the

synoptic climatology as the theoretical foundation.

By linking the synoptic patterns to a local variable such as precipitation, the climatological regime that controls the local procedure can acquire a more profound and transparent understanding at a synoptic scale. Thus, predictability of the selected predictands can be analyzed using statistical downscaling techniques. Furthermore, the synoptic climatology is also employed to select the optimum combination of large-scale predictors. In this study, the method of *self-organizing maps* (SOM) (Kohonen, 2001) is used to create the synoptic patterns around each target downscaling grid.

- **Develop a statistical downscaling model based on the above synoptic climatology methodology**. This SDSM is named SOM-SD because it is mainly based on the SOM. By selecting appropriate large-scale predictors, SOM-SD will represent simple, transparent and physically interpretable statistical relationships between the selected predictors and predictands. When applied to a changing climate, the predictors are required to carry the climate change signal.

  In brief, SOM-SD is a type of synoptic-pattern-based statistical downscaling model, which involves linking observational station data to given synoptic pattern classification schemes. A significant characteristic of SOM-SD is that it combines the advantages of a synoptic climatology classification method based on the SOM and a stochastic re-sampling technique. The former provides accurate and relatively transparent simulations of local-scale precipitation characteristics/regimes, while the latter can explore the probabilities of predictands in a Monte Carlo simulation style. With the ability to generate a full range of time series data, the SOM-SD output allows probability and risk analysis for impact studies which are essential for impact assessment, given the huge uncertainties of climate-change conditions. Therefore, SOM-SD closely follows the development trend as described by Christensen and Hewitson (2007) and Maraun et al., (2010).

- **Identify and apply a broad suite of statistical indices to assess the performance of SOM-SD**. The aims are to provide complete and explicit information for application to regional climate impact analyses and narrow the

gap between the downscaling and impact study. Depending on the application, generic needs include the correct representation of the predictands for (1) mean and extreme state, (2) temporal variability, (3) spatial variability, and (4) consistency between different local-scale variables, and these are required for future scenarios (Maraun et al., 2010).

- **Fix downscaling output biases to prevent them propagating when downscaling GCM outputs under the SRES scenarios**. There are several ways of dealing with model biases in the downscaling field and other fields (e.g., BCSD or simple delta approach). These methods have been widely applied in the *model output statistics* (MOS) methods. In this study, the *bias-correction (BC)* transformation approach is used to adjust the model-simulated ensemble according to the probability distribution functions of observed values (Ines and Hansen 2006; Sharma, et al., 2007; Piani et al., 2009). The BC technique is used as a default post processor in SOM-SD.
- **Primarily analyze the temporal *stationarity* issue that all SDSMs have to face at present.** Although it is impossible to directly analyze the stationarity since it is an essentially unverifiable assumption, it can be assessed indirectly by analyzing the evolution of large-scale atmospheric circulation in the future based on synoptic climatology (Kidson and Watterson, 1995; Hope, 2006; Hope et al., 2006).

The core objective of this study was two-fold: (1) to develop a methodological framework constructed around the tasks to be addressed (as given above); (2) to construct a simple, robust and transparent statistical downscaling model. The methodological framework consists of six components:

Component 1: assessing the performance of GCMs.

Component 2: assessing the applicability of SOM in statistical downscaling.

Component 3: constructing the downscaling model.

Component 4: assessing downscaling performance.

Component 5: performing bias correction for downscaling outputs.

Component 6: analyzing stationarity issue.

The components (1) and (2) fulfill the first task, while other components complete the corresponding other tasks. In fact, each component can stand for as an independent direction related to climate change studies. However, they are put into a generic downscaling framework, rather than handled separately in this study, because they are judged equally important from the perspective of downscaling. The downscaling method (component 3) is constructed on the theoretical foundation of synoptic climatology (component 2). Moreover, component (1) and (6) are interrelated to control the quality of GCM data for the downscaling model, while components (4) and (5) are also interrelated to control the quality of downscaling outputs.

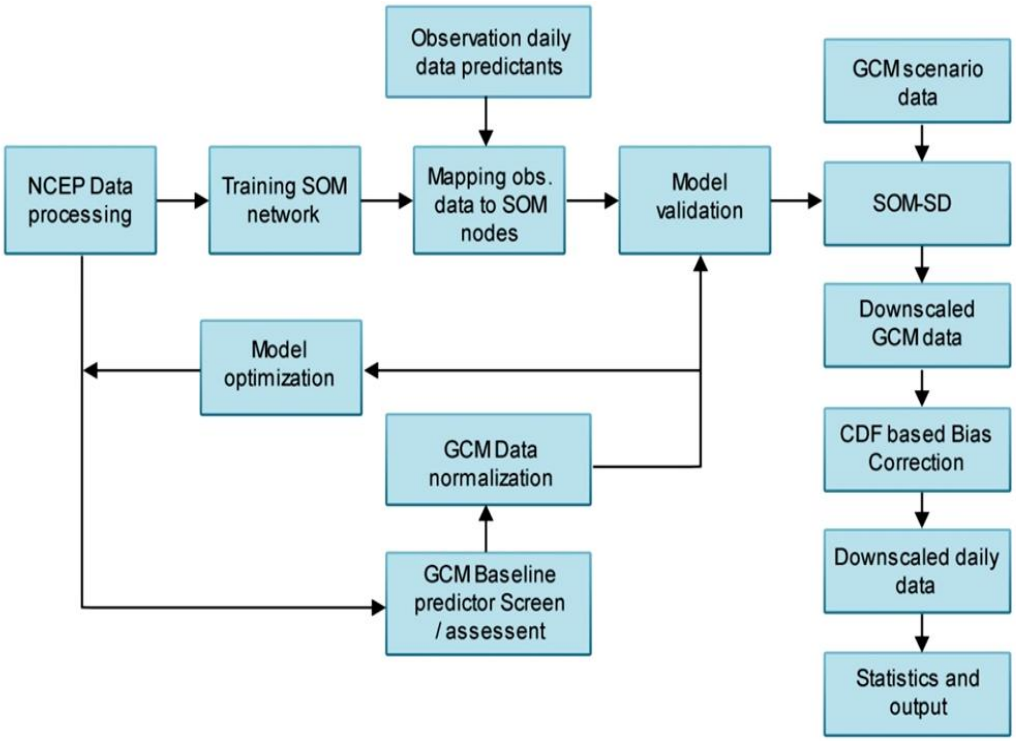

Fig. 1.3. Flow chart of the SOM-based Statistical Downscaling (SOM-SD).

A comprehensive modeling framework incorporates all of the above components (Fig. 1.3). In other words, the framework seamlessly integrates all of the components and then demonstrates the flow chart or development cycle of the SOM-based Statistical Downscaling (SOM-SD). The first step of this cycle is to identify a model structure that is appropriate for interpreting the relationship between the predictor and predictand under consideration. This is not a straightforward task, since the choice of the model structure depends on the research problems and objectives, as well as the data availability. The estimation of model parameters is the second step in the model development cycle. Next, a

model validation that consists of sensitivity and uncertainty analysis is followed, resulting in a downscaling model (SOM-SD). Finally, the model is applied to GCM scenario data. If necessary, a bias correction process is used to the downscaled data.

1.3.3 Research significance

The use of climate scenarios for impact assessment has grown steadily since 1990s. Moreover, there is a growing sense of integration of climate risk information in development planning because climate change could potentially impact all sectors at all levels of human society (Wilby et al., 2009). In the past few years, reducing vulnerability to climate change has become an urgent issue not only for developing but also developed countries.

Over the last decade, the scientific community has been developing regional climate *downscaling* techniques to reconcile the scale mismatch between coarse-resolution GCMs and location-specific information needed by adaptation planners. It is becoming apparent, however, that many downscaling techniques have serious practical limitations as being only focused on downscaling methodology. Few studies have actually looked at the role played by climate scenarios in adaptation planning (Dessai et al., 2005; Wilby et al., 2009).

This research develops a practical integrated methodological framework for regional downscaling. This framework integrates most of the important aspects related to statistical downscaling, from input data evaluation to output bias correction. At its core, the framework is not only about downscaling theory but also about its interface with impact studies. Thus, on the first hand, the framework makes the best knowledge in the fields of synoptic climatology and statistical downscaling and develops a hybrid downscaling method. On the other hand, the framework was designed to satisfy end user (in particular impact modeler) needs. This means that the framework is able to provide a set of common assessment indictors to impact study communities that convey the advantages and disadvantages of the downscaling method, which can prevent separating downscaling from impact or irrelevant studies. Another advantage of this framework is that it can provide a set of scenarios instead of a single one to describe the uncertainty involved in the downscaling process. These scenarios can

be further exploited by impact studies and then provide probabilistic information that is required by the end-users, such as government institutions for well-informed policy-making and forward planning (Cawley et al., 2007).

The strong emphasis of the framework is its flexibility, which underpins its application in a development context. In this study, the framework is developed based on the self-organizing maps algorithm and is validated over southeast Australia. However, it can be generalized to other algorithms (suitable for downscaling) and regions where similar data exist. In some regions, many conditions will limit the practical application of a downscaling method with the main one being the quality of the meteorological data needed for model calibration. Thoug good quality observed data are not available, this framework still can carry out downscaling and provide regional climate change scenarios by using high-resolution global reanalysis data and the simple bias-correction method (Fig. 1.3).

However, it should keep in mind that climate change scenarios developed by downscaling methods can meet some, but not all, of the needs for adaptation planning. The role played by these scenarios depends on not only the adaptation assessment approach, availability of technical and financial capacity to handle scenario information, but also the type of adaptation being considered (Wilby et al., 2009). Moreover, downscaling is only a link of the classic top-down approach for evaluating and responding to climate risks, and there are many alternative frameworks available to do such a job (Wilby et al., 2009, 2010).

1.4 Thesis outline

Chapter 2 describes all the data sets used in the case study area. Chapter 3 introduces the self-organizing map (SOM) algorithm and its applicability for statistical downscaling. Chapters 4 - 6 describe how to construct the downscaling model for precipitation based on reanalysis data and the comparison of the results with other models. Chapter 7 and 8 depict the application of downscaling method for GCM outputs, while Chapter 9 exhibits the bias correction procedure for downscaled precipitation. The final summary and future research needs are discussed in Chapter 10.

CHAPTER TWO

CASE STUDY AREA AND DATASETS

The development of statistical downscaling models is not only region specific, but also depends on data availability. This Chapter firstly introduces the case study area and then describes all the data-sets used in this research, which include observed, reanalysis as well as GCM output data.

2.1 Case study area

The study area, located in southeast Australia between 138-154^{o} E and 28-39^{o} S, encompasses most New South Wales (NSW) and Victoria (VIC) (Fig. 2.1). Australia is a particularly suitable region for testing the performance of various downscaling methods, since its regional climate variability as well as global changes has demonstrated a strong impact on regional ecological and economic fluctuations (Nicholls, 1997). To the east and south of the study area is the Pacific Ocean and to the west is the dry inland area of South Australia. The region has a wide variety of climatic conditions and highly diverse landscape ranges that are characterized by sub-tropical conditions in the far north, a humid marginal coastal band in the east, cool humid eastern uplands, high alpine country of the Snowy Mountains, the temperate south-east coastal area, and the hot and dry semi-arid and arid western plains. The Great Dividing Range (GDR) strides across the marginal east coastal band from north to south, which forms a natural barrier preventing the humid Pacific Ocean air from entering the region. Therefore, the spatial distribution of rainfall is markedly uneven, gradually decreasing from east to west, with sharp gradients over the GDR. The temperature shows a spatial pattern opposite to that of precipitation, gradually increasing from east to west, in addition to the latitudinal increase from south to north.

The area covers most of the Murray-Darling Basin made up of the catchments of the Murray River, the Darling River, and all the rivers and creeks that flow into them. The basin is of great national significance with many important social, economic and environmental values. It is Australia's most important agricultural region, mostly dominated by irrigated agriculture (ca 70% of all water used in Australia) (Crabb, 1997). The basin accounts for more than 40% of agricultural

production in Australia, valued at an estimate of $34 billion AUD, broadacre properties grazed around 5.9 million beef cattle and 51 million sheep in 1999 - 2000. Wheat production exceeded 12 million tons in the same year (Beare and Heaney, 2002). Water is the most vital natural resource and in high demand for the region. Changes in precipitation are the prime driver of change in the variability of water resources. However, a number of other factors can significantly affect regional water balances as well, and they are likely to be influenced by climate change. For example, changes in climatic factors of solar radiation, humidity, temperature and wind speed at ground level will have a direct effect on evapo-transpiration. Beare and Heaney (2002) stated that the projected impacts of climate change on river flows, water quality and economic returns in the Murray Darling Basin could vary considerably with different change scenarios. There is a strong demand for appropriate downscaling methods to obtain fine resolution climate information from coarse resolution climate model simulations. This is critical where topography and extreme weather phenomena are important such as for the GDR.

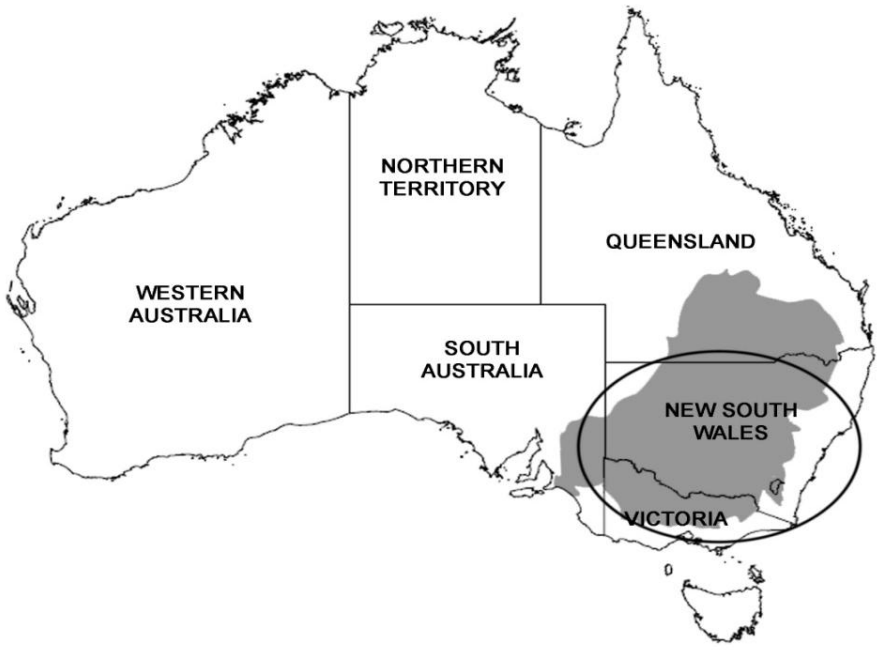

Fig. 2.1. Location of the case study area in the circle. The most important Australian agricultural region located in the shading area.

2.1.1 Climatic zones

The study area covers a wide variety of climatic conditions and highly diverse landscape ranges, which is of particular interest for downscaling studies. However,

it is very difficult to build a uniform statistical downscaling model across different climatic zones. In other words, building a model usually depends on specific regions under consideration (e.g. Timbal et al. 2009; Chu et al. 2010).

To investigate the applicability of the newly developed statistical downscaling model, the study area was divided into 9 climatic zones according to Hutchinson et al. (2005), who adopted the global agro-climatic classification by using elevation-dependent thin plate smoothing splines to clarify the spatial extents of the 18 global classes found in Australia. The clarified class boundaries were interpolated from known classes at 822 points across Australia. The climate classes reflect major patterns in plant growth temperature and moisture indices and seasonality. The agro-climatic classification provided an explicit global context for analysis (Hutchinson et al. 2005). Detailed information on the climatic zones is shown in Fig. 2.2 and Table 2.1.

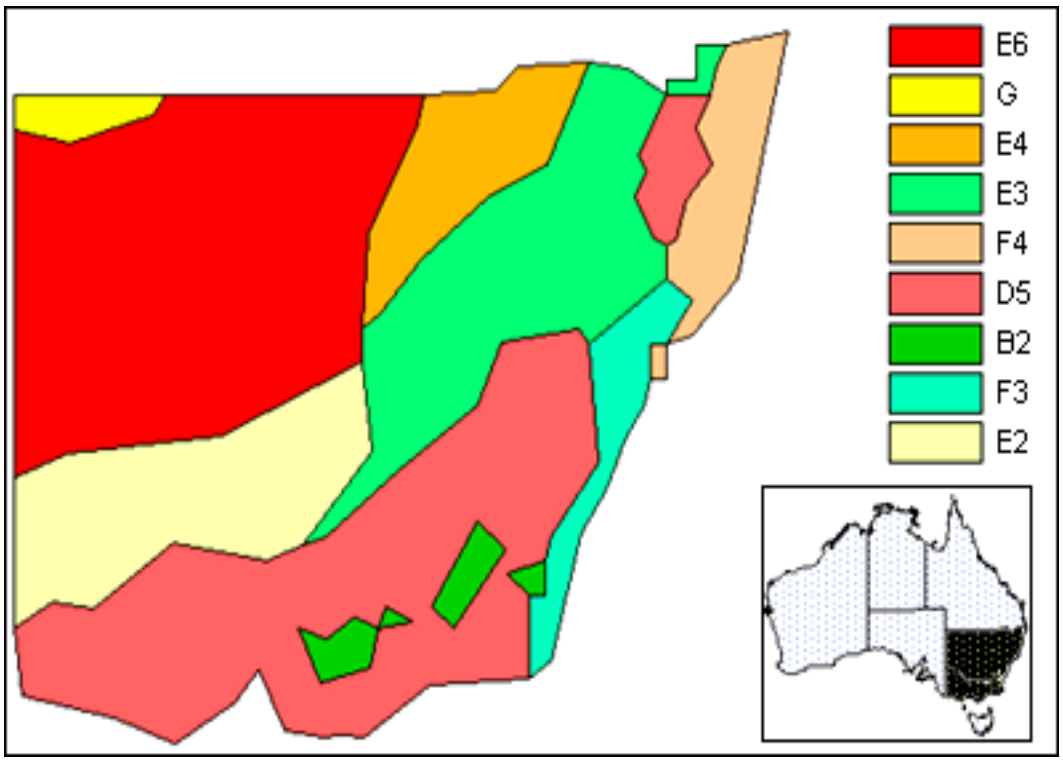

Fig. 2.2. Climatic zones in the case study area.

2.2 Data set

The development and validation of the SDSM are performed using the high quality gridded data available for both surface predictands and large-scale predictors in order to limit the impact of data quality on the statistical linkage

being developed. The data is generally open for public access and are widely used among the climatological community.

Table 2.1. Description of 9 agro-climatic zones over southeast Australia used in this study according to Hutchinson et al. (2005).

B2	Less severe winters and longer moist summers suitable for some crops
D5	Moisture availability high in winter-spring, moderate in summer, most plant growth in spring
E2	"Mediterranean" climate, but with drier cooler winters
E3	Most plant growth in summer, although summers are moisture-limiting. Temperature limits growth in winter
E4	Growth is limited by moisture rather than temperature and the winters are mild. Growth is relatively even throughout the year
E6	Semi-arid climate that is too dry to support field crops. Soil moisture tends to be greatest in winter
F3	Cooler end of the warm, wet sub-tropical climates
F4	Warmer and wetter than F3
G	Desert, supporting very little plant growth due to water limitation

2.2.1 Predictands: observation data

The predictands or the variable to be downscaled is gridded daily precipitation (1958-2008) and daily extreme temperature data (including minimum and maximum values, 1961-2000) at the resolution of 0.05 degrees (an approximately square area with sides of about 5 kilometers), which were from the Australian Bureau of Meteorology. The analyses (grids) are generated using a sophisticated analysis technique, which incorporates an optimized Barnes successive correction technique that applies a weighted averaging process to the station data across Australia (Barness, 1994a, b, c). Topographical information is also included by the use of rainfall ratio (actual rainfall divided by monthly average) in the analysis process.

In this thesis, the downscaled grids were filtered using a moving spatial window at a spatial resolution of 0.25°×0.25° (about 25 kilometers). That is to say, only one grid in the moving window had a change to be selected. On one hand, such a method of selection is sufficient to investigate the applicability of the downscaling

model across different climatic zones and orographic features. On the other hand, it can efficiently relieve computing requirements for downscaling in this study. As experiments showed, a complete run over the whole case study area will take one week (even more) for a single predictand with 3-4 predictors, using a Pentium class PC with Microsoft Windows XP and 1GB RAM. However, it should be pointed out that some downscaling values will lose in such a doing way.

2.2.2 Predictors: large-scale atmospheric circulation data

The predictors are large-scale atmospheric field data consist of the *NCEP/NCAR Reanalysis data* (NNR) and GCM simulation results under the climate change scenario A2. The NNR are produced using a global data assimilation system based on historical data (1948 onwards) (http://dss.ucar.edu/pub/reanalysis/, Kalnay et al., 1996; Kistler et al. 2001). It was found that NNR from 1961 provided the best results and is therefore applied in this study as the basis to construct the statistical downscaling method in combination with the predictands. While there are other reanalysis data publicly available such as the *ECMWF 40 Year re-analysis data* (ERA-40) and *Japanese 25-year Reanalysis data* (JRA-25), this study does not involve them because the NNR have been widely used over the case study area (e.g., Timbal et al., 2009).

The GCM outputs were obtained from the *Coupled Model Intercomparison Project No. 3* (CMIP3, http://www-pcmdi.llnl.gov/ipcc/info_for_renalysts.php). As part of the IPCC AR4 (Solomon et al., 2007), up to 23 GCMs contributed to the CMIP3 dataset. The open nature of output availability represents a major advance both for the evaluation of models, and for the generation of climate projections. However because the statistical downscaling methods rely on daily outputs for the predictors, which were not provided by every GCM modeling group, only a subset of this database could be used (Table 2.2). Thus, only GCMs that have daily data for both the simulations of the 20th and 21st century under the emission scenarios A2 were used.

Although six future emission scenarios were available, only the A2 scenario for the 21st century was used in this study. The scenario is based on a heterogeneous world with continuously increasing population and a technologically fragmented economic development leading to one of the highest emission scenarios available.

Therefore, the A2 scenario is at the high end of the SRES emissions scenarios (but not the highest), and this was preferred because, from an impacts and adaptation point of view, if one can adapt to a larger climate change then the smaller climate changes of the lower end scenarios can also be adapted to. A simulation of the 20th century was also used to complement the scenarios. Daily data are available for three time slices for which daily model predictors were available and downscaled: 40 years from 1961 to 2000 from the 20th century simulation and two 20 year periods ranging from 2046 to 2065 in the middle, and from 2081 to 2100 at the end, of the 21st century.

Table 2.2. Different GCMs from the CMIP3 database.

Model Name	***Institute***	***Country***	***Resolution(Lat×Lon)***
CCCMA_CGCM3	Canadian Centre for Climate Modeling and Analysis	Canada	$3.75^{o} \times 3.75^{o}$
CNRM_CM3	Meteo-France	France	$2.8125^{o} \times 2.8125^{o}$
CSIRO_MK35	CSIRO	Australia	$1.875^{o} \times 1.875^{o}$
MPI_ECHAM5	Max Planck Institute for Meteorology	Germany	$1.875^{o} \times 1.875^{o}$
GFDL_CM21	Geophysical Fluid Dynamics Laboratory	U.S.A	$2.0^{o} \times 2.5^{o}$
MRI_CGCM2	Meteorological Research Institute	Japan	$2.8125^{o} \times 2.8125^{o}$

The NNR and GCMs provide a number of atmospheric variables. Only variables that are most relevant to precipitation and temperature were extracted as potential predictors to reduce the amount of data used. These variables mainly involve humidity, dynamics and thermodynamics of the large-scale atmospheric circulation. Table 2.3 gives a brief description. All variables are direct outputs from the above GCMs and no derived predictor variables are employed such as vorticity or divergence. It is worth noting that although there are many variables in the NNR, only the common variables that also exist in the GCM archives were selected as predictors so that the downscaling method derived from the NNR could be applied to downscale the GCM outputs of future climate data for climate change scenario constructions.

2.2.3 Data standardization

Table 2.1 shows that different GCMs have different spatial resolutions. Some GCMs have a high resolution of 1.875^{o} (latitude) ×1.875^{o} (longitude), such as MPI-ECHAM5 and CSIRO-MK35, while the CCCMA_CGCM3 uses a relatively coarse resolution of 3.75°×3.75°. Other GCMs have similar resolutions to the NNR. Moreover, these GCMs use different coordinate systems such as Gauss or regular grids. All of the potential predictor variables were firstly converted into the same regular latitude and longitude coordinate, and then were re-gridded to use the same horizontal resolution of 2.5º latitude×2.5º longitudes, that is the resolution of the NNR observational data.

Table 2.3. List of large-scale potential predictor variables at different levels.

Variable Name	***Atmospheric Level***	***Acronym***
Sea Level Pressure	Surface	SLP
Specific Humidity	850 hPa; 700 hPa; 500 hPa	Q8; Q7; Q5
Zonal Wind	Surface (10m); 850 hPa; 700 hPa; 500 hPa	U0; U8; U7; U5
Meridional Wind	Surface (10m); 850 hPa; 700 hPa; 500 hPa	V0; V8; V7; V5
Temperature	Surface (2m); 850 hPa; 700 hPa; 500 hPa	T0; T8; T7; T5
Precipitation Rate	Surface	Pr

Moreover, the standardization of GCM predictors is widely used prior to statistical downscaling to reduce biases in the mean and variance of GCM atmospheric fields relative to observations (or reanalysis data; e.g. Wilby et al., 2004). The procedure involves subtraction of the mean and division by the standard deviation of the predictor for a predefined baseline period (i.e.1961-1990). Means and standard deviations used for standardization were derived from the baseline period 1961-1990.

The standardization procedure can be represented as:

$$\widehat{X_{ij}}(t) = \frac{X_{ij}(t) - \mu}{\sigma} \qquad (2.1)$$

where $\widehat{X_{ij}}(t)$ is the standardized atmospheric variable for grid (i, j) in the spatial downscaling domain at time *t*, $X_{ij}(t)$ is the original data, μ and σ are the mean and standard deviation of the spatial domain grids during the calibration period (Chu et al. 2010).

2.2.4 Period splitting: calibration and validation

To assess the performance of the novel downscaling method proposed by this study, the whole period of baseline was divided into two independent periods - a training period and a validation period. The novel statistical downscaling model is constructed and validated independently. However, the period splitting is highly dependent on the length of data available and is explained in the following chapters. The location of each precipitation or temperature grid cell is defined as the target location of the downscaling predictands.

CHAPTER THREE

SELF-ORGANIZING MAP AND SYNOPTIC FORCING OF PRECIPITATION OVER VICTORIA

3.1 Introduction

Synoptic climatology provides a powerful tool for studying regional climatic conditions by classifying large-scale atmospheric circulation variables into a small number of categories (so called synoptic patterns) on a physically meaningful basis (Barry and Perry, 2001; Cassano and Cassano, 2010). By linking these synoptic patterns to regional variables, a profound and transparent understanding can be acquired on the climatological regime that controls the local and regional climatic conditions at a synoptic scale (Barry and Perry, 2001; Harman and Winkler, 1991).

Over recent decades, synoptic climatology has made rapid progress because of the advance in computer techniques. A wide array of computer-assisted synoptic classification techniques, from traditional Hess–Brezowsky catalog (e.g., Hess and Brezowsky, 1952) and correlation-based maps (e.g., Kirchhofer, 1974) to more recent self-organizing maps (SOM; Cassano and Cassano, 2010), Bayesian objective classification (e.g., Little et al., 2008) and fuzzy clusters (e.g., Wetterhall et al., 2009), have been gradually employed to take over the earliest manual map classifications (e.g., Lamb, 1972).

Synoptic climatology, as a complement to the more theoretically based process studies, plays an important role in understanding and interpreting of atmospheric processes and modeling the linkage between atmospheric circulation and earth surface climate. Recently, synoptic climatological analysis has been expanded to climate change studies because of the availability of GCM outputs from the *Coupled Model Intercomparison Project* (CMIP3) and the reanalysis data sets such as NNR (Kalnay et al., 1996) and ERA-40 (Uppala et al., 2005) along with a concomitant increase in impact studies (e.g., Huth et al., 2008; Sheridan and Lee, 2010). Synoptic climatological analysis can be carried out at different spatial

scales from local, regional to global. For example, the teleconnections[1] analysis between circulation changes associated with the El Niño phenomenon or the Indian Ocean dipole (IOD) and Australian rainfall has identified a suite of large-scale drivers of rainfall variability for the Australian region (Risbey et al., 2009). Theoretically, after regional changes in the surface circulation induced by global warming are extracted from GCM outputs, the suite of large-scale drivers of regional precipitation can be employed to provide estimates of future precipitation changes (e.g., Cassano et al., 2006, 2007). More detailed discussion of synoptic methods can be found in El Kadi and Smithson (1992), Yarnal (1993), Barry and Perry (2001) and Huth et al. (2008).

Self-organizing maps (SOM), as a more recently developed technique, have been widely applied in the field of synoptic climatology. This chapter firstly introduces the self-organizing maps (SOM) algorithm and its characteristics for synoptic climatology analysis. Then, it presents the application of the method to study the synoptic forcing of precipitation over the state of Victoria in Australia during the late 20th Century using the NNR sea level pressure data (SLP) and observed precipitation data.

3.2 SOM algorithm and its climatologic applications

3.2.1 Artificial Neural Networks

Artificial Neural Networks (ANN) is one of the many algorithms used for automated analysis and visualization of the multi-dimensional data to find regularities and relationships (or reveal patterns) in the massive datasets, thereby gaining access to hidden and potentially useful information and insight on the data (Fischer, 2001). It is inspired by the structure and/or functional aspects of biological neural network of the natural thinking mechanisms that make it possible for human beings to learn from previous experience. For ANN, the most elementary computing unit is the Node, similar to the fundamental processing element of the brain, the neuron. Information is exchanged or communicated among interconnected neurons. A main advantage of ANN is that it can be trained to adaptively learn knowledge from previous experience (these are so-called

[1] Teleconnection in atmospheric science refers to climate anomalies being related to each other at large distances (typically thousands of kilometers). The most well-known one is the Southern Oscillation which is defined by linking sea-level pressure at Tahiti and Darwin, Australia.

training and learning processes), and then make inferences for new input data (this is also referred to as an inference process). The learning process can be competitive, meaning that some particular nodes can learn more knowledge than other nodes during the training process. Moreover, depending on whether *priori* patterns are known in the input, ANNs can be divided accordingly into supervised and unsupervised neural networks (Bishop 1995; Fischer, 2001; Pijanowski et al., 2002).

There are numerous applications that involve the ANN algorithm, including the application of classification analysis, which groups items in the input so that they share common (similar) features within each group. This process of finding similar items is generally referred to as clustering. In this chapter, the word "group" has a meaning similar to "cluster" or "pattern"; all these terms are used interchangeably. Especially if good visualization support is available, clustering can provide a helpful first impression of the way the data is distributed (See Fig. 3.1).

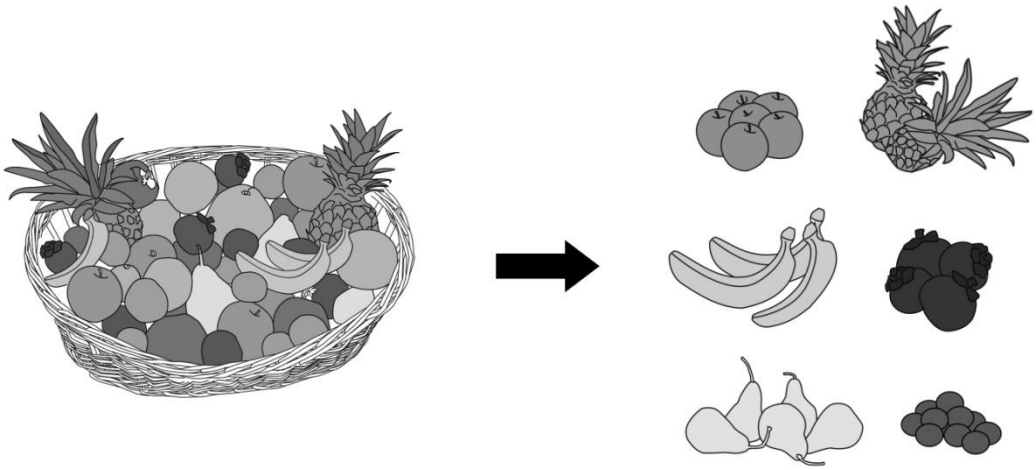

Fig. 3.1. Clustering provides a concise overview of the data.

The Self-Organizing Map (SOM) is a well-known ANN and indeed one of the most popular unsupervised learning algorithms (Kohonen, 2001). Moreover, it is also an excellent tool for visualization. The next section presents a brief introduction of the SOM method.

3.2.2 Self-Organizing Map (SOM)

The Self-Organizing Map was originally proposed by Kohonen (1982, 1990). Therefore, the SOM sometimes is also called the Kohonen Map. The typical

structure of the SOM consists of one input layer and one output layer (Kohonen layer, Fig. 3.2). The input layer of neurons is fully connected to the output layer. Without any *prior* knowledge about the clusters in the input data, the SOM network applies unsupervised and competitive learning procedure to group similar input data records which are multi-dimensional into a low-dimensional discrete lattice of nodes. The discrete lattice of nodes is referred to as a map in a general term (note that the terms map and SOM will be used interchangeably below) (Kohonen, 2001).

The map is typically two-dimensional in practice (see Fig 3.2). Higher dimensional map are not generally used although possible because they are difficult to visualize. The map is topology-preserving, meaning that the more alike two data samples are in the input data, the closer they will appear together on the final map (combining clustering and ordering processes in SOM). This allows the large and multidimensional input data to be reduced to more easily interpreted forms, and easily identified clusters, i.e. large groups with certain common characteristics. Like most ANN methods, SOM operates in two modes: training and mapping. Training builds the map using input data. It is a competitive learning process, also called vector quantization. Mapping automatically classifies a new input data record.

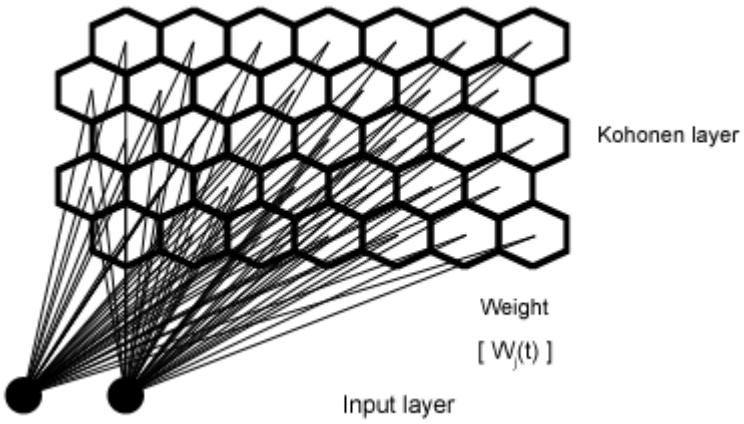

Fig. 3.2. Structure of a 5×7 two-dimensional self-organizing map (SOM).

3.2.2.1 Training

The size and topology type of output layer need to be determined before training a SOM. There is no theoretical principle for determining the optimum size of the output layer, albeit the output layer needs to be sufficiently large to ensure that the

optimum number of clusters is formed from the training data. Generally, the less the size, the more generalized the finally attained patterns or clusters. The size of a SOM is given as the number of neurons to be used in the two directions: landscape orientation and longitudinal direction. The total number is equal to the product of the number of neurons in two directions. Two topology types are frequently used (Fig. 3.3). The first one is the rectangular topology (A), where each neuron is connected to four neighboring neurons. The second one, also the more frequently used type, is the use of a hexagonal topology (B), with six neighbors to every neuron.

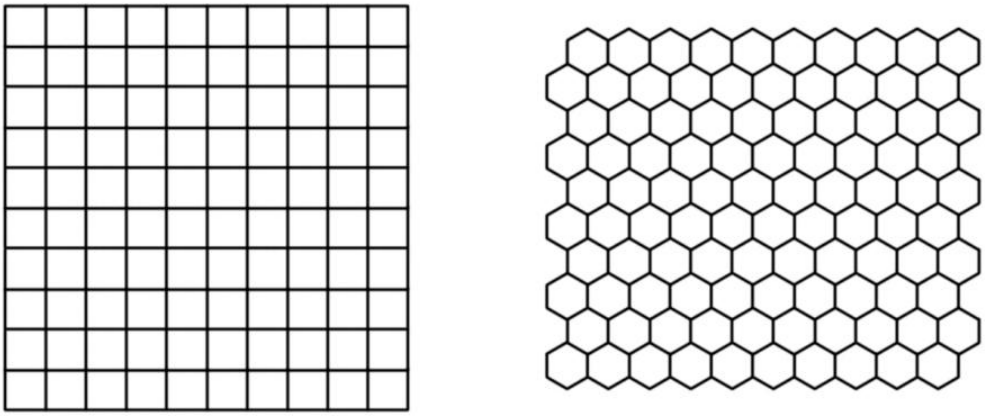

(A) (B)

Fig. 3.3. Network size and topology type of a SOM are chosen before training begins. Note that two topology types have identical size of 10×10, only the structure is different.

After assigning the size and topology type of output layer, a general training procedure can be carried out and the training algorithm used by Lin and Chen (2006) and Nishiyama et al. (2007) is adopted in this study.

The input layer on a SOM was composed of the input data that are generally multi-dimensional. Each dimension of the input data consists of a neuron of the input layer. Therefore, the input layer has an array of *M* neurons, if the input data is *M*-dimensional. The input data or the input layer can be denoted by

$$X = [x_1, x_2, \dots, x_M]^T \qquad (3.1)$$

where X is the input data. The output layer consists of the output neurons, determined by the assigned size. Figure 3.2 gives a typical example, where each output neuron is linked to each input neuron. Moreover, each connection line denotes a value of weight from the input layer neuron to the output layer neuron. Thus, the weight vector of each neuron has the same dimension as the input data

(i.e., M). If the output layer has N neurons, these neurons can be donated by $u_j, j = 1,2, \dots N$, while the weights from the input layer neurons to the jth output neuron can be donated by $w_{ij}, i = 1,2, \dots M$ and then the weight vector for all output neurons can be written as

$$W_j = \left[w_{1j}, w_{2j}, \dots w_{Mj}\right]^T, j = 1,2, \dots, N \qquad (3.2)$$

The training process begins with all weights initialized to small random numbers or some values randomly extracted from the input data. The SOM algorithm firstly calculates the Euclidean distance between an input vector X and all the weight vectors W_j $(j = 1,2, \dots, N)$ to find the "winner" neuron c with the weight vector being the closest to the input vector (i.e., the smallest Euclidean distance) as shown by Eq. 3.3. The "winner" neuron c is also called the best-matching unit (BMU).

$$c = \arg\min_j\{\|X - W_j\|\}, j = 1,2, \dots N \qquad (3.3)$$

where $\| \|$means the Euclidean distance. The Euclidean distance d_j between the weight vector W_j and input vector X is formulated as

$$d_j = \|X - W_j\| = \sqrt{\sum_{i=1}^{M}(x_i - w_{ij})^2} \qquad (3.4)$$

Next, the SOM updates the weights of both the winning neuron and its topological neighborhood towards the direction of the input vector. The winning neuron is at the center of the topological neighborhood. Moreover, the update rate for the neighbor neurons decays symmetrically from the winning neuron location. The updating process is shown by Eq. 3.5 and Fig. 3.4.

$$W_j(t+1) = W_j(t) + h_j(t)(X - W_j(t)) \qquad (3.5)$$

The weight vectors at step $t+1$ is modified on time t depends on the neighborhood function $h_j(t)$. Eq. (3.5) is applied to all neurons neighboring to the winning neuron. A typical choice of topological neighborhood function is the Gaussian function

$$h_j(t) = \alpha(t) \cdot \exp\left(-\frac{\left\|u_j - u_j^*\right\|^2}{2\sigma^2(t)}\right) \qquad (3.6)$$

where $\alpha(t)$ is the learning-rate parameter, σ is the "effective width" of the topological neighborhood, and u_j^* is the winning neuron. The neighborhood function h_j decreases with the distance from the BMU. Therefore, the closer a weight vector to the BMU, the higher update rate it is given. Moreover, the neighborhood function decreases with the iteration step *t*, which is controlled by the learning-rate $\alpha(t)$ and the width of the neighborhood function $\sigma(t)$. They both monotonically decrease with the iteration step t. $\alpha(0)$ is generally set to a value between 0 and 1.0, while $\sigma(0)$ is frequently set to about half of the map size (Kohonen, 2001; Lin and Chen, 2006; Nishiyama et al., 2007). A comprehensive schematic of training a SOM is shown in Fig. 3.5.

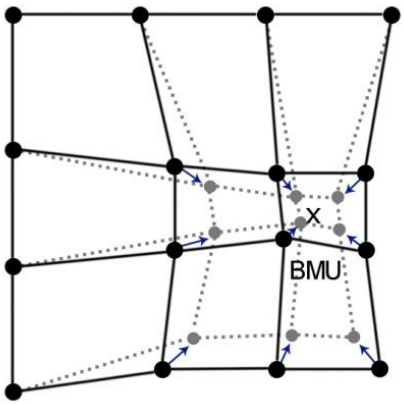

Fig. 3.4. The updating process involves the best matching unit (BMU) and its neighbors toward the input sample marked with x. The black and gray circles correspond to the situation before and after updating. The solid and dashed lines show neighborhood relations, respectively.

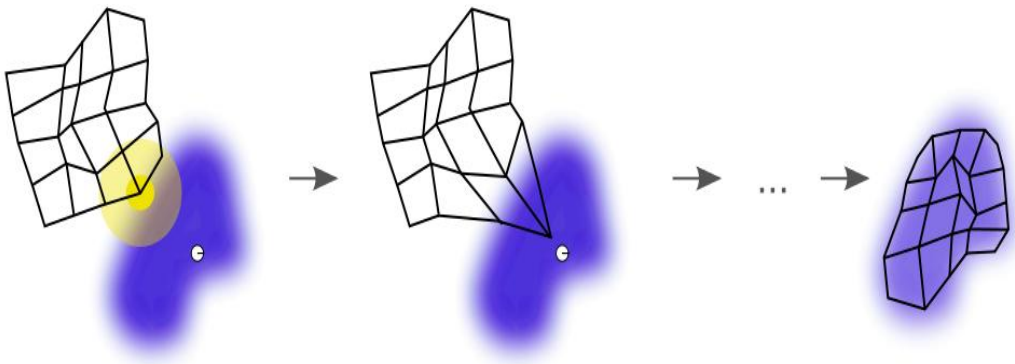

Fig. 3.5. An illustration of the training of a self-organizing map. The blue blob is the distribution of the training data, and the small white disc is the current training sample drawn from training data. At first (left) the SOM nodes are arbitrarily positioned in the data space. The node nearest to the training node (highlighted in yellow) is selected, and is moved towards the training datum, as (to a lesser extent) are its neighbors on the grid. After iterations the grid tends to approximate the data distribution (right) (source: http://en.wikipedia.org/wiki/Self-organizing_map).

To keep the stability of the SOM training, the series of computation procedures from Eq. (3.3 – 3.6) should be repeated until there are no further changes in the weight vectors related to the output neurons. The iterative calculation drives the weight vectors toward the general characteristics in input data due to the neighborhood updating. Thus, similar input data samples are projected onto an identical neuron in a map whose weight vector represents a general pattern of the input data.

In practice, the training is carried out in two stages that start with a large update kernel (close to the size of the smaller SOM dimension) for the first set of iterations. Then, using that final SOM as the starting point, a second training is run with a smaller update kernel to refine the mapping. As a general rule, the number of iterations must be at least 500 times the number of neurons in the network (Haykin, 1994).

3.2.2.2 Mapping

Once the training process is completed, a set of generalized characteristics or patterns of the training data are obtained. By presenting a new input vector to the trained SOM, it can identify the associated pattern for the new input through calculating the distances between the input vector and the weight vectors from the trained SOM. Then the weight vector is chosen with the smallest distance as the most associated pattern to the input vector. This procedure is called *mapping*. In addition, if the input vector can be mapped to a pattern, its features should be similar to this pattern. Therefore, the features of the new input vector can be estimated through the properties of the selected pattern.

Obviously, the data used for training can also be mapped to the trained SOM. In fact it is also a useful practice for frequency analysis. Frequency analysis investigates how frequent each of the patterns is (Cassano and Cassano, 2010). The percentage of occurrence, or frequency, of each node over a period is the number of occurrences divided by the total number of input data. The probability (p) that any record of the input data would map to any particular node is $1/N$, where N is the number of nodes. The significance of the frequency for which each record maps to each node can be determined by calculating a 95% confidence interval around the expected probability. Assuming that the process is binomial, the 95% confidence limits are calculated by

$$p \pm 1.96 \left[\frac{p(1-p)}{n}\right]^{1/2} \qquad (3.7)$$

where p is the probability that any record would map to any node, and n is the number of samples. If the observed frequency of a node is outside this calculated interval, it is considered significantly different at the 95% confidence level from the expected value of p (i.e., $1/N$).

3.2.2.3 Related software

One of the most widely used software package for implementing SOM is the SOM-PAK program (Kohonen et al., 1996; http://www.cis.hut.fi/research/som-research/). Use of SOM-PAK involves four main steps: map initialization, map training (in multiple stages if desired), evaluation of quantization error, and visualization. SOM-PAK only creates output in PostScript format. Another freely available software package is the SOM Toolbox (http://www.cis.hut.fi/somtoolbox/), which is good for visualization and easy to use.

3.2.2.4 SOM applications to synoptic climatology

One of the first applications of SOM in climatological analysis was the evaluation of the seasonality of circulation in southern Africa (Main, 1997). Since then, SOM began to enter the field of the analysis of climate data as a new approach and was adopted in a number of climate applications. Although, in many aspects, it is analogous to more traditional forms of cluster analysis such as principal component analysis (PCA) (Wilks, 2006), SOM has some specific advantageous characteristics that make it more attractive to climatological analysis than the traditional approaches (Hewitson and Crane, 2002; Crane and Hewitson, 2003). The traditional PCA generally requires a linear combination of orthogonal principal components (PCs) to explain a maximum possible fraction of the variability contained in the original data. Although it is powerful in reducing the dimensionality of a data set, the physical interpretation of PCs is difficult because real-world processes are generally non-linear and do not need to have orthogonal PCs at all. Moreover, the traditional PCA is less conducive to examining the continuum of data. SOM circumvents many of these shortcomings.

SOM describes the multi-dimensional distribution function of the input data by

finding a set of representative and continuous nodes spanning the input data space. The attained nodes are output in the clustering style. That is, the clustering is only a post-processing step for mapping the input data to associated nodes in SOM. Furthermore, SOM makes no assumptions about the underlying data, and the iterative training allows it to describe any distribution function regardless whether it is linear or non-linear. Another significant characteristic is that SOM has proven to be an effective tool for visualizing the relationships between the nodes, since the training procedure ensures that the most different patterns will move to opposite corners of the SOM array.

Focusing particularly over the past ten years, the main applications of SOM can be assembled into general categories based on research goals:

- Analysis of Circulation Variability (e.g., Hewitson and Crane, 2002; Morioka et al., 2010);
- SOM-based Conditional Interpolation (e.g., Crane and Hewitson, 2005; Kalteh and Berndtsson, 2007);
- Evaluation of the ability of GCMs to replicate synoptic circulation patterns (e.g., Cassano et al., 2006; Finnis et al., 2009);
- Synoptic methods and GCM generation of precipitation (e.g., Cassano and Cassano, 2010; Brown et al., 2010);
- Time Evolution of the Seasonal Climate (e.g., Main, 1997; Hope, 2006; Hope et al., 2006).

3.3 Synoptic forcing of daily precipitation in Victoria Australia

The remainder of this chapter investigates the synoptic forcing of daily precipitation, or the relationship between large-scale atmospheric circulation patterns and observed precipitation, which is a typical application of SOM in synoptic climatology. Victoria in Australia was chosen as the study area because numerous similar studies have been done for the same area, which provide a practical guide or a comparison to this study (e.g., Verdon-Kidd and Kiem, 2008; Pook et al., 2006, 2009).

3.3.1.1 Data preprocessing

In synoptic climatologic analysis, the sea level pressure (SLP) is the most used climate variable to depict the large-scale atmospheric circulation characteristics. The 40 year NNR daily SLP data over Victoria and the adjacent region (120–180°E, 20–50°S) from 1961 to 2000 were used to acquire regional-scale circulation patterns based on SOM (Fig. 3.6). The observed daily precipitation data were also selected for the same period. SLP anomalies were used as the basis for the synoptic climatology because the SLP gradients, rather than absolute values, were responsible for determining the near-surface circulation and therefore were of most interest in our analysis. SLP anomalies were calculated for each day by subtracting the mean SLP over the analysis domain for all days from the grid point values of SLP.

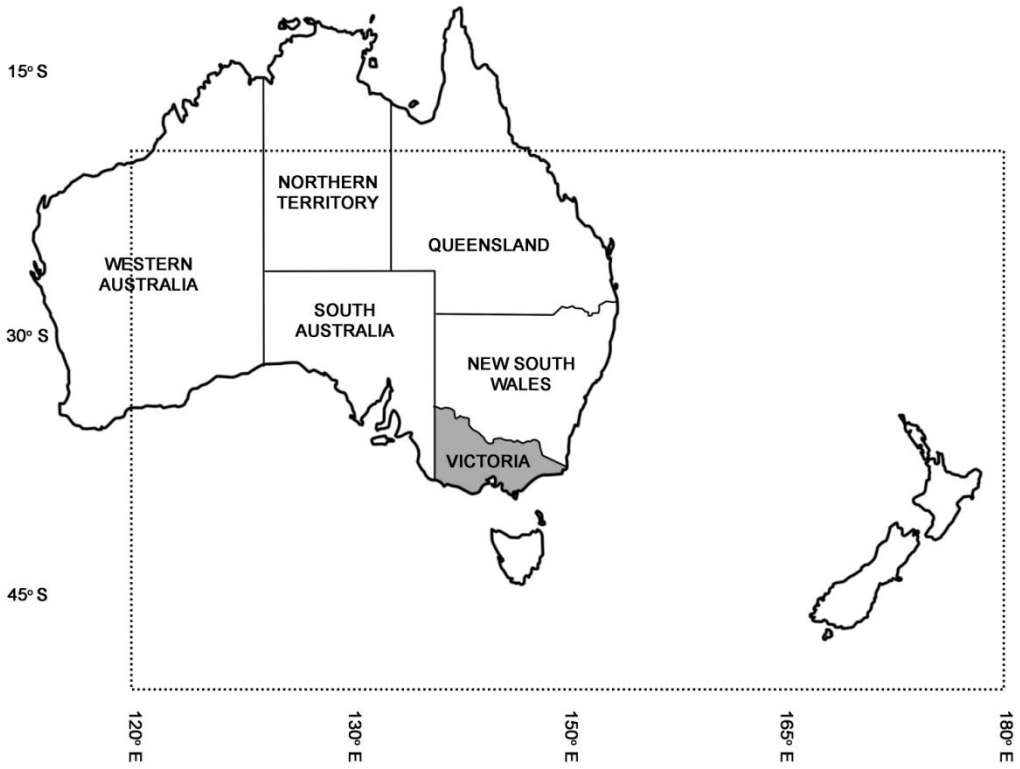

Fig. 3.6. Location of the study area of Victoria. The region over which synoptic patterns were analyzed is shown by the dashed rectangle.

3.3.2 Observed precipitation climatology

Daily rainfall characteristics can be analyzed in terms of intensity and frequency of rainfall events. Generally, the intensity and frequency of rainfall are represented

in different categories such as “light” (1-10 mm/day), “heavy” (> 10 mm/day) and “very heavy” (>30 mm/day) (Sun et al. 2006; Brown et al., 2010). Following Sun et al. (2006), rainfall less than 1 mm/day is excluded as it generally contributes little to rain gauge observations. In the Southern hemisphere, seasons are defined as spring from September to November (SON), summer from December to February (DJF), autumn from March to May (MAM) and winter from June to August (JJA).

The climate of Victoria is characterized by a range of different climate zones, from the warm, dry region of the northwest to the alpine snowfields in the northeast. Mean annual rainfall ranges from less than 300 mm in the northwest to above 2000 mm in the mountainous regions (left panel, Fig. 3.7). In general, the areas with high rainfall are associated with high elevations. The number of rain days per year (i.e., days with at least 1.0 mm rain) and the annual totals decrease towards inland from the coast (right panel, Fig. 3.7), accompanying an increasing rainfall variability.

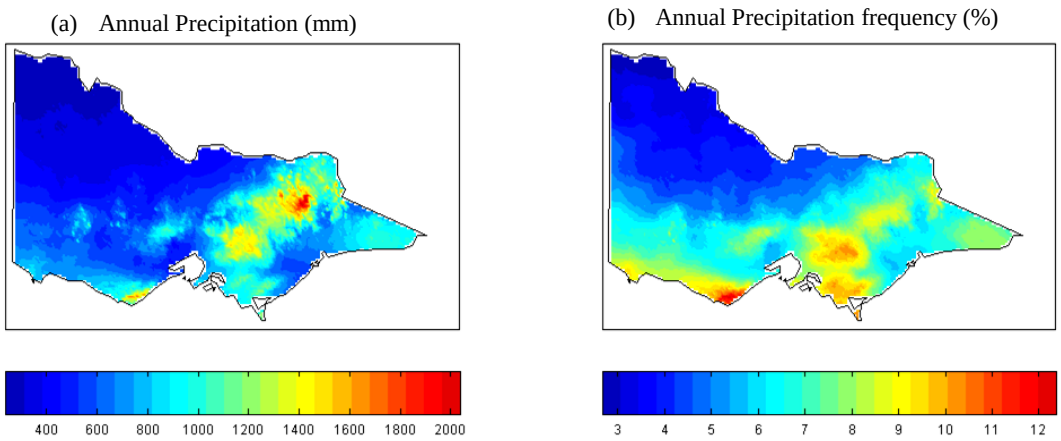

Fig. 3.7. Annual mean precipitating total (mm) and frequency (%) during 1961-2000. A wet day is defined with daily precipitation >1.0mm.

On a seasonal basis, more rainfall occurs in winter than in summer (Fig. 3.8). In summer, substantially more uplift is required than winter for air to reach saturation and produce cloud. However, because of the high moisture content of warm air, summer rainfalls may be much heavier than other seasons. Except the inland area, rainfall reaches maximum in late winter or early spring, and minimum in summer or early autumn. Over inland Victoria, a significant proportion of rain is from bands or areas of cloud that are transported across Australia from the

northwest. Rain can be particularly heavy when these northwest cloud bands interact with eastward moving frontal systems that cross the Southern Ocean (http://www.bom.gov.au/watl/about-weather-and-climate/australian-climate-influences.htm). The frequency of these cloud systems and the amount of rain associated with them varies from season to season.

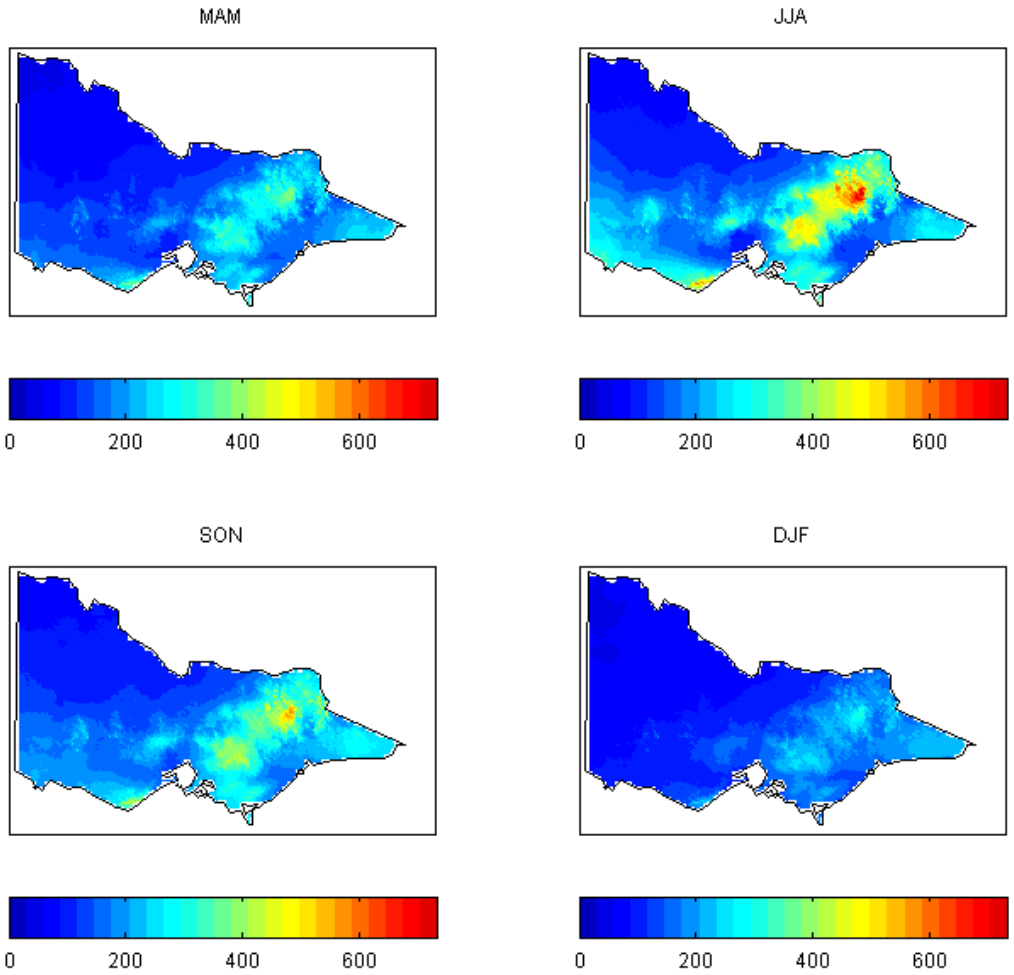

Fig. 3.8. Seasonal mean precipitation total (mm) from 1961-2000.

Another significant characteristic related to precipitation is the heavy and extreme precipitation. The frequencies of heavy and very heavy precipitation are shown in Fig. 3.9, while extreme precipitation over the 99th percentile and its frequency are displayed in Fig. 3.10. As can be seen, large precipitation including heavy, very heavy and extreme precipitation, mainly occurs in the wettest parts of the mountainous regions and decreases from the coast towards inland. For the frequency of extreme precipitation, there is no obvious spatial difference (Fig. 3.10 b).

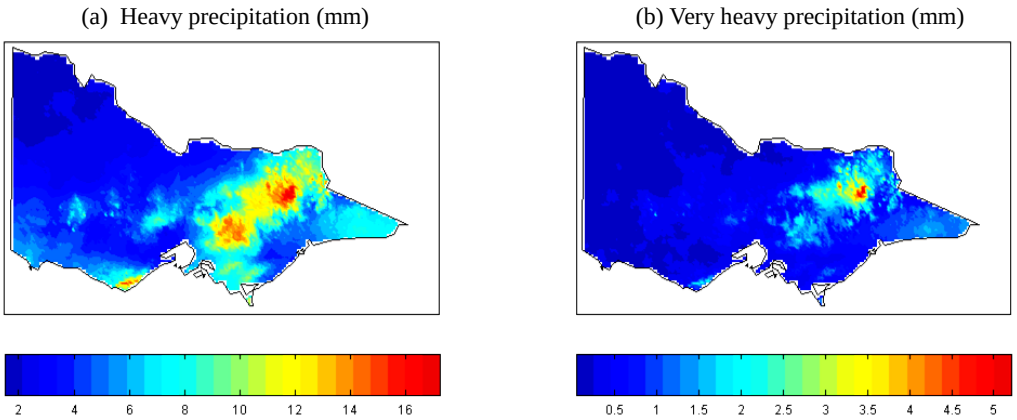

Fig. 3.9. Heavy and very heavy precipitation frequency distribution (% days) during 1961-2000 (P>=10.0mm and P>=30.0mm).

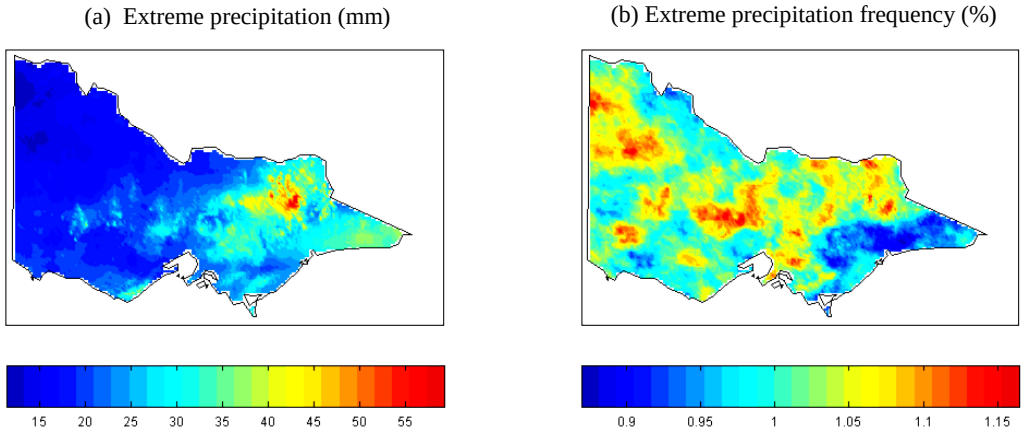

Fig. 3.10. Extreme precipitation (mm) and frequency distribution (%) during 1961-2000 (P>99th percentile long-term).

3.3.3 Synoptic regimes

A set of 20 SOM patterns (5 × 4) was attained to span the range of synoptic conditions for all seasons after training the NNR gridded daily-anomaly SLP data over the Australian region (120–180°E, 20–50°S) for the period of 1961–2000, similar to previous studies in the Victoria region (e.g. Hope et al., 2006; Verdon-Kidd and Kiem, 2008; Nicholls et al., 2009; Alexander et al., 2009). No attempt was made to further optimize the number of the synoptic patterns as there were not any significantly different patterns occurring any more (subtle changes would take place, but it did not matter). Victoria is influenced by a range of regional synoptic systems and large-scale climate phenomena due to its location to the Pacific, Indian and Southern Oceans (Fig. 3.11). Although SOM could identify all

possible SLP patterns, the patterns are in so large-scale that they could not represent important small-scale synoptic systems governing the weather of southeastern Australia, such as cut-off lows and east coast lows (Pook et al., 2006; Nicholls et al., 2009). This is because the small-scale synoptic systems are spatially unstable, i.e., they typically do not stay consistently in the same area. Therefore a multivariate clustering procedure will always struggle to identify these smaller-scale synoptic features.

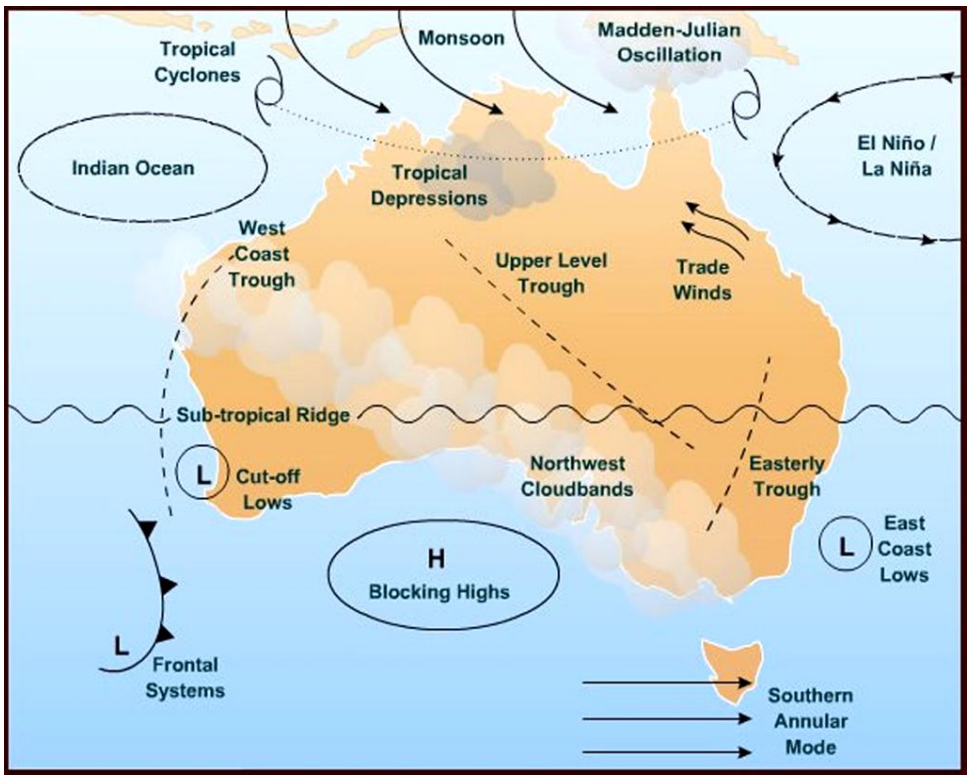

Fig. 3.11. Schematic diagram indicating the main influences on Australia's climate including easterly troughs, east coastal low-pressure systems, the Southern Annular Mode, the subtropical ridge and the ENSO phenomenon (From http://www.bom.gov.au/).

The 20 key synoptic patterns are shown in Fig.3.12, which capture a range of significant synoptic features known to influence the weather of the Victoria region. Similar types are clustered together with the most dissimilar types located at the far corners of the SOM map. The types displaying the expected deep troughs are in the lower portion of the SOM and types with broad regions of high pressure are near the top. Synoptic types with a trough to the west of the region are in the bottom left of the SOM; types of a zonal nature are in the centre; and types with a trough to the east of the region are in the top right of the SOM. These patterns also include the clear seasonal trend in the location and intensity of the semi-

permanent Pacific and Indian Ocean high pressure systems that are associated with the Sub-tropical Ridge (STR). The degree of similarity between the nodes can be analyzed by using the Sammon mapping algorithm (Sammon, 1969; Cassano and Cassano, 2010). However, here the similarity can be identified intuitively from Fig. 3.12 as the small SOM size assigned (20 patterns in this case), and thus no further analysis is carried out. Further analysis would be necessary if the size of the SOM is quite large.

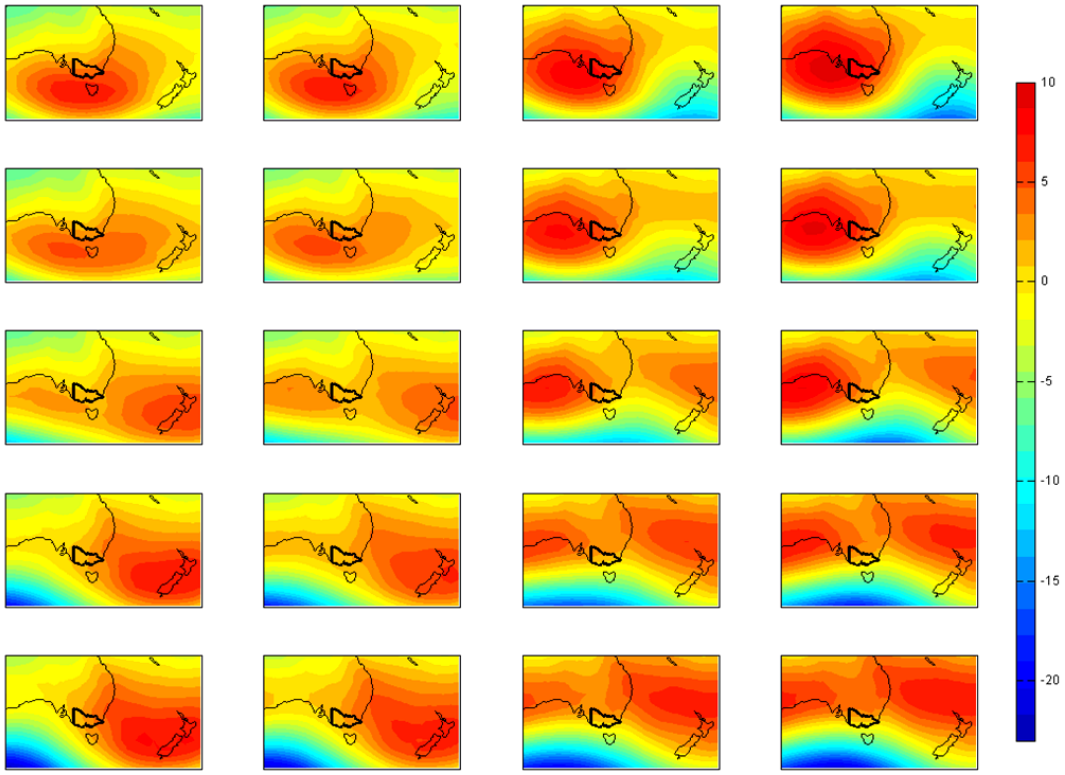

Fig. 3.12. Twenty key regional synoptic patterns were characterized using SOM (Unit of legend bar is hPa). Victoria is in bold outline.

The frequency of occurrence (*F*) of each SOM node is represented in Fig. 3.13. The frequency of each pattern is determined by mapping the daily-anomaly SLP data to the trained SOM. Nodes that have frequencies of occurrence significantly greater (less) than 1/20 or 5.0% (i.e. the node frequency that would occur if each node occurred equally) are highlighted by grey shading boxes. The figure shows that most of patterns are not significantly different from the expected frequency of 5.0%, indicating that the synoptic patterns attained by SOM are an even distribution across the whole training data. The most frequently occurring patterns are nodes (1, 4) and (3, 1), representing a strong high over southeast Australian continent and a blocking high over Tasman Sea respectively. Less frequent patterns are westward shifted weaker troughs at nodes (4, 2), (4, 3) and (4, 4).

Analysis of node frequencies on a seasonal basis provides further insight into the synoptic climatology of this region and how the occurrences of the synoptic patterns vary from season to season (Fig. 3.14). Each bar represents the node frequency of occurrence for each individual season. The *x*-axis gives the seasons and the *y*-axis the frequency of occurrence of each synoptic pattern. The most frequently occurring patterns during autumn (MAM) and spring (SON) are gradually northward shifted high pressure systems with gradually strengthened troughs in the Tasman Sea at the nodes (1,2), (1,3) and (1,4). The strong contrasts of the node frequencies occur between opposite seasons of winter (JJA) and summer (DJF). The most frequently occurring patterns during winter are strong high pressure systems over the Great Australian Bight, while the most frequently occurring patterns during summer are strong high pressure system over the Tasman Sea.

Due to the continuity of atmospheric motion, similar synoptic patterns can be found in each season. The difference of frequencies among patterns is more significant for the contrasting season of summer and winter than the bridging seasons of spring and autumn.

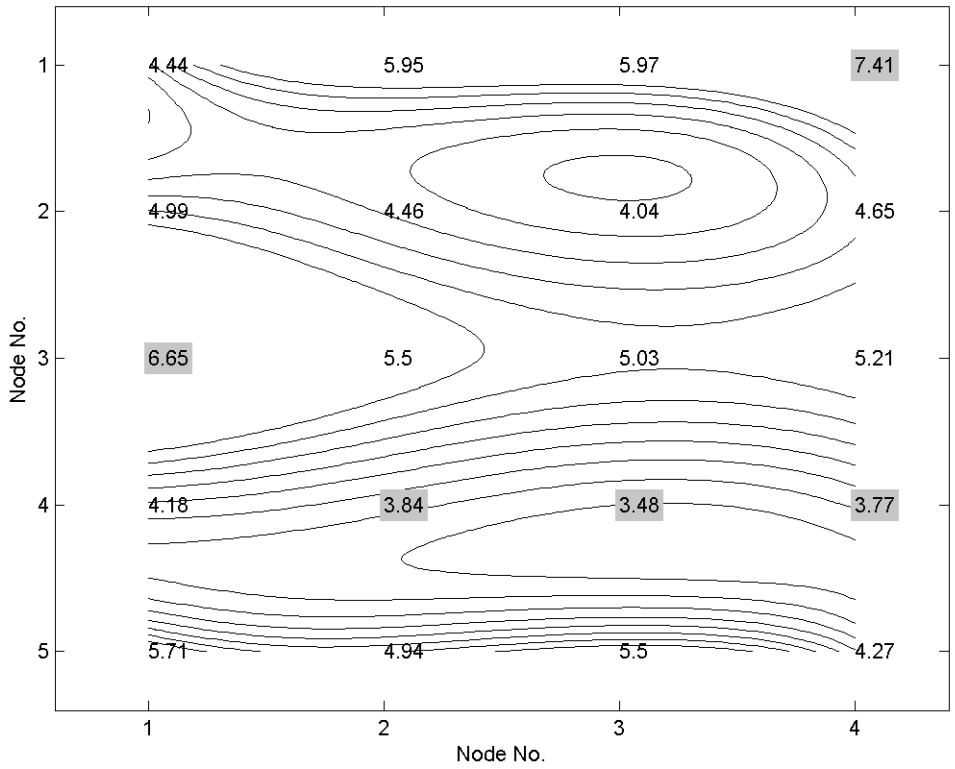

Fig. 3.13. Frequency of days that map to each SOM node annually. The grey shading indicates statistical significance as discussed in the text. Each number on the figure represents the percentage frequency of daily occurrence on an annual basis for that particular node.

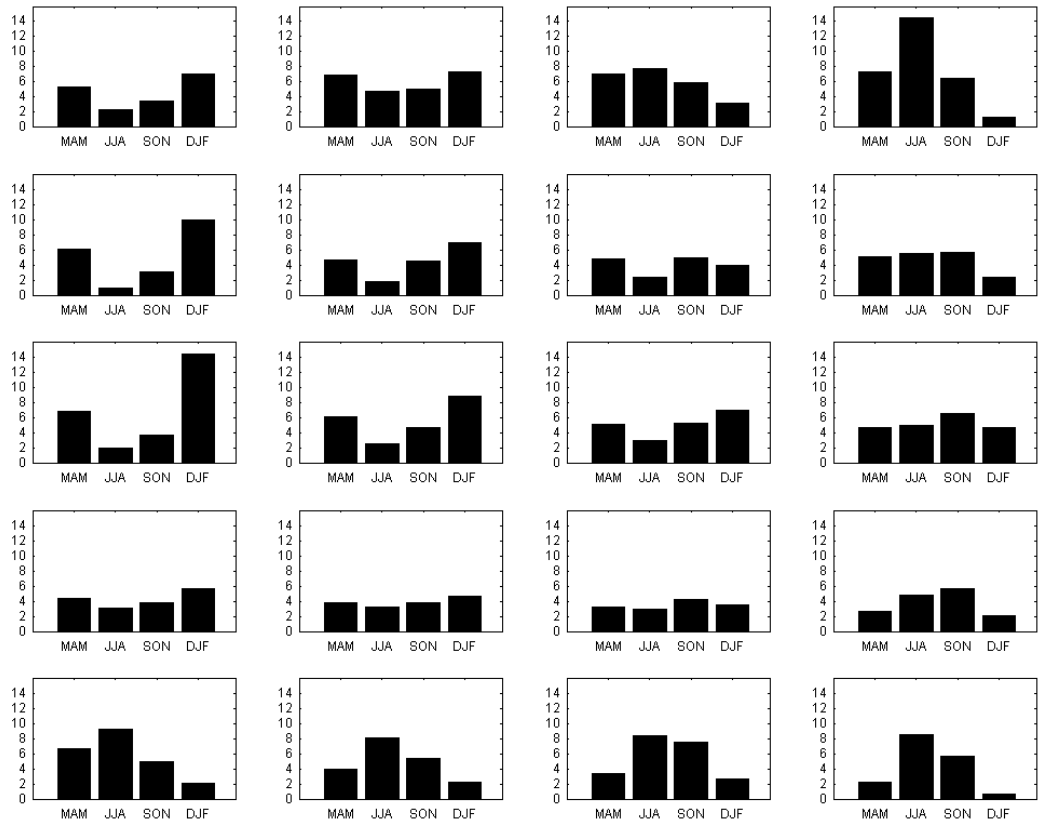

Fig. 3.14. Frequency of occurrence (%) that map to each SOM node seasonally. Each bar represents the percentage the pattern frequency in terms of daily occurrence. Each graph corresponds to a SOM node. The order is the same orientation as in Fig. 3.13.

3.3.4 Synoptic forcing of precipitation

3.3.4.1 General characteristics

The synoptic forcing for precipitation can be evaluated by mapping the observed daily precipitation data to each pattern of the SOM (e.g., Verdon-Kidd and Kiem, 2008; Cassano and Cassano, 2010). The value on each graph in Fig. 3.15 is a node mean precipitation across all grids of the Victoria region at a spatial resolution of $0.05^{o}\times0.05^{o}$. The first row shows the mean precipitation while the other panels display the mean precipitation for each season. The maximum daily precipitation values are always associated with the synoptic patterns from (3, 3) to (4, 4), which occur in JJA, MAM and SON. This is due to northward movement of high pressure systems and the presence of a pre-frontal trough (Tapper and hurry, 1996; Verdon-Kidd and Kiem, 2008). The synoptic patterns with the east coast trough characteristics (i.e., from (3, 1) through (4, 2)) also generate high precipitation. The low pressure trough deepens and moves towards the coast as the temperature rises. Stormy conditions often occur along the trough line during the

warmer months. This is due to the interaction with other low pressure troughs or cold fronts moving through southern Australia (Sturman and Tapper, 2004). When high pressure systems (e.g., pattern (1, 4)) or blocking highs (e.g., pattern (5, 1)) control the Victoria region, they generally produce less precipitation. However, if the high is associated with a cut-off low forming a blocking pattern, then affected areas could experience sustained heavy rainfall.

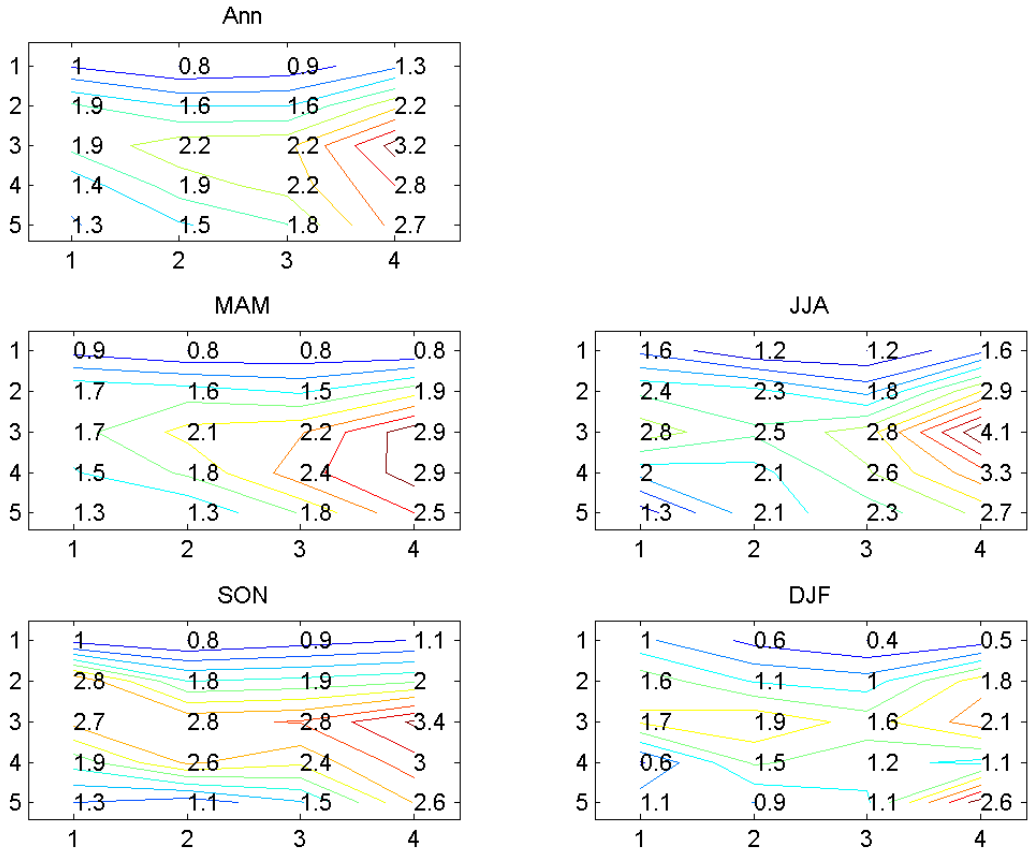

Fig. 3.15. Precipitation mapped to the SOM nodes at annual and seasonal scales. Each number on the figure represents the average daily precipitation in mm/day that occurs on an annual or seasonal basis for that particular node.

To understand the contribution of each SLP pattern to the total annual precipitation, it is necessary to simultaneously consider both the frequency and averaged daily precipitation for each node. This is because although a synoptic pattern may be associated with a large average daily precipitation, it would not contribute much to the annual total if that pattern did not occur frequently or *vice versa*. For each node in the SOM, its contribution to annual precipitation was calculated as $T = P \times F \times 365$ day/year where T is the node contribution to annual total precipitation, P is the average daily precipitation associated with that node (the first row in Fig. 3.15) and F is the frequency of occurrence of that node (Fig. 3.13). Here only the contribution of each synoptic pattern to the total annual

precipitation is calculated, however, similar analysis can be carried out for each season. The results are shown in Fig. 3.16. Higher contributions mainly occur in the middle of the figure in the landscape direction. These are associated with the synoptic patterns with easterly trough or northward high pressure systems plus a pre-frontal trough, which are the most important contributors to precipitation in the Victoria region. Moreover, these patterns do not have significantly higher or lower frequencies than the other patterns (Fig. 3.13). Therefore, higher contributions must be dominated by the node mean precipitation (Fig. 3.15). The pattern (1, 4) also makes a relatively high contribution to the annual total. The pattern is associated with the small node mean daily precipitation amounts (Fig. 3.15) but has a high frequency of occurrence (Fig. 3.13). For the pattern, the high frequency dominates its contribution to the total annual precipitation. For most of the synoptic patterns, their contributions mainly result from their node mean precipitation amounts, since their frequencies distributions do not have significant differences from the expected mean frequency value 5.0% (Fig. 3.13).

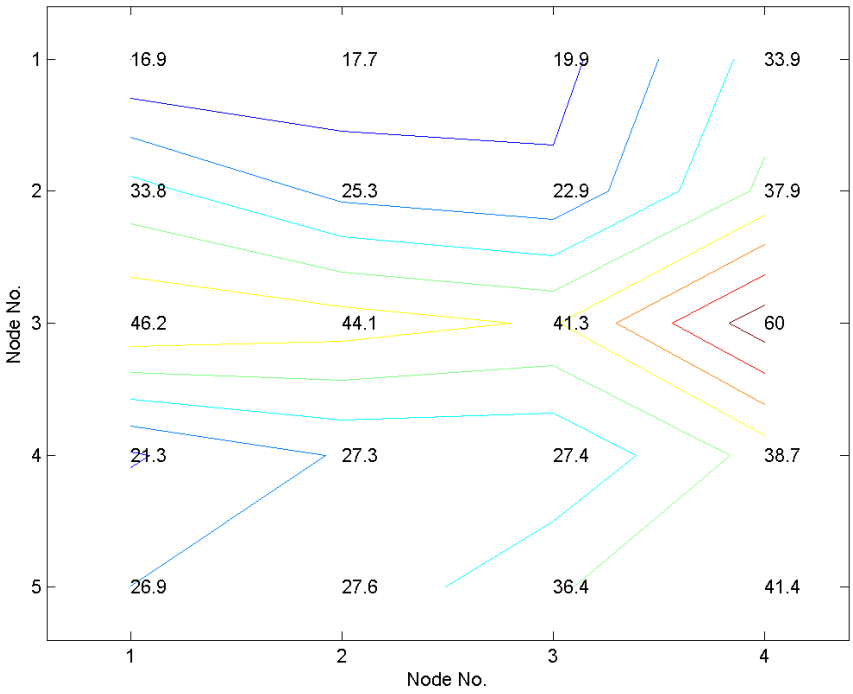

Fig. 3.16. Node contribution to Victorian mean annual precipitation (mm /year), where each number represents the node in the same position in the SOM (Fig. 3.12).

3.3.4.2 Details at a grid scale

The previous analysis considers the Victoria region as a whole. Further detailed analysis was carried out for grids covering the region (Fig. 3.17). After mapping gridded daily observed precipitation to the SOM, it was found that the same

synoptic pattern would generate different node mean precipitation intensities in different regions. Except for the wettest parts of the mountainous regions, precipitation generally decreases away from the coast for each synoptic pattern. However, the higher intensity of the node mean precipitation at each grid is still associated with the synoptic patterns with easterly trough or northward high pressure plus a pre-frontal trough, which is in agreement with the analysis in Fig. 3.15. Furthermore, the maximum daily mean precipitation amounts for these synoptic patterns mainly occur in the wettest parts of the mountainous regions. The high elevation must play an important role in producing the high precipitation by interacting with the synoptic patterns.

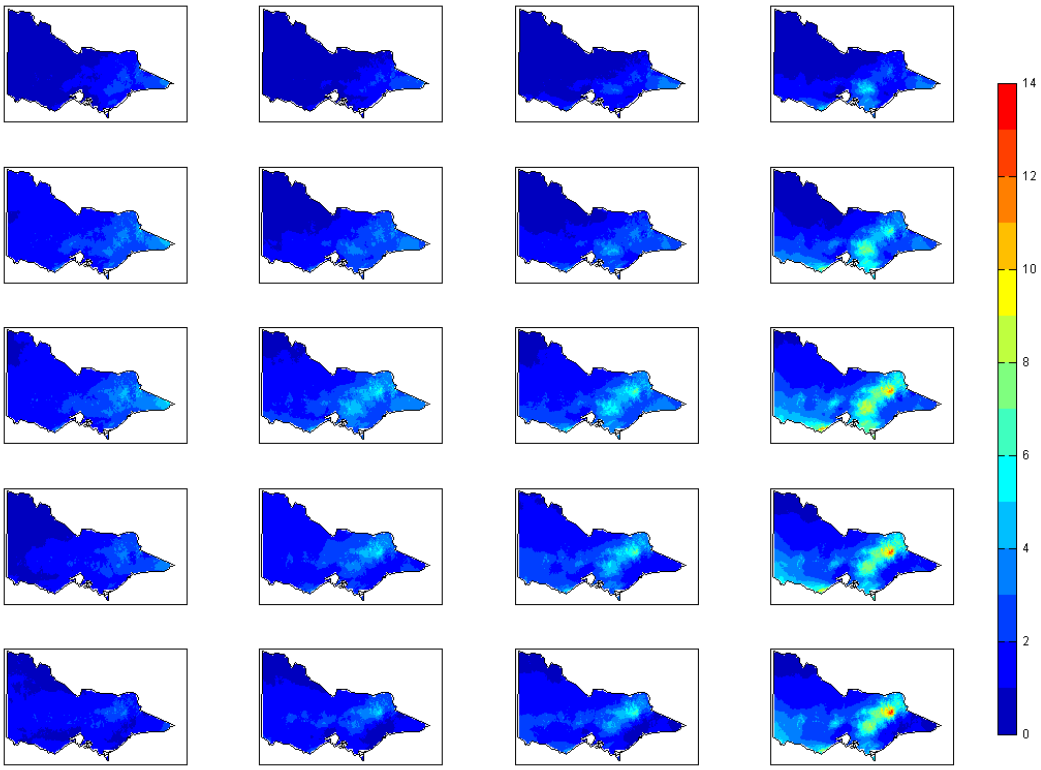

Fig. 3.17. Gridded daily precipitation mapped to the SOM (mm/day). The location of each graph corresponding to the same position in the SOM (Fig. 3.12).

For each synoptic pattern, the simple precipitation intensity on wet days (SDII) was also analyzed (Fig. 3.18). The SDII was calculated as $\mathrm{SDII} = \mathrm{NW}/\mathrm{NT}$, where the NW and NT are the rain total and rain days under each synoptic pattern. The synoptic patterns (2, 1) and (3, 1) generate high SDIIs over the whole Victoria region, while other patterns only produce high SDIIs in some local areas. The easterly trough in pattern (2, 1) can penetrate into the Victoria region more deeply

than other similar patterns such as pattern (3, 2). As a result, it can have an impact on wider areas.

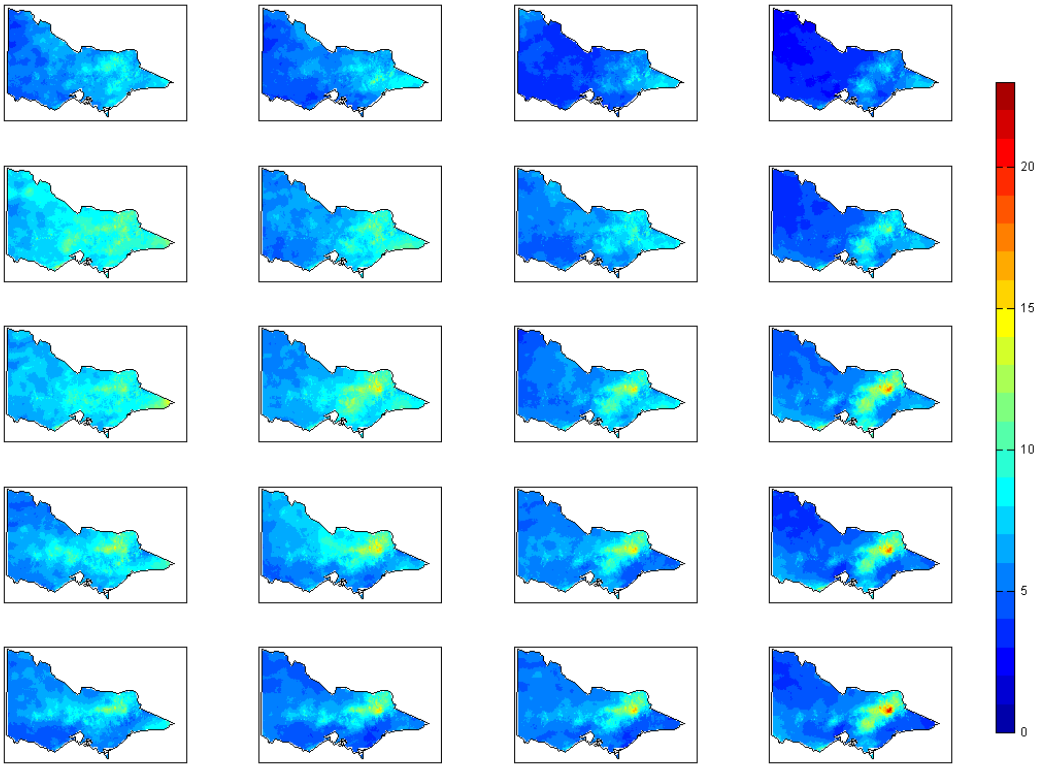

Fig. 3.18. Simple daily precipitation intensity on wet days (SDII) in each synoptic pattern. The location of each graph corresponding to the same position in the SOM (Fig. 3.12).

An additional analysis was performed to determine which of the synoptic patterns identified by the SOM were associated with the heavy and extreme precipitation events. An extreme precipitation is defined as daily precipitation greater than the 99th percentile value of the long-term series of daily precipitation from 1961 to 2000 (see section 3.2.2 for more information). The results are shown in Fig. 3.19 and Fig. 3.20. The figures demonstrate that different synoptic patterns would have different abilities to produce heavy and extreme events. Synoptic patterns with an easterly trough extending more deeply into Victoria and with a stronger pre-frontal trough passing the east coast have strong relationship with heavy and extreme precipitation at wide areas, which are at the middle of the SOM in the landscape direction. However, the maximum heavy precipitation frequency occurs in the pattern (3, 4) (Fig. 3.19), while the maximum extreme precipitation frequency takes place in the pattern (3, 1) (Fig. 3.20). For other synoptic patterns, heavy and extreme precipitation occurs in much localized areas (Figs. 3.19-3.20).

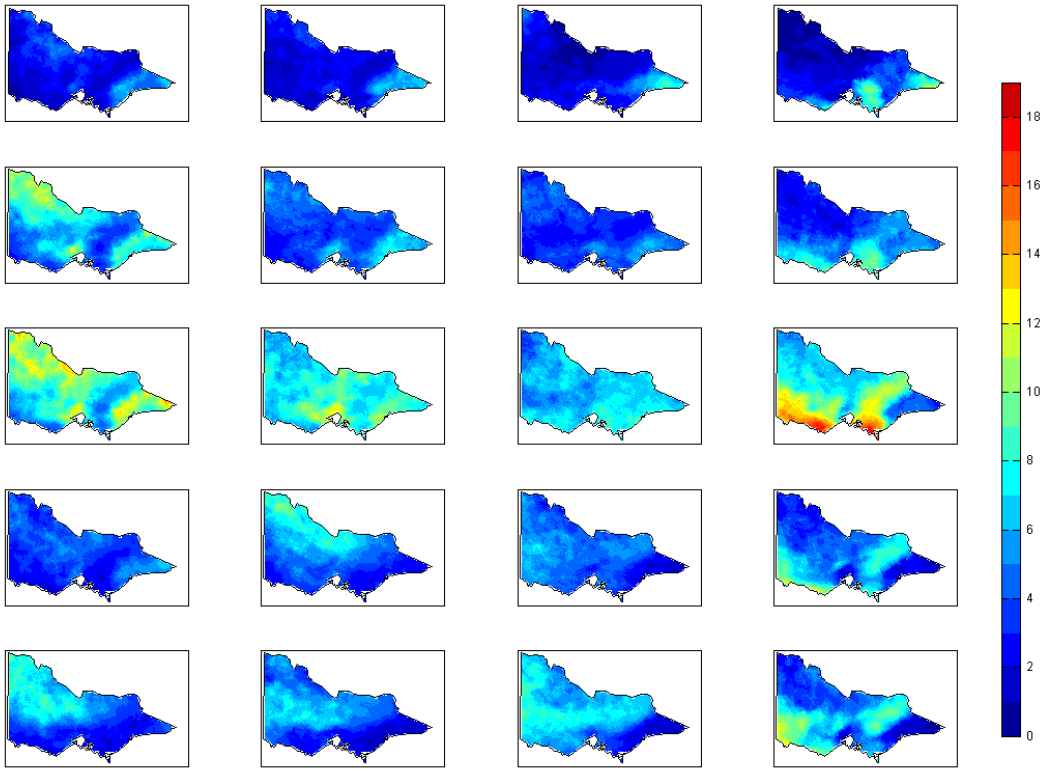

Fig. 3.19. As Fig. 3.18 but for heavy precipitation (P>10.0mm) days.

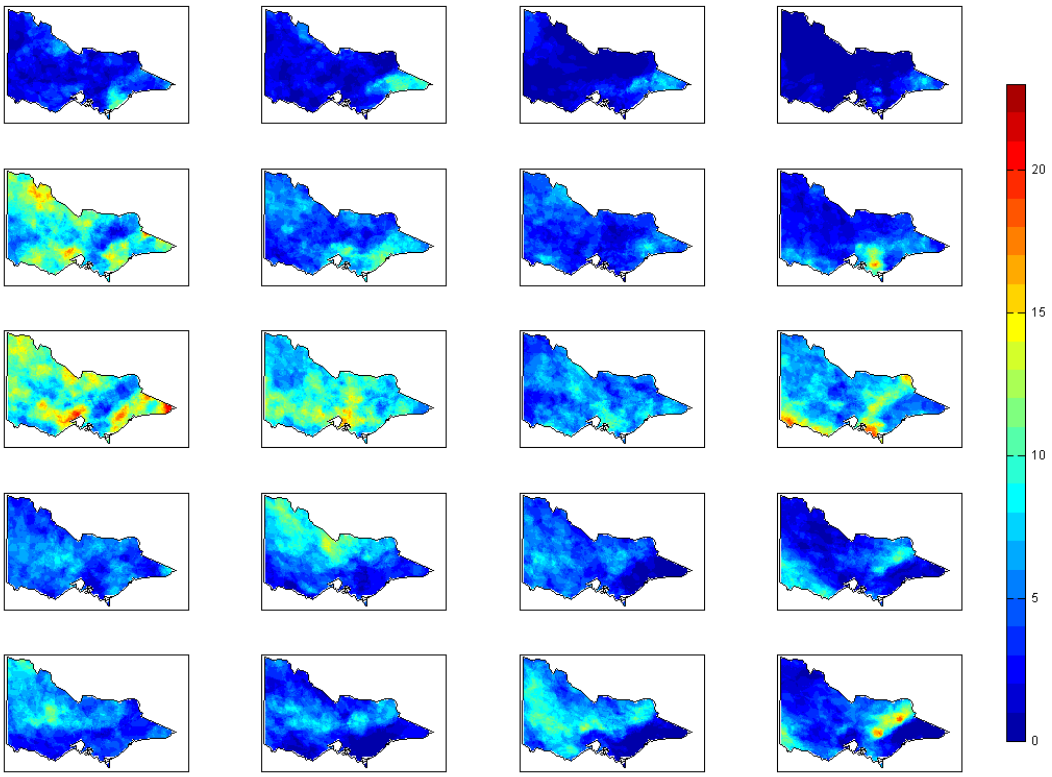

Fig. 3.20. As Fig. 3.18 but for extreme precipitation (99th percentile) days.

3.4 Conclusion and discussion

This chapter introduced the basic concept of synoptic climatology, and self organizing maps (SOM) and its advance in synoptic climatology applications. The remainder of this chapter explored the relationship between large-scale synoptic patterns and precipitation for the Victoria region in Australia based on the theory of synoptic climatology and SOM. The first step in this process was to create a classification of synoptic patterns over the Victoria region and adjacent regions by using SLP daily-anomalies from the NNR reanalysis dataset.

This analysis identified a range of significant synoptic features that influence the climate of the region and illustrated the shift of the dominant synoptic patterns throughout the seasons. These include a clear seasonal difference in the location and intensity of the semi-permanent Pacific and Indian Ocean high pressure systems that are associated with the Sub-tropical Ridge (STR) and the variation in the strength and location of the east coast trough located between the two semi-permanent high pressure systems.

Each pattern identified by the SOM was then related to precipitation. The spatial distribution of precipitation was clearly tied to the synoptic patterns. The relationship between the synoptic patterns and precipitation in the Victoria region was then further explored based on the characteristics such as rainfall frequency and intensity, which are essential for understanding and predicting the response of rainfall to climate change (e.g. Trenberth et al. 2003; Brown et al., 2010). The results show that different synoptic patterns generate different precipitation characteristics due to the shift in intensities and locations of the dominant synoptic patterns throughout the seasons. Patterns with a stronger easterly trough or a pre-frontal trough generate more precipitation than other patterns, resulting in a heavy and/or extreme precipitation. In other words, the synoptic patterns attained by the SOM can very well describe different precipitation regimes. For example, in the wettest parts of the mountainous regions (left panel of Fig. 3.7), the interaction between synoptic pattern and high elevation would have a stronger impact on local precipitation than in other regions. In this chapter, only SLP was used to identify major synoptic patterns of precipitation, as in other studies (Verdon-Kidd and Kiem, 2008; Cassano and Cassano, 2010; Brown et al., 2010). However, some studies suggested that adding more precipitation-relevant climate variables,

such as humidity, should depict the large-scale precipitation regimes more accurately (e.g., Cassano and Cassano, 2010; Yang et al., 2010). This issue is further explored in the following chapters related to downscaling daily precipitation.

The methodology used here identifies well the regionally-specific climate drivers, which provides confidence in application of the method to other synoptic climatology analyses, especially for assessing the performance of GCM outputs and statistical downscaling.

CHAPTER FOUR

STATISTICAL DOWNSCALING OF DAILY PRECIPITATION BASED ON REANALYSIS DATA

4.1 Introduction

The statistical downscaling model (SDSM) has been considered as an important tool to bridge the gap between GCM or RCM outputs and local-scale climate required to assess climate change impacts (Maraun et al., 2010). The basic idea behind SDSM is to relate synoptic climatology to local climate variables (Klein and Glahn, 1974; von Storch, 1999). In the simplest form, the basic idea of SDSM can be formulated as:

$$Y = F(X, \beta) + \epsilon \qquad (4.1)$$

where Y is the local-scale predictand, X is the large- (or larger-) scale predictors, β represents unknown parameters of the transfer function F between X and Y that must be estimated to calibrate the F, and ε is the uncertainty (error) term (van Storch et al. 2000; Fowler et al. 2007). Earlier SDSMs do not take the ε into consideration, and are therefore also called deterministic models. However, more and more SDSMs now explicitly model the variability that is not explained by the dependence of Y upon X, i.e., the ε, and these models are generally called stochastic models (Maraun et al., 2010).

The work presented in Chapter 3 showed that there was a good relationship between large-scale atmospheric circulation patterns and local precipitation regimes. The relationship is further explored in this chapter to construct a SDSM over southeast Australia. The SDSM is directly based on the synoptic climatology theory, and was named SOM-SD because the self-organizing maps (SOM) algorithm is used for synoptic classification. The SOM algorithm has some specific advantageous characteristics in its application to synoptic climatology (See Chapter 3; Hewitson and Crane, 2006). Furthermore, for a specific atmospheric state, an ensemble of possible values is generated for the

precipitation through a stochastic resampling scheme. Thus, the SOM-SD combines elements of deterministic transfer functions and stochastic components following the recommendation of IPCC AR4 on the most effective SDSMs (Christensen and Hewitson, 2007, Maraun et al., 2010). In addition, this chapter also discusses how to select predictors and assessment indices, which are important steps in constructing a downscaling model.

4.2 Study area and data

The region that including states of New South Wales (NSW) and Victoria (VIC) of Australia was taken as the case study area (Fig. 2.1). As described in chapter 2, the region has a wide variety of climatic conditions and highly diverse landscape ranges, which make it an ideal place for assessing the performance of various downscaling methods. To investigate the applicability of the SOM-SD, the region is divided into 9 climatic zones according to Hutchinson et al. (2005).

The predictand or the dependant variable is daily precipitation for the period from 1958 to 2008. These data are high-quality gridded data at a spatial resolution of 0.05°. The large-scale predictors used are from the NNR data (Kalnay et al., 1996; Kistler et al., 2001), which consist of mean sea-level pressure (SLP), specific humidity (Q), zonal wind (U), meridional wind (V), surface air temperature (T), and precipitation rate (Pr) (See Table 2.3 in Chapter 2 for more information).

The full dataset of the predictors and predictand for 1958-2008 was split into two independent intervals: a calibration period also called training period, and a validation period. The calibration period was 30 years from 1958 to 1987, and the validation period was 21 years from 1988 to 2008. The SOM-SD was trained and validated independently. For each downscaling target grid, the large-scale predictors are standardized according to Eq. 2.1. Furthermore, the means and standard deviations of the spatial domain during the calibration period were used in standardizing the corresponding predictors in the validation period. The spatial domain of large-scale atmospheric predictors is 3×3 spatial grids (resolution 2.5×2.5 degrees) whose central point is right over the downscaling target grid.

The precipitation downscaling was carried out at 0.25°×0.25° resolution, which is sufficient to investigate the applicability of the novel downscaling method across different climatic zones and orographic features.

4.3 Methodology

4.3.1 The downscaling method

There are three principal steps in constructing the SOM-SD. Firstly, a *training* process employed the SOM algorithm to identify all possible synoptic patterns around the target grid (i.e., creating a SOM) using the large-scale predictors. Secondly, the predictand data were *mapped* to the obtained SOM and a set of corresponding predictands-candidate-data-bank (PCDB) was constructed related to each synoptic pattern (also referred to as a SOM node); and finally *downscaling* was achieved by extracting predictand values from the relevant PCDB based on the predictors by matching them to a particular synoptic pattern in the trained SOM.

The three steps are discussed in detail below. For simplicity, only one precipitation grid is taken as an example to describe the downscaling procedure. Similar methodology can be applied to other precipitation grids.

4.3.1.1 SOM and Synoptic Classification (Training)

The training procedure is a standard process for the SOM algorithm that has been described in detail in Chapter 2. In brief, the SOM algorithm employs a neural network technique that uses unsupervised competitive learning procedure to determine generalized patterns or characteristics in input data. This algorithm groups or clusters similar data records together and organizes them into a two-dimensional array, referred to as a map.

The large-scale NNR predictors surrounding the target grid are inputted to the SOM training procedure. After training (see section 3.2.2.1), the final SOM is acquired on a two-dimensional rectangular grid. Here a spatial domain of 5×7 grids is used, since a SOM with this size has been found suitable for synoptic climatology studies (e.g., Hewitson and Crane, 2002; Cassano et al., 2006; Lynch et al., 2006). Certainly, a SOM with a different size can be used such as 5×5 and 9×9, which is further discussed in the following section. As a consequence of training, for the target grid a unique set of possible synoptic states described by their own spatially coincident localized synoptic climatology was created.

It should point out that the SOM was a kind of unsupervised learning algorithm

(see Chapter 3). That is to say, the learning procedure did not take the precipitation into account at all. Thus, an equal weight was given to each predictor to identify synoptic patterns in the training data, which was a typical synoptic climatologic application.

4.3.1.2 On the relationship between regional synoptic patterns and grid predictands (mapping)

Once the training process is completed, the relationship between the set of synoptic patterns and the predictand (precipitation) can subsequently be constructed for the target grid. For a given day in the calibration period, the atmospheric predictors on the day were compared with each synoptic pattern based on the Euclidean distance. A total of 35 distances were attained using a SOM with 5×7 nodes. The best matching synoptic pattern was obtained by finding the minimum distance among them. This pattern is generally called the *nearest neighbor* to the input sample in the analog-like downscaling method (e.g., Zorita and von Storch, 1999; Timbal and McAvaney, 2001; Wetterhall et al., 2005).

Then the predictand value (precipitation) on that day was mapped to the best matching synoptic pattern (i.e. SOM node). In this way, the procedure was repeated throughout the calibration period. Thus for the target grid, the atmospheric predictor variables on each day were uniquely mapped to one of the trained 35 synoptic patterns, so that there was an independent subset of predictand values under each synoptic pattern. Each subset was called a predictands-candidate-data-bank (PCDB) for the corresponding synoptic pattern. Up to now, the relationship between the predictand and the predictors was built with the target grid being described by 35 different PCDBs related to the 35 generalized synoptic patterns. These two steps are a standard synoptic climatology analysis procedure (see Chapter 3), which has been shown to be an effective tool for studying synoptic forcing of regional precipitation (Cassano et al., 2006; Nishiyama et al., 2007; Schuenemann et al., 2009).

4.3.1.3 Downscaling-validation

The NNR data in the validation period (1988-2008) was used to assess the accuracy of the downscaling model. For the target downscaling grid, the predictor variables are compared with the trained synoptic patterns day by day of validation

period, and find best matching synoptic patterns (BMSPs) for each day. The comparison was again carried out using the Euclidian distance (Toch, 1991). Through the BMSP, the predictors on each day were linked to the corresponding predictands-candidate-data-bank (PCDB) generated in the earlier mapping process. Thus, the precipitation value associated with the predictors on a particular day can be estimated through the PCDB determined by the BMSP (e.g., Bensmail et al., 1997). There are two ways to determinate a precipitation value: using the mean value of the PCDB (e.g., Gutiérrez et al., 2005) or stochastically re-sampling a value from the PCDB. The former is a deterministic approach by ignoring the intra-pattern variability, while the latter follows a stochastic approach including explicitly the climate variability that cannot be explained by SDSM. Though the stochastic approach has the advantage of including the variability in its model structure, its resampling scheme still has potential limitations (e.g., Young, 1994; Yates et al., 2003; Beersma and Buishand, 2003). For example, it does not produce precipitation amounts that have not been observed in the past, which is a universal issue for analog-like SDSMs (e.g., Wetterhall et al., 2005; Timbal et al., 2009). Here, the re-sampling index (where on the PCDB the predictive value should be read) is determined according to the conditional probability density distribution developed by Lall and Sharma (1996). This distribution is:

$$p(i) = \frac{1/i}{\sum_{j=1}^{k} 1/j} \qquad (4.2)$$

where $p(i)$ is the probability that the ith index will be re-sampled, and k is the total number of precipitation values in the corresponding PCDB. This procedure was repeated 500 times so that 500 time series data were produced and each had the equal length of the test data (larger resampling times are recommended but require more computing time). Such Monte Carlo simulations are valuable to generate probability distributions for the change in the precipitation indices under climate-change conditions and these would be of great benefit to constructing probabilistic scenarios of extremes (Haylock et al., 2006). A complete schematic of SOM-SD is shown in Fig. 4.1.

For stochastically resampling of the precipitation values, some studies suggested fitting each PCDB to some theoretical distributions such as two-parameter gamma distribution (e.g., Aksoy, 2000), Log-Logistic Distribution (e.g., Shouki et al.,

1988) and exponential distribution (e.g., Madi and Raqab, 2007), and then determining the resampling location on these distributions according to Eq. 4.2, which becomes a typical weather generator procedure (e.g., Richardson and Wright, 1984; Semenov and Barrow, 1997). However, a single theoretical distribution does not always work well (Vlček and Huth, 2009), particularly for regions with very complicated climate types and orographic features such as the case study area in this study. Therefore, only the empirical distribution (i.e., sorted arrays of observations) was used here. However, a theoretical distribution, such as two-parameter gamma distribution (e.g., Aksoy, 2000), is useful if the downscaling is carried out at a single grid or station. It also has the big advantage of generating new precipitation values, which are not observed historically, because the sampling procedure is implemented on a theoretical distribution function, rather than from the historical observed data set.

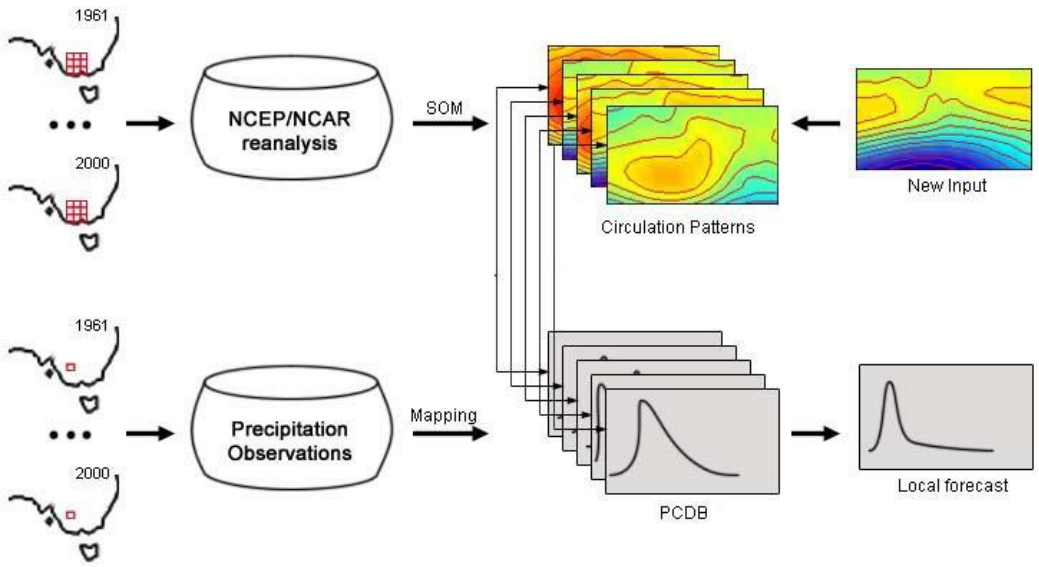

Fig. 4.1. Downscaling schematic of SOM-SD (including 3 steps).

4.3.2 Accuracy of the downscaling method

Up to now, there is still no consensus on how to assess the accuracy of downscaling methods. To a certain extent, it is due to the fact that there is no single SDSM that can perform well on all aspects of downscaled local predictands, especially for precipitation. Moreover, many SDSMs are assessed only from the perspective of climatological studies. Very few downscaling studies consider their use in other area such as climate change impact studies, and they seldom provide

any help to impact study community how to select an appropriate downscaling model partly due to the high uncertainty involved in the downscaling process. As described in Chapter 1, there is a gap between SDSMs and climate change impact analyses. This study tried to fill such a gap by collecting the assessment indices of interest for both fields of SMSD and impact studies.

Climate change can have impacts on all sectors at various levels of society, especially for those economies with greater dependence on climate-sensitive sectors, such as agriculture (e.g., Ines et al., 2006; Lobell, 2007, 2008), infrastructure (e.g., Wilbanks et al., 2007; Newton, 2009; Norena et al., 2009), and coastal zones (e.g., Dawson et al., 2009; El-Nahry and Doluschitz, 2010). The majority of these impact analyses requires that the SDSM used can not capture one or more of the following commonly-observed weather features (1) general performance (e.g., mean and bias), (2) distributions (e.g., variance and quantiles), (3) time series (e.g., correlation, wet/dry-day persistence, and forecast ability). The above three metrics capture a large portion of the information required for impact assessments. Each of the above metrics could evolve into more specific indices for particular impact studies. However, given the vast range of impact analyses that rely on climate projections, it is impossible to synthesize and list all of them here.

The intercomparison of different downscaling methods is a continuous process. For example, the STARDEX project provided a large intercomparison of statistical downscaling methods to date involving 22 downscaling methods over Europe (Goodess et al., 2010; http://www.cru.uea.ac.uk/cru/projects/stardex/). As a result, more and more statistical tests are used in common to evaluate the performance of downscaling methods. Taking the STARDEX project as an example, its statistical tests have been widely used in the latest downscaling studies (e.g., Chu et al., 2010; Hayhoe, 2010; Maraun et al., 2010). Among these studies, relevant tests can be grouped into four categories: climatological means and biases; correlations; distribution functions, thresholds and quantiles; and wet/dry-day persistence.

To develop a concise set of statistical tests, only those that are mostly concerned in both downscaling and impact studies should be selected. In addition, the performance of the downscaling method should be assessed in a seasonally

stratified style to ensure that the model is capable of capturing both the annual and seasonal variability of precipitation.

Table 4.1. summarizes the applied indices for daily precipitation. The indices represent the statistics of daily precipitation with regard to precipitation amount (SDII, ppSD, RMSE and pSSNSD), variance (ppSD and pSSNSD) and frequency (nr001, nr020, nr200, Pww and Pdd), and extreme event (P95, P95T, CWD and CDD), as well as prediction accuracy (PCF and CSI). Other statistics, such as 50 or 100 year return levels for extreme precipitation intensities (e.g., Katz et al., 2002; Naveau et al., 2005), could also be developed since the SOM-SD can generate the full time series (daily data for the length of record being used). Here, a threshold for a wet day is defined as a day with daily rainfall greater than or equal to 0.1 mm.

Table 4.1. Diagnostics of daily precipitation.

Acronym	***Definition***	***Unit***
SDII	Simple daily intensity(mean daily precipitation on wet days)	mm/day
ppSD	Standard deviation of daily precipitation on wet days	mm/day
RMSE	Root mean square error of daily precipitation time series	mm/day
nr001	Mean number of rainy days for daily precipitation >=0.1mm	Day
nr020	Mean number of rainy days for daily precipitation >=2.0mm	Day
nr200	Mean number of rainy days for daily precipitation >=20.0mm	Day
pSSNSD	Standard deviation of season precipitation	mm/season
P95	95-th percentile value of precipitation (extreme precipitation)	mm/day
P95T	Percentage of rainfall from events beyond the 95-th percentile value of overall precipitation	%
Pww	Mean wet persistence	%
Pdd	Mean dry persistence	%
CWD	Maximum consecutive wet days	Day
CDD	Maximum consecutive dry days	Day
PFC	Percentage of Forecast Correct	%
CSI	Critical Success Index	%

The inter-annual variability is analyzed through the Spearman rank correlation (RC; Corder and Foreman, 2009) between indices calculated from the observed and downscaled daily precipitation time series. Such a statistical test is of particularly importance because it indicates whether the method can reproduce correctly the predictor-predictand relationships by assessing if the inter-annual variability has been successfully captured by a model. The non-parametric unbiased estimation of RC was employed instead of the Pearson correlation in order to minimize the effect of outliers from the possibly non-Gaussian distributed variables. The term 'correlation' from now on will refer to the Spearman rank correlation. In addition, a non-parametric goodness-of-fit test was applied to compare the cumulative distribution function (CDF) of observed and downscaled daily precipitation time series.

4.3.3 Uncertainty analysis

A SDSM's ability to represent the baseline (present-day) climate is a necessary condition for use in downscaling GCM outputs from the scenarios runs, but it is not a sufficient condition. Another measure of the "goodness" of a SDSM in reproducing the observed meteorological variables is the uncertainty analysis (Castrup, 1995). One complementary method has been employed to analyze the uncertainty of the output of the statistical downscaling model, namely confidence intervals (Khan et al., 2006; Dibike et al., 2008). A confidence interval is a measure of uncertainty regarding the true value of a statistics or estimate.

The non-parametric technique known as Bootstrapping simulation (Efron and Tibshirani, 1993; Davison and Hinkely, 2006) is employed to the observed time series and the corresponding ensemble of 500 simulations generated by the SOM-SD to estimate the confidence intervals of the ensemble means and variances for the above indices (Khan et al., 2006; Dibike et al., 2008). One thousand statistics are calculated from the bootstrapping samples (i.e., corresponding to the 500 simulations) and 90% confidence interval (5th percentile for the lower confidence limit and 95th percentile for the upper confidence limit) is selected. Without specification, only the ensemble means are used to compare with the observed values.

4.4 SOM-SD application to Southeast Australia

4.4.1 Additional parameters

To make an objective downscaling, the SOM-SD should not use any tunable parameters. However, there are still two particularly important parameters that are required to be predefined and assessed before carrying out downscaling:

- The size of the geographical domain used for the large scale predictors (latitude and longitude) in order to achieve the best performance in downscaling local climate variables (e.g. Wilby et al., 2004; Maraun et al., 2010). The domain size may vary by region and selected SDSM. For example, Hidalgo et al. (2008) took the whole USA continent as the downscaling domain while Chu et al. (2010) only took one spatial grid as the domain in the Haihe River Basin in northern China. In this present study, 4 domain sizes were tested (i.e., 3×3, 5×5, 9×9 and 11×13 spatial grids). The last size is the one presented in Chapter 3 to investigate the applicability of the SOM algorithm for analyzing large-scale synoptic forcing of local precipitation over the Victoria region.

- The number of synoptic patterns or SOM nodes. There is no consensus on how many nodes (patterns) that should be used for SOM training. As a general rule, a large size presents more detail in the pattern differentiations, while smaller arrays produce greater generalization - but the underlying structure remains the same (e.g. Hewitson and Crane, 2002, 2006; Crane and Hewitson, 2003). In this study, three options were chosen and tested: 4×5, 5×7 and 9×11. These 3 sizes also were used for the SOM application in synoptic climatology in the previous studies (e.g., Hope, 2006; Hope and Nicholls, 2006; Cassano and Cassano, 2010; Hewitson and Crane, 2006).

Test results revealed that increasing the size of the spatial domain for each target downscaling grid did not always improve the downscaled results for the whole case study area, compared with the most basic size of 3×3. The results became better in some regions but worse in others. Therefore, the basic size of 3×3 was used. The basic number of synoptic patterns of 35 (i.e., 5×7) is chosen in that the

increase of the number of synoptic patterns around each downscaling grid showed a similar skill. In addition, the risk of generating pseudo synoptic patterns, i.e., patterns do not occur in the training data, will become high with increase in the number of synoptic patterns (Hewitson and Crane, 2006). The size of the spatial domain and the number of synoptic patterns were setup according to the comprehensive performance of the SOM-SD for the whole case study area, not for a specific grid. In fact, there is actually an optimum setting up for each target downscaling grid. Taking the number of synoptic patterns as an example, a larger number (more than 35) should be used to a grid located in regions with complicated climate conditions, while a smaller number (less than 35) should be used to a grid located in regions with relatively homogeneous climate conditions. The optimized number can be acquired by an iteration procedure until the SOM training cannot find any further significant different synoptic patterns. If a site-based impact study is carried out, such as a crop simulation, an optimal setting up should certainly be used. In this study, a common setting up of 3×3 grids and 35 synoptic patterns appeared acceptable for most the climatic zones.

4.4.2 Selection of predictors

The selection of appropriate predictors is crucial when developing a statistical downscaling model (Hewitson and Crane, 1996; Brinkmann, 2002; Wilby et al., 2004; Cavazos and Hewitson, 2005; Maraun et al., 2010). The choice of predictors could vary from region to region depending on the characteristics of the large-scale atmospheric circulation and the predictand under consideration (Fowler et al., 2007; Anandhi et al., 2008; Maraun et al., 2010). Any variable can be used as predictor as long as it has a reasonable relationship to the predictand (Wetterhall et al., 2005).

In general, three basic criteria have been widely accepted in selecting predictors for statistical downscaling (e.g., Giorgi et al., 2001; Benestad et al., 2008): (1) the selected predictors are reliably represented by GCMs; (2) they have physically interpretable relationship to the predictand; i.e., they (alone or combined) are able to account for most of the observed variations in the predictand and the statistical relationships are temporally stationary; (3) they should "carry the climate change signal" when applied to a changing climate.

This study followed these criteria for predictor selection. In practice, the selection was guided by an exhaustive search procedure combined with "expert" knowledge (Wilby et al., 2004). Precipitation over southeast Australia is dependent the advection of water from the surrounding ocean and thermodynamic effects of moisture and temperature which modify the local vertical static stability. Also took into account were the previous studies in Australia (Timbal and McAvaney, 2003; Timbal et at., 2009) and other studies in similar areas (Charles et al., 1999, 2003, 2004). Based on these "expert" knowledge, all possible combinations among the potential predictors (listed in Table 2.3) were exhausted, where Q at each level and Pr or their combinations were always included due to their strong relationship to precipitation. Then these combinations were built into downscaling models and their performances were assessed according to the diagnostics indices in Table 4.1. To a great extent, the procedure of selecting predictors is equivalent to construct downscaling models.

During the exhaustive search process, it was found that SLP was the most stable predictor. Its downscaling skill did not show significant spatial difference across the whole case study area. However, a model that just uses SLP would only reproduce a small proportion of variance of the observed precipitation data with low variability. SLP is a critical predictor for a synoptically driven technique such as the analogue approach, but it did not appear to be a useful predictor if none of the other available predictors is selected to compensate its lack of skill. A model using Q as predictor always outperformed models without Q in reproducing variability. In addition, thermal predictors of temperature could improve the skill in generating a high variance. When measures of air flow, either the zonal (u) or meridional (v) component of the wind, were used, a model showed obvious spatial differences with significant improvements in the coastal regions but worse performances in the inland regions; hence they were location-specific predictors and were not suitable for the whole case study area.

The exhaustive search revealed that the combinations among SLP, Q5, Q7 and T8, T7, T0 usually had similar and stable performances in terms of the assessment indicators (Table 4.1) across the whole study area. However, they would still produce a relatively poor skill in the rank correlation. When Pr was added as another predictor, there was a significant improvement in modeling the inter-annual variability.

Finally, these predictors (i.e., SLP, Q5, Q7, T0, T7 and T8) were compared with their GCM counterparts to validate that they were reliably reproduced by GCMs. The comparison method was described in details in the section 4.3.1 of Chapter 7. The comparison analysis showed that only the combination of SLP, Q5, T7 and Pr were acceptable as the common predictors for all GCMs and for all of climatic zones (Fig. 2.2).

It is worth noting that the combination does not mean an optimal combination for each individual climatic zone, but rather provided a relatively consistent performance across the study area. On the other hand, a single combination of predictors could not always produce superior results for all diagnostics indices used. Hence a trade-off between the importance of the various predictors and their role in generating precipitation needed to take into account. In this study, the predictors that could improve the indices of precipitation variance and variability were preferred, as it was believed that the ability of a downscaling model in producing high reliable precipitation variance and variability was more important than producing good means for hydrological simulations. t The secondary importance was given to the cumulative distribution of frequency (CDF), i.e., the CDF of observed and downscaled daily precipitation on wet days should be similar to each other (See 4.4.3.1).

This predictor selection method was also applied to temperature downscaling (Chapter 7).

4.4.3 Validation of SOM-SD

4.4.3.1 Precipitation amount

Based on the parameters obtained by using the above predictors and observed precipitation over the calibration period 1958–1987, precipitation for each downscaling grid for the validation period 1988 – 2008 was simulated to test the quality of the model. The ability to reproduce probability distribution functions (PDFs) of observed daily precipitation on wet days was evaluated by the first two moments of the PDFs: the daily mean precipitation (SDII) and the standard deviation (ppSD).

SDII is generally well reproduced by the downscaling method, as shown in Fig.

4.2. The first row of the figure displays the observed SDII in each season while the second row represents the difference between downscaled and observed SDII. The downscaled SDII was computed as the ensemble mean for 500 runs at each grid. SDII shows similar spatial patterns in the 2 transition seasons of spring and autumn and different patterns in summer and winter. The high SDII occurs for the grids located in the northern region in summer, but for the grids in the southeastern region in winter. The high elevation also plays an important role in generating high precipitation in the snowy mountainous region in Victoria. The second row of the figure demonstrates a close match in both magnitude and spatial distribution between the observed and the downscaled SDII. The differences between the observed and downscaled SDIIs are negligible with a range between -1.0 and 1.0mm in most of the grids for all seasons. Obvious discrepancies mainly occur in the northeast region on the left side of the GDR in winter.

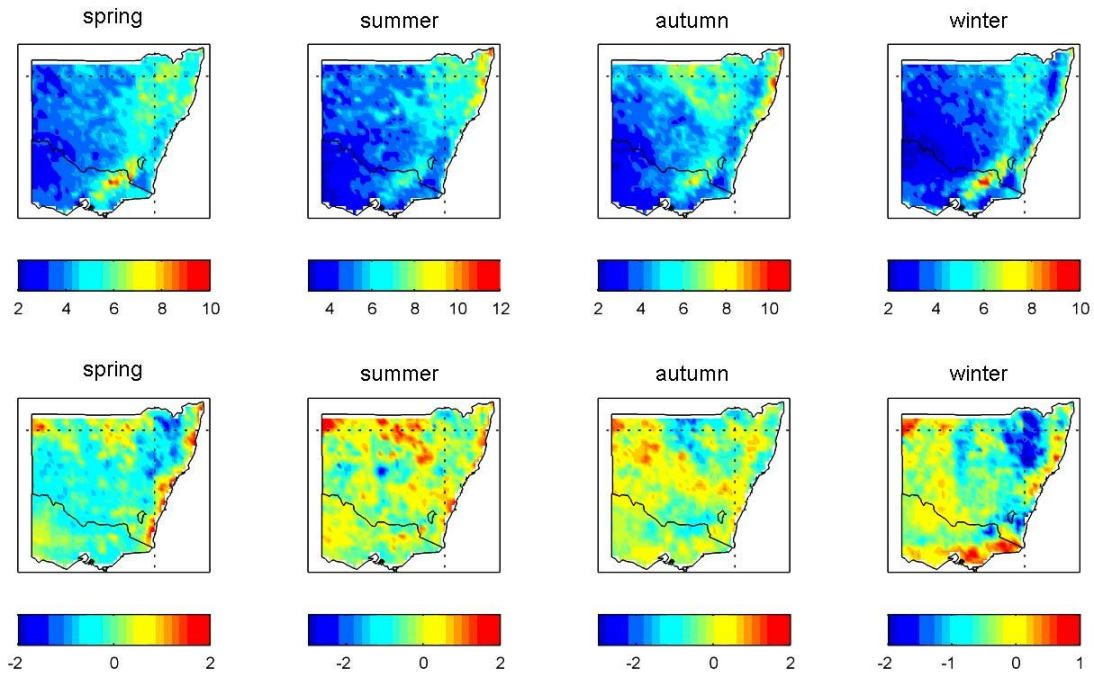

Fig. 4.2. Spatial distribution of the observed daily mean precipitation on wet days (SDII) (Top panel), and the differences between the downscaled and observed SDIIs (mm/day) (Bottom panel). The downscaled SDIIs were computed as the ensemble means of 500 runs at each grid in the validation period (1988-2008).

The general performance across different climatic zones is summarized in Fig. 4.3. On each graph, points correspond to an average across all the grids available in a particular climatic zone for a single season. Besides the means of the ensemble,

the 90% confidence intervals are also shown. The figure shows that the observed SDII is covered by the confidence intervals of the ensemble in most of the seasons and climatic zones. Overestimation occurred in zone G for spring and summer and in F4 for spring, while underestimation in E4 and F4 for autumn. Comparatively speaking, among all climate zones, zone G had the biggest 90% confidence interval in G, where the climate is very hot and dry.

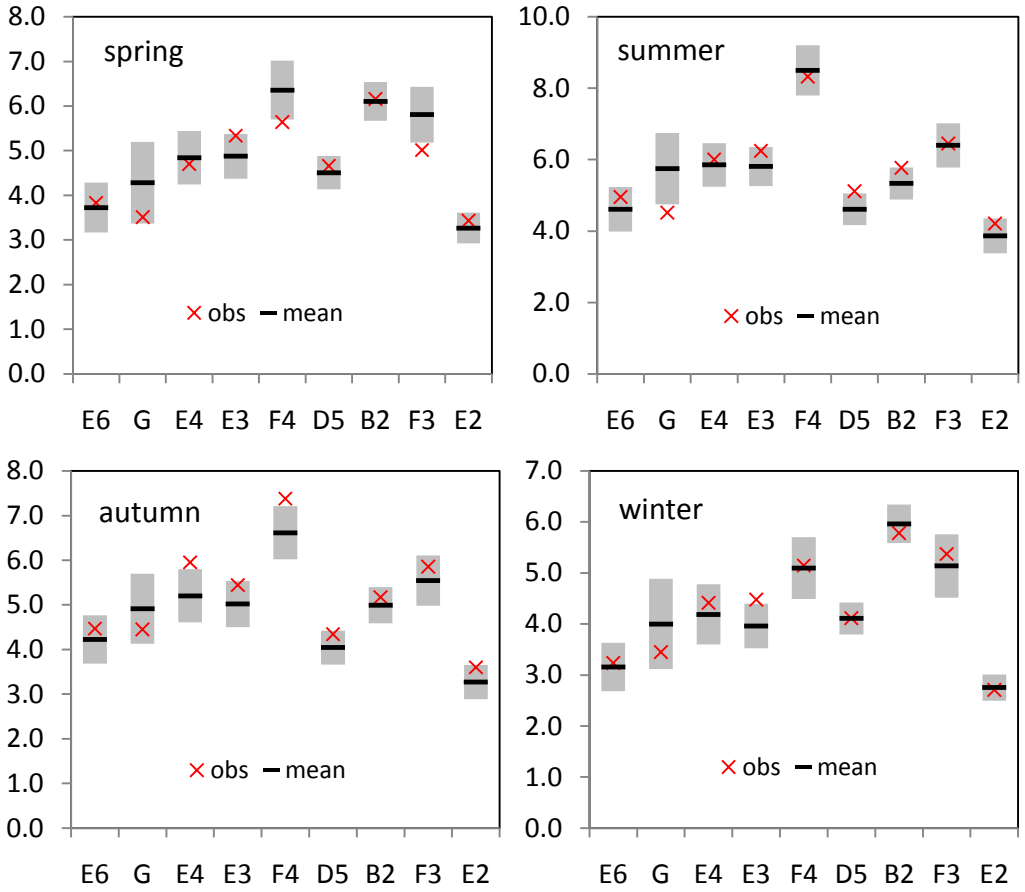

Fig. 4.3. Plot of the downscaled *versus* observed (OBS) daily mean on rainy days (SDII, mm/day). On each graph, each value is an average across all the grids available in a particular zone. The downscaled SDIIs are computed as ensemble means and 90% confidence intervals of the ensemble for 500 runs in the validation period 1988 - 2008. The X-axis shows the names of the nine climatic zones.

The SOM-SD reproduced quite well the observed standard deviation on wet days (ppSD) (Fig. 4.4). For most of the seasons, the 90% confidence intervals could cover the observed ppSDs (Fig. 4.4), and their means were close of the observed ppSD in almost all climatic zones. Moreover, the model generally gives a smaller range of the 90% confidence intervals in other zones than in G, F3 and F4. The ppSD was significantly overestimated in most zones other than F3 and F4 for spring. In combination with the downscaled SDIIs (Fig. 4.3), SOM-SD showed

relative low skill in the first two moments of the PDFs (SDII and ppSD) for zones G, F3 and F4. The method does not show any significant differences for the root mean square error (RMSE) of daily precipitation time series at each season compared with the results in the calibration period (not shown).

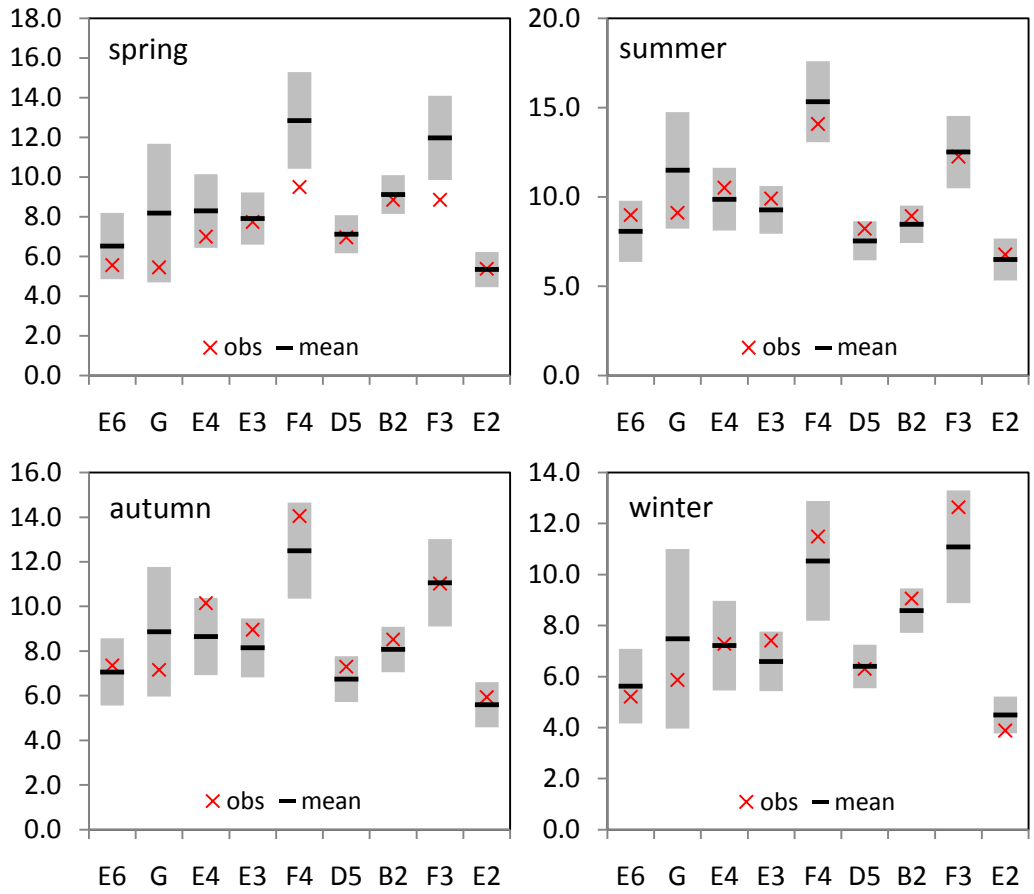

Fig. 4.4. As for Fig. 4.3 except for the standard deviation (ppSD) on wet days.

Daily precipitation belongs to a type of highly non-Gaussian distribution, so even though modeling the first two moments well cannot guarantee an unbiased estimate of the shape of its PDF. Therefore the cumulative distribution of frequency (CDF) for observed and downscaled daily precipitation on wet days was compared by using the Kolmogorov-Smirnov (K-S) goodness-of-fit test, which is a non-parametric method to test the null hypothesis of no CDF difference in paired samples (Press et al., 1992; Lopes et al., 2007; Corder and Foreman, 2009). The significant level, α, was set at 0.05, which corresponds to 5% significance level. Small probability *p*-values suggest that the null hypothesis is unlikely to be true and the null hypothesis is rejected when $p<0.05$. The test results (*p*-values) are presented in Table 4.2, where each value is an average across all the grids available for each region. The *p*-values of the goodness-of-fit

test are all above 0.05 (the 5% significance level) for the mean values of 500 runs in all climatic zones, indicating that they all pass the K-S test. In some zones, the low bounds of their 90% confidence intervals failed to pass the K-S test (p<0.05), indicating a small number of ensemble runs failed. As a whole, the SOM-SD appeared more skillful in autumn than in other seasons. The least skillful performance occurred in zone G in summer (only 0.19 for the mean).

Table 4.2. Mean of non-parametric K-S test results (p-values, p=0.05 is the 5% significance level) for comparing distribution of the downscaled and observed daily precipitation on wet days in each climatic zone. Each value is an average across all the grids available in a particular zone. These statistics are derived from the ensemble of 500 runs in the validation period (1988-2008).

	spring	**summer**	**autumn**	**winter**
E6	0.23(0.033, 0.64)	0.29(0.054, 0.69)	0.35(0.073, 0.74)	0.25(0.039, 0.64)
G	0.36(0.055, 0.79)	0.19(0.031, 0.53)	0.38(0.067, 0.84)	0.34(0.044, 0.85)
E4	0.33(0.058, 0.75)	0.28(0.050, 0.64)	0.34(0.066, 0.75)	0.34(0.054, 0.79)
E3	0.21(0.030, 0.60)	0.28(0.051, 0.68)	0.35(0.070, 0.75)	0.26(0.037, 0.67)
F4	0.30(0.051, 0.72)	0.31(0.051, 0.73)	0.25(0.046, 0.65)	0.27(0.045, 0.66)
D5	0.28(0.046, 0.67)	0.26(0.046, 0.65)	0.29(0.056, 0.68)	0.22(0.036, 0.59)
B2	0.31(0.052, 0.73)	0.26(0.048, 0.61)	0.26(0.051, 0.66)	0.20(0.041,0.47)
F3	0.34(0.065, 0.74)	0.26(0.037, 0.69)	0.22(0.039, 0.59)	0.28(0.049, 0.66)
E2	0.37(0.070, 0.79)	0.27(0.046, 0.66)	0.30(0.061, 0.70)	0.29(0.050, 0.71)

The ability to reproduce the year-to-year variability of seasonal precipitation was evaluated by the non-parametric Spearman rank correlation (RC) between the observed and downscaled time series. The correlations are shown in Fig. 4.5 where each value is an average across all grids available in each climatic zone. The 90% confidence intervals also are represented in the figure. All these correlations are significant at least at the 95% level, indicating reasonable modeling skill. There was a marked seasonal cycle, consistent across all regions (Fig. 4.5): i.e., the model appeared more successful in spring and autumn than summer and winter. However, no particular region stands out as a climatic entity where the downscaling skill in reproducing year-to-year variability is consistently lower or higher across all seasons. The mean values were generally between 0.45 and 0.60 for spring and autumn, and 0.40 for summer and winter. The least skill occurred in zone F4 with a mean value of 0.25 in summer.

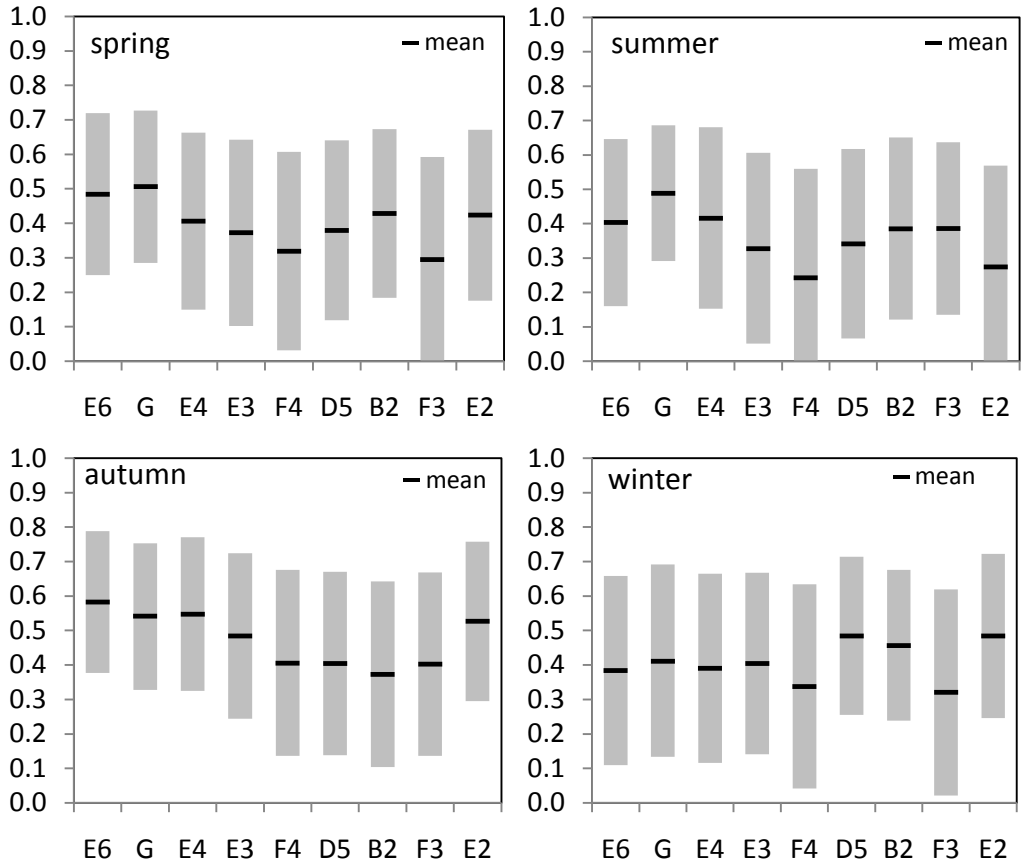

Fig. 4.5. As per Fig. 4.3 but for the Spearman rank correlation between observed and downscaled seasonal precipitation time series (α=0.05).

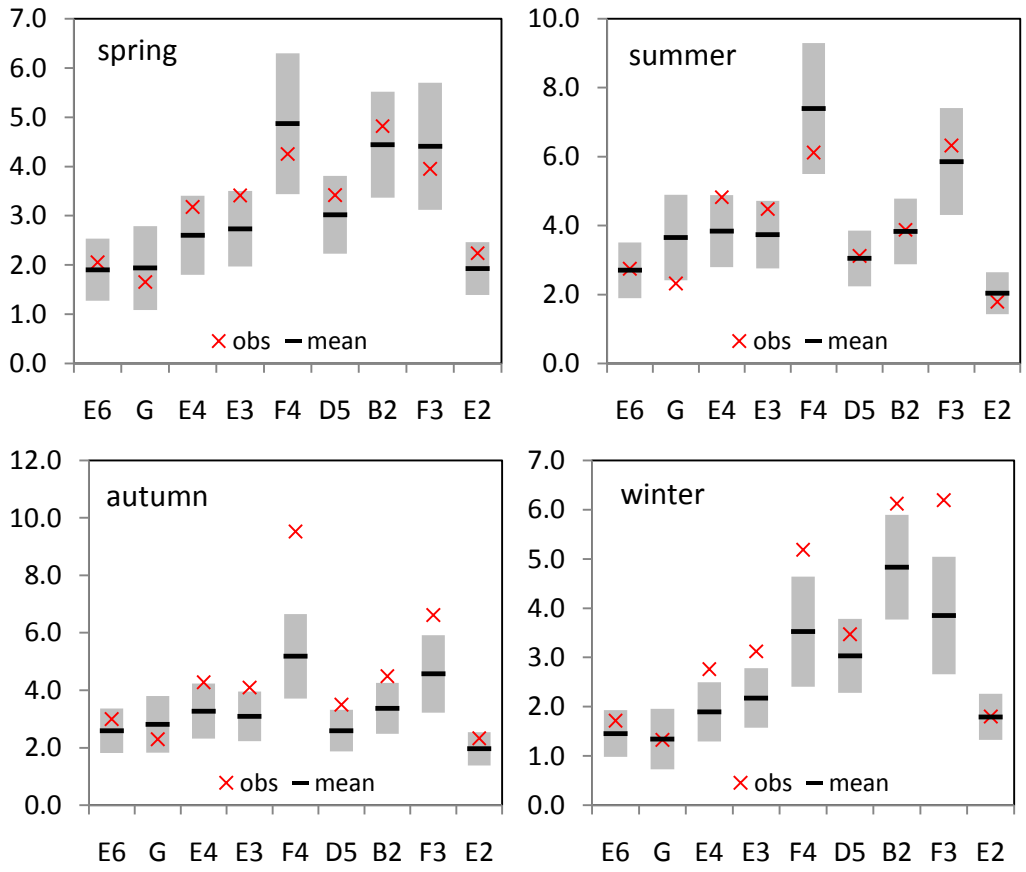

Fig. 4.6. As per Fig. 4.3 but for standard deviation of the seasonal precipitation (ppSSNSD).

The accuracy of the downscaling model relating to inter-annual variance was assessed by the standard deviations of the generated seasonal precipitation amount (pSSNSD, mm/season) (Fig. 4.6). It showed that the model had a slight tendency to underestimate the inter-annual variance, although the correlations suggested that the model was able to capture most of the inter-annual variability. The means of the ensemble for 500 runs generally were close to observed pSSNSDs, but higher in several instances. The variance was obviously underestimated in zone F4 and F3 for autumn and that for E3, E4, B2 and F3 for winter, while it was overestimated only in zone G for summer. Thus, the SOM-SD appears less skillful in reproducing inter-annual variance of observed precipitation for most of the regions in winter than for other seasons.

4.4.3.2 Precipitation frequency

Apart from the amount of precipitation, another significant characteristic related to precipitation is rainfall frequency. The ability of the SOM-SD to reproduce seasonal mean precipitation days was firstly evaluated at three different daily precipitation intensities of 0.1mm, 2.0mm and 20.0mm (nr001, nr020 and nr200). Figure 4.7 shows the spatial distributions of the observed and downscaled nr001s, while Fig. 4.8 shows the summary for the performances of nr001, nr020 and nr200 in respective climatic zones. The approach has a tendency to overestimate nr001and nr020, but has no obvious bias for either high or low values, including at the tails of the distribution (large or small observed values) (Fig. 4.7). The bias ranges were generally between -4 and 5 days for nr001, ±2 days for nr020, and ±1 day for nr200. Figure 4.7 showed that the overestimation of nr001 mainly occurs in summer and the underestimation mainly takes place in winter.

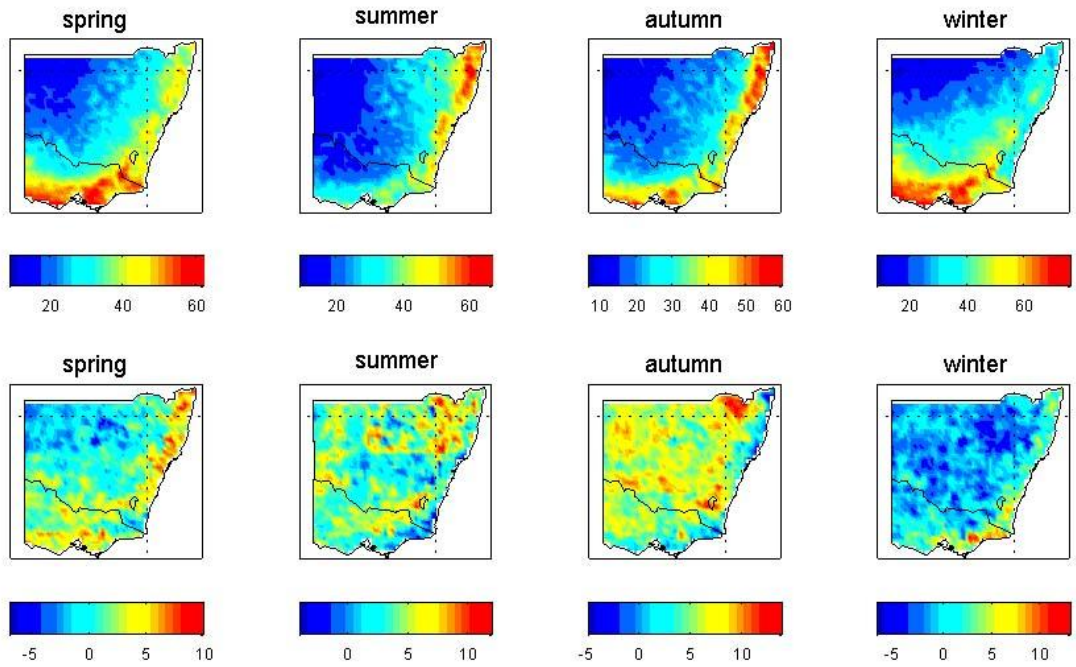

Fig. 4.7. Spatial distribution of the observed daily precipitation days (nr001, day) (Top panels), and the differences between the downscaled and observed nr001s (day) (Bottom panels). The downscaled nr001s are computed as the ensemble means of 500 runs at each grid in the validation period (1988-2008).

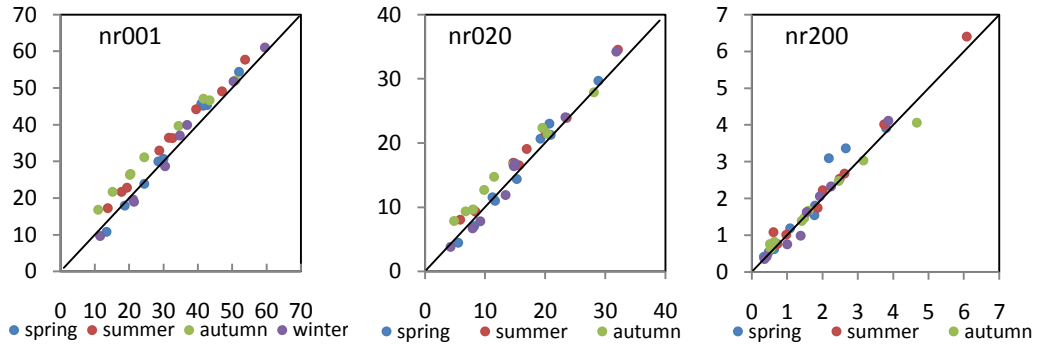

Fig. 4.8. Scatter plot of the downscaled (Y axis) *versus* observed (X axis) seasonal mean precipitation days respectively for nr001, nr020 and nr200 (see acronyms in Table 4.1). On the graph, each value is an average of all grids available in a particular zone and season, the total number of points is the number of climatic zones times four. The line of perfect fit (the diagonal) is shown. The downscaled values are computed as ensemble means of 500 runs in the validation period 1988-2008. ??

The ability to reproduce observed year-to-year variability of wet days (nr001) also was analyzed by the rank correlation separately per season and per climatic zone. The results are listed in Table 4.3, which shows that the correlation generally falls between 0.45 and 0.55(α=0.05). There are no significant seasonal cycles in different zones. The model displays the best skill in zone E2 for winter (0.65). In fact, selecting a suitable threshold for a wet day has a large impact on the statistics

of precipitation frequencies, especially for small precipitation events. This can be identified by the performances of SOM-SD for different precipitation intensities. Nevertheless, there is no consensus on the threshold selection. In this case, a subjective value of 0.1mm for daily precipitation was defined as a wet day.

Table 4.3. Rank correlations of seasonal wet days (nr001) between observed and downscaled time series (α=0.05). Each value is an average across all the grids available in a particular zone per season. These statistics were derived from the ensemble of 500 runs in the validation period (1988-2008); 90% of confidence intervals in parentheses.

E6	0.51(0.30, 0.73)	0.50(0.29, 0.71)	0.59(0.40, 0.78)	0.48(0.24, 0.72)
G	0.58(0.38, 0.78)	0.57(0.38, 0.75)	0.54(0.32, 0.77)	0.35(0.07, 0.64)
E4	0.37(0.10, 0.64)	0.44(0.19, 0.68)	0.56(0.36, 0.75)	0.39(0.12, 0.66)
E3	0.32(0.05, 0.59)	0.42(0.16, 0.68)	0.47(0.24, 0.69)	0.48(0.26, 0.70)
F4	0.32(0.02, 0.61)	0.37(0.12, 0.63)	0.40(0.14, 0.67)	0.32(0.04, 0.60)
D5	0.48(0.25, 0.70)	0.45(0.20, 0.69)	0.32(0.06, 0.59)	0.54(0.33, 0.75)
B2	0.51(0.30, 0.73)	0.44(0.19, 0.68)	0.23(-0.05, 0.51)	0.56(0.37, 0.76)
F3	0.25(-0.06, 0.55)	0.46(0.22, 0.70)	0.44(0.20, 0.69)	0.24(-0.07, 0.54)
E2	0.50(0.29, 0.70)	0.40(0.15, 0.64)	0.47(0.23, 0.70)	0.65(0.48, 0.82)

The wet-day and dry-day persistence were diagnosed using the indices of Pww and Pdd (Table 4.1). The indices were calculated seasonally. The inter-annual variability was analyzed by the rank correlation between these indices of observed and the ensemble means of the reconstructed daily precipitation time series. The SOM-SD could, to a certain extent, reproduce the observed multi-year mean wet-day persistence (Pww) and dry-day persistence (Pdd). The ratio of downscaled values to the observed values was generally above 0.6 and 0.7, respectively, for almost every season and every climatic zone (the first row in Fig. 4.9). The model did not show a significant seasonal cycle for both indices across the climatic zones. These two indices are important Markov process parameters. Rainfall occurrence generally is represented as a Markov process, the assumption being that the rainfall state on the next day is related to the state of rainfall on a finite number of previous days (Gabriel and Neumann, 1962). Although the SOM-SD showed a reasonable skill for Pww and Pdd, there was a clear systematic

underestimation for the 2 indices, as the ratio values are all less than 100% in Fig. 4.9. This indicates that though the SOM-SD has a good capability of embodying a first-order Markov process, it is not able to fully capture such an orderly process and, without introducing any other measure, the subsequent stochastic re-sampling process, obviously, could not correct this systematic error. Moreover, the definition of a wet day also has some impact on them. The second row of Fig. 4.9 shows the rank correlations between the observed and downscaled values for both the Pww and Pdd time series (i.e. Pww_CR and Pdd_CR). Although the correlation appears a little lower (generally between 0.2 and 0.4), it indicated that the SOM-SD can, to a certain extent, reproduce the inter-annual variability of the consecutive wet and dry days. The SOM-SD shows particular skills in different seasons and climatic zones (Fig. 4.9). The approach appears more skillful in autumn and spring for most zones for both Pww and Pdd. The correlations peak in spring (about 0.55 in the zone F4 for Pww_CR) and autumn (above 0.45 in zone E6, G and E2 for Pdd_CR), and the lowest correlation occurs in zone G for summer.

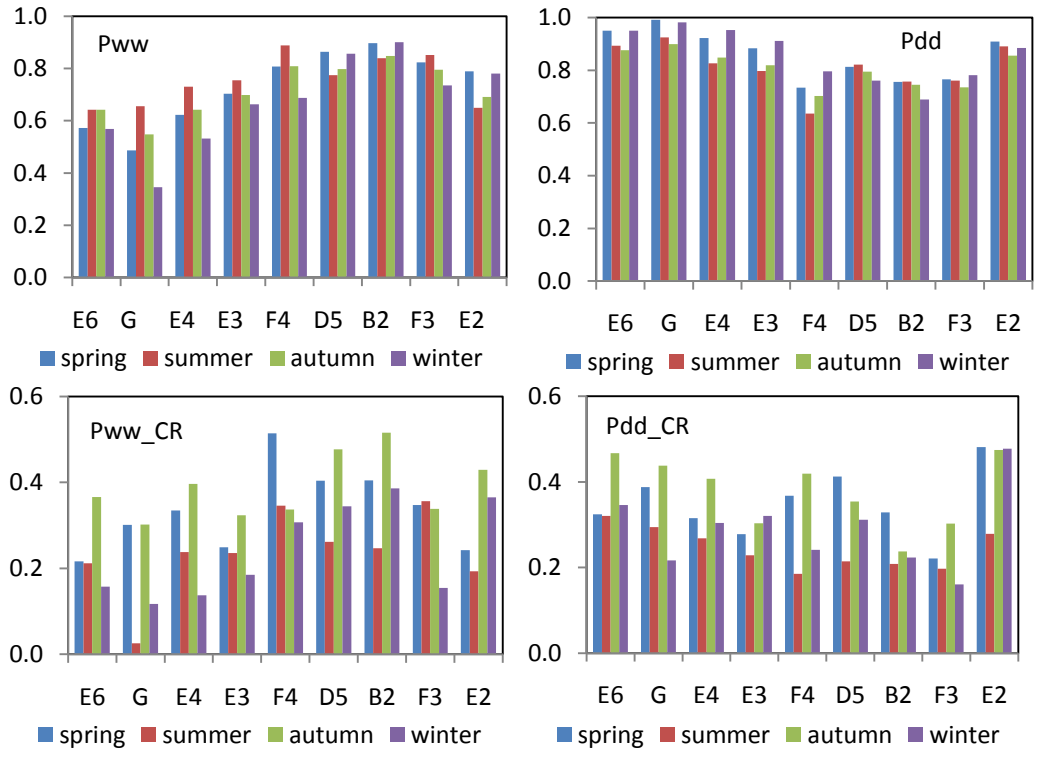

Fig. 4.9. The ratio of the downscaled seasonal mean Pww and Pdd to the observed values (top panel); Rank correlation of Pww and Pdd between the downscaled versus observed time series (α=0.05) (bottom panel). These values are shown by season (different colored bars) and climatic zones (labels on the x-axis). On each graph, each value is an average across all the grids available in a particular zone. The downscaled values are computed as ensemble means of 500 runs in the period 1988-2008.

4.4.3.3 Extreme precipitation events

One of the biggest challenges of downscaling is to correctly reproduce the extreme events, particularly extreme rainfall events. Here the P95 and P95T were used to assess the SOM-SD's capacity to reproduce extreme precipitation events, and CWD and CWW to analyze its ability to reproduce the observed maximum wet/dry spell (see Table 4.1). The extreme events of P95 and P95T were reproduced accurately (Fig. 4.10) without obvious bias toward either high or low values, including at the tails of the distribution (large or small observed values). For P95, errors in the reproduction are negligible (except for the summer in zone G, where it is overestimated) and there is no obvious seasonal cycle. However, there is a marked seasonal cycle in skill for P95T. It is overestimated in spring for all zones, while it is slightly overestimated in summer and the differences is generally between -3.0% and 5.0%.

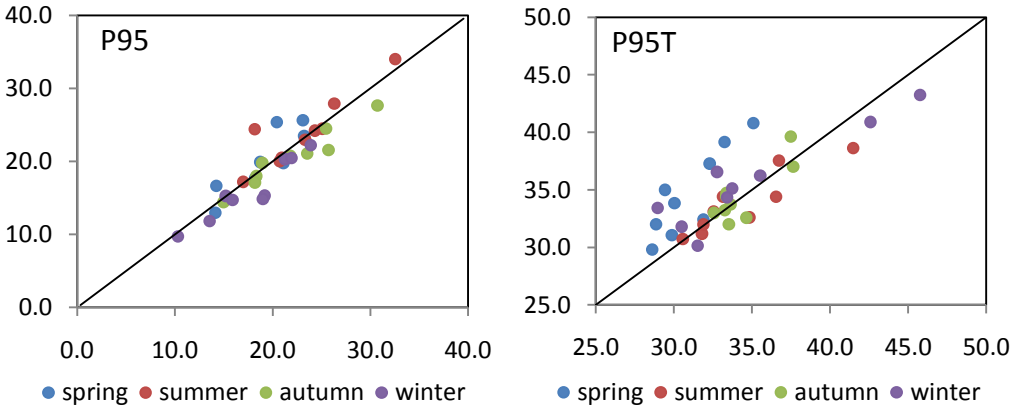

Fig. 4.10. As Fig. 4.8 but for P95and P95T (see acronyms in Table 4.1).

The SOM-SD is able to reasonably reproduce the observed maximum consecutive wet or dry days (CWD and CDD) but with slight underestimation (not shown). In the case of CWD, the biases generally lay between -5 and 5 days, and the better reproduction occurs in spring. For the CDD, the better performances occurred in summer and winter (with a bias range between -10 to 10 days) than in spring and autumn. The poor performance mostly occurred in the arid or semi-arid inland areas (zones E6 and E2 in autumn, and E6, E2 and E3 in spring). The year-to-year variability of CWD and CDD was further assessed by the rank correlation between observed and downscaled time series for each season (Fig. 4.11). The SOM-SD could reproduce the inter-annual variability of CWD with slightly

higher skill than that of CDD, probably because CWD had a more obvious seasonal cycle consistently across all regions, i.e. the downscaling approach was more successful in autumn and spring.

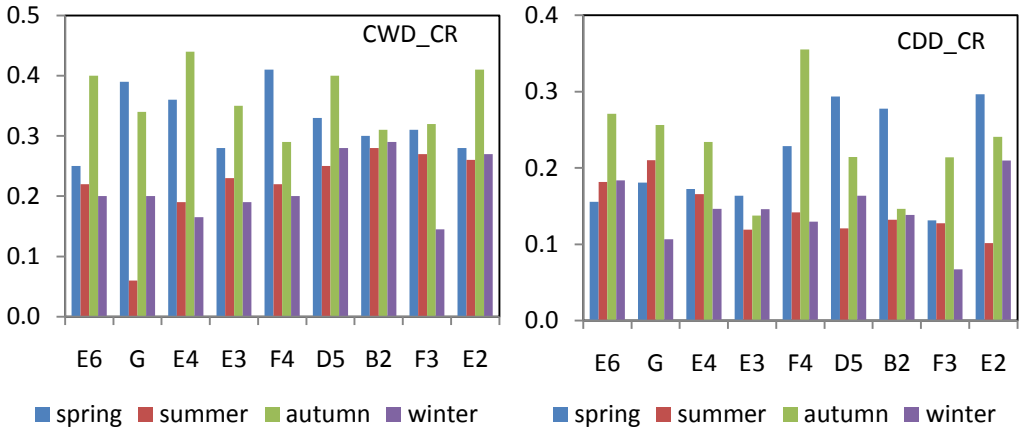

Fig. 4.11. As the second row of Fig. 4.9 but for CWD and CDD.

4.4.3.4 Forecast precision

For precipitation, its discrete joint distribution of simulations and observations in terms of relative frequencies can be defined using the following 2x2 contingency table:

		OBSERVED	
		Yes	NO
Simulation	No	M_{01}	M_{00}
	Yes	M_{11}	M_{10}

Where M_{00} is the correctly modeled dry day, M_{11} is the correctly modeled wet day, M_{10} is modeled wet but observed dry day, and M_{01} is modeled dry but observed wet day. Using the table, some measures can be computed, including *the percentage of forecast correct* (PFC), *probability of detection* (POD), *false alarm ratio* (FAR), *success ratio* (SR), *threat score* (TS) or *critical success index* (CSI), *true skill statistic* (TSS), *Gilbert skill score* (GS), *Heidke skill score* (HSS), and a categorical measure of bias. More information can be found at in Wilks (2006).

In this study, only PFC and the CSI were selected to assess the ability of SOM-SD to model the precipitation occurrence process. The CSI measure is required because the precipitation occurrence to be forecast is substantially less frequent

than the nonoccurrence (no).

$$PFC = (M_{11} + M_{00})/(M_{00} + M_{11} + M_{01} + M_{10}) \qquad (4.3)$$

$$CSI = M_{11}/(M_{11} + M_{10} + M_{01}) \qquad (4.4)$$

For both indices, the worst possible score is zero, and the best possible score is 100%. The results for PFC and CSI are represented in Fig. 4.12 and Fig. 4.13, respectively. These two indices vary among different climatic zones. For most zones, PFC is generally in the range between 55% and 70% (Fig. 4.12). High PFCs mainly occur in zones E6, G and E4. Not surprisingly, M_{00} in these zones determine their PFCs because they belong to arid or semi-arid climates. However, the conditions are opposite for CSI (Fig. 4.13). High CSIs mainly occur in wet climatic zones such as B2 and F4. The SOM-SD appears more skillful in other seasons (mostly between 30% - 50%) than in autumn (between 20%-40%). These results are similar to the results of Harpham and Wilby (2005), who used three SDSMs (a Radial Basis Function Artificial Neural Network (RBF-ANN), Multi Layer Perceptron Neural Network (MLP-ANN), and a Conditional Resampling Method (SDSM)) to downscale area-average and station daily precipitation amounts in northwest (NWE) and southeast (SEE) England.

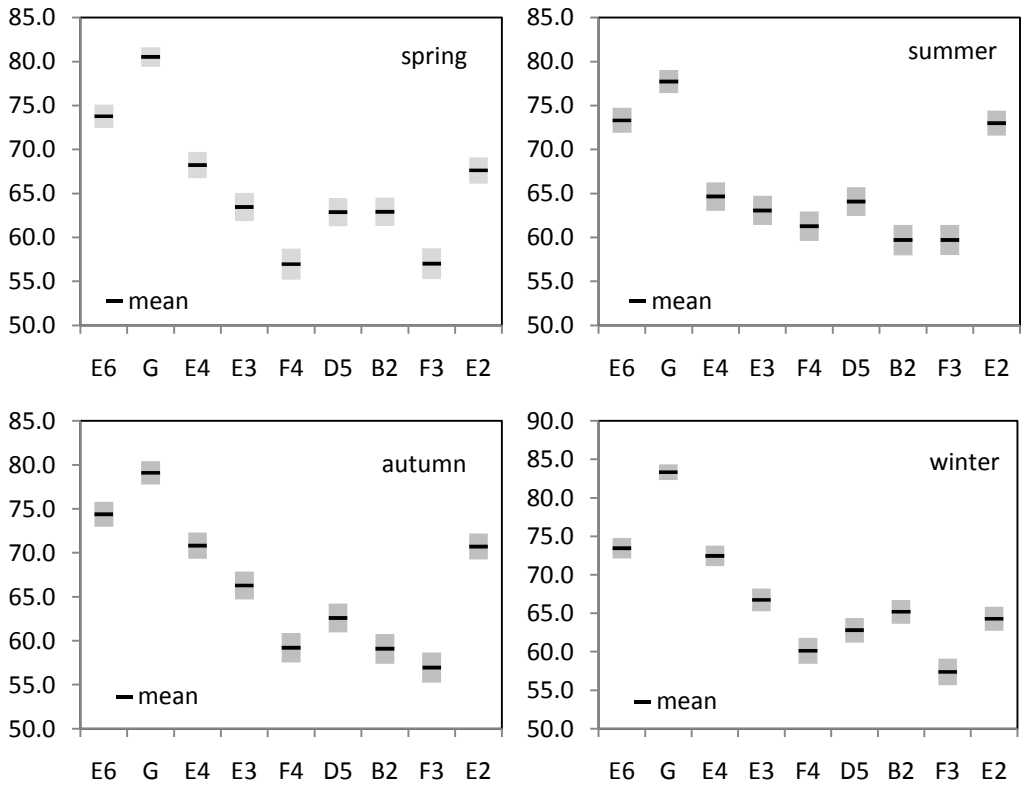

Fig. 4.12. As per Fig. 4.3 but for Percentage of Forecast Correct (PFC, %).

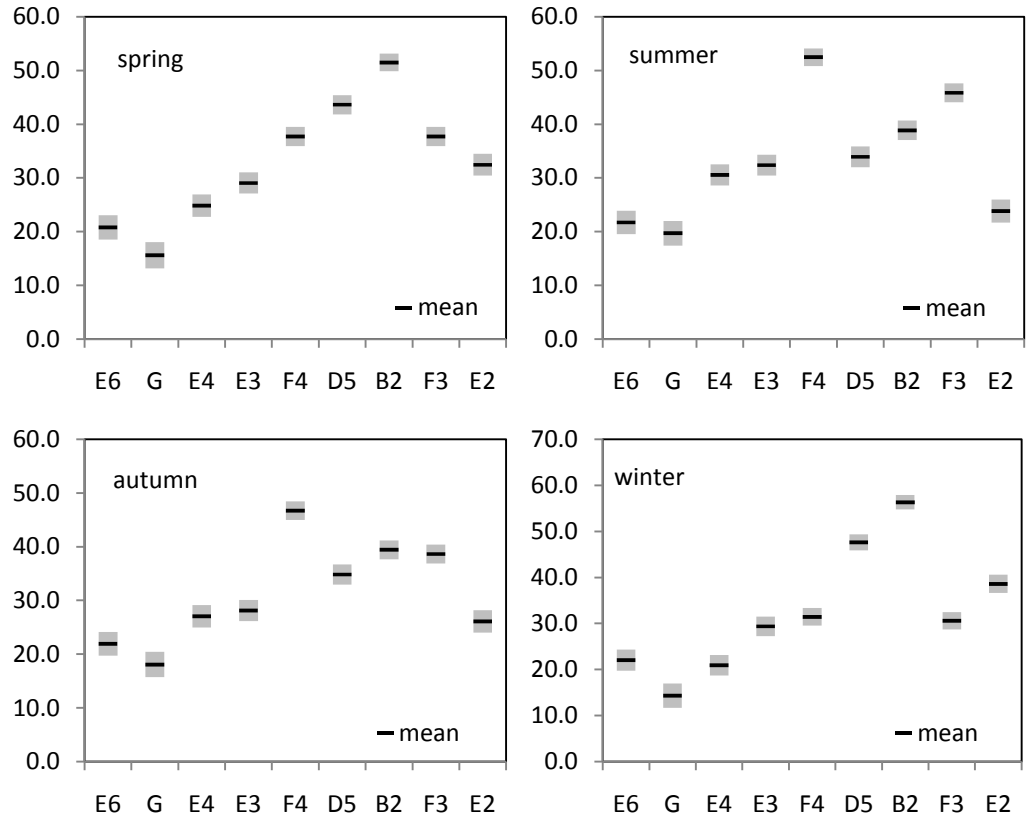

Fig. 4.13. As per Fig. 4.3 but for Critical Success Index (CSI, %).

4.5 Conclusion and discussion

This chapter described the development of a relatively simple and transparent statistical downscaling model, SOM-SD, and evaluated its applicability for downscaling daily precipitation over southeast Australia. The accuracy of the model was analyzed in a seasonally stratified style based on a series of diagnostic indices with consideration of normal precipitation amount, frequency, and extreme events. The analysis also placed a great emphasis on the skill of the method in modeling the inter-annual variability of observed daily precipitation time series. The main conclusions are:

- Circulation pattern classification is capable to capture the representative local-scale precipitation regimes. Another advantage of the method is that inter-grid relationships are preserved under a large NNR grid.
- The SOM-SD exhibits high skills in reproducing the average climatological statistics of the daily precipitation, including mean daily precipitation on wet days (SDII), rainy days (nr001, nr020 and nr200), seasonal wet/dry-day

persistence (Pww and Pdd), the cumulative distribution of frequency (CDF) and day-to-day precipitation variance on wet days (ppSD).

- The model reconstructs the observed extreme precipitation characteristics of P95 and P95T without bias. It can generate with an acceptable skill the maximum consecutive wet/dry days (CWD and CDD).
- The model can reasonably reproduce the inter-annual variability for the above indices. Moreover, the model can generate the inter-annual seasonal variance with good performance as shown in the representation of the inter-annual variability of the seasonal precipitation amount (SDII) and frequency (nr001).
- The model shows good suitability for downscaling studies across a variety of climatic zones and seasons, even along the Great Dividing Ridge where the precipitation has significant convection characteristics. Overall no particular zone stands out as a climatic entity where the downscaling skill in reproducing all statistical indices is consistently lower or higher than any other zones across seasons. Comparatively, the performance in the arid and semi-arid region is inferior to other regions owing to the extremely dry and hot climate conditions.

In addition, as a novel SDSM, a few issues require further research. Firstly, the method is incapable of predicting new daily records, because the predicted values are only taken from archives from past observations (Imbert and Benestad, 2005; Hidalgo et al., 2008; Timbal et al., 2009). Even for a stationary process, new record-breaking values are expected to occur with time.

Secondly, like other downscaling models, the SOM-SD tends to underestimate the long consecutive wet/dry days. A close look at the historical data reveals that those zones with maximum consecutive wet days mainly occur in the snowy mountain area of zone B2 and subtropical climatic area of zone F4, while the maximum consecutive dry days take place in the desert area of zone G. For the dry days in zone G, the climate is so hot and dry that it is very difficult to describe the precipitation process accurately by SDSMs. So the SOM-SD only shows a moderate performance compared with other zones. This may, however, be improved through combining the SOM-SD with other techniques, such as the Hidden Markov-Chain or the Bayesian inference (network) methods (Vrac et al., 2007).

Thirdly, SOM-SD can only simulate, to a certain extent, the inter-annual variability. This is also a common issue for almost all statistical downscaling models. For example, Timbal et al. (2003) used analog models to predict daily rain occurrences in neighboring regions to the case study area used in this study. The models were also only able to partially reproduce observed inter-annual variability. In fact, the SOM-SD's capability of modeling the inter-annual variability will improve if an optimization procedure is adopted to select the most optimal combination or the most appropriate spatial domain of the large-scale predictors, and the most optimal number of synoptic patterns for a specific climatic zone. This is not explored in this study since only a set of common configuration was used for the SOM-SD in order to investigate its applicability across different climatic zones. On the other hand, the SOM-SD does not explicitly take the seasonality of precipitation or predictors into account as other downscaling models do (e.g., Vrac et al., 2007; Timbal et al., 2009; Chu et al., 2010). If the seasonality can be taken into account, the skill in modeling the inter-annual variability may also improve (Vrac et al., 2007). However, the above-proposed schemes (i.e., optimization or seasonality consideration) would not solve the issue totally. This is because surface variables are not controlled completely by the large-scale predictors (von Storch, 1999; Timbal et al., 2009), which is very true for precipitation process.

Fourthly, like other downscaling models, the performance of the SOM-SD also depends on the length and quality of both predictor and predictand data available. It was found that the gridded precipitation data includes more drizzle events than reality, even though they were assimilated through sophisticated algorithms from the observed station data. These kinds of phenomena become more common in those regions with rare or sparse rainfall gauge stations. The issue concerning data assimilation has been beyond the scope of this study, nevertheless the downscaling practices actually call for even high quality data (Maraun et al., 2010). Due to data quality, selecting an appropriate threshold value for a wet day or rainfall day also becomes an important factor for influencing the performance of the SOM-SD.

Finally, the SOM-SD relies on an indirect link between large-scale predictors and local predictand. This is because the model must firstly classify predictors into a finite number of synoptic patterns, and map the predictand values to these patterns

to build the relationship between predictors and predictand. Thus, weather classification or clustering becomes an additional task compared with other downscaling models, so requires additional knowledge (Wilby et al., 2004; Fowler et al., 2007). However, with fast advancing computer technology, this should not be considered as an issue anymore and in fact many clustering analysis tools have been publically available. The SOM toolbox is a good example (Kohonen, 2001; http://www.cis.hut.fi/somtoolbox/).

In conclusion, the SOM-SD combines the advantages of a synoptic classification method based on SOM and a stochastic re-sampling technique, which is a type of effective statistical downscaling scheme (Christensen and Hewitson, 2007). The synoptic classification method provides accurate and relatively transparent simulations of local-scale precipitation characteristics/regimes, while the stochastic re-sampling technique can explore the probability of daily precipitation in a Monte Carlo simulation way. With the ability to generate a full range of time series data, the SOM-SD output allows probability and risk analysis which are essential for climate change impact studies, especially under the large uncertainty of climate change conditions. Moreover, the high skill of the method provides confidence for its use in regional and local impact studies from future climate change.

CHAPTER FIVE

IMPROVEMENT ON MODELING DAILY PRECIPITATION SEASONALITY IN SOM-SD

5.1 Introduction

Seasonality is an important regional/local climate characteristic that requires consideration in statistical downscaling. Regions with clearly defined seasons may imply different seasonal driving forces for precipitation. For example, precipitation in summer is driven by convection to a greater extent than in winter. The season-dependent performance of downscaling models clearly indicates that downscaling without considering seasonality could cause intra-annual anomalies in the final result (Johansson and Chen, 2003; Wetterhall et al., 2007).

However, SOM-SD presented so far did not take explicitly the seasonality into consideration. Synoptic patterns for each downscaling grid were attained by training the data from calibration period as a whole without seasonal separation; and the precipitation values that mapped to these synoptic patterns did not have seasonal separation, either. These values were then used to construct the so-called predictands-candidate-data-bank (PCDB) for each corresponding synoptic pattern in the SOM-SD. To overcome the seasonality issue, a general solution is to divide the year into four seasons or into 12 months, and then to carry out downscaling in each season (e.g. Furrer and Naveau, 2007; Timbal et al., 2009) or each month (e.g., Chu et al., 2010) accordingly. In this chapter, a different scheme is presented to try to improve the skill of SOM-SD in modeling daily precipitation seasonality.

5.2 Method

5.2.1 Seasonality issues in SOM-SD

A trained SOM based on the whole data without a seasonal separation produces generalized synoptic patterns among seasons. These patterns together with their associated PCDBs reflect the common large-scale atmospheric circulation regimes driving the local precipitation. However, atmospheric motions have seasonal variations. Consequently, synoptic patterns must have seasonal changes. During

training, the information has been reflected in the attained SOM, which can be identified clearly from the seasonal frequency of occurrence distribution after mapping the predictor data to each synoptic pattern (Fig. 3.14). From this point of view, the SOM-SD considers the seasonality of predictors implicitly. So does the predictand through the PCDBs relevant to the predictors. The above approach worked reasonably well in reproducing the precipitation events in terms of the magnitude and the wet/dry persistence (see Chapter 4; Hewitson and Crane, 2006).

However, it should not be forgotten that the frequencies are significantly different in summer and in winter for the same synoptic pattern (Fig. 3.14). Moreover, compared with large-scale synoptic patterns, precipitation shows even stronger seasonal characteristics (Fig. 3.8). As the patterns could occur in every season, there is no seasonal separation for the precipitation values under each PCDB that relates to these generalized synoptic patterns. During the downscaling, a phenomenon will be encountered that precipitation amounts are extracted with equal probabilities from a PCDB for those seasons that shares a same synoptic pattern. When the downscaled results were analyzed in a seasonally stratified style, it showed that the SOM-SD has an obvious tendency to generate too even precipitation distributions over seasons, which weakens the precipitation seasonality. The phenomena become more significant in places where precipitation has significant seasonal characteristics.

5.2.2 New seasonal re-sampling scheme

As described before, a general solution to the seasonality issue is to construct downscaling models for each season (e.g., Furrer and Naveau, 2007; Timbal et al., 2009) or for each month (e.g., Chu et al., 2010). In this study, a so-called ‘Season Precipitation Pool (SPP)’ scheme was introduced to strengthen the downscaled precipitation seasonality (Fig. 5.1). Each PCDB related to one of the 35 key synoptic patterns was subdivided into 4 corresponding SPP according to the seasons. A precipitation value can only be mapped to the SPP of its corresponding season. Thus, each synoptic pattern is linked to 4 SPPs and for a particular day, its precipitation value is re-sampled only from the season-related SPP. For example, if the prediction of precipitation on one day in spring is needed, the precipitation amount would be selected from the spring SPP under the associated synoptic pattern that is identified by the predictors on that day.

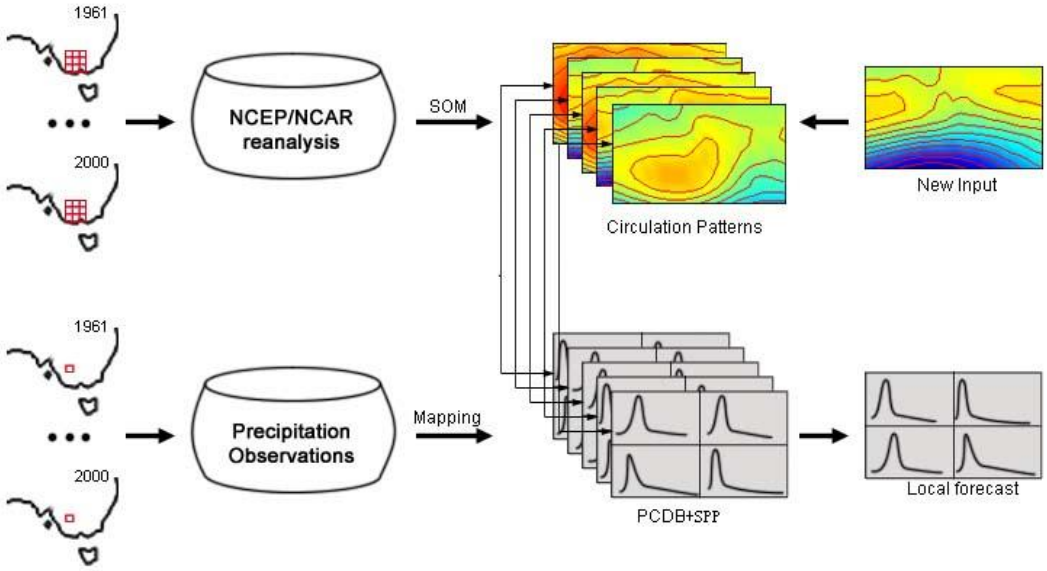

Fig. 5.1. Downscaling schematic of the SOM-SD with the SPP scheme.

The SPP scheme is helpful in terms of providing an appropriate range to re-sample the precipitation amount, after the SOM method identifies all possible synoptic patterns (irrespective of training the SOM seasonally or not). The trained synoptic patterns cover the common precipitation regimes in different seasons. This is vital for the application of the downscaling method to construct climate change scenarios, which means that they will still be able to find similar precipitation regimes even if the climate change might result in some synoptic pattern shifting from one season to another, while seasonally training the SOM might fail to do so. Generally, the smaller the time scale for training, the less true for the temporal stationarity in the future (Timbal et al., 2009). The remainder of this chapter shows the comparison of downscaled precipitation between the SOM-SD with or without the SPP scheme to investigate the improvement on the seasonality of downscaled precipitation.

5.2.3 Assessment indices

The skill of the downscaling method was assessed in a seasonally stratified style to ensure that the model is capable of capturing the seasonal variations of precipitation. The Spearman rank correlation (Corder and Foreman, 2009) for these indices between the observed and downscaled daily precipitation time series was employed to analyze the ability of SOM-SD to model the inter-annual variability for different assessment indices. Table 5.1 summarizes the assessment indices. The indices represented the statistics of daily precipitation with regard to

precipitation amount and frequency, as well as extreme events.

Table 5.1. Assessment indices for downscaled daily precipitation.

Acronym	***Definition***	***Unit***
SDII	Simple daily intensity(mean daily precipitation on wet days)	mm/day
ppSD	Standard deviation of daily precipitation on wet days	mm/day
RMSE	Root mean square error of daily precipitation time series	mm/day
nr001	Mean number of rainy days for daily precipitation >=0.1mm	Day
nr020	Mean number of rainy days for daily precipitation >=2.0mm	Day
nr200	Mean number of rainy days for daily precipitation >=20.0mm	Day
pSSNSD	Standard deviation of season precipitation	mm/season
P95	95-th percentile value of precipitation (extreme precipitation)	mm/day
P95T	Percentage of rainfall from events beyond 95-th percentile value of	%
Pww	Mean wet persistence	%
Pdd	Mean dry persistence	%
CWD	Maximum consecutive wet days	Day
CDD	Maximum consecutive dry days	Day
CSI	Critical Success Index	%

An ensemble of 500 simulations was generated by the downscaling method. The indices listed above were expressed as ensemble means with their 90% confidence intervals computed with a bootstrapping procedure (Efron and Tibshirani, 1993; Davison and Hinkely, 2006; Dibike et al., 2008). Without specification, only the ensemble means were used to compare with the observed values. In this present study, a wet day was defined as a day with daily rainfall greater than or equal to 0.1 mm.

5.3 Results

5.3.1 Precipitation amount

The SOM-SD without and with the SPP scheme was constructed for the calibration data (1958–1987). Based on the parameters obtained, precipitation was simulated for each downscaling grid for the validation period 1988 – 2008. Firstly, the ability to reproduce the daily mean (SDII) and the standard deviation (ppSD)

of observed daily precipitation on wet days was evaluated.

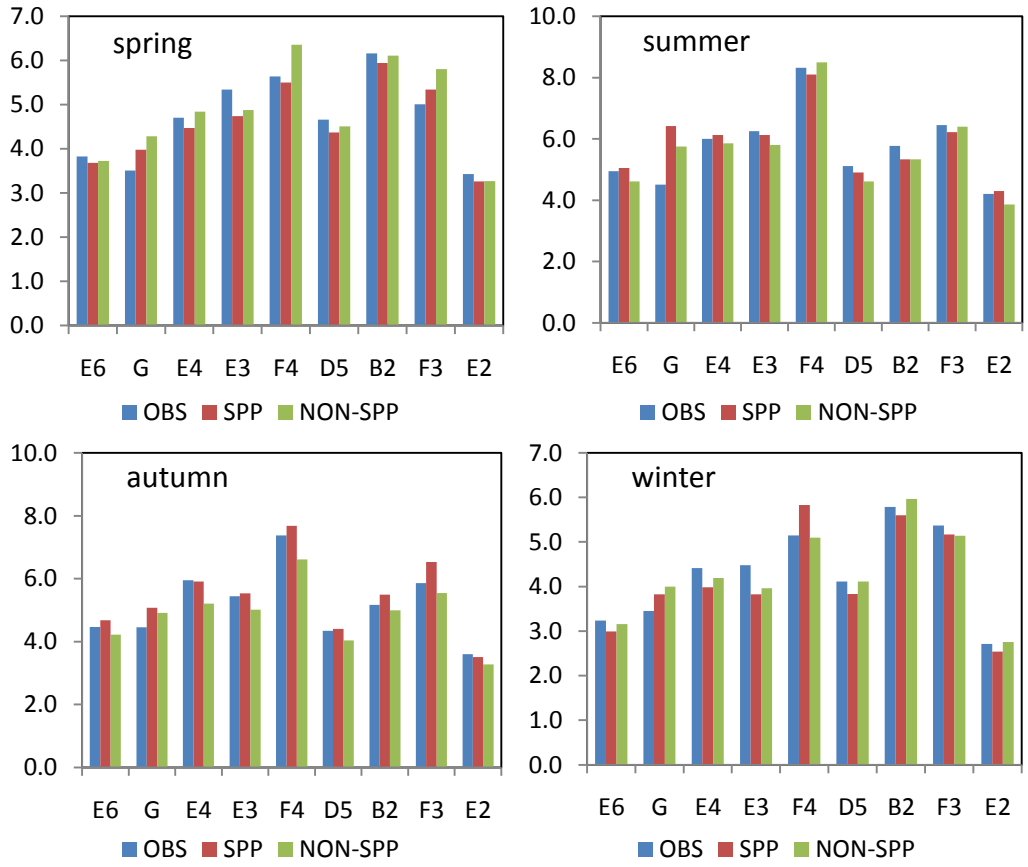

Fig. 5.2. Plot of daily mean on rainy days (SDII, mm/day) for observed (OBS) and downscaled values with and without the SPP scheme (SPP and NON-SPP). On each graph, each value is an average across all the grids available in a particular zone. The downscaled SDIIs were computed as ensemble means for 500 runs in the validation period 1988-2008. The X-axis shows the names of the nine climatic zones.

The SOM-SD with or without the SPP scheme both reproduced the SDII very well (Fig. 5.2). The differences of SDIIs among the observed and downscaled values from the SOM-SD with or without the SPP scheme were almost negligible in most climatic zones for most seasons. However, the improvements with the SPP scheme were identified by the narrowing the 90% confidence intervals across different climatic zones (not shown). The SOM-SD with or without the SPP scheme both reproduced well the observed standard deviations of daily precipitation on wet days (ppSD, Fig. 5.3). In contrast to SDIIs, the improvements on the 90% confidence intervals for ppSD with the SPP scheme were minimal.

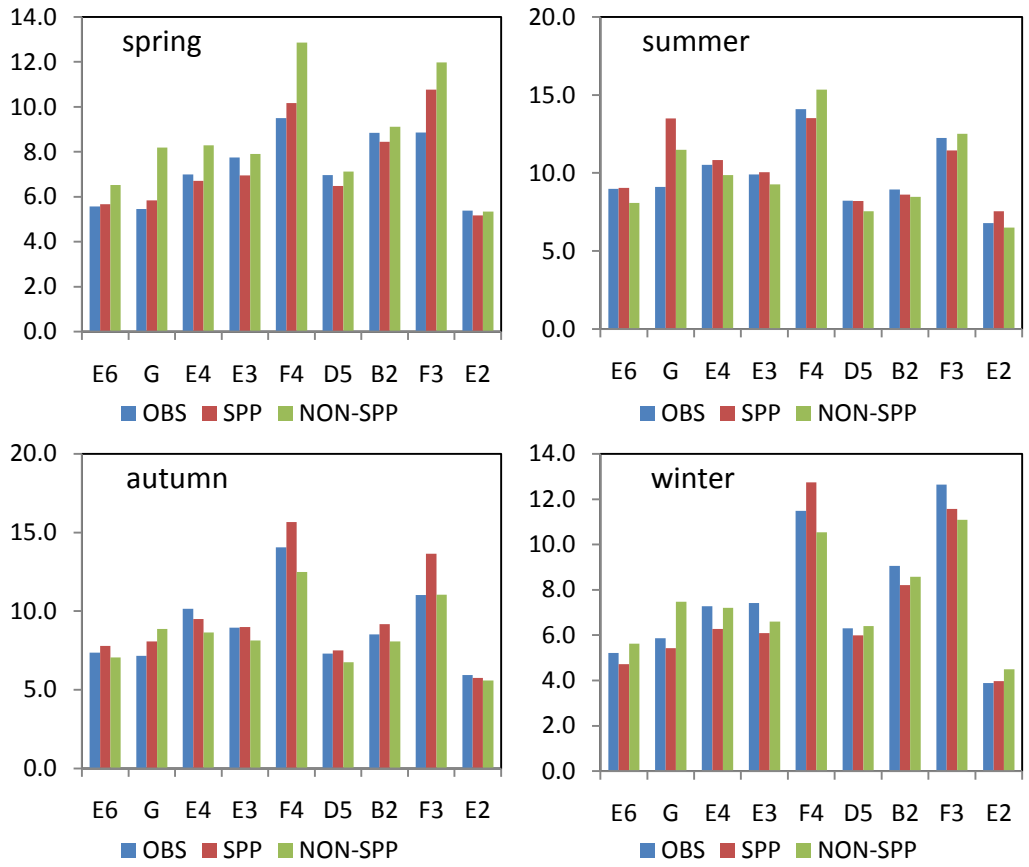

Fig. 5.3. As Fig. 5.2 but for the standard deviation (ppSD) on wet days.

The root mean square error (RMSE) is widely recognized as a useful statistics for indicating how accurately the model predicted values with regard to the observed data points. The spatial distribution of the differences in RMSE for the downscaled results with and without SPP is shown in Fig. 5.4. The figure shows that the improvements (i.e., differences in negative values) occur in most regions mainly for spring, autumn and winter. For spring, there were large improvements (<-1.0mm) along the eastern coastal band, while there were no improvements (>0.0mm) in the western arid and semi-arid regions. For summer, although there were no improvements in most of the arid and semi-arid regions, and in the southern coastal region, larger improvements (<-1.0mm) still occurred along the eastern coastal band to the right of the GDR. In contrast, the large improvements did not occur in the same regions for autumn and winter. The major improvements took place along the left side of the GDR for autumn, while they mainly occurred in the southern and middle region for winter (between -0.5 mm and -1.0mm).

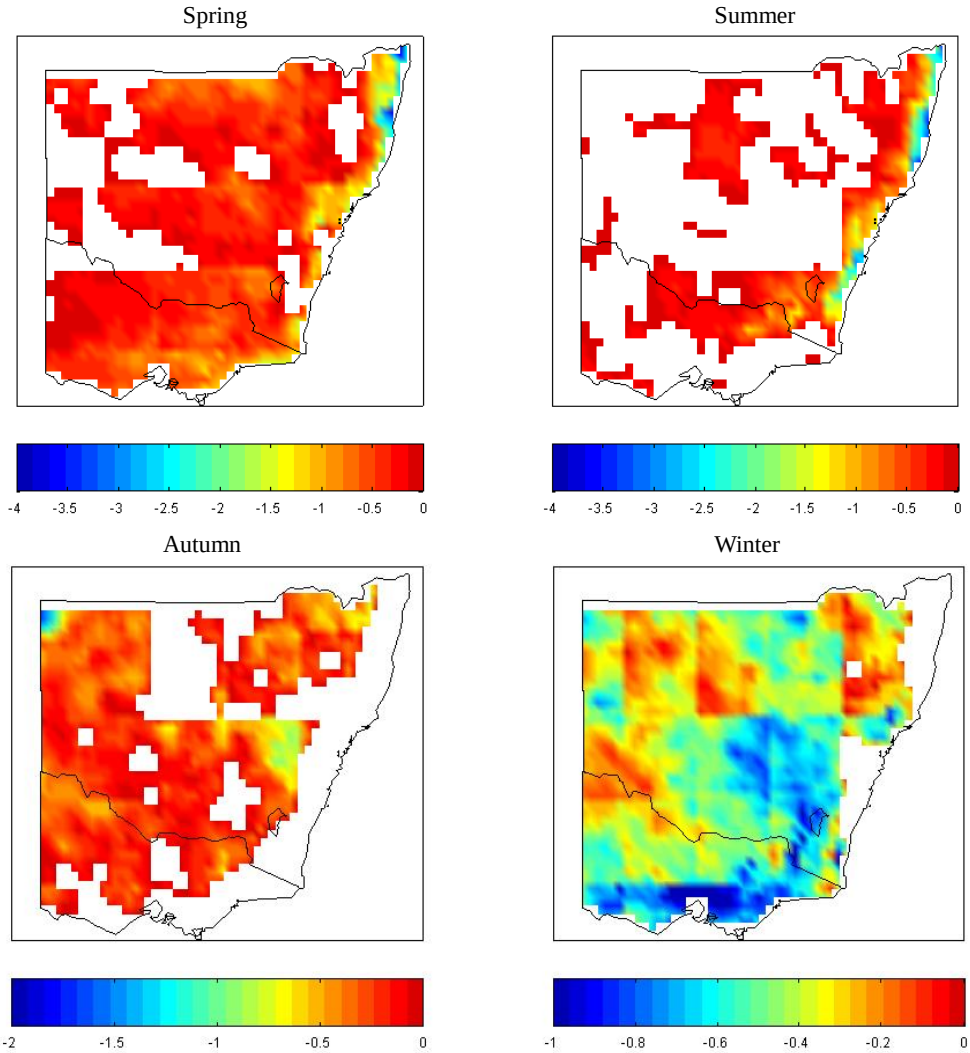

Fig. 5.4. Spatial distribution of the differences of RMSE for the downscaling with or without the seasonal resampling scheme. The RMSEs were computed as the ensemble means of 500 runs at each grid in the validation period (1988-2008). The white area indicates no improvements.

The ability to reproduce the inter-annual variability of seasonal precipitation was evaluated by computing the non-parametric Spearman rank correlation (RC) between the observed and downscaled time series. All these correlations are significant at least at the 95% level, indicating reasonable modeling skill. The spatial differences of RCs from with or without SPP are shown in Fig. 5.5. The improvements (i.e., differences greater than 0.0) of SPP scheme on modeling the inter-annual variability of daily precipitation were significant in most of the regions for all seasons (Fig. 5.5). The improvements are generally between 5.0% and 15.0% for spring and summer, and between 10.0% and 20.0% for autumn and winter. The large improvements occur in the southwest regions for spring while occur in the southeast coastal regions for summer. For autumn, they also occur in the southeast regions but along the left of the Great Dividing Ridge (GRD). The

large improvements for winter mainly occur in the north part of the case study area. However, there are still areas, particularly arid and semi-arid regions, which gain no improvements or have adverse effects. For a downscaling method, its ability to reproduce the inter-annual variability is particularly important because it indicates whether the method can reproduce correctly the predictor-predictand relationships. However, it is very difficult to capture the relationship for downscaling precipitation in SDSMs. Sometimes, the RC below 10% is still acceptable. From this point of view, the SPP is extremely useful in this regard.

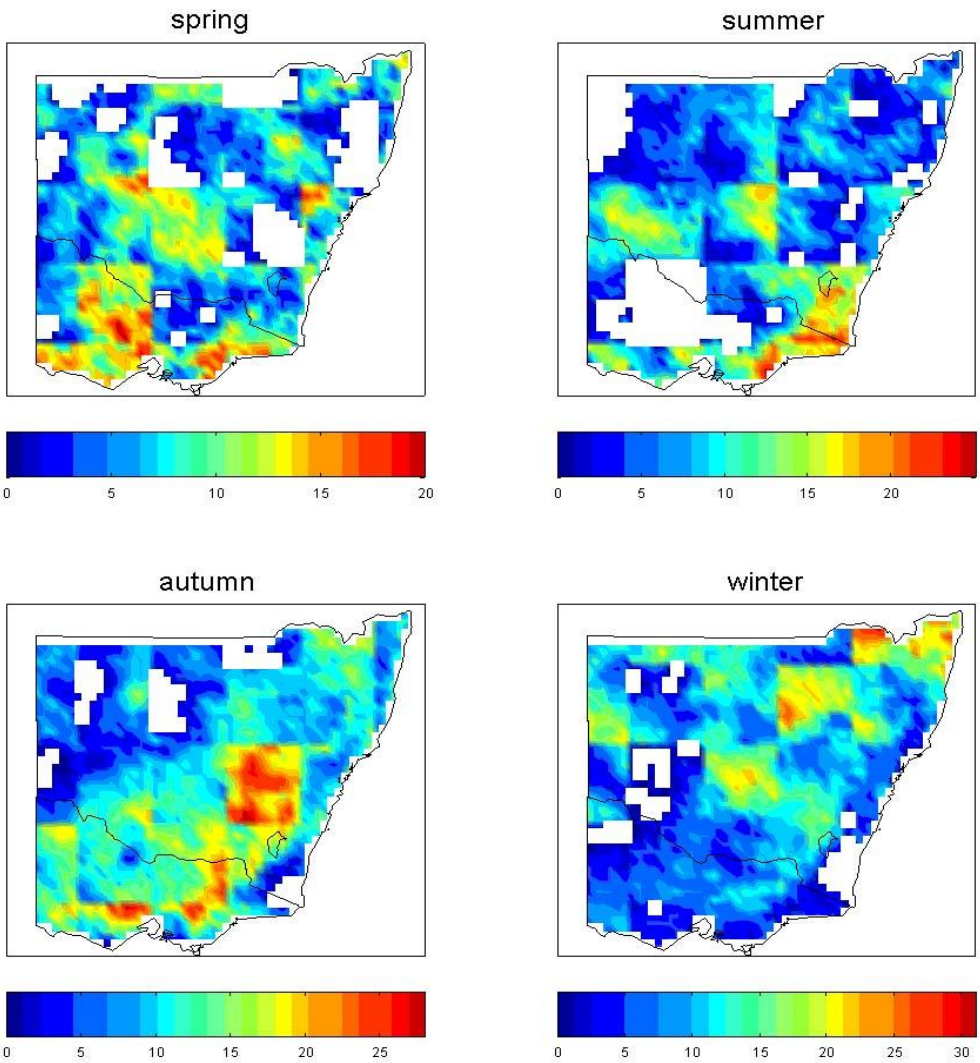

Fig. 5.5. Spearman Rank correlation (RC) differences in the seasonal precipitation downscaled with or without the seasonal resampling scheme SPP (%). The RCs are computed as the ensemble means of 500 runs at each grid in the validation period (1988-2008). The white area indicates no improvements.

Table 5.2. The ratios of the seasonal precipitation standard deviation (pSSNSD) for the downscaled results with and without the SPP scheme *versus* the observed values. Each value is an average across all the grids available in a particular zone per season. For the downscaled values, these statistics were derived from the ensemble of 500 runs in the validation period (1988-2008); 90% confidence intervals are shown in parentheses.

Season	Zone	SPP	NON-SPP
spring	E6	1.02 (0.76, 1.29)	0.92 (0.62, 1.24)
	G	1.14 (0.82, 1.16)	1.76 (0.66, 1.69)
	E4	0.79 (0.59, 0.99)	0.82 (0.57, 1.07)
	E3	0.82 (0.62, 1.02)	0.80 (0.58, 1.03)
	F4	0.97 (0.70, 1.24)	1.15 (0.81, 1.48)
	D5	0.91 (0.70, 1.13)	0.88 (0.65, 1.11)
	B2	0.95 (0.72, 1.16)	0.92 (0.70, 1.15)
	F3	1.07 (0.78, 1.37)	1.12 (0.79, 1.44)
	E2	0.97 (0.73, 1.21)	0.86 (0.62, 1.10)
summer	E6	1.34 (0.81, 1.46)	0.98 (0.69, 1.28)
	G	1.88 (1.25, 2.50)	1.57 (1.04, 2.11)
	E4	0.90 (0.66, 1.13)	0.80 (0.58, 1.02)
	E3	0.93 (0.69, 1.16)	0.83 (0.57, 1.05)
	F4	1.15 (0.88, 1.43)	1.21 (0.90, 1.52)
	D5	1.10 (0.82, 1.38)	0.98 (0.72, 1.24)
	B2	1.05 (0.80, 1.31)	0.99 (0.74, 1.23)
	F3	0.93 (0.70, 1.15)	0.93 (0.68, 1.17)
	E2	1.28 (0.90, 1.66)	1.14 (0.80, 1.48)
autumn	E6	1.05 (0.77, 1.33)	0.86 (0.60, 1.12)
	G	0.91 (0.66, 1.16)	0.94 (0.61, 1.27)
	E4	0.93 (0.70, 1.02)	0.77 (0.54, 0.99)
	E3	0.95 (0.72, 1.19)	0.76 (0.54, 0.97)
	F4	0.75 (0.55, 0.95)	0.54 (0.39, 0.70)
	D5	0.96 (0.72, 120)	0.74 (0.53, 0.95)
	B2	0.96 (0.73, 1.19)	0.75 (0.55, 0.95)
	F3	0.94 (0.70, 1.18)	0.69 (0.49, 0.89)
	E2	1.05 (0.78, 1.31)	0.84 (0.59, 1.10)
winter	E6	0.86 (0.63, 1.08)	0.84 (0.57, 1.12)
	G	1.07 (0.81, 1.34)	1.01 (0.55, 1.47)
	E4	0.70 (0.52, 0.88)	0.68 (0.47, 0.91)
	E3	0.75 (0.57, 0.93)	0.70 (0.50, 0.89)
	F4	0.93 (0.66, 1.19)	0.68 (0.46, 0.89)
	D5	0.89 (0.68, 1.09)	0.87 (0.66, 1.09)
	B2	0.81 (0.34, 0.98)	0.79 (0.62, 0.96)
	F3	0.69 (0.47, 0.90)	0.62 (0.43, 0.82)
	E2	0.96 (0.83, 1.18)	0.99 (0.73, 1.26)

The accuracy of the downscaling model related to inter-annual variance was assessed by using the standard deviations of the downscaled seasonal precipitation amount (pSSNSD). The ratios between downscaled results and observed values were presented in Table 5.2. The SOM-SD had a slight tendency to underestimate the inter-annual variance indicated by the below 100.0% values (between 80-100%). Nevertheless, the rations exceeded 100% in several cases. As a result of inserting the seasonal resampling scheme SPP into the SOM-SD, the most significant improvements mainly occurred in all of the climatic zones for autumn, meaning that the values in this season were closer to the perfect value of 100.0% and the enhancements of the values were generally above 20%. Subtle improvements occurred in other seasons.

5.3.2 Precipitation frequency

The SOM-SD performance of modeling seasonal mean precipitation days was compared at three different daily precipitation intensities of 0.1mm, 2.0mm and 20.0mm (nr001, nr020 and nr200) for both with and without SSP scheme (Figs. 5.6 – 5.8). For nr001, the SOM-SD showed significant improvements resulting from the SPP scheme for summer and autumn, some improvement for winter, but a slight deterioration for spring with the SPP scheme had a tendency to produce more precipitation days than the observed values (Fig. 5.6). Similar results were obtained for nr020 (Fig. 5.7). However, it was different for heavy precipitation (i.e., nr200). The SOM-SD could reproduce the nr200 with reasonable accuracy, irrespective of whether the SPP scheme was used (Fig. 5.8). The only significant improvements of introducing SPP scheme occurred in zone F4 for spring, summer and autumn.

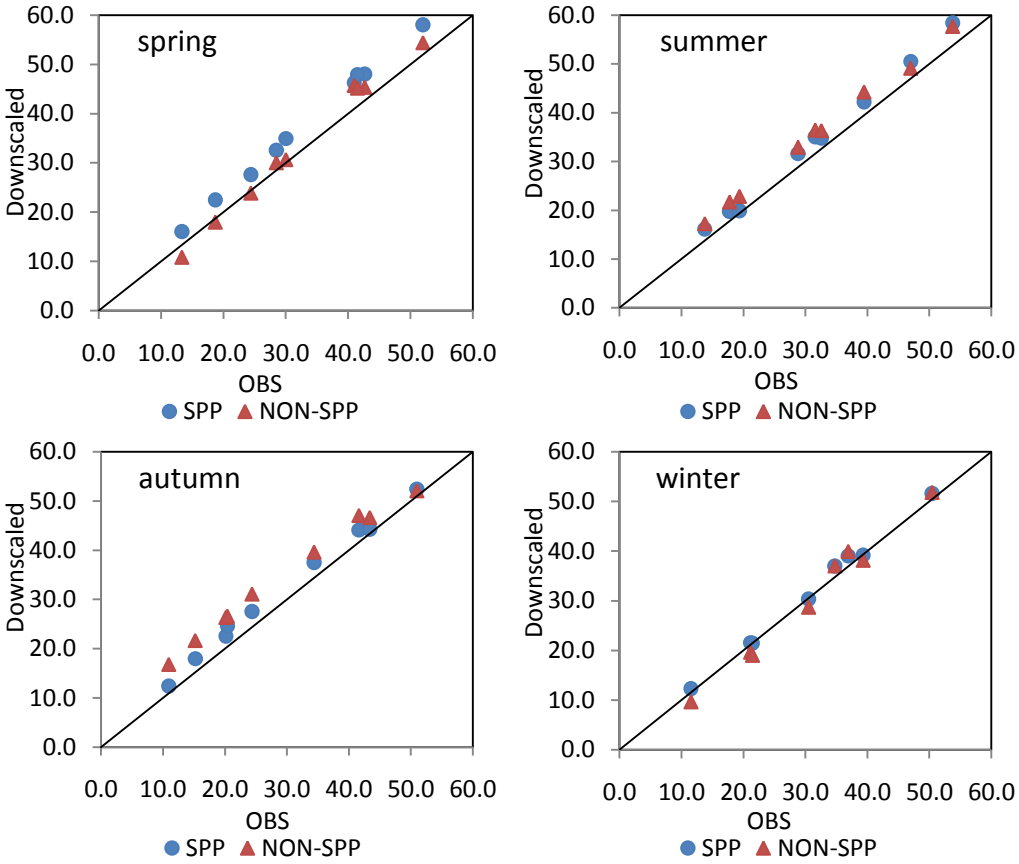

Fig. 5.6. Scatter of the seasonal precipitation days (nr001) for the observed values and the downscaled results with and without the SPP scheme, respectively.

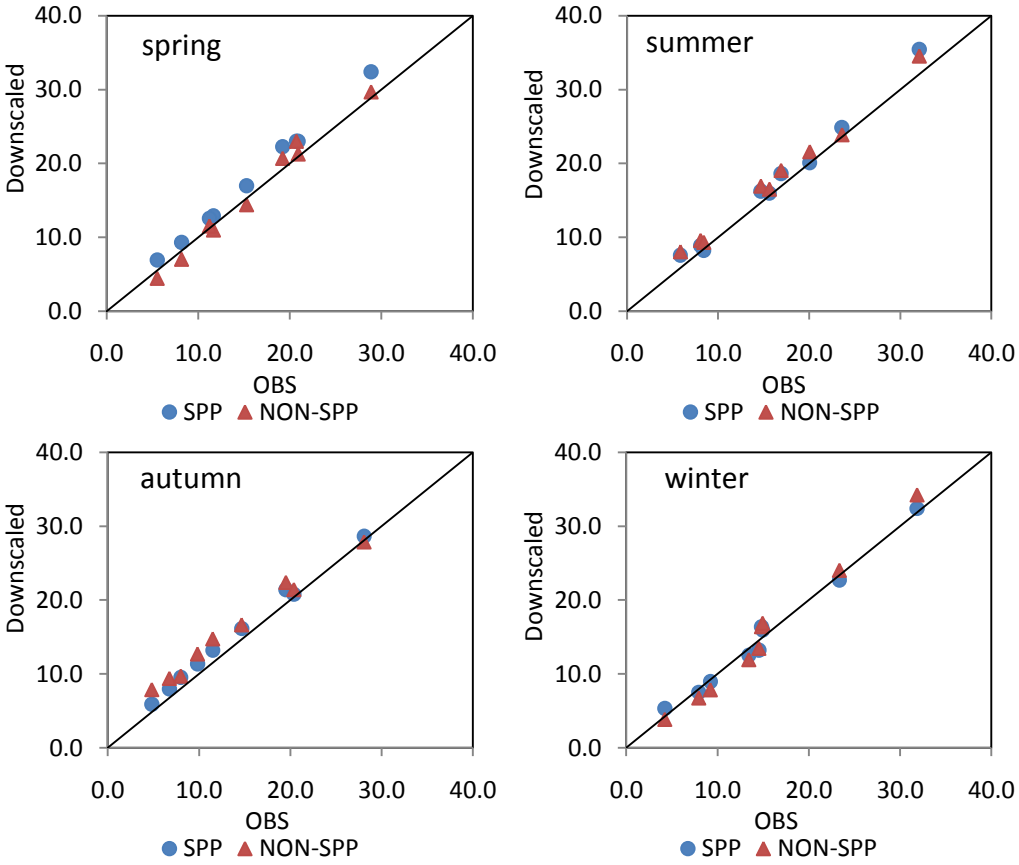

Fig. 5.7. As Fig. 5.6 but for nr020.

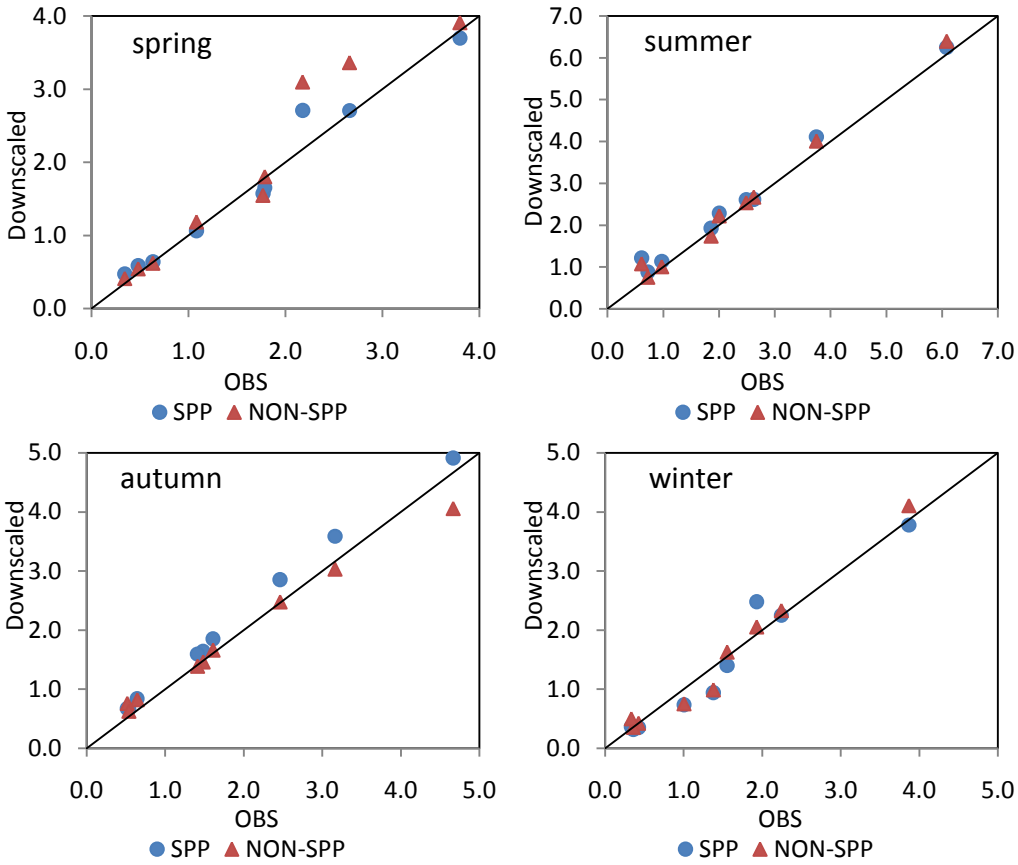

Fig. 5.8. As Fig. 5.6 but for nr200.

The ability of the SOM-SD to reproduce observed year-to-year variability of rainfall days (nr001) was analyzed by the rank correlation (Fig. 5.9). At 95% (α=0.05) statistical significance level, the correlations were generally between 0.45 and 0.60, with the best skill being for zone E2 of winter. No significant seasonal cycles was found in most climatic zones. The introducing SPP scheme led to a general improvement across the region for almost all season, with significant improvements taking place in autumn and winter. The biggest improvement occurred in zone B2 for autumn as the correlation doubled from 0.2 to 0.4. Other improvements with the SPP scheme were reflected with the narrowing in the 90% confidence intervals of these correlations (not shown).

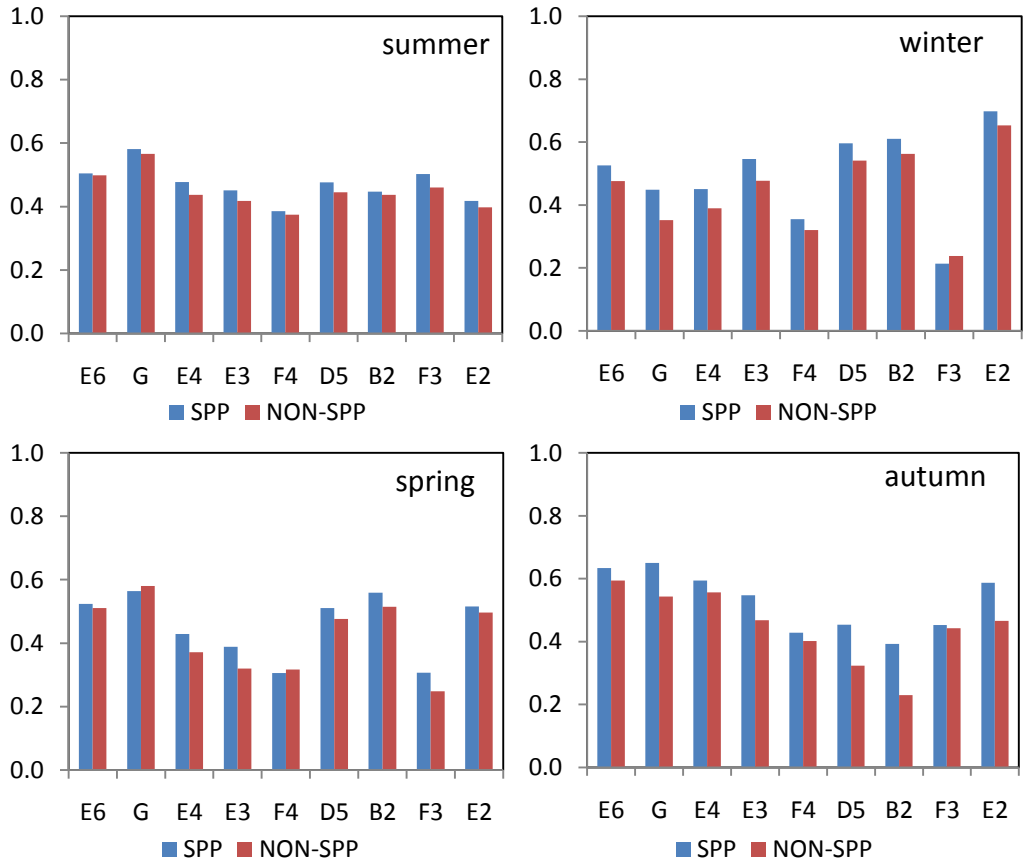

Fig. 5.9. Spearman Rank correlation of rainfall days (nr001) between the observed values and the SOM-SD downscaled results with and without the SPP scheme (SPP and NON-SPP). Each value is an average across all the grids available in a particular zone. The downscaled values were computed as ensemble means for 500 runs in the validation period 1988 - 2008. The X-axis shows the names of the nine climatic zones.

The ability of the SOM-SD to reproduce the mean wet-day and dry-day persistence was diagnosed using the indices of Pww and Pdd. The two indices represented the probability of a wet day followed by another wet day and the probability of a dry day followed by another dry day, respectively. As rainfall occurrence generally is represented as a first-order Markov process such that the rainfall state on the next day is related to the state of rainfall on a previous day (Gabriel and Neumann, 1962; Castellvi and Stockle, 2001), Pww and Pdd are obviously important Markov process parameters. The other two transitional probabilities (Pwd and Pdw) can be easily deduced from Pww and Pdd (Richardson and Wright, 1984). The SOM-SD generally reproduced well the observed multi-year mean wet-day persistence (Pww) (Table. 5.3) and dry-day persistence (Pdd) (Table. 5.4).

Table 5.3. The seasonal mean wet-day persistence of the observed values and the downscaled results with and without the SPP scheme (Pww). Each value is an average across all the grids available in a particular zone per season. For the downscaled values, these statistics were derived from the ensemble of 500 runs in the validation period (1988-2008); 90% confidence intervals are in parentheses.

Season	**Zone**	**OBS**	**SPP**	**NON-SPP**
spring	E6	0.47	0.35 (0.31, 0.38)	0.27 (0.23, 0.31)
	G	0.42	0.32 (0.28, 0.35)	0.20 (0.16, 0.25)
	E4	0.52	0.39 (0.36, 0.42)	0.32 (0.29, 0.36)
	E3	0.56	0.45 (0.42, 0.48)	0.39 (0.36, 0.42)
	F4	0.66	0.55 (0.52, 0.57)	0.53 (0.51, 0.56)
	D5	0.64	0.60 (0.58, 0.62)	0.56 (0.53, 0.58)
	B2	0.71	0.69 (0.67, 0.71)	0.64 (0.62, 0.66)
	F3	0.64	0.56 (0.54, 0.59)	0.52 (0.50, 0.55)
	E2	0.52	0.46 (0.43, 0.49)	0.41 (0.38, 0.44)
summer	E6	0.49	0.34 (0.30, 0.38)	0.32 (0.28, 0.35)
	G	0.46	0.33 (0.30, 0.37)	0.30 (0.27, 0.34)
	E4	0.59	0.45 (0.42, 0.48)	0.43 (0.40, 0.46)
	E3	0.59	0.47 (0.44, 0.50)	0.45 (0.42, 0.48)
	F4	0.75	0.69 (0.67, 0.71)	0.67 (0.65, 0.69)
	D5	0.58	0.46 (0.43, 0.49)	0.45 (0.42, 0.48)
	B2	0.63	0.53 (0.50, 0.55)	0.53 (0.50, 0.55)
	F3	0.69	0.61 (0.59, 0.63)	0.58 (0.56, 0.61)
	E2	0.49	0.32 (0.29, 0.36)	0.32 (0.29, 0.35)
autumn	E6	0.48	0.33 (0.30, 0.37)	0.31 (0.28, 0.35)
	G	0.47	0.27 (0.22, 0.31)	0.26 (0.22, 0.29)
	E4	0.57	0.39 (0.35, 0.42)	0.37 (0.34, 0.40)
	E3	0.57	0.42 (0.38, 0.45)	0.40 (0.37, 0.43)
	F4	0.74	0.62 (0.60, 0.65)	0.60 (0.58, 0.62)
	D5	0.60	0.50 (0.47, 0.52)	0.48 (0.45, 0.51)
	B2	0.65	0.55 (0.53, 0.58)	0.55 (0.53, 0.58)
	F3	0.67	0.54 (0.51, 0.56)	0.54 (0.51, 0.56)
	E2	0.51	0.39 (0.36, 0.42)	0.35 (0.32, 0.39)
winter	E6	0.49	0.35 (0.32, 0.38)	0.28 (0.24, 0.32)
	G	0.43	0.27 (0.24, 0,31)	0.15 (0.11, 0.19)
	E4	0.51	0.34 (0.31, 0.37)	0.27 (0.23, 0.30)
	E3	0.58	0.44 (0.41, 0.47)	0.38 (0.35, 0.42)
	F4	0.64	0.47 (0.44, 0.49)	0.44 (0.41, 0.47)
	D5	0.71	0.63 (0.61, 0.65)	0.61 (0.59, 0.63)
	B2	0.78	0.71 (0.69, 0.72)	0.70 (0.68, 0.72)
	F3	0.62	0.46 (0.44, 0.49)	0.46 (0.43, 0.49)
	E2	0.63	0.53 (0.50, 0.56)	0.49 (0.46, 0.52)

Table 5.4. The seasonal mean dry-day persistence of the observed values and the downscaled results with and without the SPP scheme (Pdd). Each value is an average across all the grids available in a particular zone per season. For the downscaled values, these statistics are derived from the ensemble of 500 runs in the validation period (1988-2008) and 90% of confidence intervals in parentheses.

Season	**Zone**	**OBS**	**SPP**	**NON-SPP**
spring	E6	0.86	0.79 (0.77, 0.83)	0.82 (0.81, 0.84)
	G	0.90	0.85 (0.84, 0.87)	0.89 (0.88, 0.90)
	E4	0.82	0.73 (0.71, 0.75)	0.76 (0.74, 0.78)
	E3	0.78	0.66 (0.64, 0.68)	0.69 (0.67, 0.71)
	F4	0.72	0.53 (0.50, 0.55)	0.53 (0.50, 0.55)
	D5	0.68	0.55 (0.53, 0.58)	0.56 (0.53, 0.58)
	B2	0.62	0.45 (0.42, 0.48)	0.47 (0.44, 0.50)
	F3	0.69	0.52 (0.49, 0.54)	0.53 (0.50, 0.56)
	E2	0.78	0.70 (0.68, 0.72)	0.71 (0.69, 0.73)
summer	E6	0.87	0.81 (0.80, 0.83)	0.78 (0.76 ,0.80)
	G	0.90	0.85 (0.84, 0.87)	0.83 (0.82, 0.85)
	E4	0.81	0.70 (0.68, 0.72)	0.67 (0.64, 0.69)
	E3	0.78	0.66 (0.64, 0.68	0.62 (0.60, 0.64)
	F4	0.64	0.42 (0.39, 0.45)	0.41 (0.37, 0.44)
	D5	0.76	0.66 (0.64, 0.68)	0.63 (0.60, 0.65)
	B2	0.71	0.58 (0.56, 0.61)	0.54 (0.51, 0.57)
	F3	0.65	0.50 (0.48, 0.53)	0.50 (0.47, 0.53)
	E2	0.86	0.81 (0.79, 0.82)	0.77 (0.75, 0.78)
autumn	E6	0.90	0.84 (0.83, 0.85)	0.79 (0.77, 0.80)
	G	0.93	0.89 (0.88, 0.90)	0.83 (0.82, 0.85)
	E4	0.88	0.80 (0.79, 0.82)	0.75 (0.73, 0.77)
	E3	0.85	0.75 (0.73, 0.77)	0.69 (0.67, 0.71)
	F4	0.68	0.51 (0.48, 0.53)	0.48 (0.45, 0.51)
	D5	0.76	0.65 (0.63, 0.67)	0.61 (0.59, 0.63)
	B2	0.71	0.59 (0.57, 0.61)	0.53 (0.51, 0.56)
	F3	0.71	0.57 (0.55, 0.60)	0.52 (0.50, 0.55)
	E2	0.86	0.78 (0.76, 0.80)	0.74 (0.72, 0.76)
winter	E6	0.85	0.80 (0.79, 0.82)	0.81 (0.79, 0.82)
	G	0.92	0.89 (0.88, 0.90)	0.90 (0.89, 0.91)
	E4	0.85	0.80 (0.78, 0.81)	0.81 (0.79, 0.82)
	E3	0.79	0.72 (0.70, 0.74)	0.72 (0.70, 0.74)
	F4	0.78	0.64 (0.62, 0.66)	0.62 (0.60, 0.65)
	D5	0.65	0.52 (0.49, 0.54)	0.49 (0.46, 0.52)
	B2	0.59	0.44 (0.41, 0.47)	0.41 (0.38, 0.44)
	F3	0.75	0.60 (0.58, 0.63)	0.58 (0.56, 0.61)
	E2	0.72	0.65 (0.63, 0.67)	0.64 (0.62, 0.66)

For Pww, the SOM-SD appeared more successful in the humid regions with the ratio of downscaled values to the observed being above 0.8 compared to the relatively dry regions where the ratio was around 0.6. This can be explained partly by the high frequency of precipitation events in the humid areas. The ratio was calculated as the mean of downscaled Pww *versus* observed Pww (values in Table 5.3). The SPP scheme made improvements in all climatic zones for the other three seasons except winter. Relative significant improvements occurred in the arid and semi-arid zones of E6, G, E4 and E3. For Pdd, it was reproduced more successfully than Pww as the downscaled Pdd was closer to the observed values (Table. 5.4). In semi-arid and arid zones of E6, G, E4, E3 and E2, the ratio was generally above 0.9. In relatively humid zones such as F3, F4, B2 and D5, the ratio was generally above 0.7. The lowest ratio occurred in zone F3 for summer (around 0.6). Thus, the SOM-SD appeared more skillful in the dry zones than in humid zones. The improvements on Pdd, as the result of the SPP scheme, mainly occurred in summer and autumn. Moreover, these improvements were spatially consistent across all climatic zones. In spring and winter, the SPP scheme did not degrade significantly the performance of the SOM-SD although some improvements occurred in several zones.

The inter-annual variability of Pww and Pdd was analyzed also by the rank correlation (RC) between the observed and the downscaled daily precipitation time series (represented as Pww_RC and Pdd_RC). The mean performance in each climatic zone is displayed in Figs. 5.10 and 5.11 for Pww_RC and Pdd_RC respectively. The SOM-SD could only reproduce the inter-annual variability of the wet and dry day persistence to a certain extent. For Pww_RC, the values generally were between 0.2 and 0.4. The SOM-SD appeared more successful in the two transitional seasons of spring and autumn than in summer and winter (Fig. 5.10). For the former, the Pww_RCs were generally above 0.25 and the maximum Pww_RC (above 0.5) occurred in the subtropical climate zone, F4, while the values were generally around 0.2 and the minimum value (below 0.1) occurred in the most dry desert zone G for the latter. The improvements resulting from the SPP scheme mainly occurred in spring. The biggest improvement reached 0.1 in the zones G and E4. In other seasons, the performance of the SOM-SD was almost identical irrespective of whether or not the SPP scheme was used. For Pdd_RC,

the SOM-SD also appeared more skillful in spring and autumn than in winter and summer (Fig. 5.11). For the former, the values of Pdd_RC were generally between 0.3 and 0.5, while for the latter they were between 0.2 and 0.35. The relatively significant improvements only occurred in zones G, E4 and E3 for spring, E6 and E2 for summer, G and F3 for autumn. However, the SPP scheme had adverse impacts in zone E2 for spring and autumn. Although the SOM-SD could only reproduce part of the year-to-year variability of wet and dry day persistence in each season, the results were comparable to other studies (Wetterhall et al., 2006; Yang et al., 2010).

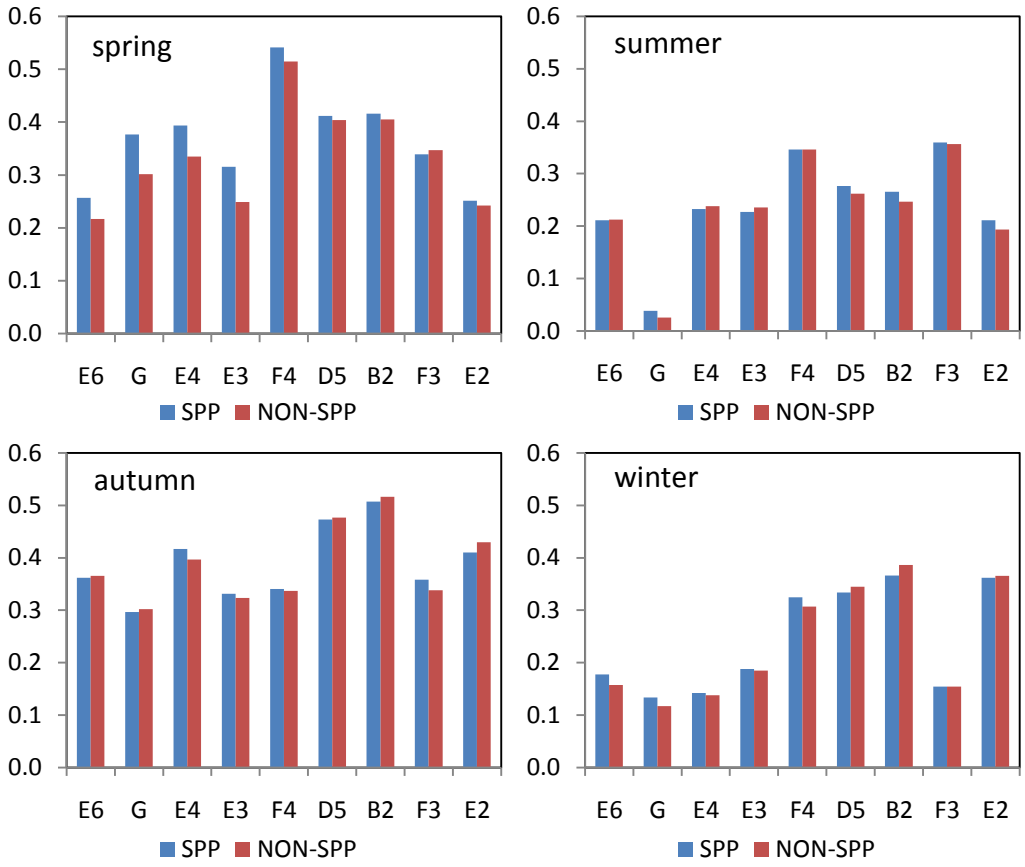

Fig. 5.10. As Fig. 5.9 but for Pww.

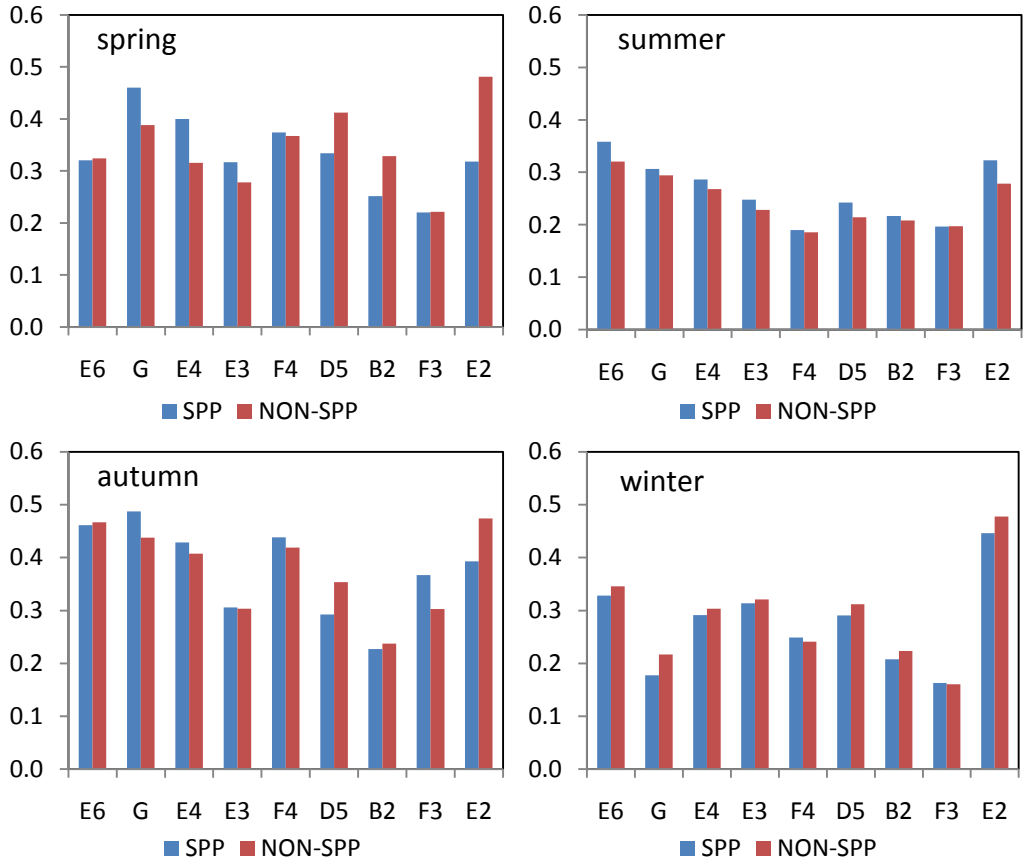

Fig. 5.11. As Fig. 5.10 but for Pdd.

As a precipitation event can be seen as a yes/no forecast, the Critical Success Index (CSI) would be a good measure of accuracy (Donaldson, 1975; Wilks, 2006). The CSI gives the correct ratio of precipitation events (i.e., yes events) downscaled by the SOM-SD. The results are given in Fig. 5.12. Again the better performance occurred in the relatively humid zones such as F4, F3, D5 and B2 with the values of CSI above 35%. For the relatively dry zones (E6, G, E4, E3 and E2), the values were generally between 20% and 30% and the best performance took place in zone E2 for winter (CSI>35%). There were no significant seasonal cycles, especially for the relatively dry zones. The main improvements from the SPP scheme occurred in the relatively dry zones for most of the seasons except for summer. The performance of SOM-SD in the CSI was relatively stable in the humid zones regardless of the SPP scheme.

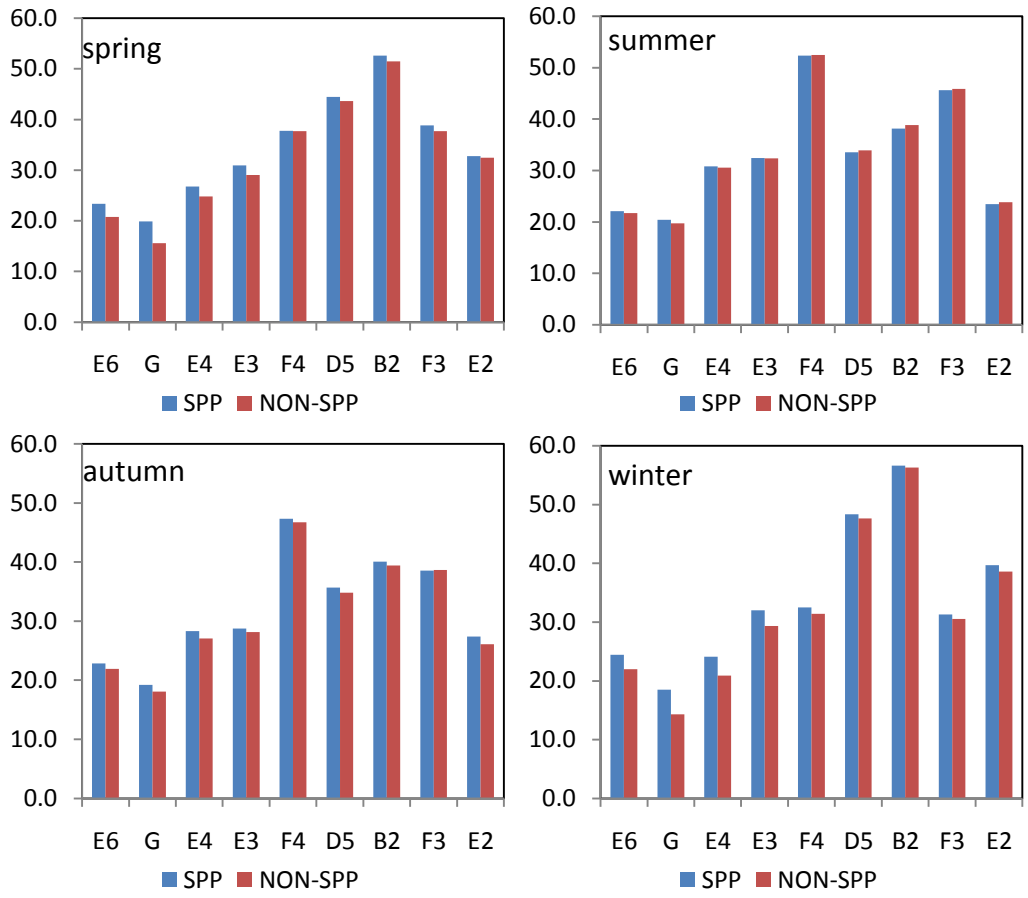

Fig. 5.12. As Fig. 5.10 but for CSI (%).

5.3.3 Extreme precipitation events

The climate changes induced by anthropogenic activities will be perceived mainly through increases in extreme weather during the 21st century (IPCC, 2001, 2007). It is always of particular interest for statistical downscaling to correctly reproduce the extreme events, particularly extreme rainfall events, which potentially have much greater socio-economic impact than the monthly mean. Here the 95% percentile value of the long-long precipitation time series was used as the threshold value for extreme precipitation (P95). Furthermore, the contribution of extreme precipitation events to annual total precipitation was taken into consideration as well (P95T).

The reproduction of the extreme events of P95 and P95T was very accurate (Figs. 5.13 and 5.14). For P95, the differences between the observed values and downscaled results were almost negligible in most of the climatic zones for all seasons (Fig. 5.13), irrespective whether the SPP scheme was applied. There was

no evidence that the SOM-SD had a bias toward either high or low values at the tails of the distribution. Only in zone G for summer, the P95 was largely overestimated. There were some subtle improvements resulting from the SPP scheme in some zones. The adverse effects of the SSP scheme mainly took place in zone G for summer and winter. In the case of P95T, there was no obvious seasonal cycle and the values were generally about 30% for each season (Fig. 5.14). For zones F4 and F3 for winter and autumn, and zone G for summer, P95T was greater than other zones for the corresponding seasons. These precipitation characteristics were captured by the SOM-SD very well. The SPP scheme caused significant improvements in most zones for spring, and some improvements in autumn. For the other two seasons, the improvements were almost negligible.

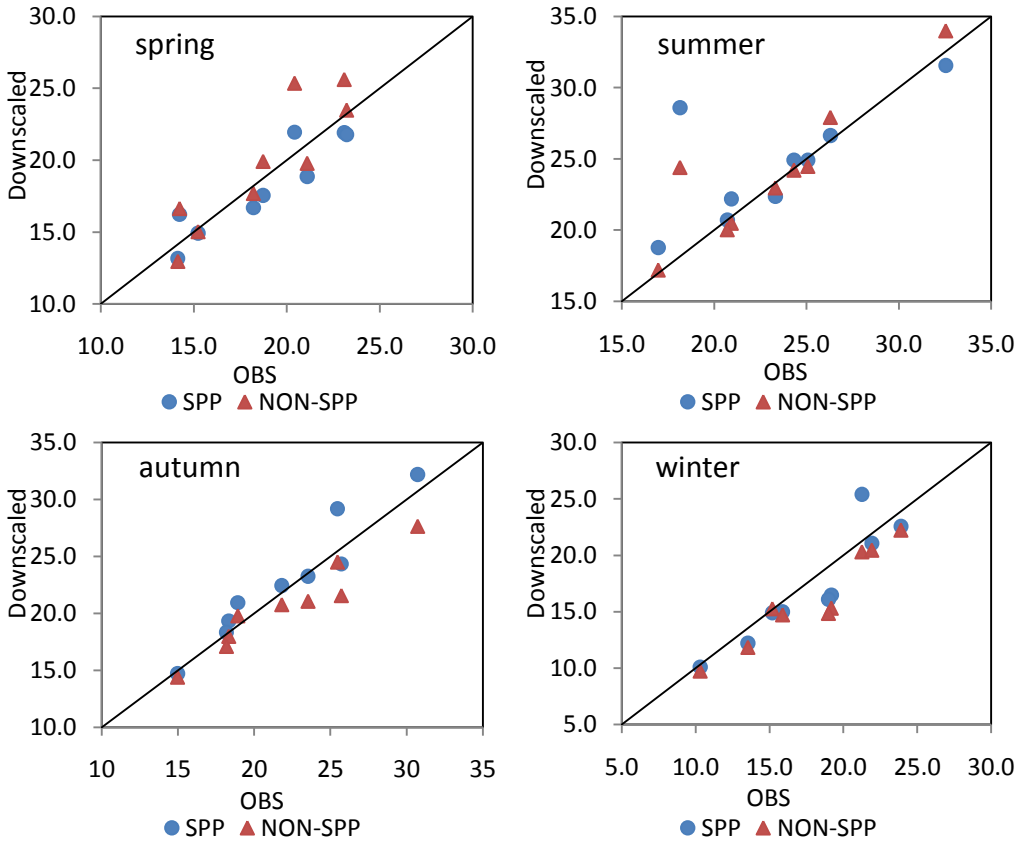

Fig. 5.13. As Fig. 5.6 but for P95.

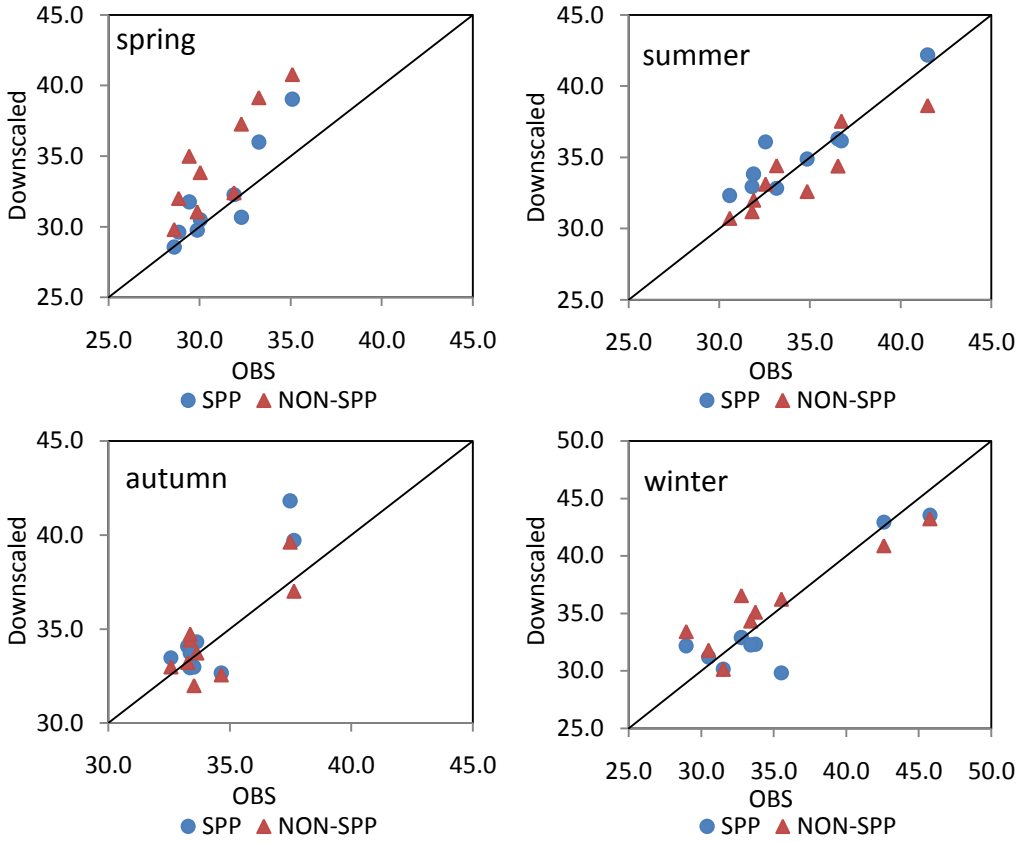

Fig. 5.14. As Fig. 5.13 but for P95T.

In addition, the analysis of the wet spells and dry spells is also of considerable importance for the management of water resources and policy making because of their strong socio-economic implications. The indices of CWD and CWW were used to analyze the ability of the SOM-SD to reproduce the observed maximum wet/dry spell. To a certain extent, the SOM-SD with or without the SPP scheme were both able to reasonably reproduce the observed maximum consecutive wet or dry days (CWD and CDD) but with slight underestimation (not shown). The differences between downscaled results from the SOM-SD with or without the SPP scheme were almost negligible. In the case of CWD, the biases generally lay between -5 and 5 days for each season, and the better reproduction occurs in spring followed by other seasons. For the CDD, the better performances occur in summer and winter (with a bias range between -10 to 10 days) rather than in spring and autumn. The poor performance mostly occurs in the arid or semi-arid inland areas (most in the climatic zone E6 and E2 in autumn, and E6, E2 and E3 in spring).

The underestimation over the CWD and CDD might be a consequence of two factors: data quality and the downscaling model itself. The data quality issue has been discussed in the previous chapters. Although the SOM-SD had a good ability to reproduce Pww and Pdd, namely the two important parameters of a first-order Markov process, there is a main deficiency associated with the first-order Markov model as it fails to reproduce well the long dry spells (Racsko et al., 1991; Guttorp, 1995; Semenov and Porter, 1995). It implies that the SOM-SD does not tend to generate long dry spells as well. In addition, the SOM-SD employed a stochastic re-sampling technique to select precipitation values, which would likely have had some impacts on the continuity of the precipitation time series.

The SOM-SD could also reproduce the observed year-to-year variability of the maximum wet and dry spell, but only to a certain extent. The variability was described as the rank correlation between the pair of observed and downscaled values, and then represented in Figs. 5.15 and 5.16, respectively, for CWD and CDD. Although the correlations appeared a little low for both indices, they showed significant seasonal cycles. For CWD, the SOM-SD gave higher correlations in spring and autumn than in summer and winter. For the former, the correlations were around or above 0.3 while the values were generally around 0.2 for the latter. The maximum and minimum values both occurred in zone G for spring and summer, respectively. The SPP scheme resulted in improvements mainly in the arid and semi-arid zones such as G and E4 for spring. In other cases, the improvements were generally negligible. However, the SPP scheme caused a significant adverse impact in zone B2 for winter. In the case of CDD, the SOM-SD appeared more skillful in some zones for spring and autumn with the correlations above 0.2. The SPP scheme could generate some main improvements in the arid and semi-arid zones for all seasons except for winter, and in all humid zones except B2 for autumn. The adverse impact of the SPP scheme occurred mainly in zones D5, B2 and E2 for spring.

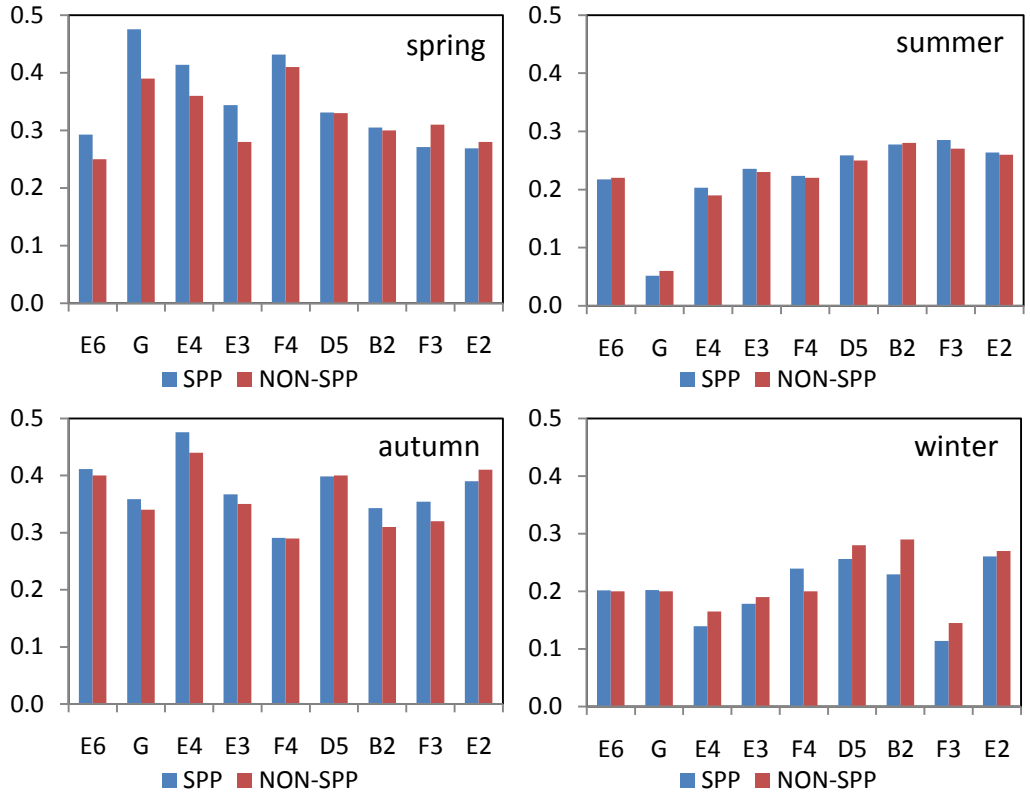

Fig. 5.15. Rank correlation of seasonal maximum consecutive wet days (CWD) for the observed values and the SOM-SD downscaled results with and without the SPP scheme (SPP and NON-SPP). Each value is an average across all the grids available in a particular zone. The downscaled values were computed as ensemble means for 500 runs in the validation period 1988 - 2008. The X-axis shows the names of the nine climatic zones.

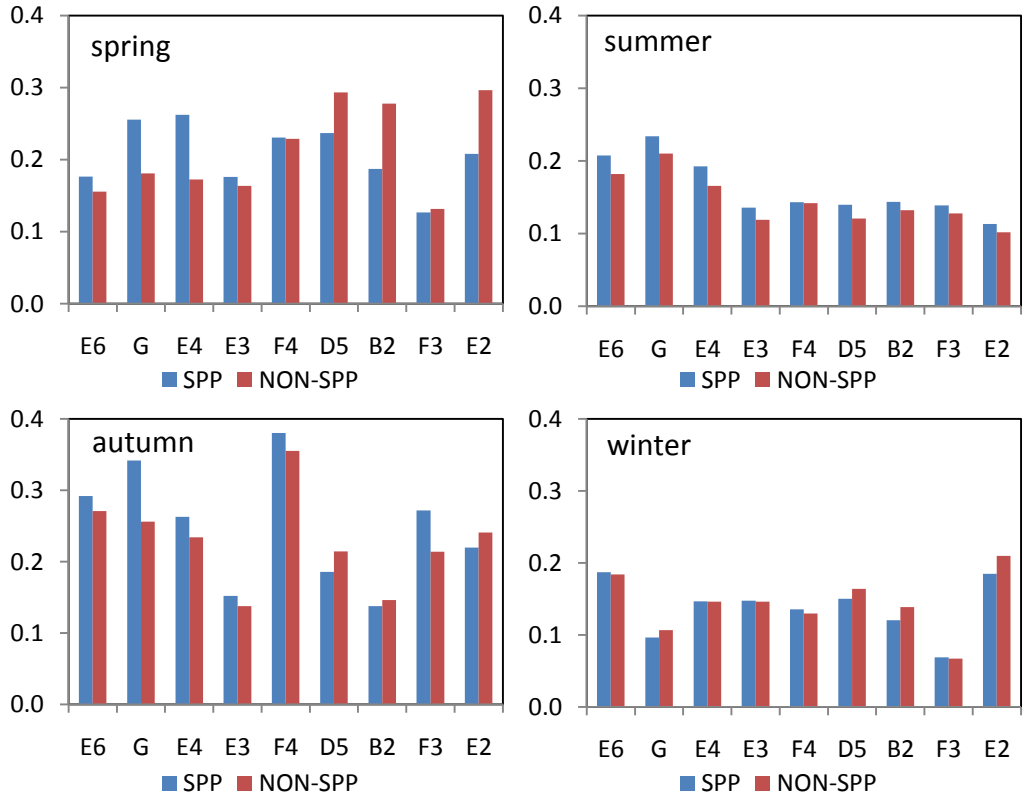

Fig. 5.16. As Fig. 5.15 but for CDD. Labels as for Fig. 2.2.

5.4 Conclusion and discussion

The SOM training procedure, one of the principal steps of the SOM-SD, does not consider the seasonality. Hence the attained synoptic patterns represent the generalized climate characteristics around each downscaling target precipitation grid during the calibration period. Due to seasonal variations of the atmospheric motions, the SOM training procedure can capture the seasonal information in the attained synoptic patterns, but in an implicit manner.

Nevertheless, it is worth noting that similar synoptic patterns are likely to appear in different seasons. Thus, the seasonality of precipitation itself does not require an explicit consideration when re-sampling a precipitation amount from a pattern. In this chapter, a seasonal re-sampling scheme was introduced to take the seasonality into consideration explicitly in the SOM-SD. All precipitation values mapped to a specific synoptic pattern were divided into 4 seasonal precipitation pools (SPP) according to their date-relevant seasons. Then, for a new input of predictors, the precipitation value was only re-sampled from the corresponding SPP under the synoptic pattern determined by the input data. Superimposed on that, the seasonality of precipitation itself is inserted into the SOM-SD explicitly.

The testing results from a series of diagnostic indices indicate that the SOM-SD performs well across different climatic zones. Overall not one particular zone stands out as a climatic entity where the downscaling skill in reproducing all statistical indices is consistently lower or higher across seasons, although the SOM-SD performance in the arid and semi-arid region is inferior to other regions owing to the extremely dry and hot climate conditions. The main conclusions for the SOM-SDs with or without the SPP are summarized as follows:

- Both approaches exhibit high skills in the average climatological statistics of the daily precipitation time series, including mean daily precipitation on wet days (SDII), rainy days (nr001, nr020 and nr200), wet/dry-day persistence (Pww and Pdd) and day-to-day precipitation variance on wet days (ppSD) in each season. However, the SPP scheme can produce significant improvements on the day-to-day and year-to-year variance (ppSD and pSSNSD), and the RMSE. For other indices, the improvements are dependent on the specific season or climatic zone under consideration. For example, the SPP scheme

would generate more drizzle events in spring than the observed values, but generate more accurate precipitation frequency in other seasons.

- Both approaches reproduce the observed extreme precipitation characteristics of P95 and P95T very well. Moreover, they can generate an acceptable skill in modeling the maximum consecutive wet/dry days (CWD and CDD). The SPP scheme makes significant improvement on the contributions of extreme precipitation events to annual total (P95T) than on the extreme precipitation values themselves (P95). For P95, the differences between them are almost negligible in most climatic zones and season.
- To a certain extent, both approaches can reproduce the inter-annual variability of the above indices. Moreover, they appear more successful in representing the year-to-year variability of the seasonal precipitation amount (SDII) and frequency (nr001) than other indices related to wet/dry day persistence such as Pww, Pdd, CWD and CDD. It is noticeable that the significant improvements on these indices resulting from the SPP scheme generally occurred in the two transitional seasons of spring and autumn. In the other two seasons of summer and winter, the improvements were usually subtle, although there are also some large improvements but these were dependent on climatic zone. This is because similar synoptic patterns occurs more often in the similar seasons (spring and autumn), rather than in the opposite seasons (winter and summer). Another important improvement is that the SPP scheme could effectively narrow the uncertainty range of the 90% confidence interval for each of the above assessment indices.

In summary, the classification of circulation patterns is good at capturing the representative local-scale precipitation regimes and *most of* the seasonality of both predictors and predictand, while the SPP scheme further strengthened the precipitation's own seasonality information in the SOM-SD. Such a combination was expected to allow for important precipitation characteristics such as conditional distributions of local simulated rainfall intensities and wet/dry spell behavior to be simulated more accurately than the approach based solely on large-scale synoptic patterns. However, it was found that the introducing of SPP scheme could only produce a subtle improvement in the skill of the SOM-SD. To some extent, it indicated that the NNR data embraced a good seasonality, while the SOM-SD could capture such seasonality very well. Thus, it appeared that the SPP

scheme was not necessary for the SOM-SD from NNR training. But the SPP scheme was very important for downscaling GCMs, which will be discussed in Chapter 8.

CHAPTER SIX

COMPARISON WITH RELATED DOWNSCALING MODELS

6.1 Introduction

As stated in Chapter 1, for the statistical downscaling family, there are many different approaches, which have been developed in the last decades. Generally, methods of statistical downscaling can be categorized into three groups: *regression models*, *weather typing schemes* and *stochastic weather generators* (Wilby and Wigley, 1997; Wilby et al., 2004). Irrespective of their particular formlations, they all share the same theoretical framework comprising some kind of mapping (statistical relationship) between large (or larger) scale predictors and the expected value of a local-scale predictand (Giorgi and Mearns 1991; Maraun et al., 2010). Each category of methods has their relative strengths and weakness, so a wide variety of combinations also exist. For instance merging neural networks and clustering analysis as the SOM-SD proposed in this thesis, or merging analog method and canonical correlation (e.g. Fernández and Sáenz, 2003).

The SOM-SD combines the advantages of a synoptic classification method based on the SOM algorithm (Kohonen, 2001) and a stochastic re-sampling technique. The downscaling methods most comparable to the SOM-SD are the unconditional stochastic and the analog methods (Zorita and von Storch 1999; Imbert and Benestad, 2005). In this chapter, the three methods are compared by producing gridded time series of precipitation. The focus is put on whether the SOM-SD model can perform better and provide more information than its simpler counterparts, the analogue model in particular.

6.2 Related models

6.2.1 Unconditional stochastic re-sampling model

The stochastic re-sampling technique is commonly used in the weather generators (WGs, Giorgi et al., 2001; Wilby et al., 2004). Early versions of WGs, such as WGEN (Richardson, 1981; Richardson and Wright, 1984), SIMMETEO (Geng et al., 1986, 1988), MARKSIM (Jones and Thornton, 2000) and EARWIG (Kilsby et al., 2007), are statistical models and mainly used to stochastically generate weather time series of (usually several) local weather variables that resemble the statistical properties of observed weather. The weather sequences are generally employed for agricultural and hydrological modeling studies in case that weather observations are too short or have missing data (Thornton et al., 1994; Neitsch et al., 1999; Yang et al., 2005). However, these early WGs are only based on the local observations, i.e. they do not directly use large-scale predictors, which is also called unconditional model. WGs were also developed by conditioning their parameters on large-scale atmospheric predictors, which made them conditional models and were used in statistical downscaling (Katz, 1996; Semenov and Borrow, 1997; Mehrotra et al., 2006; Khalili et al., 2009).

In this study, a simple unconditional stochastic re-sampling model was employed as a benchmark to compare with the SOM-SD. A precipitation value on a target day during the validation period was randomly selected directly from the calibration data according to the most relevant season. The procedure was repeated for multiple times to explore all possible precipitation states for that day. Thus, no model parameters were acquired, which is different from a common unconditional weather generator. Strictly speaking, the unconditional stochastic re-sampling model used in this study is not a downscaling model as it takes no account of the large-scale patterns, and therefore could not be applied to a future projection. In addition, the observed precipitation data were not fitted into a theoretical distribution such as gamma (e.g., Aksoy, 2000), Log-Logistic (e.g., Shouki et al., 1988) or exponential distributions (e.g., Madi and Raqab, 2007). This is because a single statistical distribution would not always work well (Vlček and Huth, 2009), let alone for a region with very complicated climate types and orographic features such as the case study area in this study. Therefore, only the empirical distribution (i.e., sorted arrays of observations) was used.

6.2.2 Analog model

Perhaps, the analog model (AM) is the simplest statistical downscaling method. The method has a long history in the field of weather forecasting (Lorenz 1969; Kruizinga and Murphy 1983) and short-term climate prediction (Barnett and Preisendorfer 1978; van den Dool 1994). Recently, the method and its derivatives have been widely used as downscaling tools across different regions due to its simplicity (Zorita et al. 1995; Cubasch et al. 1996; Biau et al. 1999; Wetterhall et al., 2005; Hidalgo et al., 2008; Timbal et al., 2009). The basic idea behind the analog model is that the local variable such as precipitation and temperature on a day is completely determined by the large-scale synoptic pattern on that day. Hence, if one could find an exact analog in the historical daily record to the projected day in the future, the predictand in the projected future should replicate the predictand value determined by historical analog (Zorita and von Storch, 1999; Obled et al., 2002). A major problem associated with this method is that it needs sufficiently long high-quality observations, so that a reasonable analog of the large-scale circulation can always be found.

The analog of the target day during the validation period is selected by analyzing circulation patterns of the predictor fields during calibration period. In this study, the entire time series during the calibration period was used to select the analog. The predictors used and other configuration for this model can be found in Sector 6.3. The target predictand $S(t)$ at time *t* is simulated by selecting the predictand at the time *u*, at which the characteristics of the predictor $F(u)$ most closely resemble those of the target predictor $F(t)$. The predictor $F(u)$ is called the analog to $F(t)$.

$$\hat{S}(t) \in S(u) \;\; u \in U,\; t \notin U,\; U \in T,\; (u,t) \in T$$

The analog is then selected as the time that minimizes:

$$min\|F(U) - F(T)\| \qquad (6.1)$$

where $\|\ \|$ is the Euclidean distance used as a similarity measure between $F(U)$ and $F(T)$. Next, a predictand (precipitation in our case) value is re-sampled from the calibration period according to the selected analog. The above procedure is

repeated over the whole validation period to generate a whole time series of the predictand.

The most significant benefit of this method is that it is very easy to use and does not need too many computing resources. Furthermore, it does not make any assumptions about underlying distribution of the predictand and is good at preserving the spatial correlation of the predictand. In many cases, the AM performs equivalent to the more complicated methods, and therefore used as a benchmark in the field of statistical downscaling (Zorita and von Storch, 1999). The AM has been successfully used for downscaling precipitation and temperature for most of the Australia (Timbal and McAvaney, 2001; Timbal et al., 2009). However, the method has a well-known drawback that it is incapable of predicting new daily records, because the predicted values are only taken from archives from past observations (Imbert and Benestad, 2005; Hidalgo et al., 2008; Timbal et al., 2009). Even for a stationary process, new record-breaking values are expected to occur with time, albeit at successively longer intervals, which possibly limits the validity in a perturbed climate (Zorita and von Storch, 1999).

6.2.3 SOM-SD

Synoptic climatology provides a powerful method to study the large-scale driver (regimes) of a region- (local-) scale climate (Barry and Perry, 2001), especially for precipitation (Hewitson and Crane, 2002; Hope et al., 2006; Cassano et al., 2007; Finnis et al., 2009). The SOM-SD belongs to the field of synoptic climatology. It employs the Self-Organizing Maps (SOM) algorithm (Kohonen, 2001) as a core technique to analyze the general characteristics (patterns) of large-scale circulation for predictors on a physically meaningful basis, which is a typical clustering analysis procedure. During the analysis process, the Euclidean distance is used to measure the similarity between patterns. Then by mapping the observed precipitation to these patterns, the synoptic forcing of local precipitation is identified, which may be hidden by monthly or seasonal mean fields (Barry and Perry, 2001; Hewitson and Crane, 2002; Hanson et al., 2004; Cassano et al., 2007).

The predictand data (observed precipitation) in the calibration period were mapped to the obtained synoptic patterns, and then the predictand values under each synoptic pattern were used to construct a corresponding predictands-

candidate-data-bank (PCDB), after identifying all possible synoptic patterns around the target grid according to the predefined number of SOM nodes(i.e., creating a SOM). To strengthen the seasonality of precipitation, the SOM-SD further divides each PCDB into four seasonal precipitation pools (SPPs) according to the season associated precipitation value under the PCDB. Thus, the synoptic regimes of precipitation were identified through the relationship between large-scale predictors and predictand. For a target day for downscaling during the validation period, the SOM-SD uses the predictors on that day to find the best matching synoptic pattern (BMSP), and in turn to find the SPP under the corresponding PCDB. Finally, *downscaling* for the target day is achieved by stochastically extracting predictand values from the relevant SPP. All resampled values shares the common precipitation regimes so that the precipitation states are explored as much as possible.

6.2.4 The relationship among the three models

From the above descriptions, it is clear that the SOM-SD shares a similar synoptic climatology foundation with the AM. They both belong to indirect statistical downscaling methods, meaning that the relationship between large-scale predictors and predictand are connected through synoptic patterns instead of the direct link between them such as regression relationship (e.g., Li and Smith, 2009; Chu et al., 2010). The most significant difference between the SOM-SD and the AM is that the pattern found by the AM is a specific pattern, while the pattern found by the SOM-SD is a generalized pattern attained by a clustering analysis, although the SOM-SD and the AM both aim at finding the most similar synoptic pattern from the historical data.

In addition, the SOM-SD used a stochastic re-sampling technique to select the precipitation values from the SPP determined by the pattern found. From this point of view, the SOM-SD is similar to the above unconditional stochastic re-sampling method (hereafter called unconditional model). However, the unconditional model is not conditioned on the synoptic pattern. Hence, the range for re-sampling precipitation values is wider in the unconditional model than in the SOM-SD.

6.3 Configuration of models

The comparison study was carried out by applying the same training data set to all models. For each downscaling target grid, the SOM-SD used a spatial domain of 3×3 grids for predictors and a total number of 5×7 for SOM nodes. The chosen predictors were SLP, Q5, T7 and Pr (see Table 2.3). The same procedure described in Chapter 4 was also used to select predictors for the AM. It was very interesting that the predictors and spatial domain used by SOM-SD was very suitable for the AM. This could be attributed to the fact that the SOM-SD and AM shared the same synoptic climatology basis. In this study, the time window for AM to select the analog was assigned as ±45 days following the previous studies of Timbal et al. (2009) and Hidalgo et al. (2008). That is to say, the analogue had to be selected from the same time of year as the downscaled one. For example, if the day to simulate was 15 January, then the analogue could be selected between 1 December and 28 February any year of the training period (Wetterhall et al., 2005). It was worth noting that an equal weight was given to each predictor in the SOM-SD and the AM. The unconditional model also generated an ensemble of 500 runs for the downscaled precipitation time series as was the case for the SOM-SD.

Precipitation distribution in the case study area is highly affected by elevation, and precipitation amounts show distinct seasonal cycles in some climatic zones, with the largest variability happening in summer. All of the three downscaling methods took the seasonality into consideration, but dealt with through different approaches. Seasonality was considered implicitly in the unconditional model so that a precipitation could only be selected from training periods in the same season around the target day. The AM also considered seasonality implicitly by using a time window, i.e., 45 days before and after the target day in the training dataset. The SOM-SD included seasonality semi-implicitly, meaning that large-scale synoptic pattern seasonality was attained through the use of seasonal variation of the predictors themselves, while precipitation seasonality was explicitly considered using the seasonal precipitation pool (SPP).

Since precipitation is inherently a stochastic and non-linear process, the evaluation was focused on the statistical properties. The evaluations of the three methods were carried out in a seasonally stratified style in order to check

seasonality performance of the methods. Table 1 summarizes the applied indices. The indices represented the statistics of daily precipitation with regard to both precipitation amount (SDII, ppSD, RMSE, pSSNSD) and frequency (nr001, nr200, Pww, Pdd), as well as extreme events (P95, P95T, CWD, CDD). In addition, the Spearman rank correlation (Corder and Foreman, 2009) calculated from the observed and downscaled daily precipitation time series was employed to analyze the ability of the three methods to reproduce the inter-annual variability for the above assessment indices.

As mentioned before, an ensemble of 500 simulations was generated by the unconditional model and the SOM-SD, and therefore the assessment indices listed above were expressed as ensemble means with their 90% confidence intervals computed with a bootstrapping procedure (Efron and Tibshirani, 1993; Davison and Hinkely, 2006; Dibike et al., 2008). Without specification, only the ensemble means were used to compare with the observed values. A wet day is defined as a day with daily rainfall greater than or equal to 0.1 mm.

Table 6.1. Assessment indices for downscaled daily precipitation.

Acronym	***Definition***	***Unit***
SDII	Simple daily intensity(mean daily precipitation on wet days)	mm/day
ppSD	Standard deviation of daily precipitation on wet days	mm/day
RMSE	Root mean square error of daily precipitation time series	mm/day
nr001	Mean number of rainy days for daily precipitation >=0.1mm	Day
nr200	Mean number of rainy days for daily precipitation >=20.0mm	Day
pSSNSD	Standard deviation of seasonal precipitation	mm/season
P95	95-th percentile value of precipitation (extreme precipitation)	mm/day
P95T	Percentage of rainfall from events beyond 95-th percentile value of overall precipitation	%
Pww	Mean wet persistence	%
Pdd	Mean dry persistence	%
CWD	Maximum consecutive wet days	Day
CDD	Maximum consecutive dry days	Day

6.4 Results

6.4.1 Precipitation amount

The summary of RMSE across all of the climatic zones and seasons is listed in Table 6.2, where each value is an average across all the grids available in a particular zone per season. The AM only provides a single time series with the same length to the validation data, so it is a deterministic downscaling method. The SOM-SD and the unconditional model are stochastic methods and provide an ensemble of 500 runs, with the 90% confidence intervals also represented in parentheses in the table. Compared with the ensemble means of the SOM-SD and the unconditional model, the AM gives the smallest RMSE across all of the climatic zones for all seasons, which indicates that the AM performs better than the other two stochastic models. This is not surprising, as the AM was designed to find the only best one analogue precipitation day from the history. At the same time, RMSE values of the ensemble means of the SOM-SD are smaller than those of the unconditional for all climatic zones in each season. Moreover, the SOM-SD shows relative high skill for summer, autumn and winter, with about half of their 90% confidence intervals being able to cover the best RMSE from the AM (Table 6.2) for these 3 seasons. Such a case occurs only once for the unconditional model in the zone G for summer.

The ability of the three models to reproduce the observed probability distribution functions (PDFs) was evaluated by looking at the first two moments of the PDFs: the mean (SDII) and the standard deviation (ppSD) on wet days, shown in Figs. 6.1- 6.2, respectively. On each figure, the left panels give the comparison for the SOM-SD, while the right panels for the unconditional model. SDII was very well reproduced by the three models (Fig. 6.1). There are no statistically significant differences between the SOM-SD and the unconditional model. In most cases, both the observed values and values simulated by the AM could be covered by the SOM-SD and the unconditional model inside their 90% confidence intervals. Compared with other models, SDII is underestimated by the AM almost in all cases, particularly in spring, when the values were all below the SOM-SD and the unconditional model. The ensemble means of the SOM-SD and the unconditional model were generally above the corresponding values for the AM in most cases, and were closer to the observed values, which indicated that the two models performed better than the AM.

Table 6.2. The root mean square error (RMSE). Each value is an average across all the grids available in a particular zone per season. For the SOM-SD and the unconditional model, these statistics are derived from the ensemble of 500 runs in the validation period (1988-2008); 90% confidence intervals are in parentheses. The numbers in bold indicate that confidence intervals could cover the values from the AM.

Season	Zone	AM	SOM-SD	Unconditional
Spring	E6	3.63	3.96 (3.63, 4.29)	4.15 (3.82, 4.48)
	G	3.01	3.38 (3.09, 3.68)	3.35 (3.07, 3.64)
	E4	4.84	5.46 (5.07, 5.85)	5.80 (5.42, 6.19)
	E3	5.93	6.52 (6.15, 6.88)	7.03 (6.66, 7.40)
	F4	8.03	9.75 (8.80, 10.70)	10.49 (9.51, 11.48)
	D5	6.27	6.87 (6.44, 7.29)	7.40 (6.97, 7.82)
	B2	8.72	9.65 (9.13, 10.18)	10.49 (9.97, 11.01)
	F3	8.53	10.01 (8.89, 11.13)	10.47 (9.37, 11.56)
	E2	4.10	4.48 (4.16, 4.81)	4.82 (4.48, 5.15)
Summer	E6	5.55	6.12 (***5.43***, 6.81)	6.35 (5.66, 7.04)
	G	6.16	6.97 (***5.64***, 8.30)	7.18 (***5.79***, 8.54)
	E4	8.38	9.12 (8.16, 10.07)	9.42 (8.52, 10.33)
	E3	8.06	8.98 (8.24, 9.72)	9.41 (8.67, 10.16)
	F4	14.45	15.36 (14.20, 16.51)	16.34 (15.17, 17.51)
	D5	6.84	7.34 (***6.77***, 7.91)	7.70 (7.13, 8.28)
	B2	8.04	8.69 (8.14, 9.24)	9.17 (8.62, 9.73)
	F3	11.25	12.23 (***11.20***, 13.26)	12.98 (11.96, 14.01)
	E2	4.99	5.02 (***4.47***, 5.57)	5.15 (4.61, 5.69)
Autumn	E6	4.12	4.71 (4.17, 5.25)	5.01 (4.47, 5.54)
	G	3.59	4.10 (***3.59***, 4.61)	4.17 (3.68, 4.67)
	E4	5.86	6.78 (6.21, 7.35)	7.21 (6.66, 7.75)
	E3	6.50	6.85 (***6.30***, 7.40)	7.36 (6.81, 7.91)
	F4	12.71	14.96 (13.52, 16.40)	16.49 (15.00, 17.99)
	D5	6.17	6.56 (***6.03***, 7.10)	7.27 (6.71, 7.83)
	B2	7.19	8.60 (7.96,9.23)	9.67 (8.99, 10.35)
	F3	10.86	11.73 (***10.55***, 12.91)	12.65 (11.41, 13.86)
	E2	4.02	4.22 (***3.86***, 4.58)	4.67 (4.29, 5.05)
Winter	E6	3.22	3.52 (3.26, 3.79)	3.72 (3.45, 3.99)
	G	2.78	3.03 (***2.76***, 3.29)	3.19 (2.94, 3.45)
	E4	4.40	4.92 (4.61, 5.24)	5.30 (4.96, 5.64)
	E3	5.24	5.73 (5.40, 6.05)	6.23 (5.87, 6.58)
	F4	8.35	10.43 (9.26, 11.60)	11.32 (10.05, 12.59)
	D5	5.84	6.50 (6.10, 6.90)	7.00 (6.59, 7.41)
	B2	9.02	9.83 (9.35, 10.32)	10.70 (10.18, 11.21)
	F3	9.16	10.94 (9.96, 11.92)	11.43 (10.41, 12.46)
	E2	3.55	3.76 (***3.51***, 4.02)	4.02 (3.76, 4.28)

Figure 6.2 showed the results for the reproduction of the standard deviation (ppSD). The AM has a tendency to underestimate the observed variance such that the downscaled values by the AM were generally below the observed values. Moreover, they were also below the ensemble means of other two models (i.e., SOM-SD and the unconditional model). The variance underestimation is a known issue for regression-based statistical downscaling methods (Von Storch, 1999) and for the AM (Timbal et al., 2009). This variance underestimation by the AM is relatively small, which is of the order of 5 – 15%, with the largest underestimations in spring. However, it was not the case for the SOM-SD, and the unconditional model. Their 90% confidence intervals were able to cover the observed variances in most of the cases. In terms of ensemble means, the SOM-SD could reproduce almost 100% variance of the observed daily precipitation time series with an exception in winter when the variance was underestimated to the order of 10%. The best performance was acquired by the unconditional model, which is based on a pure stochastic re-sampling technique, since the model could completely reproduce the observed variance irrespective of the climatic zones and seasons. Thus, the stochastic models including the SOM-SD and the unconditional model had a stronger capacity for modeling the variance than the deterministic model of AM. This implies that the ability of a deterministic model in this aspect can be improved significantly by inserting a stochastic component.

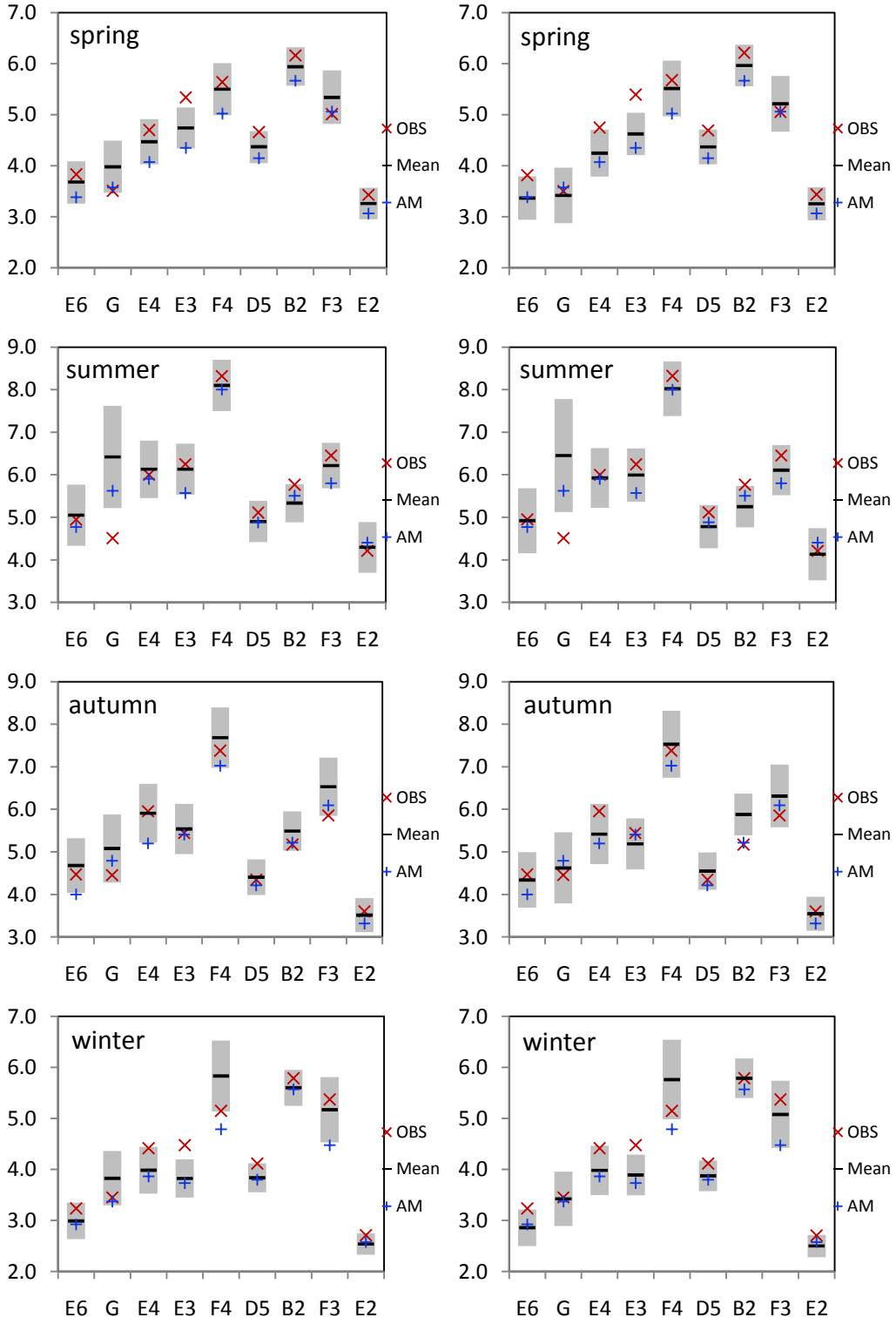

Fig. 6.1. Plot of the downscaled *versus* observed (OBS) daily mean on rainy days (SDII, mm/day). On each graph, each value is an average across all the grids available in a particular zone. The downscaled SDIIs are computed as ensemble means with 90% confidence intervals of the ensemble for 500 runs in the validation period 1988 - 2008. The X-axis shows the names of the nine climatic zones. Left panels for the SOM-SD, right panels for the unconditional model.

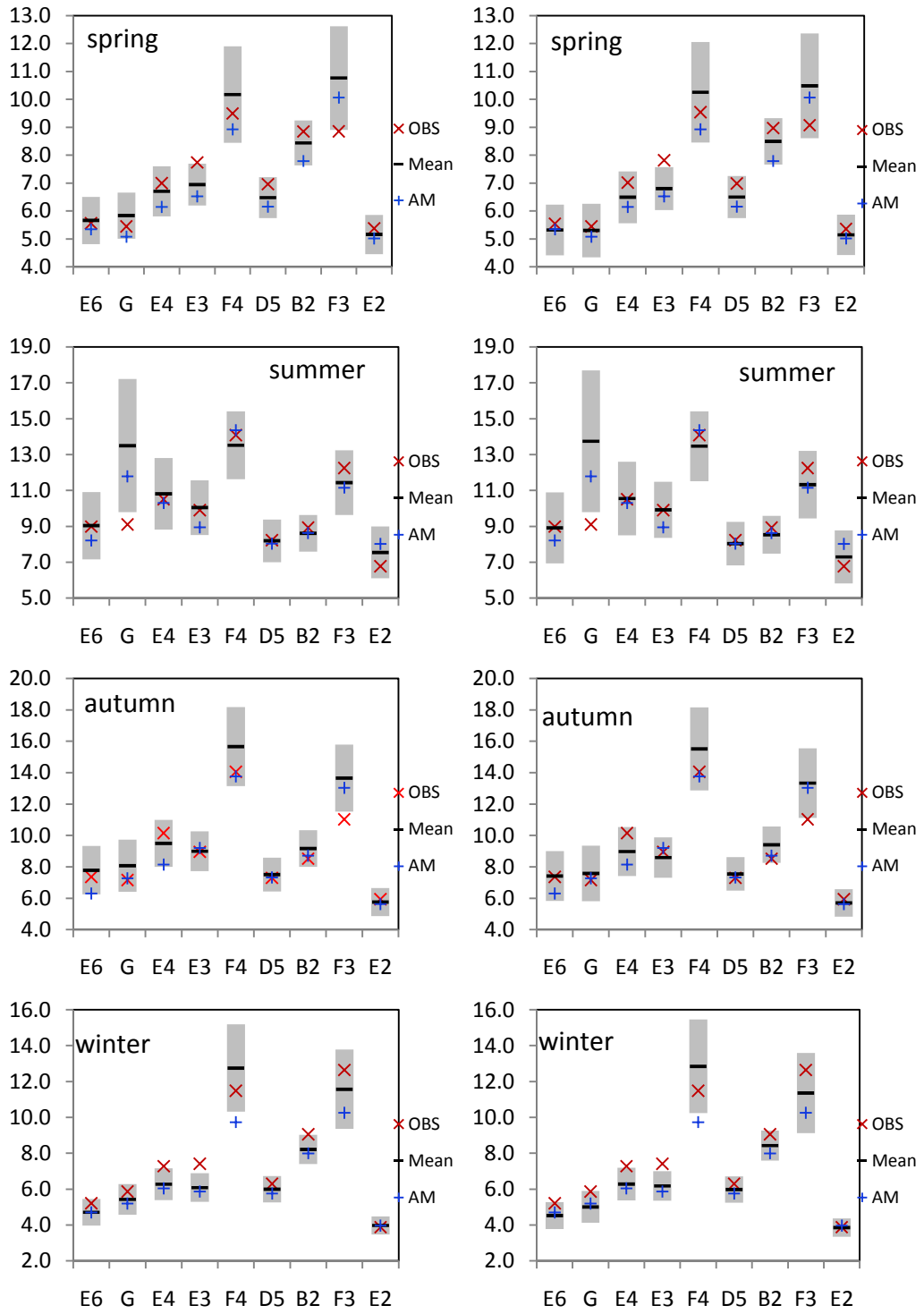

Fig. 6.2. Plot of the downscaled *versus* observed standard deviation on rainy days (ppSD). On each graph, each value is an average across all the grids available in a particular zone. The downscaled SDIIs are computed as ensemble means with 90% confidence intervals of the ensemble for 500 runs in the validation period 1988 - 2008. The X-axis shows the names of the nine climatic zones. Left panels for the SOM-SD, right panels for the unconditional model.

The three models were further analyzed of their ability to produce inter-annual variance of seasonal total precipitation time series (pSSNSD). The comparison result is given in Table 6.3, where each value is a ratio of the downscaled pSSNSD *versus* the corresponding observed value for an easy comparison. The table showed that the SOM-SD and the AM appeared more skillful, since they could reproduce more of the observed variance than the unconditional model, which indicated that the year-to-year variance of the seasonal total precipitation was highly associated with the changes of large-scale atmospheric circulations. The three models showed different seasonal cycles in their modeling skills. The AM and the SOM-SD had high skills for all seasons, while the unconditional model appeared more skillful only in summer. The three models generally displayed slightly low skills in the transition regions of E3 and E4, between dry and humid zones. Comparatively speaking, the SOM-SD performed the best, even in the driest zone G (except for summer). This is not only because the pSSNSD from the ensemble means were close or higher than the values of pSSNSD downscaled by the AM, but also because its 90% confidence intervals covered the observed values. The unconditional model failed to do that in most cases.

The capacity for reproducing the year-to-year variability of seasonal precipitation was analyzed using the Spearman rank correlation coefficients for the three models. As expected, the unconditional model, due to its pure stochastic nature, gives symmetrical confidence intervals with the ensemble means of the rank correlations as zero. Therefore, only the comparison between the SOM-SD and AM were made (Fig. 6.3). Both the SOM-SD and the AM appeared more skillful in autumn than other seasons. The performance of the AM was generally better than that of the mean of SOM-SD ensemble. The correlations were mostly between 0.50-0.65 for the AM, while they were around 0.45 for the SOM-SD. However, the confidence intervals of the SOM-SD could all cover the values of the AM, except for winter in zone F3, where the correlation for the AM was higher than the upper bound of the confidence interval of the SOM-SD. Furthermore, the ensemble means of the SOM-SD were very close to the values of the AM in many cases. All of this indicated that both models could capture most of the inter-annual variability of the seasonal precipitation time series.

Table 6.3. Ratios of seasonal precipitation standard deviation between the downscaled results to the observed values (pSSNSD). Each value is an average across all the grids available in a particular zone per season. For the SOM-SD and the unconditional model, these statistics are derived from the ensemble of 500 runs in the validation period (1988-2008); 90% of confidence intervals are in parentheses.

Season	**Zone**	**AM**	**SOM-SD**	**Unconditional**
spring	E6	0.92	1.03 (0.76, 1.29)	0.64 (0.45, 0.83)
	G	0.93	1.14 (0.84, 1.44)	0.62 (0.43, 0.81)
	E4	0.67	0.79 (0.58, 0.99)	0.56 (0.40, 0.72)
	E3	0.77	0.82 (0.62, 1.02)	0.62 (0.45, 0.79)
	F4	0.99	0.97 (0.70, 1.24)	0.81 (0.56, 1.06)
	D5	0.81	0.91 (0.70, 1.13)	0.67 (0.48, 0.85)
	B2	0.81	0.95 (0.74, 1.17)	0.67 (0.49, 0.86)
	F3	1.01	1.08 (0.78, 1.38)	0.90 (0.63, 1.17)
	E2	0.87	0.97 (0.73, 1.22)	0.67 (0.48, 0.87)
summer	E6	0.98	1.13 (0.81, 1.46)	0.79 (0.53, 1.04)
	G	1.83	1.87 (1.25, 2.50)	1.21 (0.76, 1.67)
	E4	0.83	0.89 (0.65, 1.13)	0.69 (0.49, 0.90)
	E3	0.84	0.93 (0.69, 1.17)	0.77 (0.56, 0.98)
	F4	1.09	1.16 (0.88, 1.44)	1.02 (0.77, 1.27)
	D5	1.05	1.10 (0.82, 1.39)	0.89 (0.65, 1.13)
	B2	1.06	1.06 (0.80, 1.31)	0.86 (0.64, 1.08)
	F3	0.88	0.93 (0.70, 1.16)	0.74 (0.54, 0.94)
	E2	1.18	1.29 (0.90, 1.67)	1.02 (0.70, 1.33)
autumn	E6	0.85	1.05 (0.77, 1.33)	0.55 (0.37, 0.72)
	G	1.03	1.18 (0.86, 1.51)	0.60 (0.40, 0.79)
	E4	0.76	0.93 (0.70, 1.16)	0.51 (0.36, 0.67)
	E3	0.99	0.95 (0.72, 1.19)	0.58 (0.41, 0.74)
	F4	0.81	0.74 (0.55, 0.94)	0.57 (0.40, 0.75)
	D5	0.97	0.96 (0.72, 1.20)	0.70 (0.49, 0.90)
	B2	0.99	0.96 (0.73, 1.19)	0.73 (0.52, 0.94)
	F3	0.93	0.94 (0.70, 1.18)	0.66 (0.46, 0.86)
	E2	0.94	1.05 (0.78, 1.31)	0.67 (0.47, 0.86)
winter	E6	0.86	0.86 (0.63, 1.08)	0.66 (0.46, 0.85)
	G	0.88	1.07 (0.80, 1.34)	0.73 (0.51, 0.96)
	E4	0.69	0.70 (0.52, 0.88)	0.58 (0.41, 0.74)
	E3	0.72	0.75 (0.56, 0.93)	0.59 (0.42, 0.75)
	F4	0.77	0.93 (0.66, 1.19)	0.74 (0.50, 0.97)
	D5	0.81	0.88 (0.68, 1.09)	0.63 (0.45, 0.81)
	B2	0.70	0.81 (0.64, 0.98)	0.55 (0.39, 0.70)
	F3	0.64	0.68 (0.47, 0.90)	0.57 (0.39, 0.74)
	E2	0.93	0.96 (0.73, 1.18)	0.71 (0.51, 0.91)

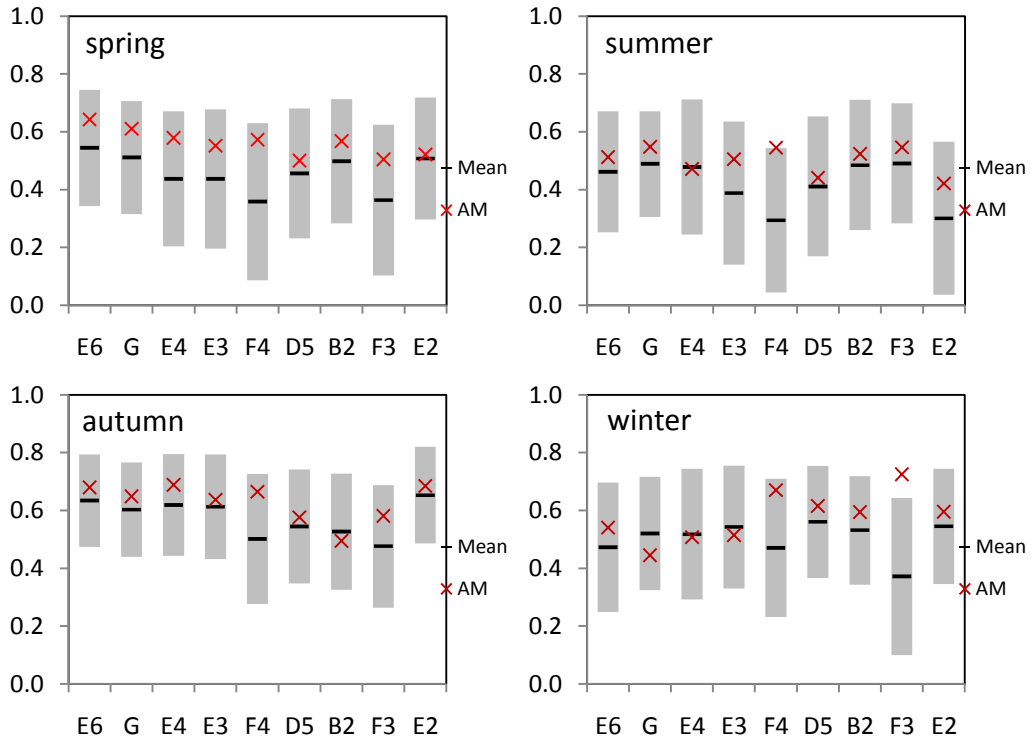

Fig. 6.3. Comparison of rank correlation coefficients of seasonal precipitation time series between the SOM-SD and the AM (α=0.05). On each graph, each value is an average across all the grids available in a particular zone. The SOM-SD values are computed as ensemble means with 90% confidence intervals of the ensemble for 500 runs in the validation period 1988 - 2008. The X-axis shows the names of the nine climatic zones.

6.4.2 Precipitation frequency

The ability of the three models to model precipitation frequency was diagnosed through total precipitation days (nr001) and heavy precipitation days (>20.0mm; nr200). The results are shown in Figs. 6.4 and 6.5, respectively. For the season mean precipitation days (nr001), three models displayed a higher skill in summer and winter than autumn and spring (Fig. 6.4). The seasonal precipitation days (nr001) were significantly overestimated in most of the climatic zones for spring by the three models. The overestimation was most obvious in the SOM-SD and the least in the AM. In the other seasons, there were no significant differences among models. They all reproduced the seasonal mean precipitation days very well, with the downscaled values along the perfect line (Fig. 6.4). For the seasonal mean heavy precipitation days (nr200), the three models generated a uniform high skill in summer (Fig. 6.5). The differences between the downscaled and observed

values were almost negligible and there was no evidence that the three models had a bias toward either high or low values, including at the tails of the distribution (large or small observed values). In spring, the best performance was attained by the unconditional model. The SOM-SD had a slight tendency to generate more heavy precipitation days in some zones, while the AM had an obvious tendency to underestimate the values. In autumn, the higher skill was found in the AM and the unconditional model, while the SOM-SD had a spatial consistent tendency to slightly overestimate the heavy precipitation days. In winter, the SOM-SD and the unconditional model performed better than the AM. In most of the climatic zones, the AM tended to produce more heavy precipitation days than observation.

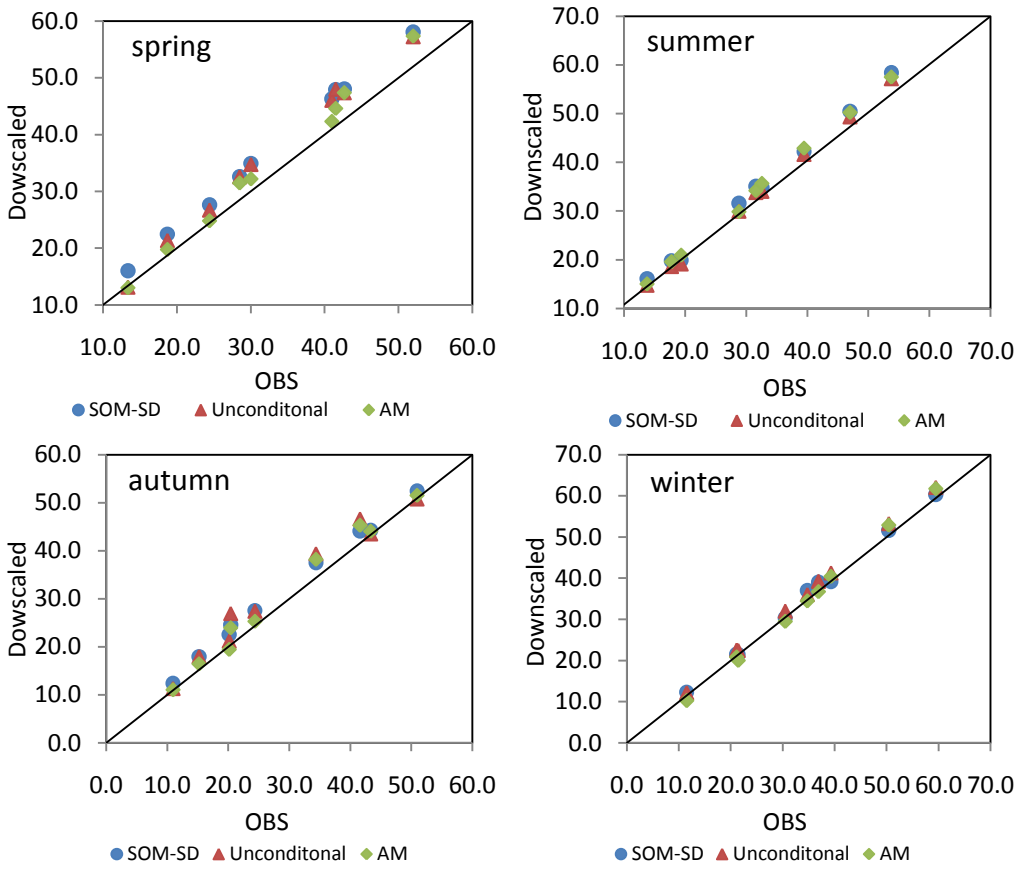

Fig. 6.4. Scatter plot of the seasonal mean precipitation days (nr001) for the observed values and downscaled results from the SOM-SD, AM and the unconditional model, respectively. On the graph, each value is an average of all grids available in a particular zone and season, the total number of points is the number of climatic zones. The line of perfect fit (the diagonal) is shown. The downscaled values are computed as ensemble means of 500 runs in the validation period 1988-2008.

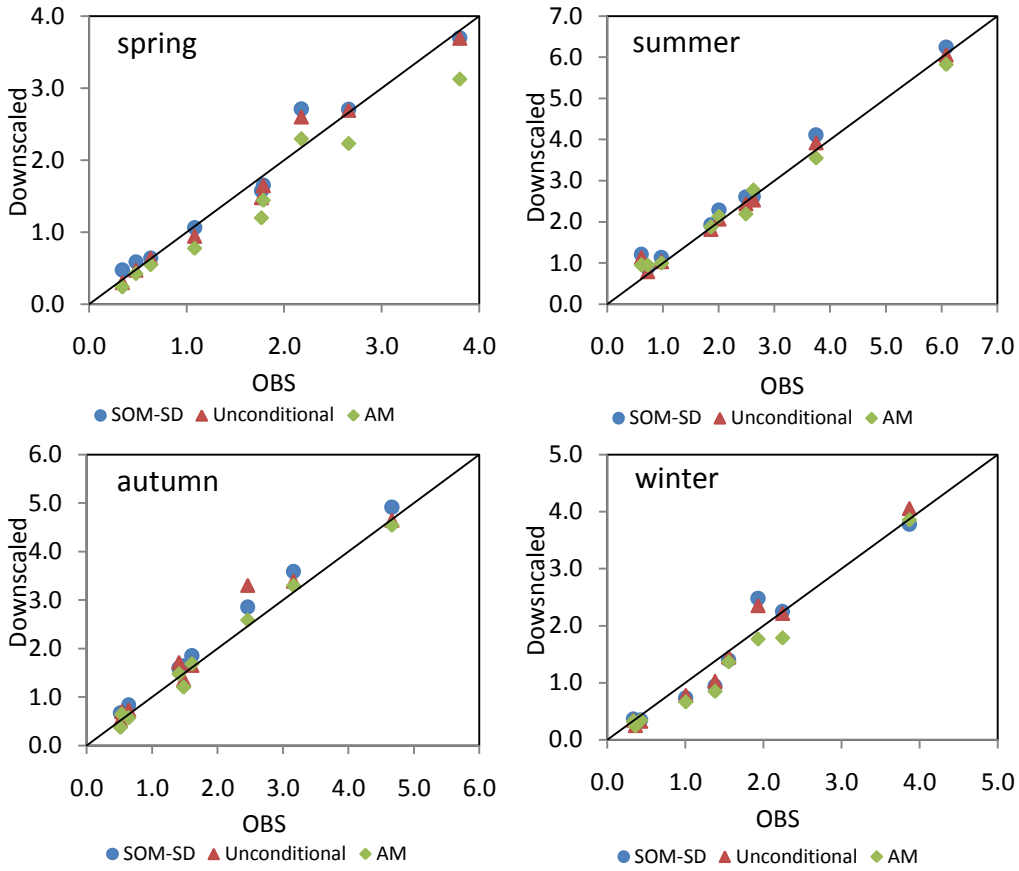

Fig. 6.5. As Fig. 6.4, but for seasonal heavy precipitation days (nr200; daily precipitation >20.0mm).

The ability of the three models to reproduce the inter-annual variability of seasonal precipitation days was analyzed again using the rank correlation between the downscaled and observed values. As expected, the ensemble means of the rank correlation resulting from the unconditional model were all nearly zero with completely symmetric confidence intervals, because the pure randomness of the stochastic nature of the model. Therefore, only the comparison between the SOM-SD and the AM is shown in Fig. 6.6. The AM performed better than the ensemble means of the SOM-SD. However, the 90% confidence intervals of the SOM-SD could nearly always cover the associated better performance of the AM. The two models did not show too significant seasonal cycles in the skill across each climatic zone. The correlation was generally around 0.6 for the AM, and about 0.5 for the ensemble means of the SOM-SD. In autumn, they appeared more successful in the arid and semi-arid zones (above 0.7 for the AM and above 0.6 for the SOM-SD), than the humid zones (below 0.6).

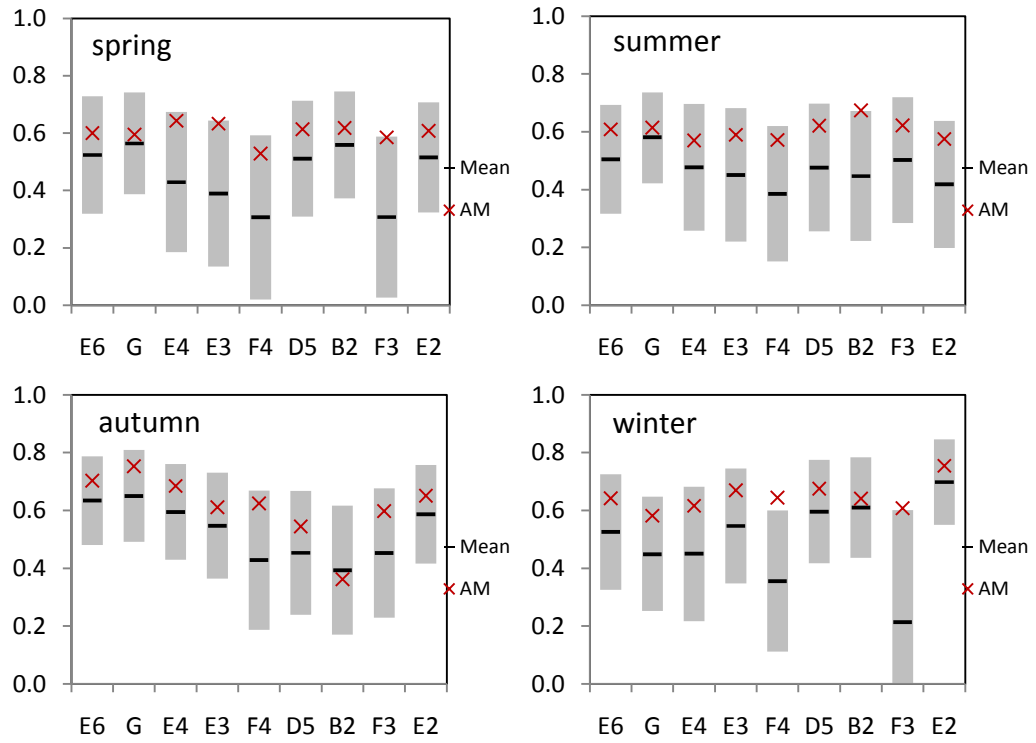

Fig. 6.6. Comparison of rank correlation of seasonal precipitation days between the SOM-SD and the AM (α=0.05). On each graph, each value is an average across all the grids available in a particular zone. The downscaled values from the SOM-SD are computed as ensemble means with 90% confidence intervals of the ensemble for 500 runs in the validation period 1988 - 2008. The X-axis shows the names of the nine climatic zones.

The precipitation occurrence is generally represented by a two-state (wet- or dry-day), first-order Markov process in which precipitation probabilities depend only on whether or not precipitation occurred on the previous day (Gabriel and Neumann, 1962; Castellvi and Stockle, 2001). The ability of the three models to reproduce the mean wet-day and dry-day persistence was diagnosed in each season and climatic zone by using the indices of Pww and Pdd (See acronyms in Table 6.1). The three models could generally reproduce well the observed multi-year mean wet-day persistence (Pww) (Fig. 6.7) and dry-day persistence (Pdd) (Fig. 6.8). In each graph, each value is a ratio between the downscaled results and the observed value. The performance of all models displayed significant regional characteristics in that they all showed a higher skill in the humid regions for Pww and higher skill for Pdd in the dry regions. In General, the reproduction of the two indices were more accurate for the SOM-SD and the AM. For Pww, this was true for all of cases, particularly in the arid and semi-arid zones such as E6 and G,

where the values of Pww were above 0.7 for the SOM-SD and the AM and below 0.5 for the unconditional model (Fig. 6.7). The differences between the SOM-SD and the AM were nearly negligible. For Pdd, the three models performed better than for Pww, which could be explained partly by the fact that the events without precipitation are more frequent than precipitation events (Fig. 6.8). The values of Pdd are generally above 0.8, or even above 0.9 in the very dry regions. The differences among the three models are smaller than those for Pww. The lowest values for Pww and Pdd occurred in the driest zone, G, and the wettest zone, B2, respectively.

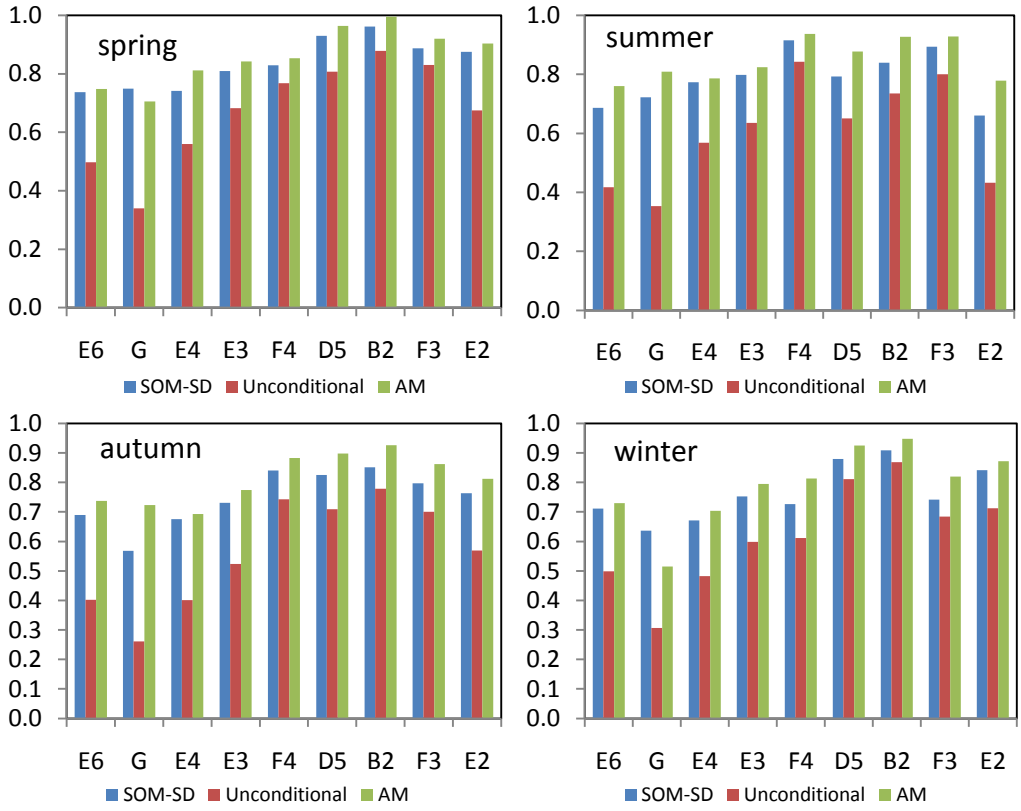

Fig. 6.7. The ratio of the downscaled seasonal mean wet-day persistence (Pww) to the observed values from the SOM-SD, the AM and the unconditional model. These values are shown by season and climatic zones (labels on the x-axis). On each graph, each value is an average across all the grids available in a particular zone. The downscaled values for the SOM-SD and the unconditional model are computed as ensemble means of 500 runs in the period 1988-2008.

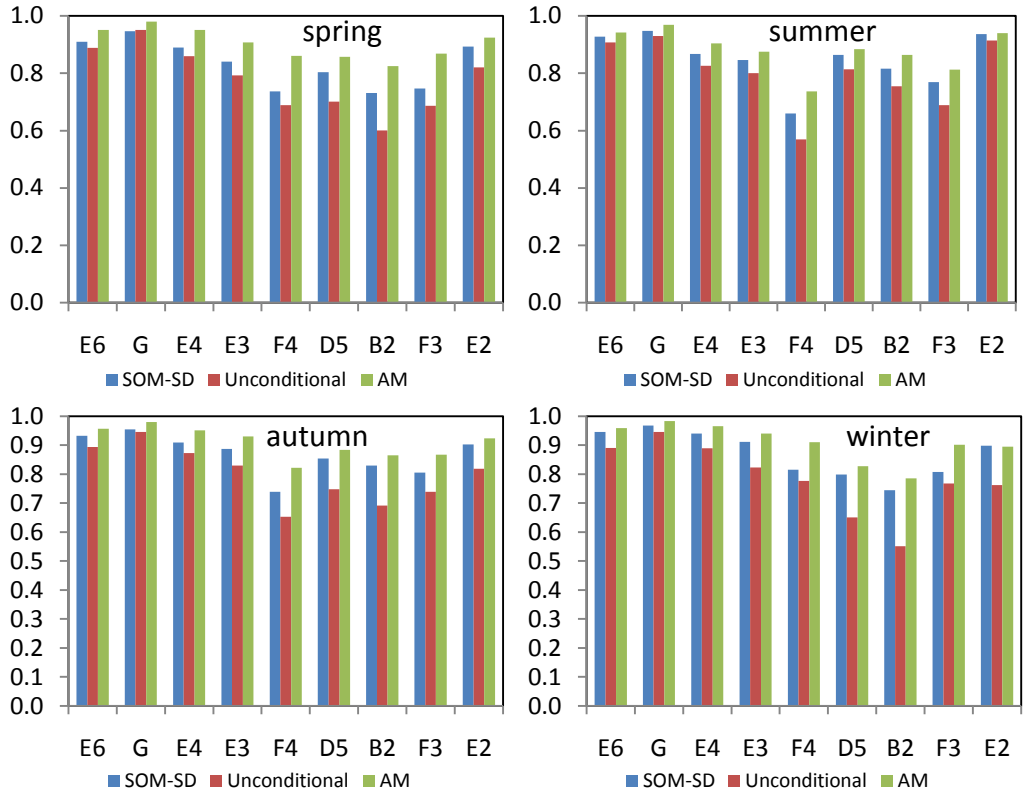

Fig. 6.8. As Fig. 6.7 but for the seasonal mean dry-day persistence (Pdd).

The unconditional model could not reproduce the year-to-year variability of the seasonal mean Pww and Pdd due to its pure stochastic nature. The SOM-SD and the AM could reproduce the interannual variability to a certain extent. The rank correlations were generally between 0.25 and 0.60 for Pww and between 0.35 and 0.65 for Pdd (Table 6.4). The SOM-SD and AM appeared more successful in the transitional seasonal period of spring and autumn than in summer and winter. In most cases, the AM appeared more skillful than the mean performance of the SOM-SD with higher correlations, especially for winter. Nevertheless, the better performance of the AM was not above the 90% confidence intervals of the SOM-SD.

6.4.3 Extreme events

The three models could reproduce P95 very well (Fig. 6.9). Errors were almost negligible and there was no evidence that the three models had a bias toward either high or low values, including at the tails of the distribution (large or small observed values). Only exception occurred in the driest zone G for summer; P95 was overestimated significantly by all models. The SOM-SD performed better than the other 2 models (Fig. 6.9). The models appeared more skillful in summer and autumn than in spring and winter. In the latter two seasons, P95 was underestimated by the unconditional model and the AM. The underestimation was more obvious in spring for the AM. The contributions of extreme precipitation events to the seasonal total precipitation were between 30% and 35% for most zones for most seasons (Fig. 6.10). The highest contributions occurred in summer for the driest zone G, and in winter for the humid zones of F3 and F4. The three models could reproduce this property very well. The differences in the reproduction were negligible in most cases.

To a certain extent, the three models were able to reproduce reasonably well the observed maximum consecutive wet or dry days (CWD and CDD) but with underestimations (not shown). In the case of CWD, the biases generally lay between -5 and 5 days, and the best reproduction season occurred in spring. For the CDD, the best performances occur in summer and winter (with biases ranging between -10 to 10 days). Comparatively, the AM performed slightly better than the SOM-SD and the unconditional model. The year-to-year variability of CWD and CDD was assessed further by the rank correlation between observed and downscaled time series for each season in the climatic zones (Table 6.5). Again, as a stochastic model, the unconditional model did not show any correlation in terms of the ensemble means for the 500 runs. The SOM-SD and the AM could capture only a small part of the inter-annual variability of CWD (from 0.3 to 0.5) and CDD (from 0.2 to 0.5). Moreover, the reproductions were slightly higher in spring and autumn than in other seasons for both indices.

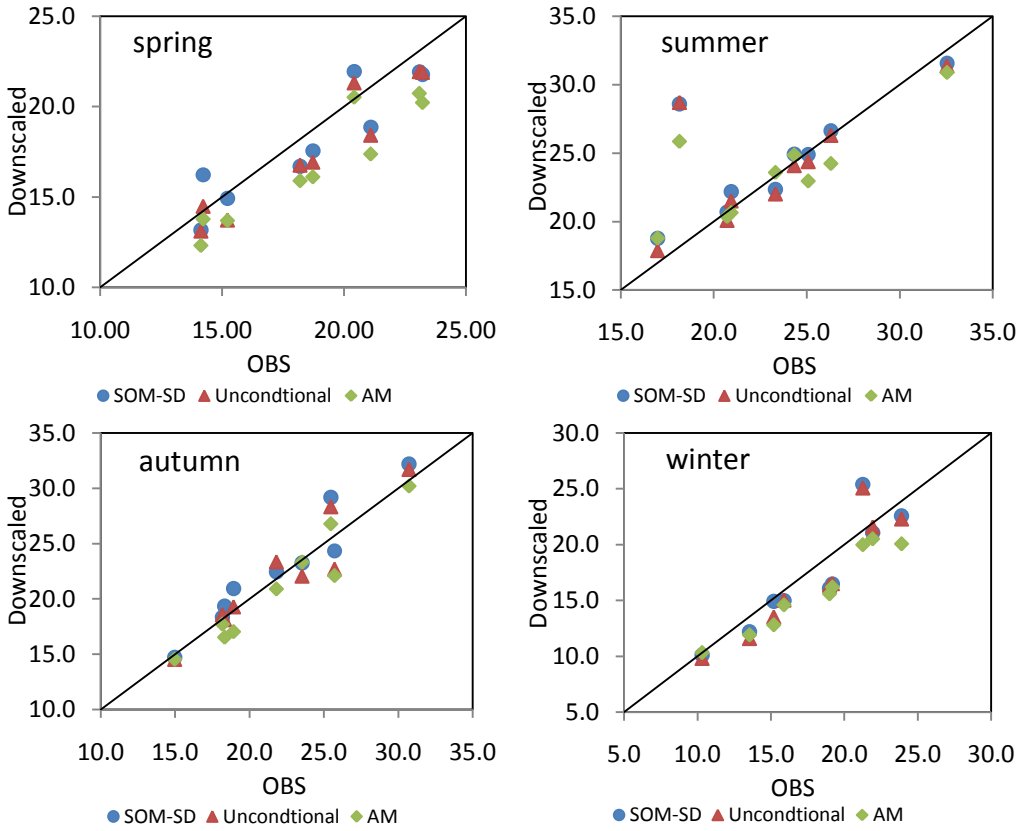

Fig. 6.9. As Fig. 6.4 but for P95.

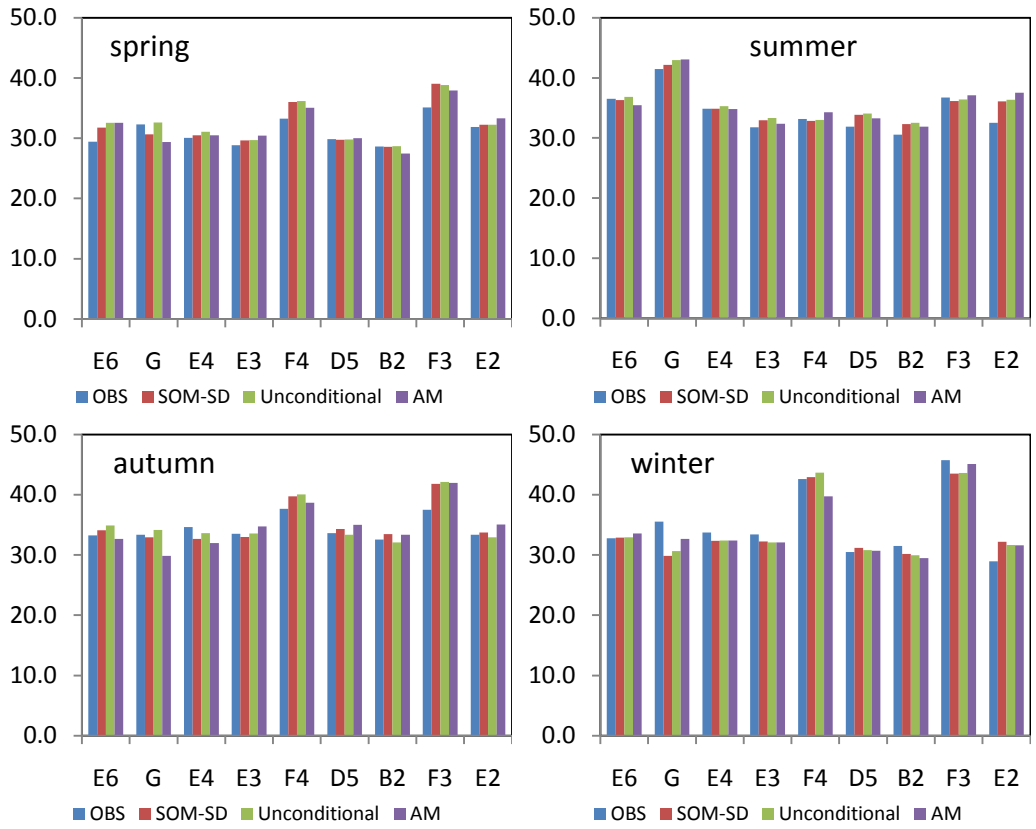

Fig. 6.10. As Fig. 6.7 but for P95T.

Table 6.4 Rank correlations of Pww and Pdd between observed values and downscaled results for the AM and the SOM-SD. Each value is an average across all the grids. For the SOM-SD and the AM model, these statistics are derived from the ensemble of 500 runs in the validation period (1988-2008); 90% confidence intervals in parentheses. For the acronyms, see Table 6.1.

Index	zone	**spring**		**Summer**		**Autumn**		**winter**	
		AM	SOM-SD	AM	SOM-SD	AM	SOM-SD	AM	SOM-SD
Pww	E6	0.24	0.26 (-0.02, 0.53)	0.29	0.21 (-0.08, 0.50)	0.40	0.36 (0.10, 0.62)	0.28	0.18 (-0.13, 0.48)
	G	0.31	0.38 (0.13, 0.62)	0.04	0.04 (-0.24, 0.32)	0.54	0.30 (0.03, 0.57)	0.15	0.13 (-0.17, 0.44)
	E4	0.32	0.39 (0.16, 0.63)	0.29	0.23 (-0.04, 0.32)	0.43	0.42 (0.19, 0.65)	0.22	0.14 (-0.18, 0.46)
	E3	0.30	0.32 (0.07, 0.56)	0.22	0.23 (-0.06, 0.51)	0.33	0.33 (0.09, 0.57)	0.29	0.19 (-0.11, 0.49)
	F4	0.61	0.54 (0.34, 0.74)	0.36	0.35 (0.08, 0.61)	0.44	0.34 (0.11, 0.57)	0.54	0.32 (0.05, 0.60)
	D5	0.41	0.41 (0.17, 0.65)	0.32	0.28 (-0.01, 0.56)	0.52	0.47 (0.26, 0.69)	0.41	0.33 (0.07, 0.59)
	B2	0.46	0.42 (0.19, 0.65)	0.37	0.27 (-0.03, 0.56)	0.54	0.51 (0.29, 0.72)	0.45	0.37 (0.12, 0.61)
	F3	0.45	0.34 (0.08, 0.60)	0.24	0.36 (0.10, 0.62)	0.45	0.36 (0.14, 0.58)	0.44	0.15 (-0.17, 0.48)
	E2	0.28	0.25 (-0.03, 0.53)	0.29	0.21 (-0.10, 0.52)	0.46	0.41 (0.17, 0.65)	0.40	0.36 (0.09, 0.63)
Pdd	E6	0.40	0.32 (0.06, 0.58)	0.41	0.36 (0.13, 0.59)	0.61	0.46 (0.26, 0.67)	0.45	0.33 (0.05,0.61)
	G	0.32	0.46 (0.26, 0.66)	0.35	0.31 (0.07, 0.54)	0.70	0.49 (0.27, 0.70)	0.35	0.18 (-0.13, 0.49)
	E4	0.43	0.40 (0.18, 0.62)	0.36	0.29 (0.04, 0.53)	0.60	0.43 (0.23, 0.63)	0.47	0.29 (0.00, 0.58)
	E3	0.43	0.32 (0.06, 0.57)	0.39	0.25 (-0.02, 0.51)	0.50	0.31 (0.08, 0.53)	0.44	0.31 (0.03, 0.60)
	F4	0.45	0.37 (0.10, 0.65)	0.24	0.19 (-0.13, 0.51)	0.59	0.44 (0.19, 0.68)	0.53	0.25 (-0.06, 0.55)
	D5	0.51	0.33 (0.06, 0.56)	0.37	0.24 (-0.06, 0.55)	0.52	0.29 (0.03, 0.56)	0.38	0.29 (-0.01, 0.59)
	B2	0.50	0.25 (-0.06, 0.56)	0.34	0.22 (-0.10, 0.54)	0.34	0.23 (-0.07, 0.53)	0.34	0.21 (-0.12, 0.54)
	F3	0.44	0.22 (-0.11, 0.55)	0.32	0.20 (-0.12, 0.52)	0.58	0.37 (0.10, 0.63)	0.38	0.16 (-0.18, 0.50)
	E2	0.60	0.32 (0.06, 0.57)	0.44	0.32 (0.04, 0.60)	0.63	0.39 (0.16, 0.62)	0.50	0.45 (0.19, 0.70)

Table 6.5 Rank correlations of CWD and CDD between observed values and downscaled results for the AM and the SOM-SD. Each value is an average across all the grids. For the SOM-SD and the AM model, these statistics are derived from the ensemble of 500 runs in the validation period (1988-2008); 90% confidence intervals in parentheses. For the acronyms, see Table 6.1.

Index	zone	**spring**		**Summer**		**Autumn**		**winter**	
		AM	SOM-SD	AM	SOM-SD	AM	SOM-SD	AM	SOM-SD
CWD	E6	0.34	0.29 (0.02, 0.56)	0.30	0.22 (-0.07, 0.50)	0.48	0.41 (0.16, 0.66)	0.31	0.20 (-0.11, 0.51)
	G	0.29	0.48 (0.25, 0.70)	0.18	0.05 (-0.22, 0.32)	0.62	0.36 (0.11, 0.61)	0.29	0.20 (-0.10, 0.50)
	E4	0.43	0.41 (0.17, 0.66)	0.29	0.20 (-0.09, 0.49)	0.56	0.48 (0.24, 0.71)	0.34	0.14 (-0.19, 0.46)
	E3	0.35	0.34 (0.08, 0.61)	0.27	0.24 (-0.07, 0.54)	0.40	0.37 (0.12, 0.62)	0.30	0.18 (-0.14, 0.50)
	F4	0.56	0.43 (0.18, 0.69)	0.26	0.22 (-0.08, 0.53)	0.38	0.29 (0.01, 0.58)	0.44	0.24 (-0.07, 0.54)
	D5	0.36	0.33 (0.05, 0.61)	0.35	0.26 (-0.04, 0.56)	0.47	0.40 (0.15, 0.65)	0.30	0.26 (-0.05, 0.55)
	B2	0.41	0.30 (0.02, 0.59)	0.42	0.28 (-0.04, 0.59)	0.30	0.34 (0.08, 0.61)	0.31	0.23 (-0.06, 0.51)
	F3	0.43	0.27 (-0.03, 0.57)	0.34	0.29 (-0.01, 0.58)	0.47	0.35 (0.10, 0.61)	0.37	0.11 (-0.23, 0.45)
	E2	0.35	0.27 (-0.04, 0.57)	0.36	0.26 (-0.04, 0.57)	0.46	0.39 (0.13, 0.65)	0.33	0.26 (-0.04, 0.56)
CDD	E6	0.22	0.18 (-0.14, 0.49)	0.19	0.21 (-0.10,0.51)	0.44	0.29 (0.01, 0.57)	0.21	0.19 (-0.15, 0.51)
	G	0.15	0.26 (-0.03, 0.54)	0.17	0.23 (-0.07, 0.53)	0.50	0.34 (0.06, 0.63)	0.12	0.10 (-0.23, 0.42)
	E4	0.21	0.26 (-0.02, 0.55)	0.19	0.19 (-0.12, 0.50)	0.33	0.26 (-0.02, 0.54)	0.16	0.15 (-0.18, 0.48)
	E3	0.28	0.18 (-0.13, 0.48)	0.15	0.14 (-0.18, 0.45)	0.26	0.15 (-0.14, 0.44)	0.17	0.15 (-0.18, 0.48)
	F4	0.34	0.23 (-0.08, 0.54)	0.18	0.14 (-0.19, 0.47)	0.57	0.38 (0.11, 0.65)	0.39	0.14 (-0.20, 0.47)
	D5	0.38	0.24 (-0.07, 0.54)	0.22	0.14 (-0.20, 0.48)	0.33	0.19 (-0.13, 0.49)	0.27	0.15(-0.19, 0.48)
	B2	0.39	0.19 (-0.14, 0.51)	0.20	0.14 (-0.20, 0.49)	0.28	0.14 (-0.19, 0.47)	0.25	0.12 (-0.22, 0.46)
	F3	0.29	0.13 (-0.22, 0.48)	0.16	0.14 (-0.20, 0.48)	0.40	0.27 (-0.04, 0.57)	0.21	0.07 (-0.29, 0.42)
	E2	0.44	0.21 (-0.10, 0.51)	0.14	0.11 (-0.22, 0.45)	0.35	0.22 (-0.08, 0.52)	0.26	0.18 (-0.14 ,0.50)

6.5 Conclusion and discussion

In this chapter, the performance of the SOM-SD was compared with two related statistical downscaling techniques: an analog model and an unconditional stochastic re-sampling model, by downscaling daily precipitation over southeast Australia.

The three models did not show obvious differences in reproducing the mean (SDII) and the standard deviation (ppSD) of daily precipitation on wet days. Generally, the 90% confidence intervals of the SOM-SD and the unconditional model could cover the observed values and the results from the AM. Comparatively speaking, the SOM-SD performed slightly better than the other models, since its ensemble means of 500 runs were closer to the observed values. However, SDII was underestimated significantly by all three models across all climatic zones in spring. The ppSD was reproduced very well by three models. However, the AM had a slight tendency to underestimate the observed variance compared with the other models. In fact, the variance underestimation is a known issue for regression-based statistical downscaling methods (Von Storch, 1999). This is was overcome by the SOM-SD and the unconditional model. The three models also showed a high skill in reproducing the inter-annual variance of seasonal precipitation time series (represented by pSSNSD). The SOM-SD and the AM could reproduce more of the observed pSSNSD than the unconditional model. In addition, the AM could generate the smallest RMSE, while the 90% confidence intervals of the SOM-SD could cover the best performance from the AM in some cases. The unconditional model always gave the largest RMSE.

The three models could reproduce the precipitation frequencies very well with the intensities greater than 0.1mm/day and 20.mm/day (nr001 and n200). There was no evidence that the three models had a bias toward either high or low values, including at the tails of the distribution (large or small observed values). However, they showed different seasonal cycles across the two statistical indices. For nr001, the models appeared more skillful in other seasons than in spring when it was overestimated. In the case of nr200, the AM had a slight tendency to underestimate the values compared with the SOM-SD and the unconditional model. Besides precipitation frequency, the three models also have a good capability of reproducing the observed dry-day and wet-day persistence (Pdd and

Pww), but with a little underestimation. The performances of the three models displayed significant regional characteristics in that they all showed high skills in the humid regions for Pww and high skills in the dry region for Pdd. Comparatively speaking, the reproduction of Pww and Pdd were more accurate for the SOM-SD and the AM than for the unconditional model. To some extent, this indicates that the probability of precipitation occurrence would be likely conditioned on large-scale atmospheric circulation patterns.

The ability of the three models to reproduce extreme events was also assessed by 4 diagnostic indices: extreme seasonal precipitation at the 95% percentile of overall precipitation (P95), contributions of seasonal 95% percentile or higher precipitation to seasonal total (P95T), seasonal maximum consecutive dry days, and wet days (CDD and CWD). Comparatively, the SOM-SD performed the best in reproducing P95. All models showed a seasonal cycle particularly in summer and autumn. In spring and winter, the AM and the unconditional model displayed a tendency to underestimate P95. However, it is very interesting that the three models did not show significant differences in reproducing the P95T. In terms of CWD and CDD, the SOM-SD and the AM only performed slightly better than the unconditional model.

However, there are significant differences among the three models in modeling the inter-annual variability. The AM gave the best performance, while the SOM-SD showed a large improvement compared with the unconditional stochastic model. Furthermore, the best performance from the AM can mostly be covered by the SOM-SD. Not surprisingly, the unconditional model, not a genuine SDSM, failed to reproduce the observed inter-annual variability, because the precipitation was completely determined stochastically (i.e., unconditional on predicators). It confirms that the inter-annual variability of precipitation, to a certain extent, is actually associated with the large-scale circulation patterns, rather than a totally random phenomenon. However, the SOM-SD and AM performed better in reproducing the inter-annual variability of SDII and nr001 than those of Pww, Pdd, CWD and CDD.

In summary, conditional re-sampling models (the SOM-SD and the AM) are better than the unconditional re-sampling model in estimating the inter-annual variability of observed daily precipitation, even though similar performance were obtained

by all three models to reproduce the observed multi-year mean climatological statistics. Moreover, the 90% confidence intervals of the SOM-SD generally can cover the results from the AM. On the one hand, it reveals that the performance of the AM is not beyond the confidence scope simulated by the SOM-SD. On the other hand, it indicates that the nearest neighbor (synoptic pattern) found by the AM in the historical time series was not always the most suitable synoptic pattern so as to make its performance beyond the scope of the SOM-SD. As the GCM outputs are rarely able to reproduce very well the observed climate represented by the NNR data, particularly for areas where strong localized precipitation drivers exist beside the large scale circulation patterns (Mullan et al., 2001), it leaves us a question: can the AM find its most suitable synoptic pattern in the GCM outputs as it does in the reanalysis data? A further diagnosis would be necessary to test this. Lorenz (1969) showed that it would be highly unlikely to find an acceptable analog, given the relatively short historical records of observations and the high number of degrees of freedom of atmospheric circulations. However, the uncertainty can, to a certain degree, be relieved by the SOM-SD because it uses a set of generalized synoptic patterns to find their neighbors in the GCM outputs (which maybe more robust).

As a whole, it was found that, in general, the AM performed the same as the more complicated method of SOM-SD, even better in some aspects. This was expected as both methods shared not only the same theoretical foundation, but also the same model configuration. However, while the AM used an optimized synoptic pattern, the SOM-SD used a generalized pattern to derive precipitation. As an optimized case of the SOM-SD, the AM would outperform the median performance of the SOM-SD. The AM used in this study was a deterministic method with a single analog, which was the most common form of analog model in statistical downscaling studies. It further demonstrated the existence of good relationship between precipitation and synoptic patterns. Obviously, the single analog just produced a specific sample from infinitive climate scenarios, but it had limited use in climate change assessment and particularly in impact studies.

Compared with the AM, the SOM-SD could provide a set of scenarios that is able to reveal the probabilistic characterization of the uncertainty from downscaling process. This uncertainty can be further exploited in impact studies. In most cases, the distribution of plausible impacts (driven by a set of downscaling outputs),

rather than one possible impact consequence (driven by on downscaling output), is the critical information required by end-users, such as government institutions or the insurance industry, for well-informed policy-making and forward planning (Cawley et al., 2007).

In fact, the AM can also be used to generate a probabilistic downscaling output (Schmidli et al., 2007), which involves the selection of a set of analogs from a reference data set on the basis of the similarity of large-scale synoptic patterns, and to build a probabilistic model for precipitation based on the analogs for each day of a season. Although this two-step analog model was not tested in this study, it can be expected that it should have a similar performance as the SOM-SD as both methods share the same synoptic climatologic foundation.

CHAPTER SEVEN

STATISTICAL DOWNSCALING OF DAILY TEMPERATURE FOR CLIMATE CHANGE SCENARIOS

7.1 Introduction

In this chapter, the applicability of SOM-SD to other local surface variables was tested following the methodology of downscaling precipitation. Since rainfall and temperature generally are the most important local climate variables for impact studies, downscaling daily maximum temperature and minimum temperature were used as an example. Furthermore, the SOM-SD was extended to construct future temperature change scenarios based on the large-scale predictors derived from six different GCMs.

7.2 Data and method

7.2.1 Data

The predictands or the dependent variables are daily gridded minimum and maximum temperature at a spatial resolution of 0.05° from 1961-2000. The data were acquired from the Australia Bureau of Meteorology and extracted from the whole data set to cover the case study area. The downscaling was carried out at 0.25°×0.25° resolution, which is sufficient to investigate the applicability of the downscaling method across different climatic zones and orographic features.

Daily large-scale atmospheric predictors consist of the NCEP/NCAR Reanalysis data (NNR; available from 1948 to real-time; Kalnay et al. 1996; Kistler et al. 2001) and GCM simulation results under the climate change scenario A2. The predictors consist of mean sea-level pressure (SLP), specific humidity (Q), zonal wind (U), meridional wind (V), air temperature (T), surface mean temperature (Ts), surface minimum and maximum temperature (Tn and Tx). Among them, the predictors of Q, U, V and T were represented at different pressure levels as NNR (see Table 2.3). The GCMs used included CCCMA, CNRM, CSIRO, GFDL, MPI and MRI (see Table 2.2 for more information about these GCMs).

The data of the predictors and predictand during the baseline period of 1961-2000 were split into two independent intervals: a calibration period, also called the training period, and a validation period. The calibration period was 30 years from 1961 to 1990, and the validation period was 10 years from 1991 to 2000, so that the method was trained and validated independently. The GCM predictor data were used to construct future temperature change scenarios during two 20-year periods ranging from 2046 to 2065 and from 2081 to 2100. Moreover, all data have been re-gridded to have the same spatial resolution of 2.5°×2.5° and have been standardized. More detailed information about these data and relevant processing approaches can be found in Chapter 2.

7.2.2 Downscaling temperature using SOM-SD

One temperature grid was taken as an example to describe the downscaling procedure. Spatial statistical downscaled data over the case study area were obtained by applying the same procedure to other grids.

In this chapter, the SOM-SD was used to characterize the atmospheric circulation on a localized domain of 3×3 grids around the target location and to generate a set of possible values for the minimum and maximum temperature for each atmospheric pattern by using the data from the NNR and observed temperature data during the validation period. A total of 5×7 patterns were used. To downscale GCM data, the data were matched to the SOM characterization of the atmospheric patterns through the similarity measure (i.e., Euclidean distance), and for each circulation pattern in the GCM data, temperature values were randomly re-sampled from the associated set of possible values according to the conditional probability density distribution developed by Lall and Sharma (1996). Further details on the SOM-SD were described in Chapter 4.

7.3 Accuracy of the downscaling method

7.3.1 Assessment indices

The performance of the downscaling method was assessed in a seasonally stratified style to ensure that the model was capable of capturing the annual variability of temperature. Table 7.1 summarizes the applied indices. Most of these statistics are collected from the STARDEX indices. The indices representing

the statistics of daily extreme temperature with regard to both mean and extreme events were selected.

Table 7.1. Diagnostics of daily temperature. The unit is in °C in all cases.

Acronym	Definition
mTmax	Daily mean maximum temperature
TxSD	Standard deviation of daily maximum temperature
TxSSNSD	Standard deviation of seasonal mean maximum temperature
TxRMSE	Root mean square error of daily maximum temperature
Tx90	90-th percentile of maximum temperature
mTmin	Daily mean minimum temperature
TnSD	Standard deviation of daily minimum temperature
TnSSNSD	Standard deviation of seasonal mean maximum temperature
TnRMSE	Root mean square error of daily minimum temperature
Tn10	10-th percentile of minimum temperature

Apart from the mean climatological statistics, the inter-annual variability was also analyzed by the Spearman rank correlation between indices calculated from the observed and downscaled daily temperature time series, which is particularly important because it indicates whether the method can reproduce correctly the predictor-predictand relationships. The non-parametric unbiased estimation of RC was employed instead of the Pearson correlation in order to minimize the effect of outliers from the possibly non-Gaussian distributed variables. Hereafter, the term "correlation" will refer to the Spearman rank correlation without particular specification.

7.3.2 Uncertainty analysis

Another measure of the "goodness" of a SDSM in reproducing the mean value and variability of observed meteorological variables is the uncertainty analysis (Castrup 1995). In this study, confidence intervals were used as a complementary method to analyze the uncertainty of the output of the SOM-SD (Khan et al., 2006; Dibike et al., 2008). As mentioned before, an ensemble of 500 simulations were generated by the SOM-SD, with the statistical parameters listed above expressed as ensemble means with their 90% confidence intervals (5th percentile for the

lower confidence limit and 95th percentile for the upper confidence limit) computed with a bootstrapping procedure (Davison and Hinkley, 2006). Generally, a good simulation result was identified with the small confidence interval. Without particular specification, only the ensemble means were used to compare with the observed values.

7.4 Downscaling result

7.4.1 Selection of predictors

The selection of predictors can vary from one region to another depending on the characteristics of the large-scale atmospheric circulation and the predictand to be downscaled. There is not a consensus on the selection of predictors in different parts of the world (Holfer et al., 2010). The predictor selection procedure described in Chapter 4 was also used in this chapter. Specifically, the predictors were chosen on the basis of "expert" knowledge including previous experience (Yin et al., 2010) and literature review from other studies in similar areas (Timbal and McAvaney, 2001; Timbal et al., 2009). However, the core procedure was still to use an exhaustive search method to exploit all possible combinations among the potential predictors listed in Table 2.3. Furthermore, the selected predictors must be modeled reliably by GCMs (See section 7.4.3).

Finally, it was found that the predictor set of SLP, Tn and Q at the 850mb level could produce a comparably stable and good performance for the daily minimum temperature, while the combination of SLP and Tx was appropriate for the daily maximum temperature across the different climatic zones (Fig. 2.2). It is worth noting that statistical downscaling studies generally did not recommend using the surface fluxes such as mean, minimum and maximum temperatures as predictors (e.g., Holfer et al., 2010). It is possible that these predictors would have been assimilated by the reanalysis procedure, or they would have been determined completely by the model and therefore associated with larger uncertainty. Nevertheless, the predictor selection in this study did not solely depend on the NNR, but also the GCMs. Here, it seemed that it was not an issue for the inclusion of these predictors in the SOM-SD as they were modeled reliably by GCMs.

7.4.2 Downscaling from reanalysis data

Based on the parameters obtained by using the above NNR predictors and

observed temperature over the calibration period 1961–1990, the local temperature was simulated for each downscaling grid for the validation period 1991 – 2000 to test the quality of the downscaling model.

The ability of the technique to reproduce the observed probability distribution functions (PDFs) was evaluated by looking at the first two moments of the PDFs: the mean and the standard deviation. The reproductions of the mean values and standard deviations are shown in Figs. 7.1 and 7.2, respectively. In each graph, points correspond to a single climatic zone for a single season with the observed values on the X-axis and the reconstructed results along the Y-axis, and each value was computed as an average across all the grids available in a climatic zone and season. The validation revealed interesting features of the downscaling technique. Firstly, the downscaling method was unbiased: the observed probability density functions (PDFs) of daily minimum and maximum temperature (T_{min} and T_{max}) were both reproduced quite accurately for almost all climatic zones in each season. The differences of the mean values and the standard deviations between the observed and downscaled values were almost negligible for both T_{min} and T_{max}. The SOM-SD did not show any bias in reproducing either high or low of mean values and standard deviations, including those at the tails of the distribution (large or small observed values), the mean values in particular (Fig. 7.1). The underestimate of observed standard deviations is a known problem for many SDSMs, particularly for regression-based methods (Von Storch 1999). However, this is not shown in the SOM-SD result, which could be explained partly by the fact that a stochastic re-sampling technique was used to generate daily time series inside the SOM-SD (Fig. 7.2).

Besides the ability to reproduce the observed shape of the PDFs, the skill of the SOM-SD in reproducing the year-to-year variability of seasonal temperature driven by large-scale synoptic changes was evaluated by computing the non-parametric Spearman rank correlation between the observed and downscaled time series. The correlations are displayed in Fig. 7.3, where each value is an average across all grids available in each climatic zone (to save space, 90% confidence intervals are not shown). All of these correlations were significant at least at the 95% level (α = 0.05). There was no consistent seasonal cycle in the skill for T_{min}, with the mean correlations generally between 0.6 and 0.8 (left panel, Fig. 7.3). It appeared that the SOM-SD had high skill for autumn and winter in the arid and

semiarid climatic zones, while had high skill for summer in the relatively humid zones. In the case of T_{max} (right panel, Fig. 7.3), the model showed a marked seasonal cycle in skill, consistent across all regions, i.e., the SOM-SD appeared to have the highest skill in summer (above 0.8) and the lowest skill in winter (about 0.4), with the two transition seasons (spring and autumn) moderately simulated in between (the correlations were generally around 0.65). All of this indicated that the SOM-SD could reproduce most of the observed inter-annual variability of T_{min} and T_{max}.

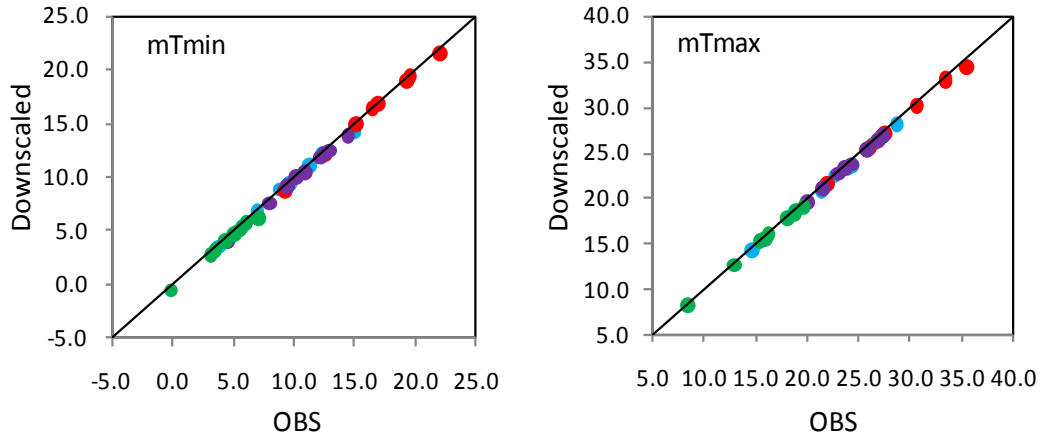

Fig. 7.1. Scatter plot of the downscaled *versus* observed mean (OBS) of the series for the two temperature predictands. On each graph, there is one point per climatic zone and per season, the total number of points per graph is the number of climatic zones times four. The line of perfect fit (the diagonal) is shown. The color code refers to season: blue is winter, green is spring, and red is summer and purple is autumn. The downscaled values were computed as ensemble means of the ensemble for 500 runs in the validation period 1991 - 2000.

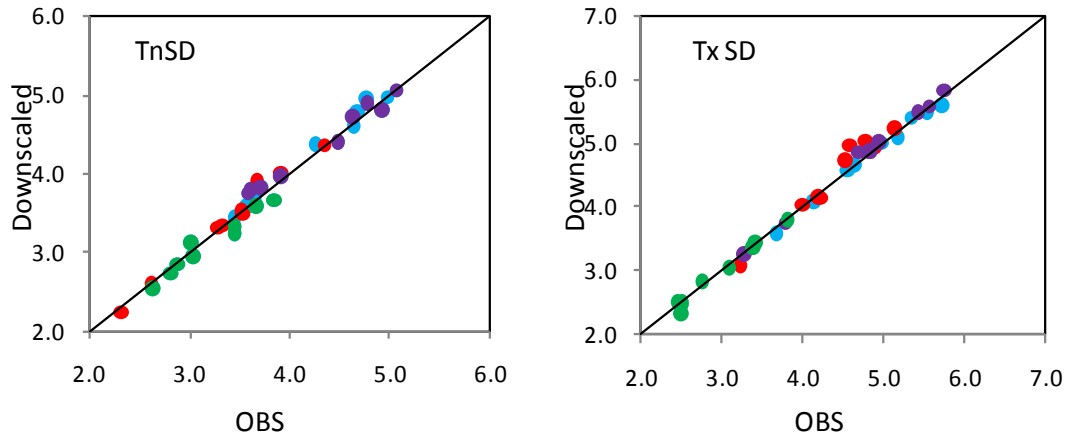

Fig. 7.2. As Fig. 7.1 but for standard deviations.

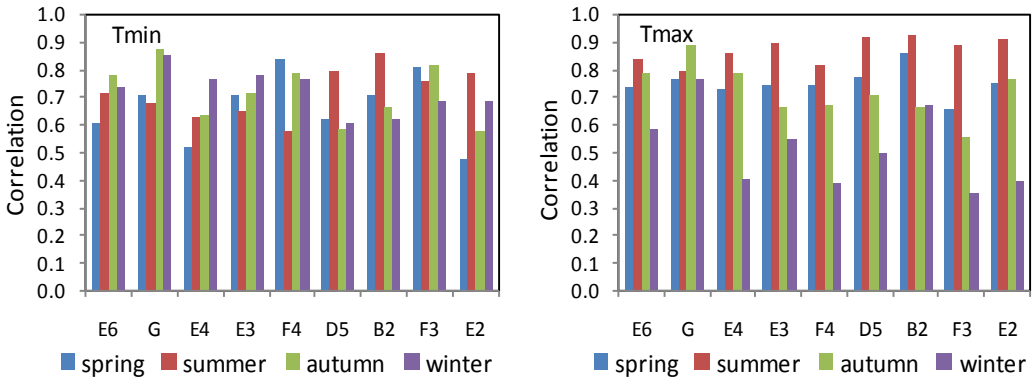

Fig. 7.3. Correlation between observed and reconstructed time series of seasonal mean values (different colored bars for seasons) in the different climatic zones (names on the X-axis) for the two predictands considered (labels in the upper left corner). Each correlation was an average across all the grids available in a particular climatic zone. The downscaled values were computed as ensemble means of the ensemble for 500 runs in the validation period 1991 - 2000.

The accuracy of the downscaling model relating to the inter-annual variance was assessed using the standard deviations of the generated time series of the seasonal means, T_{min} and T_{max}. The percentage of observed inter-annual range (i.e. the difference between the highest and lowest seasonal totals in the observed record) reproduced by the reconstructed series is shown in Fig. 7.4. For T_{min} (left panel, Fig. 7.4), the SOM-SD was able to capture observed variance in the other three seasons (90-130%) except winter. The SOM-SD could reproduce most of the variance in winter (above 60%) but had systematic underestimation. Similar results were acquired for T_{max} (right panel, Fig. 7.4), but with systematic underestimation for all seasons. The SOM-SD appeared more skillful in summer and autumn (mostly close to 100%), followed by spring (mostly above 80%). Clearly, the downscaling model did not have difficulty to reproduce the inter-annual variance in most seasons.

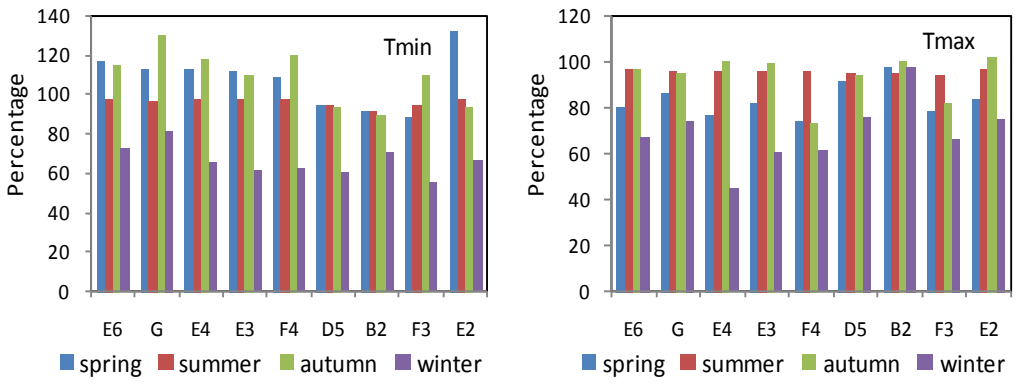

Fig. 7.4. As per Fig. 7.3 but for the percentage of the observed inter-annual variance reproduced by the downscaled series.

Moreover, additional temperature extreme indices have been used to evaluate the performance of the SOM-SD in capturing the extreme temperature events, which is one of the biggest challenges for GCM downscaling due to their huge potential of socio-economic impacts. Fig. 7.5 shows the scatter plots of observed *versus* downscaled seasonal values for the 10th percentile of daily T_{min} (Tn10) and the 90th percentile daily T_{max} (Tx90) calculated during the validation period from 1961 to 2000. The 10th percentile represented the value of daily T_{min} which were not exceeded only 10% of the time while the 90th percentile represented the value of daily T_{max} which were not exceeded 90% of the time. They represented the extreme low and high temperature conditions, respectively. The SOM-SD displayed excellent skills for both indices (Fig. 7.5). Errors in the reproduction of both indices were small and no obvious bias was found toward either high or low values, including those at the tails of the distribution (large or small observed values).

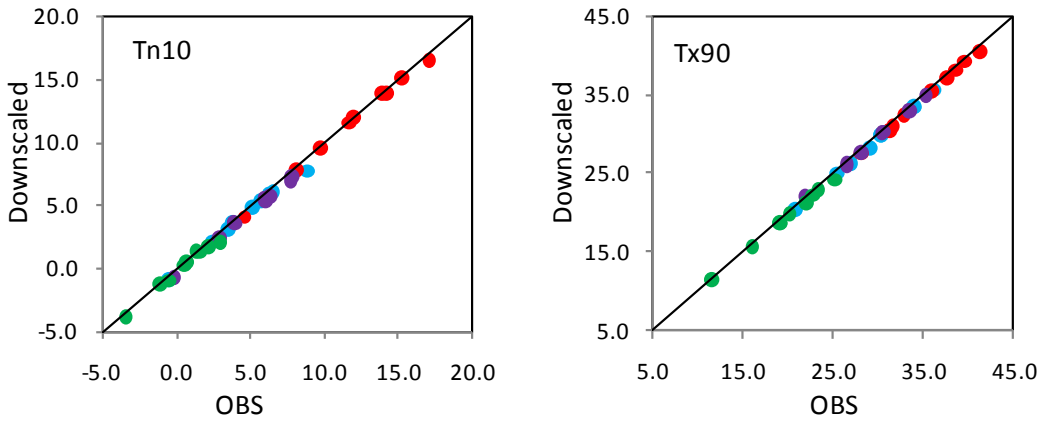

Fig. 7.5. As per Fig. 7.1 but for the 10th daily percentile daily T_{min} (Tn10) and the 90th percentile daily T_{max} (Tx90) during the validation period from 1991 to 2000.

7.4.3 Downscaling from GCM outputs

7.4.3.1 Assessment of GCM circulation

Once the downscaling models have been calibrated and validated, the next step is to use these models to downscale the future climate change scenario simulated by GCMs. At first, it is essential to consider the performance of GCMs in simulating present-day climate, and then to analyze the projected changes (compared with present-day climate) in atmospheric circulation, and how this relates to the issue of stationarity (Hewitson and Crane, 2006).

The stationarity issue results from the two basic assumptions that SDSMs are based on:

a) There is a relationship between the larger-scale predictors and the local-scale climate variables, and an appropriate downscaling transfer function can be generated.

b) The relationship or the transfer function will remain valid, i.e., temporally stable in the future.

The first assumption has been widely validated by may SDSMs, meaning that an empirical downscaling of present climate is eminently feasible, given that the relationship really exists between the predictors and the predictands. However, whether the relationship derived from the present climate could be employed to future climate conditions can only be verified after the fact. Therefore, empirical downscaling implicitly assumes that the observational data from which the relationship is developed encompasses the required information for future cross-scale relationships (Wilby et al., 2004; Hewitson and Crane, 2006).

For a target downscaling grid, a set of large-scale atmospheric circulation patterns with the number of 5×7 was identified by the SOM algorithm from the predictors at a spatial domain of 3×3 grid domain during the calibration period (1961-1990). Thereafter, the data from the reanalysis and GCMs (during different time periods) could be mapped to the attained SOM. Thus, the frequency of occurrence of each node in the SOM could be acquired. The difference in the node frequency of occurrence between the reanalysis and GCM data sets provides an indication of the differences in the synoptic climatology represented by the two data sets. The above method has been used widely to assess the ability of GCMs to replicate synoptic circulation patterns represented by the reanalysis data, although different synoptic classification methods have been used (e.g., Cassano et al., 2006; Hewitson and Crane, 2006; Finnis et al., 2009).

An ideal GCM would recreate the same synoptic patterns that take place in the real atmosphere, represented by the NNR in this study, and therefore, the same node frequencies as the NNR. Here the Pearson correlation was used between the reanalysis and model's node frequencies to evaluate the individual model's

depiction of the synoptic climatology around each downscaling target during the baseline period (Cassano et al., 2007). The basic synoptic patterns were acquired using 30-year calibration NNR data. The correlations of the GCMs with these patterns were computed across all grids in the case study area at the annual scale. The results are shown in Figs. 7.6 and 7.7, for the combinations of the predictors for T_{min} and T_{max} during the calibration and validation period. It is clear that all GCMs could quite well reproduce the observed synoptic patterns with relatively high correlations between 0.6 and 1.0. However, the correlations were not spatially consistent for any GCM, revealing a model bias that varies among the climatic zones. No significant changes in the correlations were found between the validation and the corresponding calibration period, which is of extreme importance, since it indicates to a certain extent that the atmospheric circulation conditions remained stable during the validation period.

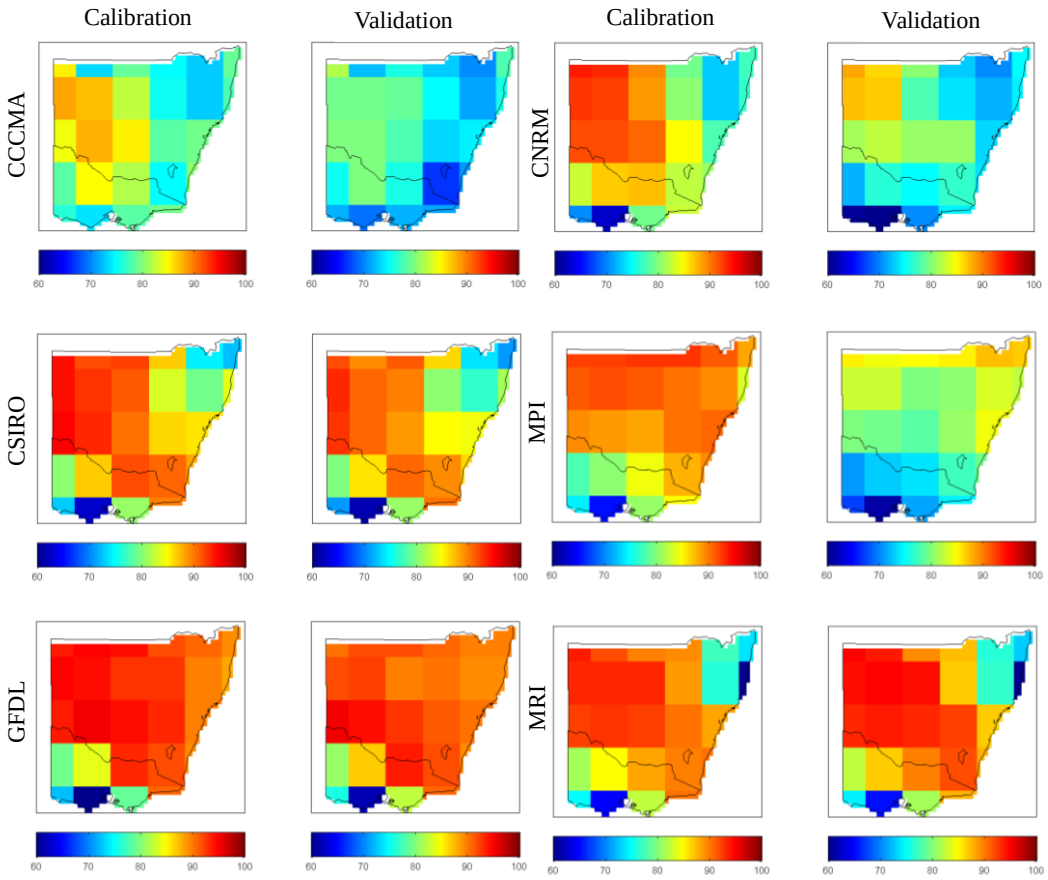

Fig. 7.6. Correlations between the NNR and GCM modeled synoptic pattern frequencies of the combination of predictors for $T_{\min}$ during the calibration period (1961 - 1990) and the validation period (1991 - 2000).

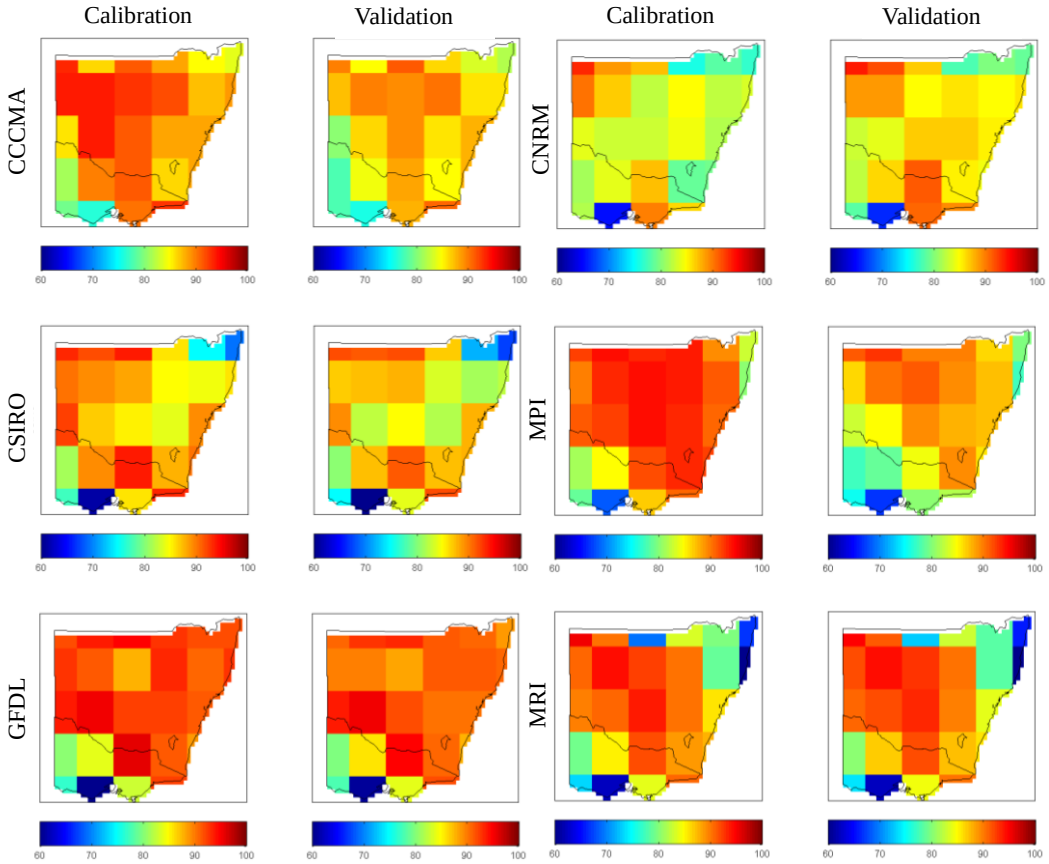

Fig. 7.7. As for Fig. 7.6 but for T_{max}.

7.4.3.2 Downscaling GCM baseline

The performance of each GCM in reproducing the large-scale circulation patterns was further analyzed by the SOM-SD reflected synoptic mechanisms controlling southeast Australia daily temperature variability. This was a kind of indirect assessment method (Busuoic et al., 2001; Chen et al., 2006). GCM data were used during the validation period (1991 – 2000), and the comparisons between observed and downscaled values are displayed in Figs. 7.8 – 7.11, where the first two moments of the PDFs for T_{min} and T_{max} are shown. For the mean values of both $T_{min}$and T_{max}, the downscaled results from the GCMs were comparable to those of the observed values and downscaled results from the NNR for all of the four seasons (Figs. 7.8 – 7.9), though the CNRM model showed relative large overestimation in autumn for both T_{min} and T_{max}. For the standard deviations, there were different performances among the GCMs in different seasons (Figs. 7.10 – 7.11). However, the skill in reproducing the observed variance was still acceptable. All of the above analyses showed that the statistical relationship between the predictors and the predictand derived from the calibration period could be employed at least to the validation period.

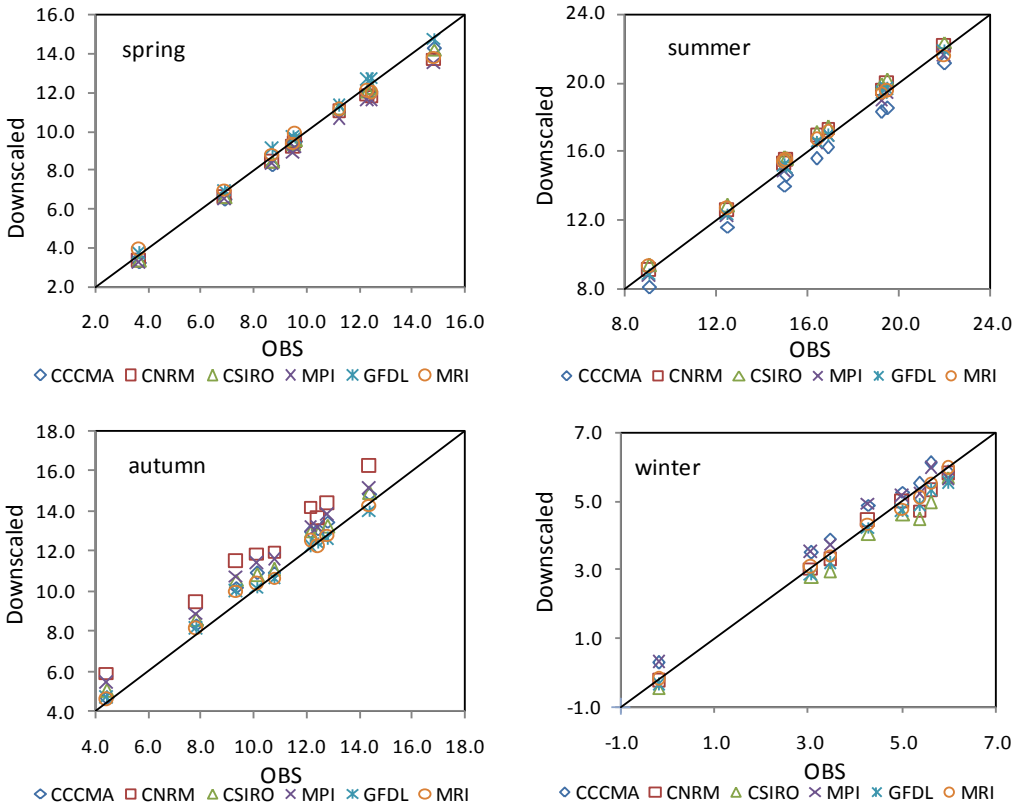

Fig. 7.8. As Fig. 7.1 but for the downscaled from GCMs *versus* observed mean (OBS) of the series for T_{min}.

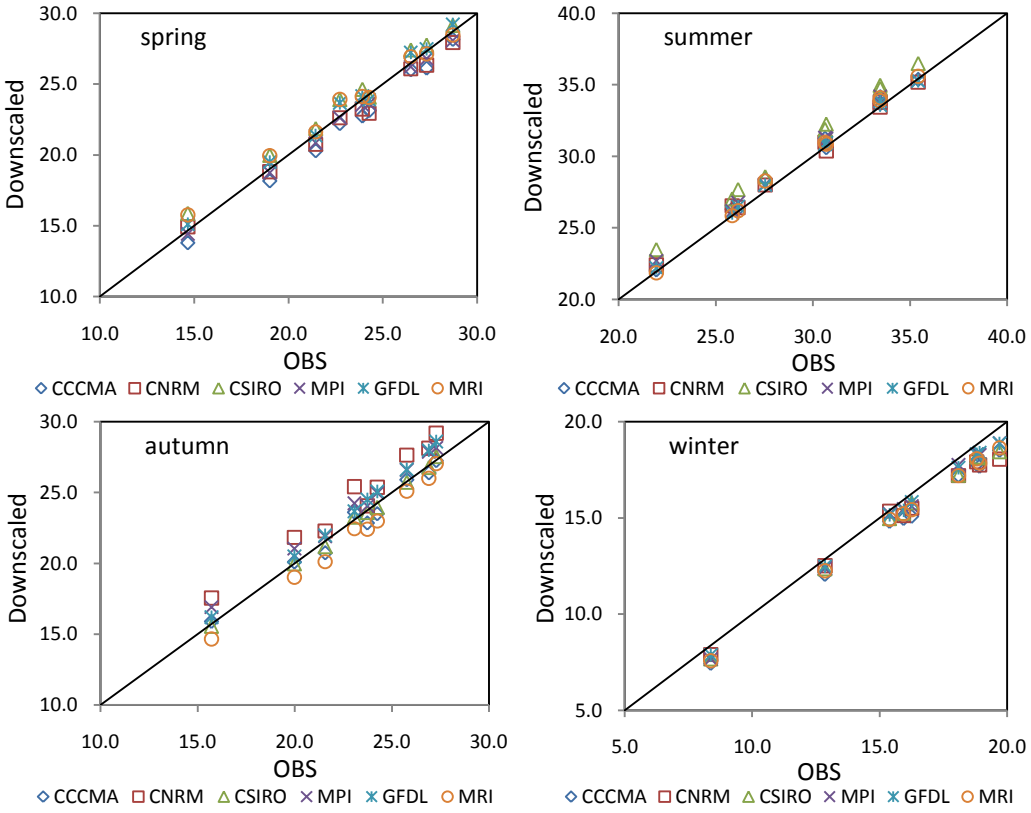

Fig. 7.9. As for Fig. 7.8 but for T_{max}.

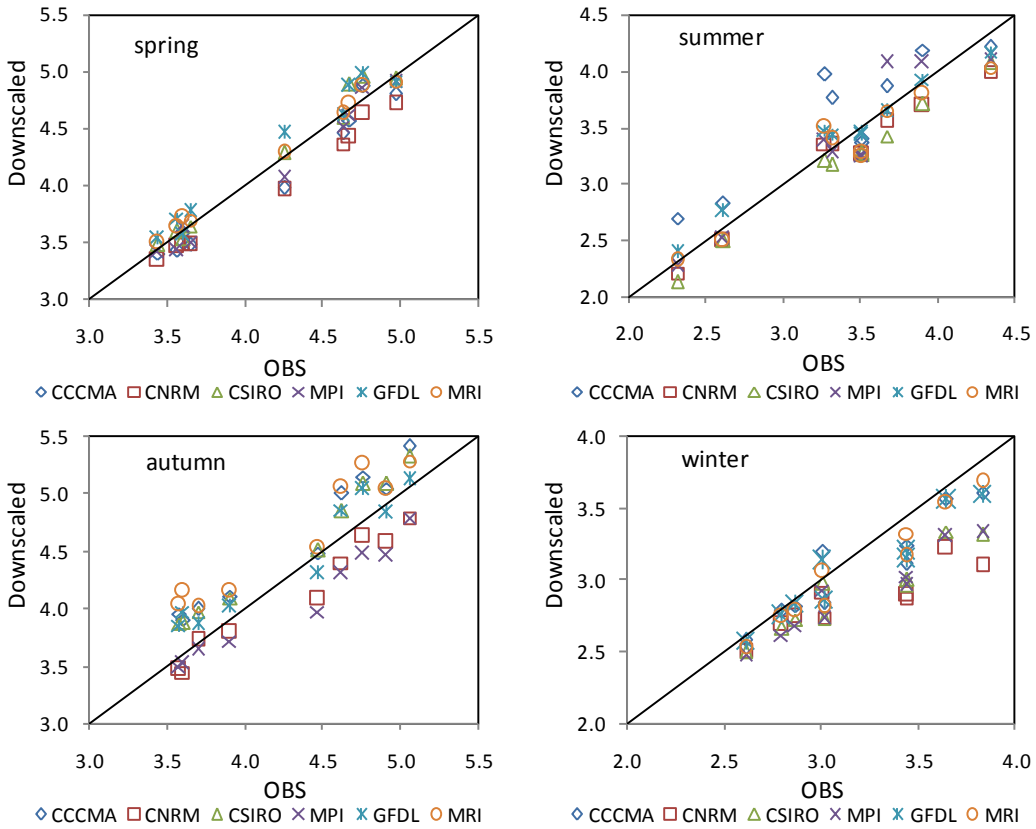

Fig. 7.10. As for Fig. 7.8 but for the standard deviations of T_{min}.

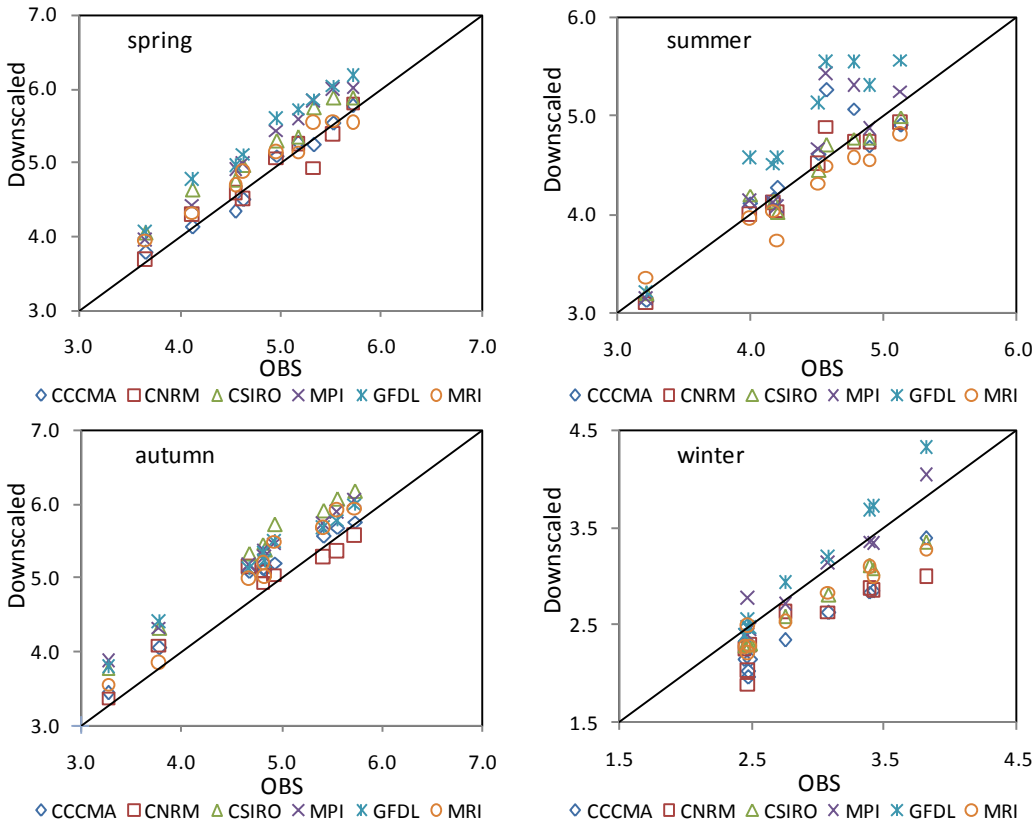

Fig. 7.11. As for Fig. 7.8 but for the standard deviations of T_{max}.

The A2 scenario is at the high end of the SRES emissions scenarios (but not the highest), since it is characterized by a very heterogeneous world with a continuously increasing population and a technologically fragmented economic development leading to one of the highest emission scenarios. It is expected that climate would go through much extensive changes in the future under this scenario, which makes it difficult to assess the possibility the change of the transfer function in the future. Nevertheless, the difference in the SOM node frequency of occurrence between the future and present climate could still be useful to quantitatively analyze whether the same synoptic patterns are present in the future if climate change will manifest itself as a change in the timing, persistence, and frequency of these synoptic-scale events.

For a given region, some studies analyzed the changes in frequency of SOM nodes one by one (e.g., Cassano et al., 2006; Hewitson and Crane, 2006; Hope 2006; Finnis et al., 2009). Not surprisingly, these studies indicated that changes of the frequency of occurrence really occurred in the GCM future data, resulting from changes in the temporal characteristics of the projected atmospheric circulation. A different method was used in this study to check the frequency changes based on an assumption that a substantial difference in frequencies for GCMs between the baseline and future could be identified by a different frequency distribution clustered in the SOM represented by the NNR. Taking all frequencies on the SOM nodes from both the GCM baseline and scenarios data as a whole, the non-parametric Kolmogorov-Smirnov (K-S) test was employed to compare their cumulative distribution function (CDF), which is a non-parametric method used to test the null hypothesis of no CDF difference in paired samples (Corder and Foreman, 2009). The CDFs should be similar to each other, as long as the atmospheric circulation does not over-cluster at several synoptic states (represented by abnormal frequencies). Although the above approach was not totally different from the direct analysis method (e.g., Hewitson and Crane, 2006), it has significant advantage since it could be applied easily to many downscaling target grids simultaneously as in the present study.

The K-S test requires calculating the test statistic and p value for the null hypothesis and either accept or reject the hypothesis at a given significant level α based on the p value. The p value is the probability of wrongly rejecting the null hypothesis if it is in fact true. An α value of 0.05 which corresponds to 5%

significance level was used in this study. Small *p*-values suggest that the null hypothesis is unlikely to be true and the null hypothesis is rejected when $p<0.05$. The test results indicated that the *p*-values were all above 0.05 (i.e., passed the K-S test, not shown) across all grids during the two 20 year future periods ranging from 2046 to 2065 (Future-A) and from 2081 to 2100 (Future-B). It indicated that the future synoptic-scale states may still be similar in CDF to the present-day synoptic patterns. Thus, to a certain extent, it provided the confidence in applying the statistical relationship between the predictors and the predictand derived from the baseline period to the future scenarios.

In addition, the SOM-SD is a type of conservative downscaling method, because the future atmospheric states could always map to the closest SOM nodes through the similarity computations, even though they might fall outside of the envelope of climate as defined by the data used to train the SOM. Thus, the future climate response can be conservatively estimated and, at worst, the change is underestimated.

7.4.3.3 Projected future temperature changes

The downscaled T_{min} and T_{max} changes under the A2 scenario in summer and winter are displayed in Fig. 7.12 – 7.13 for Future-A, and in Fig. 7.14 – 7.15 for Future-B, respectively. The changes were calculated as the differences between the downscaled results from the scenario periods and the baseline period (1961 – 1990). The downscaled results showed a spatially consistent increase in mean daily $T_{min}$and T_{max} for the Future-A and Future-B, with more significant warming trend in summer than in winter. For both T_{min} and T_{max}, the changes varied among the GCMs.

For Future-A, the increases in daily T_{min} were generally above 0.6 °C in summer and above 0.4 °C in winter across all climatic zones (Fig. 7.12). In summer, the CCCMA, MPI and GFDL produced greater increase (between 0.8 $^{\circ}$C and 1.2 $^{\circ}$C) than other GCMs (below 0.8 $^{\circ}$C). Most of the GCMs showed no obvious differences in the increases across different climatic zones. In winter, only CCCMA gave a relative large increase. Moreover, the mean daily T_{min} rose the largest in zones E4, E3 and F4 (above 0.6 $^{\circ}$C) and the smallest in those of D5, B2, F3 and E2 (about 0.4 $^{\circ}$C). Similar results were acquired in the case of mean daily

T_{max} (Fig. 7.13). In summer, the temperature increases were generally above 1.5 °C in most of climatic zones. MRI showed the smallest increase slightly above 0.5 °C, while CSIRO gave the largest increase of above 2.0 °C in most of climatic zones. Moreover, the warming trend appeared faster in other zones than that in the subtropical zones of F3 and F4. In winter, the increases were about 1.0 °C and more significant in E6, G, E4 and E3 than in other zones.

For Future-B, the mean daily T_{min} increased between 1.0 °C and 2.0 °C in summer, with the largest increase acquired by CCCMA and the smallest increase by CSIRO (Fig. 7.14). Moreover, the increase did not display an obvious spatial pattern for each GCM. In winter, the mean daily T_{min} increased highly in zones E4, E3 and F4 (between 1.2 °C and 1.8 °C) and lowly in the zones of D5, B2, F3 and E2 (between 0.5 °C and 0.8 °C). There were no significant differences among GCMs. In the case of the mean daily T_{max}, it would increase above 2.5 °C and below 3.5 °C (except for the subtropical zones of F3 and F4) in summer (Fig. 7.15). In winter, the increase appeared more significant in the zones of E6, G, E4 and E3 (mostly above 2.0 °C) than in other zones (mostly about 1.5 °C). Moreover, CNRM and CSIRO would produce the higher warming than other GCMs in most of the arid and semi-arid zones.

The temperature increase could also be found in the two extreme temperature indices of Tn10 and Tx90. Here only the changes in Tn10 for winter and in Tx90 for summer were taken as examples because in these seasons they occurred more frequently than other seasons. The downscaling showed that Tn10 increased higher in the arid and semi-arid zones D5, B2, F3 and E2 than in humid zones in Future-A. Moreover, MRI always gave the smallest increase, while CCCMA almost always gave the largest increase (Top panel, Fig. 7.6). However, Tn10 increased similarly high for almost all GCMs in Future-B (Bottom panel, Fig. 7.16). For Tx90, the GCMs showed a very similar spatial pattern across the climatic zones during the two future periods (Fig. 7.17). The increasing appeared slightly more marked in D5, B2, F3 and E2 than in other zones. The increases in Tx90 were from 1.0 to 1.5°C for Future-A and from 1.5 °C to 2.0 °C for Future-B.

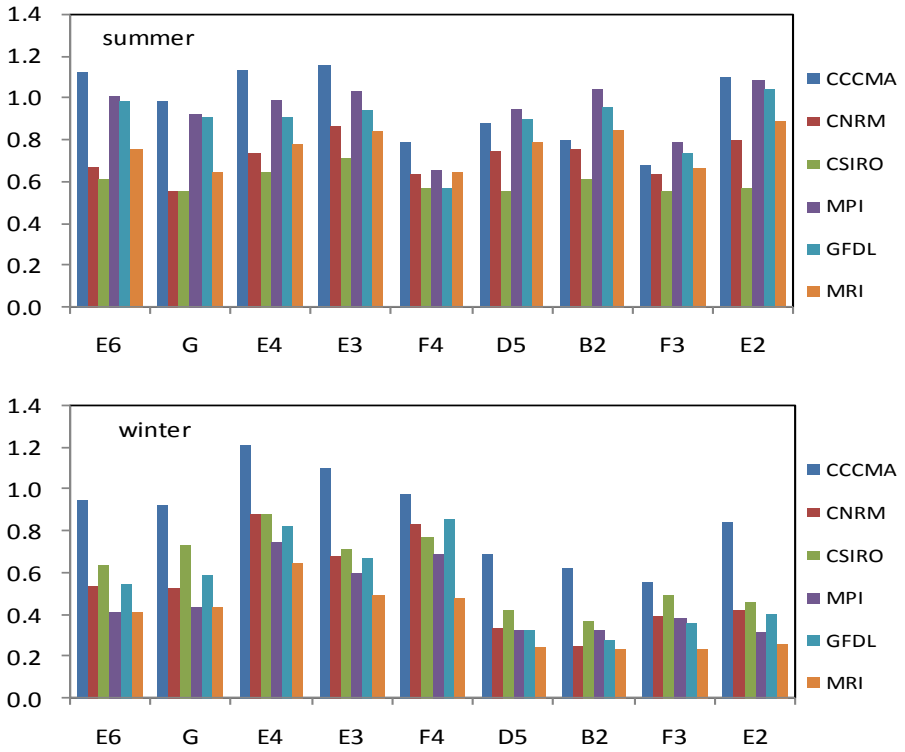

Fig. 7.12. Daily T_{min} change estimates under the A2 scenario during the Future-A (2046 – 2065 minus 1961 – 1990) derived from the GCMs (different color bar) in different climatic zones (names on the X-axis). The top panel is for summer, while the bottom panel is for winter. Each value was an average across all the grids available in a particular climatic zone. The downscaled values are computed as ensemble means of the ensemble for 500 runs. The units are $^{\circ}$C.

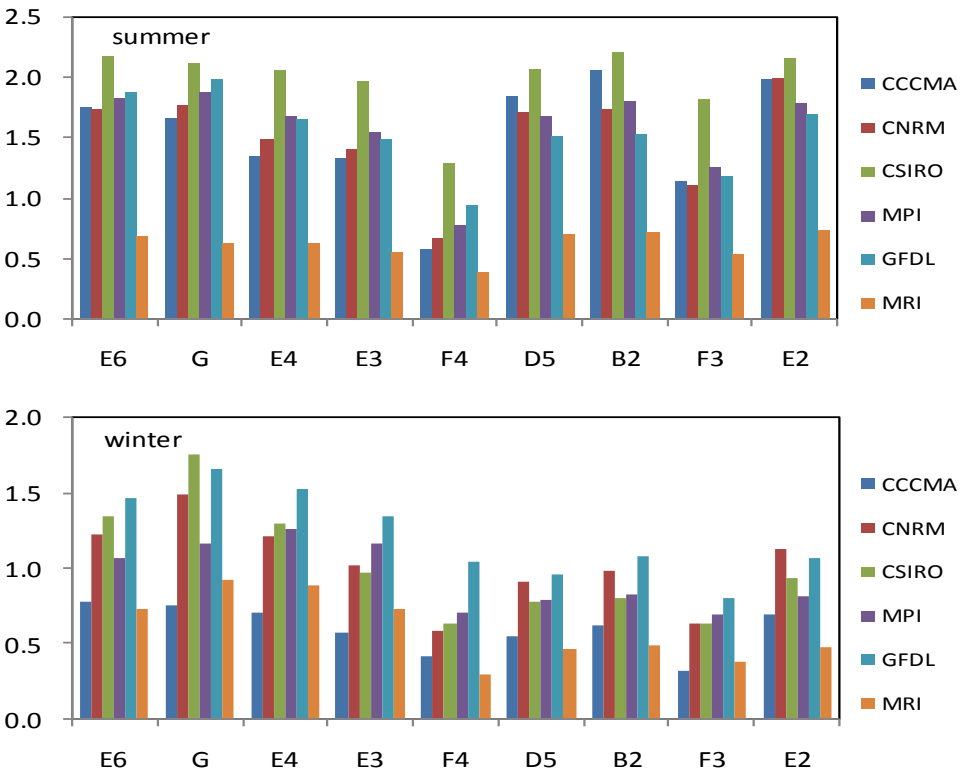

Fig. 7.13. As Fig. 7.12 but for T_{max}.

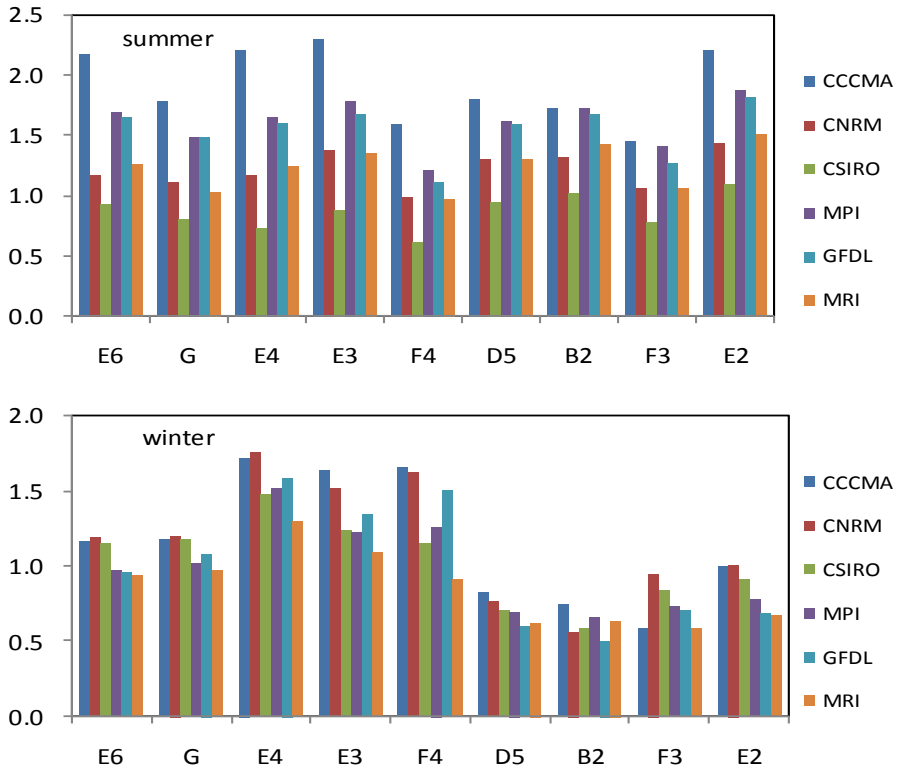

Fig. 7.14. Daily T_{min} change estimates under the A2 scenario during the Future-B (2081 – 2100 minus 1961 – 1990) derived from the GCMs (different color bar) in different climatic zones (names on the X-axis). The top panel is for summer, while the bottom panel is for winter. Each value was an average across all the grids available in a particular climatic zone. The downscaled values were computed as ensemble means of the 500 runs.

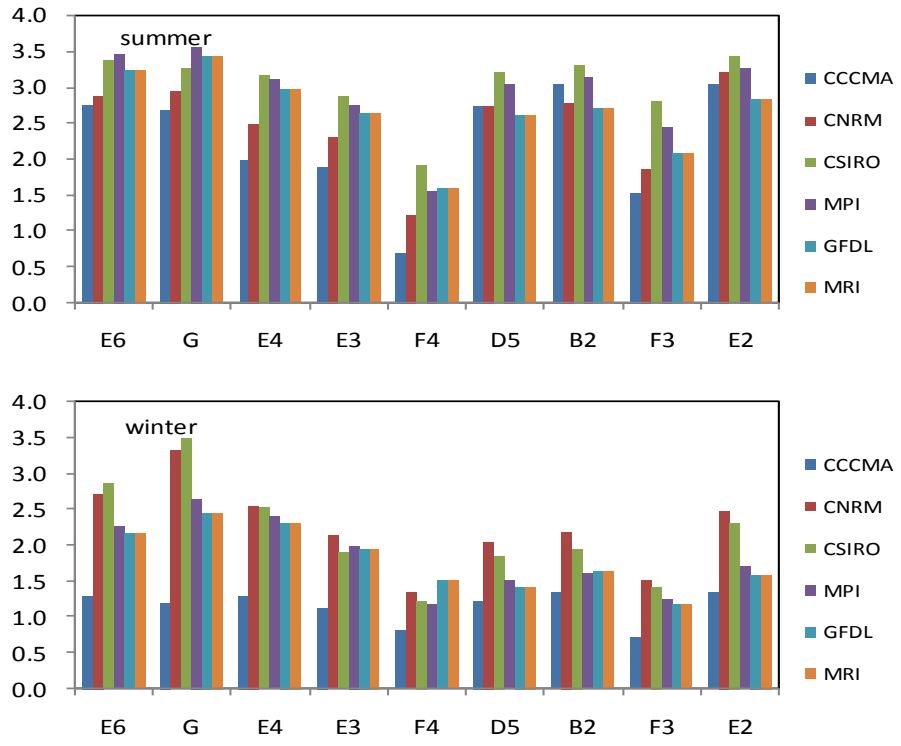

Fig. 7.15. As Fig. 7.14 but for T_{max}.

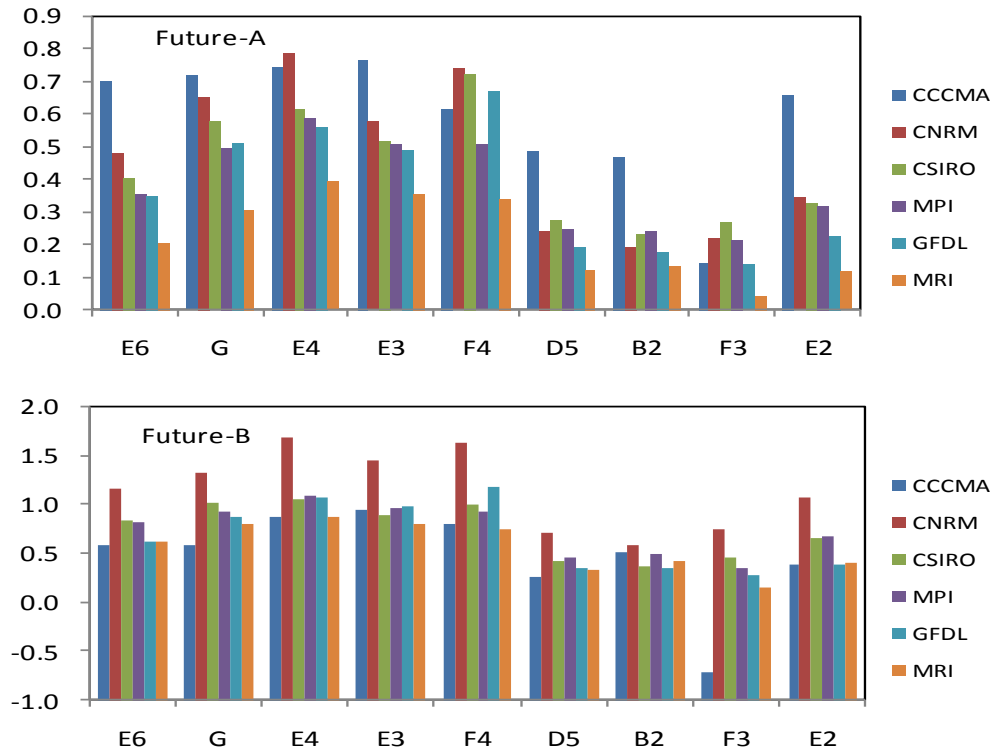

Fig. 7.16. The 10th daily percentile daily T_{min} (Tn10) change estimates in winter under the A2 scenario during the Future-A (2046-2065 minus 1961-1990) and the Future-B (2081 – 2100 minus 1961 – 1990) derived from the GCMs. Each value was an average across all the grids available in a particular climatic zone.

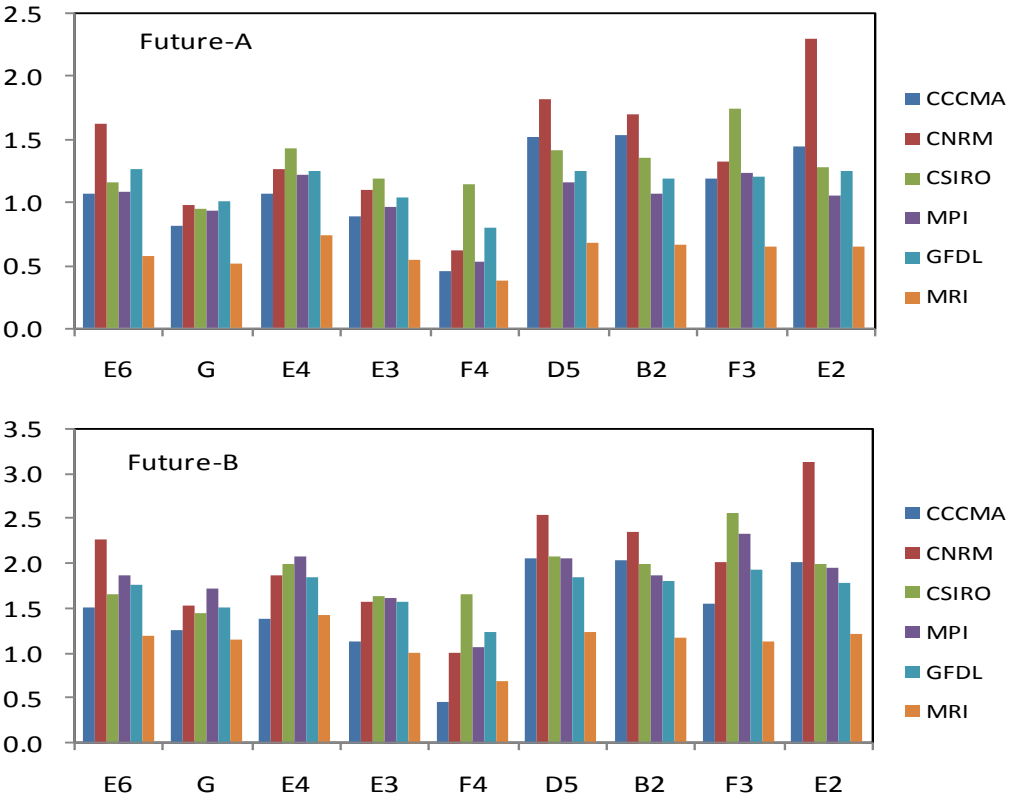

Fig. 7.17 as Fig. 7.16 but for Tx90 in summer.

7.4.3.4 Trend correction

Compared with the direct GCM output, the downscaled temperature changes from downscaled outputs, or the warming trends in most cases, were projected much lower. The underestimations were consistent across all GCMs and more significant in winter than in summer. In winter, the downscaled projections showed only half the temperature increase projected by GCM outputs.

A set of expanded analyses was carried out, which showed that there were several combinations of predictors that could have similar modeling performance for both NNR and GCM baseline data. However, it was found that none of these combinations could generate larger temperature increases for the downscaled T_{min} and T_{max} than the combination of predictors used at present. On the one hand, this indicated that the used predictor combination was robust. On the other hand, the reduced warming in the downscaled projections must be due to other reasons, such as that the SOM-SD could not extrapolate record-breaking temperatures. However, it is very likely that record-breaking temperatures may take place more frequently in the future as current observations showed and GCMs projected. Thus re-sampling values from historical data for future climate will distort the tails of the distributions of the downscaled temperatures as temperatures rise. This is not only a common issue for analog-like models (e.g., Timbal et al., 2003, 2009; Benestad et al., 2008), but also for bias correction methods (e.g., Wood et al., 2004; Maurer, 2007).

There were a few attempts to improving the above problem (e.g., Maurer, 2007; Benestad, 2010), for example, a scheme to superimpose a linear trend from a regression-based model onto the results of the analog-like model (Imbert and Benestad, 2005). Nevertheless, such a scheme was not adopted by this study, because the linear trend generally is not the best representation of the long-term temperature evolution (Benestad, 2003). Here another simple approach was used to ensure that the difference of the downscaled temperature between the scenario period (SCE) and the baseline period (BSL, 1961-1990) for a particular GCM matches the counterpart of the direct GCM output. This adjustment was done for each month and each downscaling grid as:

$$Y_{m,SD}^{SCE\,\prime}(t) = Y_{m,SD}^{SCE}(t) + [(\overline{Y_{m,GCM}^{SCE}(t)} - \overline{Y_{m,GCM}^{BSL}(t)}) - (\overline{Y_{m,SD}^{SCE}(t)} - \overline{Y_{m,SD}^{BSL}(t)})] \qquad (7.1)$$

where *t* donates a day from a particular month *m*, *SD* and *GCM* represents the

value of the predictand Y from the downscaling model of SOM-SD and a particular GCM, respectively, Y' is the adjusted value and $\bar{Y}$ is the mean value for a period of SCE or BSL. It is worth noting that the $\bar{Y}$ for a GCM also is the mean value of the spatial domain of 3×3 grids around the target grid. This is because a spatial mean might be more reliable than that of single grid for a GCM. For both the downscaled T_{min}, and T_{max}, the above adjustment procedure generated very similar changes to the direct GCM outputs. Taking Future-A as an example, seasonal local warming averaged over the whole case study area are shown for both T_{max} and T_{min}, in both the original downscaled and corrected projections (Fig. 7.18).

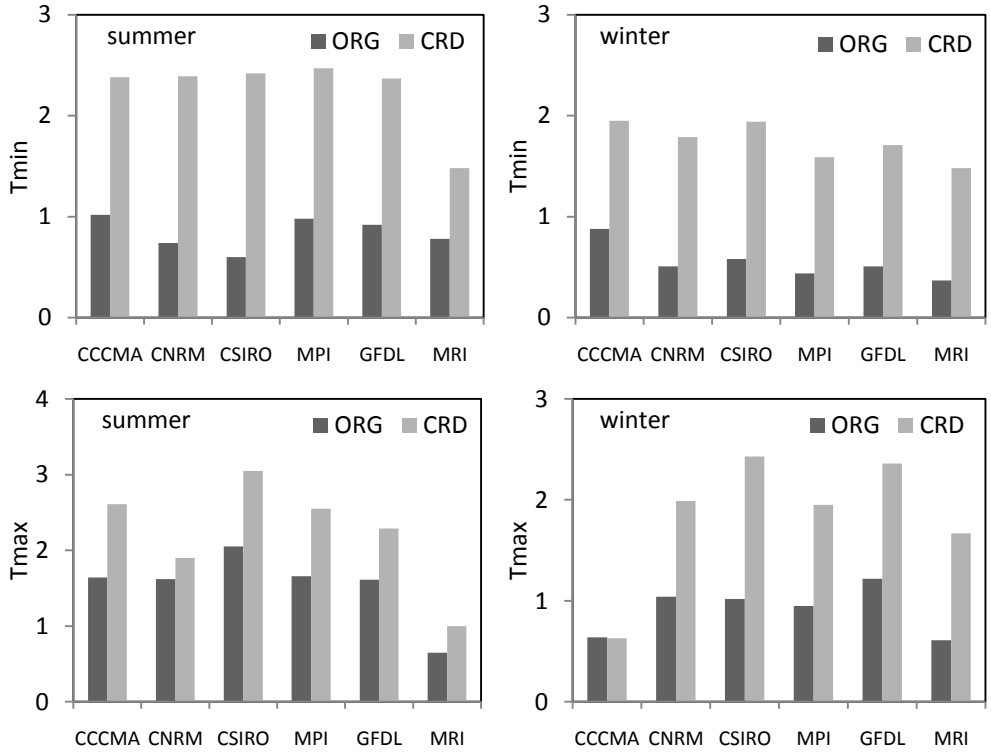

Fig. 7.18. Seasonal local warming averaged over the whole case study area for both T_{max} and T_{min}, in both the original downscaled (ORG) and corrected projections (CRD) during Future-A (2046-2065).

The above adjustment is based on the assumption that the GCMs could generate correctly the future temperature change trend, even though they might fail to reproduce the observed records. Moreover, the adjustment also followed the principle of downscaling methods to refine the details as to the GCM results, rather than producing a completely different projection. The proposed adjustment corrected the downscaled temperature trend to produce representative values for impact studies. However, it dealt with new values outside the range of the

observed data by shifting the downscaled PDF according to the mean difference between the two periods projected by a GCM. Such a shift of the statistical distribution, although easy to use, seems a little artificial. More complicated schemes can be further explored in the future.

7.5 Conclusion and discussion

In this chapter, the SOM-SD was used to downscale daily maximum and minimum temperature across southeast Australia. The validity of the SOM-SD was investigated with evaluation of six GCM models (CCCMA, CRNM, CSIRO, MPI, GFDL and MRI; see Table 2.2) for projecting climate change under the scenario A2 across southeast Australia. Based on the NNR, the SOM-SD gave an unbiased reproduction of the probability density functions (PDFs) for the observed daily T_{min} and T_{max}. The SOM-SD could reproduce both the high and low of the mean values and the standard deviations, including the tails of the distribution (large or small observed values). Moreover, it also offered unbiased estimates of the extreme low and high temperature (Tn10 and Tx90). The GCMs were evaluated directly by the similarity of the frequency of occurrence for each of the observed synoptic patterns represented by the NNR, and then were indirectly assessed by the SOM-SD. The correlation results showed that all GCMs could reproduce the observed synoptic climatology reasonably well (mostly above 0.8 for the predictor combination associated with T_{min} and T_{max}). The downscaled results using GCM control data were comparable to those using the NNR during the baseline period.

One of the biggest challenges for SDSMs is the stationarity issue. Although the stationarity issue could not be verified immediately, the non-parametric K-S test was used to analyze the projected atmospheric state changes in their CDFs of the frequencies of occurrence associated with present synoptic patterns. The tests indicated that the future atmospheric states were very likely to remain stable and within the scope of the present synoptic patterns. Together with the conservative downscaling of the SOM-SD, the confidence increased for surface variables derived from GCMs. When forced by several different GCMs, the downscaled results across southeast Australia showed a spatially consistent increase for T_{min} and T_{max} as well as their extreme values, with more significant warming trend in summer than in winter. However, for both T_{min} and T_{max}, the changes

varied among the GCMs.

In addition, it was found that the local warming projected by the SOM-SD was consistently lower than that in the direct GCM output. This feature might be due to three factors: (1) though the set of used predictors were optimized for the whole area, they were not the optimum one for each downscaling grid; Moreover, the parameters also were not the optimum for training the SOM, including the size of spatial domain and the number of synoptic patterns; (2) the SOM-SD could reproduce only part of the observed long-term trend; (3) the SOM-SD, like other analog-like models, is incapable of making predictions of values outside the observed data, and thus is unable to predict new record-breaking values. As global warming becomes more significant than at present, this issue will also become more serious. Under such a case, analog-like models including the SOM-SD must be combined with other methods such as linear models to extrapolate new values outside the observed data (Imbert and Benestad, 2005).

In this study, to produce representative values for impact studies, the downscaled results were simply adjusted by ensuring that the difference of the downscaled temperature between the scenario period and the baseline period for a particular GCM matches the counterpart of the direct GCM output. This method was titled as "trend correction". For both the downscaled T_{min} and T_{max}, the adjustment procedure generated very similar changes to the direct GCM outputs. However, it should be noted that such a trend correction appears a little artificial. More practical correction methods will be assessed in the coming future.

It was also found that large-scale temperature variables were more informative predictors of local surface daily temperature than large-scale circulation fields. Other combinations of predictors could produce similar downscaling results. One of the objectives of this study was to analyze the applicability of the SOM-SD across different climatic zones and seasons with respect to temperature changes. Thus, the combination of predictors selected did not mean an optimum combination for any zone and/or any season, where/when an extensive diagnosis indicated that other predictors also have different impacts on downscaled temperature (e.g., Timbal et al., 2009). If climate change impact studies are carried out in small (smaller) regions, the optimum combination of predictors should be selected in order to further improve the performance of the SOM-SD.

In addition, the SOM-SD used a moving spatial domain to characterize the differences in atmospheric states around each target downscaling location. For the target grids that were most co-located with the center of the domain, the spatial coherence of the downscaled predictands could be well depicted. That is to say, the spatial coherence was achieved in each independent grid of large-scale predictors. However, it became difficult to keep the spatial coherence as the spatial domain moved. This is not necessarily the limitation of the SOM-SD, rather a common constraint for most SDSMs (Maraun et al., 2010). This issue could partly be explained by the discontinuity in the similarity of the atmospheric states in the selected downscaling domains. With regard to other strengths and weaknesses of the SOM-SD, they are referred in Chapter 4-6.

CHAPTER EIGHT

STATISTICAL DOWNSCALING OF DAILY PRECIPITATION FROM GCM OUTPUTS

8.1 Introduction

Precipitation projection plays a crucial role in regional impact studies. Alterations of precipitation characteristics are expected to be significant because of global warming (Allen and Ingram, 2002; Trenberth et al., 2003; Randall et al., 2007). However, it remains a challenge for GCMs to capture observed precipitation characteristics even at the global scale (e.g., Trenberth et al., 2003; Meehl et al., 2005; Randall et al., 2007).

Precipitation in Australia is characterized by complex features. It encompasses both tropical and mid-latitude processes, and includes both extremely arid regions and regions with high annual and seasonal rainfall. Combined with the highly diverse landscape ranges, a number of synoptic processes (Fig. 3.11) are responsible for the interannual rainfall variability, which include the large-scale El Niño-Southern Oscillation, the Southern Annular Mode and Indian Ocean Dipole, also the small-scale low pressure systems cut-off from the westerlies (Qi et al., 2006; Hopkins and Holland, 1997; Holland et al., 1987) and easterly troughs (Speer and Leslie, 1998; Speer and Geerts, 1994).

These regional-scale synoptic processes usually are not included in GCMs, due to limited knowledge and imperfect representation of the physical processes leading to many assumptions and over simplifications in parameterizations. This has been witnessed by the inter-model differences in simulating a precipitation response to a given forcing scenario. Rainfall events tend to be simulated more frequently and more moderately by GCMs than in real climate (Trenberth et al., 2003). Hence regional impact studies that made use of the direct GCM-simulated precipitation are always subject to debate (von Storch et al., 1993). In general, downscaling is required before GCM data can be used for regional scale impact studies.

In this chapter, the SOM-SD is evaluated and extended to downscale GCM transient simulations so that future precipitation change scenarios could be constructed.

8.2 Data and method

8.2.1 Data

The predictands or the dependent variables are daily gridded precipitation at a spatial resolution of 0.05°provided by the Australian Bureau of Meteorology. To match the GCM simulations of present-day climate, only the period from 1961-2000 was used. Although the dependent variables have a fine resolution of 0.05°×0.05°, the downscaling was only carried out at a resolution of 0.25°×0.25° mainly due to the high computational demand. Nevertheless, such a resolution is sufficient to reflect different climatic zones and orographic features across the case study area.

Daily large-scale atmospheric predictors consist of the NCEP/NCAR Reanalysis data (NNR; available from 1948 to real-time; Kalnay et al., 1996; Kistler et al., 2001) and GCM simulation results under the climate change scenario A2 from the CMIP3 project (https://esg.llnl.gov:8443/index.jsp). Although many climate variables are available, only the mean sea-level pressure (SLP), specific humidity at 500hPa (Q5), air temperature at 700hPa (T7) and precipitation rate (Pr) were selected as predictors here. These predictors from NNR and observational precipitation data were used to build the relationship between synoptic driver and precipitation over the case study area and had shown a good performance (see Chapter 4). The GCMs used included CCCMA, CNRM, CSIRO, GFDL, MPI and MRI. The GCM simulations in present-day climate cover the baseline period (1961-2000). All of the above predictors have been regridded to have the same spatial resolution of 2.5°×2.5°. More detailed information about these data and relevant processing approaches can be found in Chapter 2.

Because the SOM-SD was calibrated and validated according to the NNR for the 1961-2000, the data of the predictors and predictand of the same period were employed as a whole in order to evaluate the performance of the SOM-SD in downscaling the GCM outputs. The GCM predictor data used to construct future

precipitation change scenarios were two 20-year periods ranging from 2046 to 2065 and from 2081 to 2100.

8.2.2 Configuration of SOM-SD

The details in constructing the SOM-SD for downscaling have been described in Chapters 4 – 6, and therefore only the particular set-up for downscaling GCM simulations for precipitation is given here. For each downscaling precipitation grid, a set of 5×7 general synoptic pattern was identified on the spatial domain of 3×3 grids. Firstly, predictors from both NNR and GCMs were standardized by subtracting the mean value and then dividing by the standard deviation of the whole domain during the baseline period (Eq. 2.1, Chapter 2). Secondly, for the GCM simulation data of future climate, the predictors were standardized using the means and standard deviations of the simulation data for the present-day climate. Other SOM-SD configurations were the same as those in Chapter 5, such as the seasonal re-sampling scheme and the conditional stochastic re-sampling algorithm.

8.2.3 Accuracy of the downscaling method

Regional rainfall characteristics can be analyzed by examining its frequency and intensity, which are important statistical properties for hydrological studies. Table 8.1 lists several diagnostics for daily precipitation characteristics concerning first and second moments of PDF, extremes and wet/dry day persistence. A wet day was defined as a day with the daily precipitation greater than or equal to 0.1mm. These diagnostics have now been recognized as common indices for downscaling studies (e.g., STARDEX; Maraun et al., 2010). As discussed previously, the SOM-SD can produce an ensemble of 500 runs for each precipitation grid at a daily time-step. From that, the 90% confidence intervals (5-95%) can be calculated for these indices through a bootstrapping technique (Khan et al., 2006; Dibike et al., 2008). Downscaling results were evaluated for the entire learning period (1961 to 2000) and were assessed in a seasonally stratified style to ensure that the model was capable of capturing the annual variability of precipitation.

Table 8.1 Diagnostics of daily precipitation

Acronym	*Definition*	*Unit*
SDII	Simple daily intensity(mean daily precipitation on wet days)	mm/day
ppSD	Standard deviation of daily precipitation on wet days	mm/day
RMSE	Root mean square error of daily precipitation time series	mm/day
pSSNSD	Standard deviation of season precipitation	mm/season
P95	95-th percentile value of precipitation (extreme precipitation)	mm/day
nr001	Mean number of rainy days for daily precipitation >=0.1mm	Days
nr020	Mean number of rainy days for daily precipitation >=2.0mm	Days
nr200	Mean number of rainy days for daily precipitation >=20.0mm	Days
Pww	Mean wet persistence	%
Pdd	Mean dry persistence	%
Ldd	Mean dry spell length	Days

8.3 Results

8.3.1 Assessment of GCMs

Downscaling methods are generally constructed based on the reanalysis data, and then are applied to GCMs. A basic assumption is that the predictors must be reliably represented by GCMs. So assessing the performance of GCMs is an important step to construct a successful downscaling method.

Here the method described in Chapter 7 was used to assess the performance of GCMs. For a target downscaling grid, a set of large-scale atmospheric circulation patterns with the number of 5×7 was identified by the SOM algorithm from the predictors at a spatial 3×3 grid domain. The data from the reanalysis and GCMs (during different time periods) then were mapped to the attained SOM. The difference of the SOM node frequency of occurrence between the NNR and GCM data was used as an indication of differences in the synoptic climatology represented by the two data sets. The correlation between each GCM and the NNR are listed in Table 8.2, where each value is a mean value across all down

target grids in a specific climatic zone. All GCM could reproduce quite well the observed synoptic patterns represented by the NNR predictors. In most of the climatic zones, the correlations were generally above 0.80 with the exceptions in zone E4 for CNRM, CSIRO, MPI, GFDL and MRI and zone F4 for CSIRO, MPI and MRI. Overall, there was no particular GCM that stands out as always performing better than others in all the climatic zones hence all GCMs were suitable to be downscaled.

Table 8.2 Mean correlation of the SOM node frequencies between the GCMs and the NNR across the climatic zones during the baseline period of 1961-2000.

zone	CCCMA	CNRM	CSIRO	MPI	GFDL	MRI
E6	0.88	0.85	0.87	0.85	0.87	0.89
G	0.84	0.85	0.86	0.86	0.86	0.92
E4	0.87	0.75	0.79	0.78	0.76	0.85
E3	0.90	0.83	0.86	0.86	0.86	0.86
F4	0.89	0.82	0.77	0.75	0.87	0.69
D5	0.87	0.87	0.87	0.85	0.86	0.88
B2	0.89	0.89	0.87	0.87	0.89	0.91
F3	0.87	0.85	0.81	0.82	0.90	0.84
E2	0.88	0.90	0.81	0.87	0.89	0.91

8.3.2 Evaluation of the GCM-based downscaling

Based on the GCM predictors, the skill of the SOM-SD in reproducing the observed probability distribution functions (PDFs) was firstly evaluated by the first two moments of the PDFs: the mean (SDII) and the standard deviation (ppSD) on wet days, as shown in Fig. 8.1. In each graph, each point corresponds to a single climatic zone for a specific GCM with the observed mean value across all grids in that zone on the X-axis and the downscaled mean along the Y-axis. It is worth mentioning that the downscaled values were computed as the means of the ensemble for 500 runs. However, in the case of GCMs, the downscaled values appeared closer to the observed values in summer and winter than in spring and autumn. The points of spring and autumn were slightly below the diagonal,

indicating a bias toward drier values for the downscaled series. Overall, the downscaled results were comparable to the observed values.

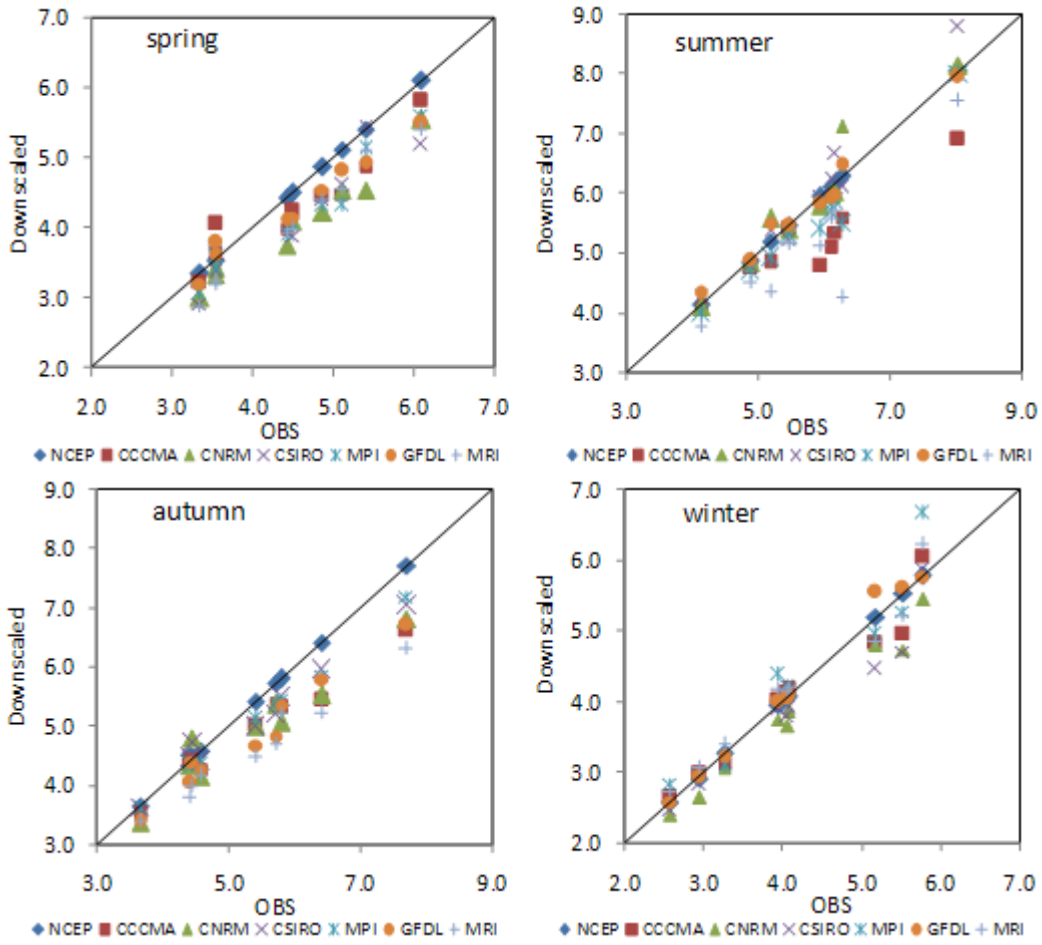

Fig. 8.1. Scatter plot of the downscaled *versus* observed mean (OBS) of daily precipitation on wet days (SDII; mm/day). On each graph, there is one point per climatic zone and per GCM, the total number of points per graph is the number of climatic zones times seven (one for NCEP and six for GCMs). The downscaled values are computed as ensemble means of 500 runs during the baseline period 1961 – 2000[2].

The production of the standard deviation for daily precipitation on wet days (ppSD) is shown in Fig 8.2. The best reproduction was acquired in winter, when errors in the reproduction for most of the GCMs were negligible and there was no bias toward either high or low values, including at the tails of the distribution (large or small observed values). Relative better performance was also attained in summer, when only CCCMA and MRI had a tendency to underestimate the observed values. However, in spring and autumn, the downscaled values showed a

[2] The observational precipitation data were not divided into calibration and validation data, while used as a whole. It could be imagined that NCEP points should lie perfect on the straight line.

slight tendency to underestimate the observed values. This underestimation is a known issue for regression-based statistical downscaling methods (Von Storch, 1999), but the SOM-SD could reproduce most of the observed variance and this variance underestimation was relatively small. Accordingly, there was no further "variance inflation" techniques employed to artificially adjust the downscaled rainfall series in order to enhance the variance (e.g., Von Storch, 1999; Timbal et al., 2009).

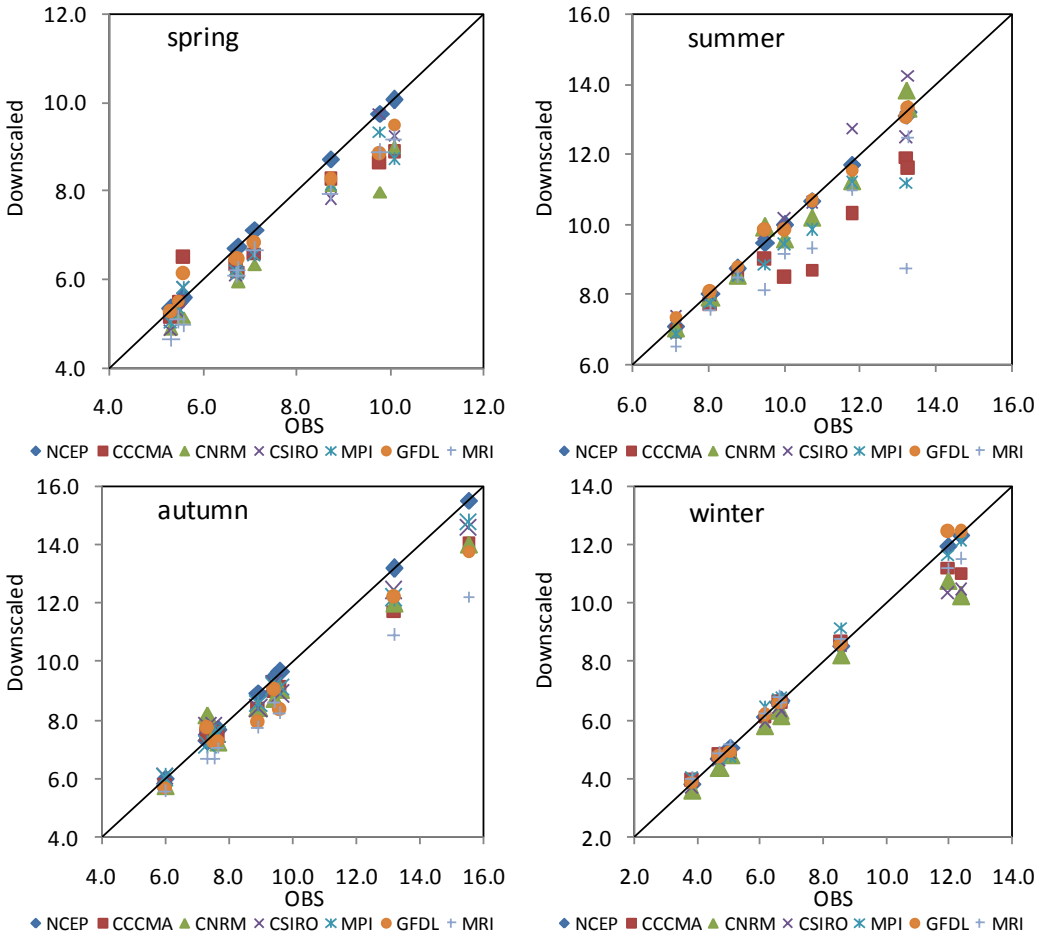

Fig. 8.2. As Fig 8.1 but for standard deviations (ppSD).

In addition, the root mean square error (RMSE) between downscaled and observed time series did not show any significant differences between the NNR and those from GCMs in each climatic zone for each season (Fig. 8.3). This implied that the downscaled results from the selected GCMs were comparable to those from the reanalysis data. The RMSEs generally appeared larger in the sub-tropic climatic zones of F3 and F2 and the high elevation mountain zone of B2 than in other zones. As daily precipitation typically belongs to non-Gaussian distribution, the correct modeling of the first two moments of PDF would not

prevent a biased estimate of the shape of the PDF. The Kolmogorov-Smirnov (K-S) goodness-of-fit test was further used to assess the cumulative distribution of frequency (CDF) for observed and downscaled daily precipitation on wet days. As before, an α value of 0.05 which corresponds to the 5% significance level was used in this study, with small *p*-values suggesting that the null hypothesis is unlikely to be true and the null hypothesis being rejected when $p<0.05$.

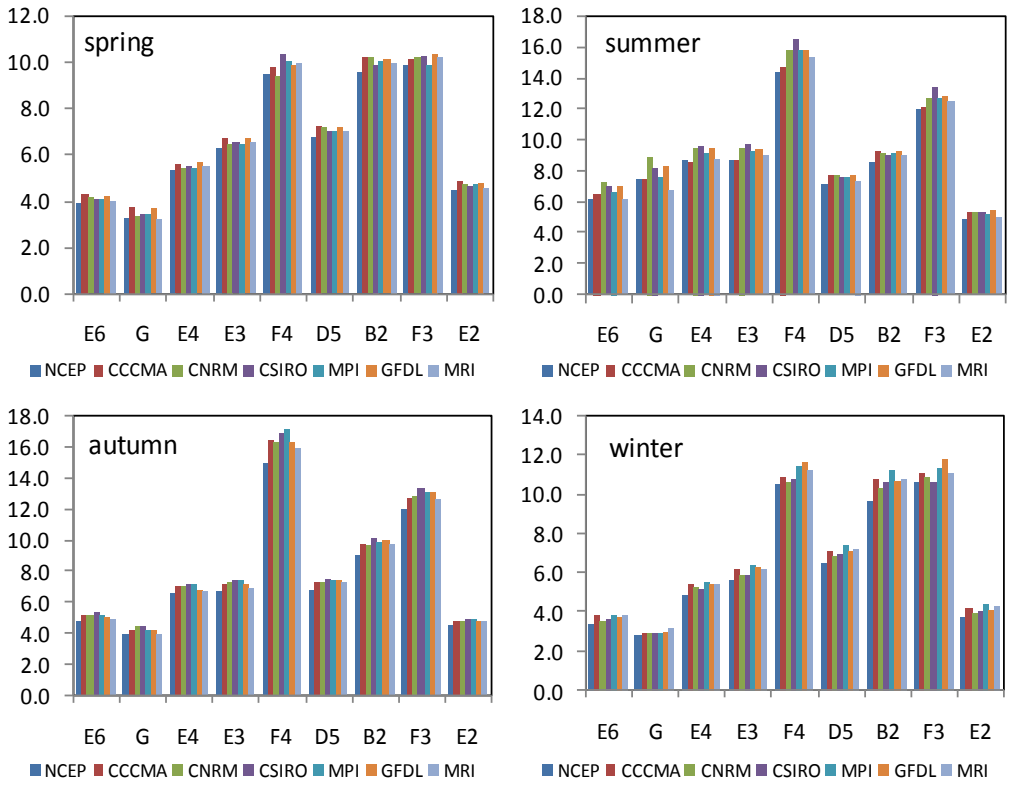

Fig. 8.3 Root mean square error for the downscaled and observed daily precipitation series (RMSE) specified by the named GCMs (different colored bars) and the climatic zones (names on the X-axis). Each value was an average across all the grids available in a particular climatic zone.

The test results (*p*-values) are presented in Table 8.3, where each value was an average across all the grids available for a particular region and a GCM. The *p*-values of the goodness-of-fit test were almost all above 0.05 (the 5% significance level) for the means of 500 runs in all climatic zones, indicating that they all passed the K-S test. Moreover, the best performance was acquired by the downscaled values from the NNR, since the lower bounds of the 90% confidence intervals also passed the K-S test across all climatic zones and seasons. However, that was not the case for the GCMs. Although most of the runs in the ensemble succeeded in passing the K-S test at the 5% significance level, there were still some runs failed. Overall, the K-S tests for GCMs appeared better in other

seasons than in spring.

Table 8.3. Mean of non-parametric Goodness-of-fit test results (*p*-values) for comparing cumulative frequency distribution of the downscaled and observed daily precipitation on wet days in each of the climatic zones. Each value is an average across all the grids available in a particular zone. These statistics are derived from the ensemble of 500 runs in the baseline period (1961-2000); 90% confidence intervals are in parentheses.

Spring	NCEP	CCCMA	CNRM	CSIRO	MPI	GFDL	MRI
E6	0.90(0.37, 0.99)	0.71(0.21, 0.97)	0.54(0.13, .88)	0.53(0.12, 0.90)	0.65(0.17, 0.95)	0.72(0.21, .97)	0.48(0.08,0 .92)
G	0.88 (0.33, 0.99)	0.56 (0.10, 0.96)	0.73 (0.19, 0.99)	0.74 (0.20, 0.99)	0.70(0.19, 0.99)	0.71 (0.22, 0.98)	0.68 (0.16, 0.99)
E4	0.89 (0.36, 0.99)	0.39 (0.08, 0.82)	0.12 (0.01, 0.46)	0.29 (0.03, 0.82)	0.17(0.02, 0.67)	0.44 (0.10, 0.86)	0.23 (0.02, 0.74)
E3	0.89 (0.37, 0.99)	0.38 (0.06, 0.88)	0.10 (0.01, 0.47)	0.15 (0.01, 0.59)	0.11(0.01, 0.55)	0.33 (0.05, 0.83)	0.18 (0.02, 0.70)
F4	0.90 (0.37, 0.99)	0.42 (0.07, 0.91)	0.15 (0.03, 0.39)	0.55 (0.13, 0.91)	0.18(0.04, 0.46)	0.33 (0.06, 0.81)	0.44 (0.11, 0.73)
D5	0.90 (0.37, 0.99)	0.52 (0.12, 0.92)	0.26 (0.05, 0.68)	0.04 (0.00, 0.19)	0.16(0.02, 0.62)	0.14 (0.02, 0.53)	0.08 (0.01, 0.43)
B2	0.89 (0.38, 0.99)	0.59 (0.16, 0.95)	0.16 (0.02, 0.55)	0.00 (0.00, 0.04)	0.11(0.01, 0.52)	0.05 (0.01, 0.23)	0.03 (0.00, 0.26)
F3	0.90 (0.36, 0.99)	0.22 (0.03, 0.61)	0.27 (0.05, 0.73)	0.13 (0.02, 0.50)	0.04(0.00, 0.24)	0.42 (0.07, 0.91)	0.11 (0.01, 0.51)
E2	0.90 (0.36, 0.99)	0.68 (0.18, 0.98)	0.24 (0.03, 0.78)	0.08 (0.01, 0.43)	0.30(0.04, 0.82)	0.39 (0.07, 0.78)	0.14 (0.01, 0.58)
Summer	NCEP	CCCMA	CNRM	CSIRO	MPI	GFDL	MRI
E6	0.89 (0.36, 0.99)	0.51 (0.13, 0.85)	0.57 (0.14, 0.93)	0.73 (0.22, 0.98)	0.72 (0.23, 0.96)	0.65 (0.18, 0.96)	0.27 (0.04, 0.75)
G	0.89 (0.38, 0.99)	0.41 (0.06, 0.92)	0.25 (0.04, 0.81)	0.84 (0.31, 0.99)	0.69 (0.20, 0.98)	0.78 (0.23, 0.99)	0.05 (0.00, 0.35)
E4	0.89 (0.36, 0.99)	0.03 (0.00, 0.22)	0.68 (0.20, 0.97)	0.75 (0.23, 0.99)	0.33(0.04, 0.83)	0.64 (0.16, 0.97)	0.15 (0.01, 0.64)
E3	0.88 (0.35, 0.99)	0.07 (0.01,0.30)	0.72 (0.21, 0.98)	0.72 (0.22, 0.98)	0.47(0.09, 0.94)	0.66 (0.17, 0.97)	0.37 (0.06, 0.87)
F4	0.88 (0.36, 0.99)	0.04 (0.00, 0.22)	0.49 (0.10, 0.89)	0.16 (0.02, 0.58)	0.65(0.17, 0.97)	0.70 (0.20, 0.98)	0.38 (0.07, 0.83)
D5	0.89 (0.35, 0.99)	0.29 (0.06, 0.62)	0.65 (0.17, 0.96)	0.48 (0.11, 0.81)	0.61(0.14, 0.97)	0.70 (0.20, 0.98)	0.32 (0.04, 0.82)
B2	0.90 (0.36, 0.99)	0.39 (0.08, 0.79)	0.71 (0.21, 0.98)	0.48 (0.13, 0.84)	0.66(0.14, 0.99)	0.78 (0.22, 0.99)	0.37 (0.06, 0.90)
F3	0.89 (0.37, 0.99)	0.10 (0.02, 0.35)	0.60 (0.15, 0.94)	0.50 (0.10, 0.93)	0.60(0.14, 0.98)	0.64 (0.14, 0.98)	0.28 (0.03, 0.81)
E2	0.89 (0.34, 0.99)	0.49 (0.11, 0.90)	0.76 (0.22, 0.99)	0.73 (0.20, 0.99)	0.75(0.23, 0.99)	0.72 (0.20, 0.99)	0.48 (0.08, 0.95)
Autumn	NCEP	CCCMA	CNRM	CSIRO	MPI	GFDL	MRI
E6	0.88 (0.38,0.98)	0.57 (0.14, 0.94)	0.57 (0.14, 0.94)	0.72 (0.22, 0.97)	0.77(0.25, 0.98)	0.39 (0.07, 0.84)	0.28 (0.05, 0.70)
G	0.90 (0.36, 0.99)	0.69 (0.19, 0.98)	0.71 (0.21, 0.99)	0.72 (0.19, 0.99)	0.78(0.24, 0.99)	0.71 (0.18, 0.99)	0.54 (0.10, 0.97)
E4	0.90 (0.37, 0.99)	0.46 (0.08, 0.94)	0.55 (0.11, 0.96)	0.46 (0.09, 0.92)	0.67(0.17, 0.98)	0.18 (0.02, 0.63)	0.06 (0.00, 0.37)
E3	0.90 (0.37, 0.99)	0.39 (0.06, 0.86)	0.36 (0.06, 0.82)	0.47 (0.10, 0.88)	0.59(0.15, 0.90)	0.18 (0.02, 0.67)	0.09 (0.01, 0.39)
F4	0.90 (0.39, 0.99)	0.04 (0.00, 0.25)	0.11 (0.01, 0.36)	0.24 (0.04, 0.65)	0.30(0.07, 0.59)	0.16 (0.03, 0.42)	0.03 (0.01, 0.11)
D5	0.90 (0.39, 0.99)	0.37 (0.07, 0.78)	0.20 (0.03, 0.61)	0.56 (0.14, 0.89)	0.46(0.09, 0.87)	0.39 (0.08, 0.84)	0.38 (0.09, 0.71)
B2	0.91 (0.39, 0.99)	0.13 (0.01, 0.59)	0.04 (0.00, 0.25)	0.36 (0.08, 0.81)	0.19(0.02, 0.66)	0.28 (0.05, 0.78)	0.31 (0.07, 0.61)
F3	0.90 (0.39, 0.99)	0.08 (0.01, 0.35)	0.07 (0.01, 0.37)	0.38 (0.08, 0.81)	0.34(0.07, 0.71)	0.34 (0.06, 0.83)	0.11 (0.02, 0.30)
E2	0.89 (0.36, 0.99)	0.67 (0.16, 0.98)	0.28 (0.03, 0.84)	0.77 (0.23, 0.99)	0.78(0.23, 0.99)	0.45 (0.08, 0.92)	0.59 (0.16, 0.95)
Winter	NCEP	CCCMA	CNRM	CSIRO	MPI	GFDL	MRI
E6	0.89 (0.37, 0.99)	0.72 (0.20, 0.97)	0.36 (0.06, 0.84)	0.74 (0.22, 0.97)	0.59(0.17, 0.88)	0.80 (0.26, 0.98)	0.64 (0.17, 0.95)
G	0.90 (0.36, 0.99)	0.76 (0.25, 0.99)	0.72 (0.18, 0.99)	0.68 (0.16, 0.98)	0.72(0.22, 0.99)	0.77 (0.21, 0.99)	0.63 (0.15, 0.98)
E4	0.89 (0.36, 0.99)	0.71 (0.20, 0.98)	0.54 (0.12, 0.95)	0.63 (0.15, 0.97)	0.64(0.17, 0.96)	0.75 (0.24, 0.98)	0.66 (0.18, 0.97)
E3	0.89 (0.35, 0.99)	0.74 (0.23, 0.99)	0.26 (0.04, 0.72)	0.55 (0.13, 0.93)	0.39(0.08, 0.82)	0.80 (0.27, 0.99)	0.66 (0.18, 0.97)
F4	0.90 (0.36, 0.99)	0.51 (0.12, 0.91)	0.31 (0.06, 0.73)	0.27 (0.05, 0.61)	0.58(0.15, 0.88)	0.69 (0.18, 0.98)	0.45 (0.12, 0.76)
D5	0.89 (0.37, 0.99)	0.52 (0.13, 0.87)	0.43 (0.10, 0.82)	0.48 (0.13, 0.83)	0.12(0.02, 0.28)	0.67 (0.20, 0.96)	0.28 (0.06, 0.58)
B2	0.91 (0.38,0.99)	0.39 (0.10, 0.75)	0.41 (0.10, 0.80)	0.55 (0.15, 0.87)	0.06(0.01, 0.13)	0.66 (0.21, 0.96)	0.15 (0.03, 0.38)
F3	0.90 (0.35, 0.99)	0.64 (0.17, 0.95)	0.63 (0.18, 0.96)	0.36 (0.08, 0.71)	0.56(0.15, 0.87)	0.54 (0.10, 0.97)	0.65 (0.19, 0.96)
E2	0.89 (0.36,0.99)	0.60 (0.13, 0.98)	0.52 (0.11, 0.95)	0.77 (0.24, 0.99)	0.05(0.00, 0.32)	0.74 (0.23, 0.98)	0.26 (0.04, 0.74)

The reproduction of the observed inter-annual variance was assessed by using the standard deviation of the seasonal precipitation amount (pSSNSD, mm/season). The percentage of the observed inter-annual variance covered by the downscaled series is shown in Fig 8.4. The GCMs (including the NNR) had a slight tendency to underestimate the inter-annual variance as they generally could reproduce 60-100% of observed pSSNSDs. There were no obvious differences in the ability to reproduce pSSNSD among the GCMs and the NNR for most of the climatic zones and seasons, except zones G and F4, where showed significant seasonal cycles. For zone G, the GCMs could reproduce more of the inter-annual variance in winter than in summer, but was exactly the opposite for zone F4.

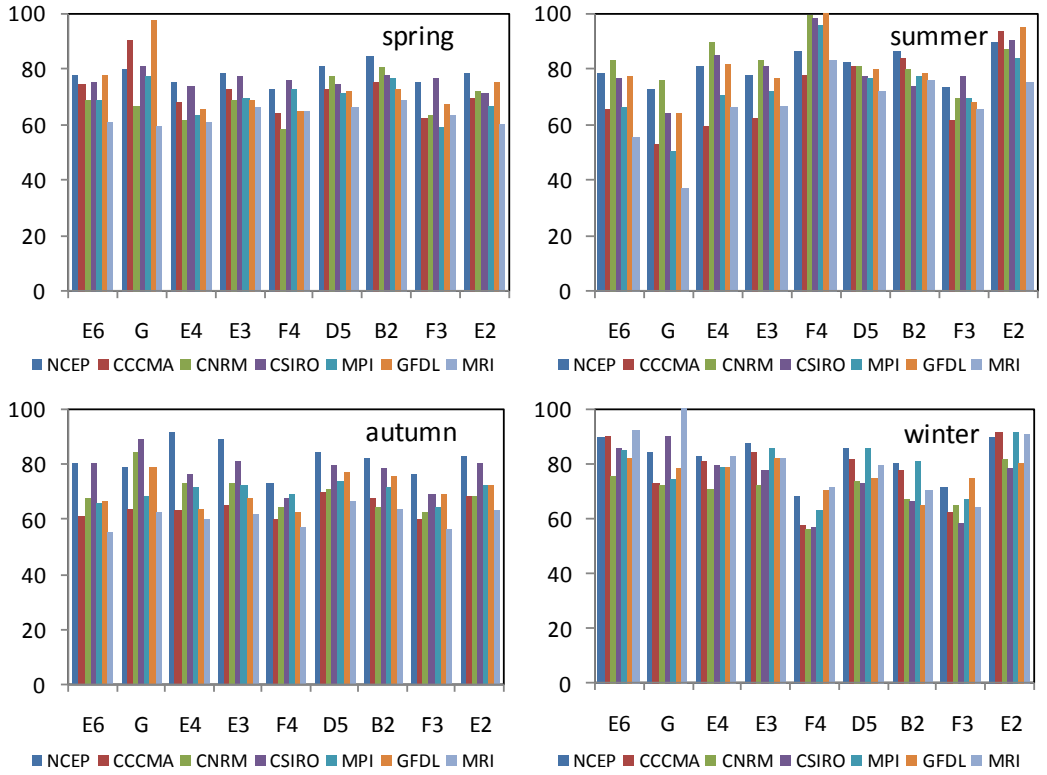

Fig. 8.4. As Fig. 8.3 but for the percentage of the observed inter-annual variance reproduced by the downscaled series (pssnSD).

In this study, the value at the 95% percentile of the overall precipitation series was used as the threshold to define an extreme precipitation event (P95, mm/day). The production of P95 is displayed in Fig 8.5. The best performance was still acquired by the NNR. In the case of GCMs, P95 was reproduced quite well in winter. Errors were negligible and no obvious bias was found, with only the CCCMA, CSIRO and CNRM had a little difficulty to generate the very high P95. A similar performance occurred in summer except for the CCCMA, in which the P95 was significantly underestimated in most of the climatic zones. In the other two

seasons, P95 was reproduced well, particularly for the low values. However, the high values were obviously underestimated. In general, the reproduction of P95 was acceptable.

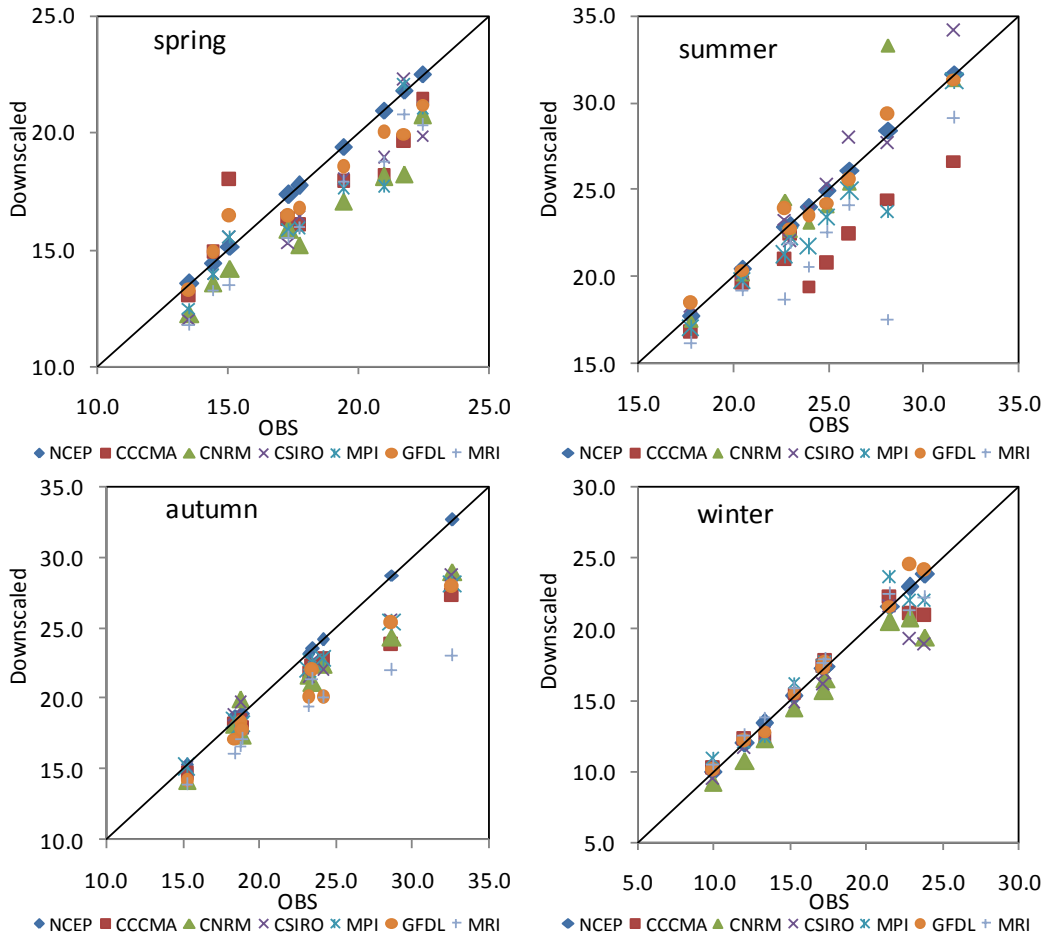

Fig. 8.5. As Fig 8.1 but for P95.

The reproductions of the observed precipitation frequencies by the downscaled results were analyzed at three different daily precipitation intensities of 0.1mm, 2.0mm and 20.0mm, represented as nr001, nr020 and nr200, respectively. The comparisons of these indices between the observed values and downscaled results are given in Figs 8.6 – 8.8. The downscaled results from the GCMs could reproduce the observed precipitation frequencies very well for all seasons, particularly for the precipitation events with the small rainfall intensities (e.g., nr001 and nr020). The differences in the reproduction of these frequencies were negligible and there was no evidence that the downscaled results had any bias toward either high or low values or the tails of the distribution (large or small observed values). However, this was only true for nr200 in winter and summer (except for the CCCMA). In spring and autumn, the observed nr200 was slightly underestimated, especially for the high values.

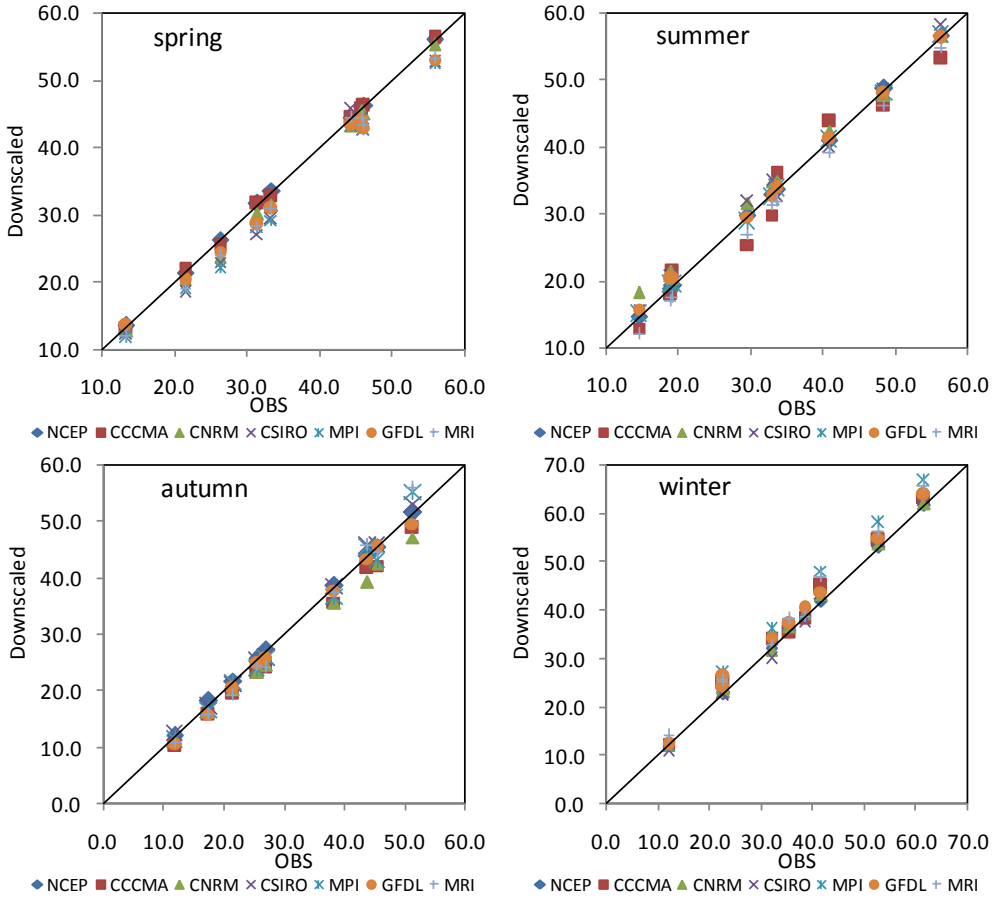

Fig. 8.6. As Fig 8.1 but for the total precipitation days (nr001).

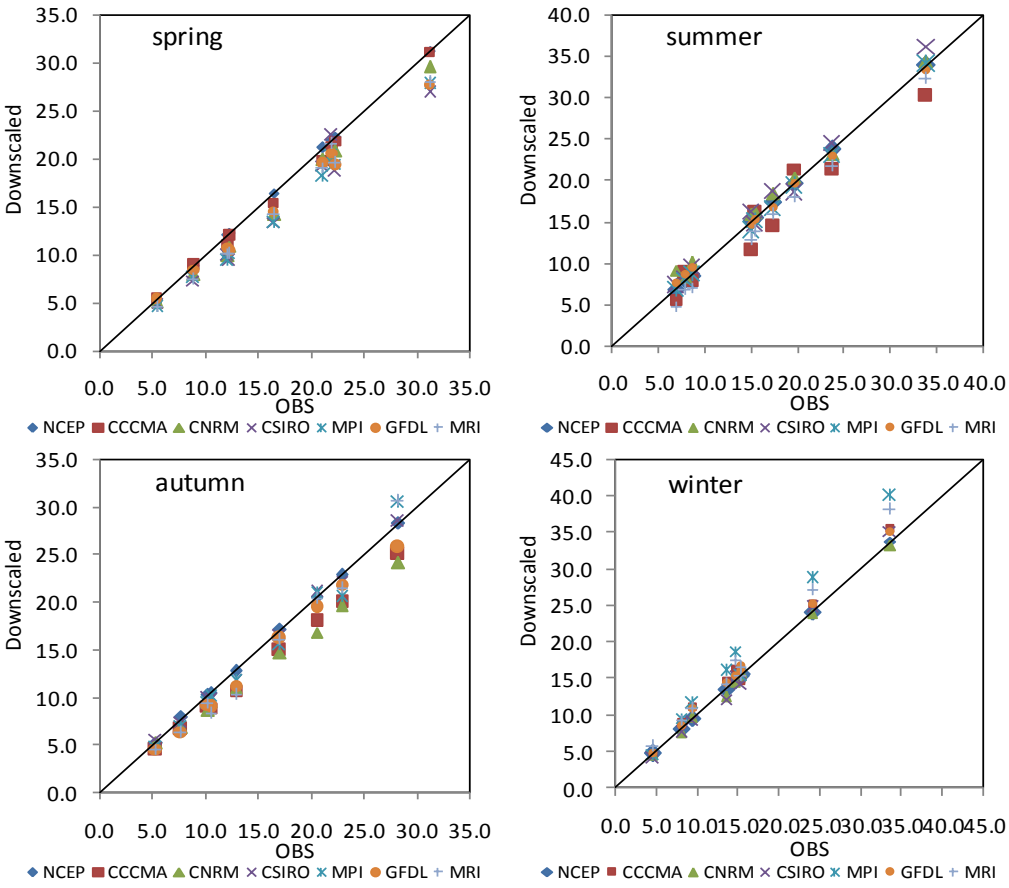

Fig. 8.7. As Fig .8.1 but for precipitation days >=2.0mm.

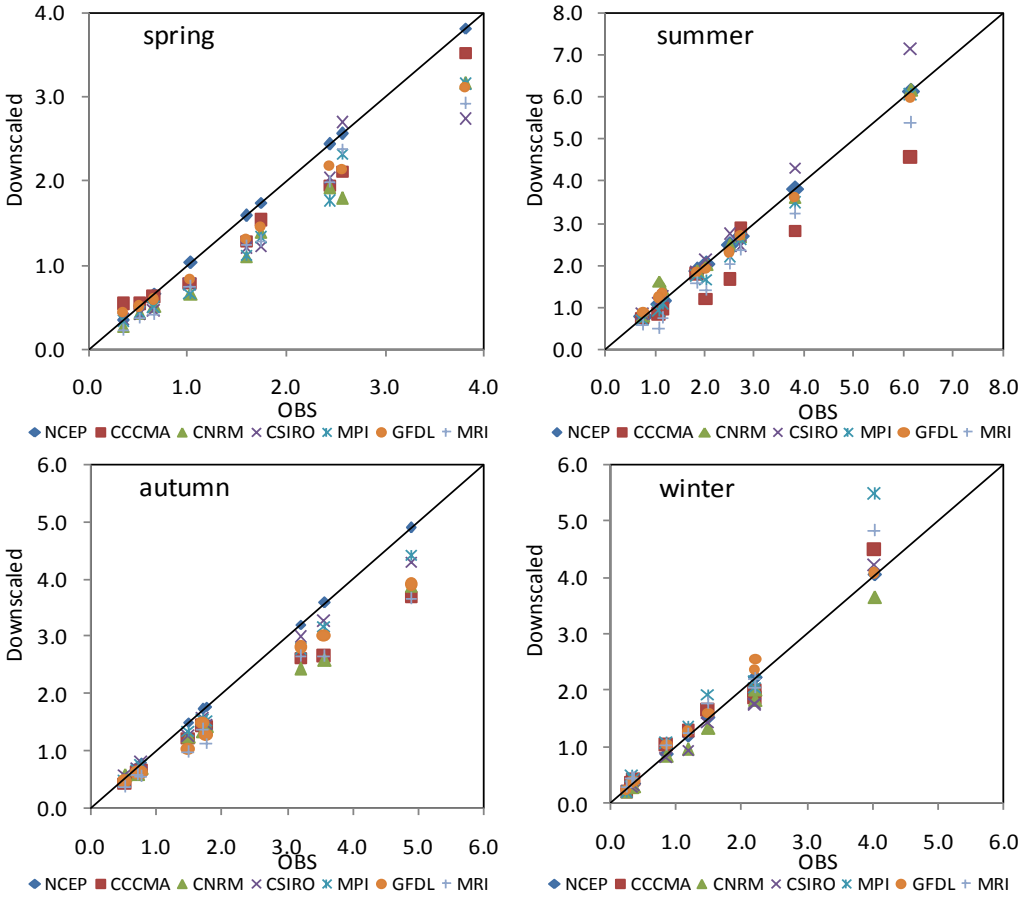

Fig. 8.8. As Fig. 8.1 but for precipitation days >=20.0mm.

The reproductions of the observed wet/dry–day persistence were analyzed through the two indices of Pww, the probability of a wet day followed by another wet day; and Pdd, the probability of a dry day followed by another dry day, the two important Markov process parameters as discussed previously (Chapter 4). The Figures 8.9 – 8.10 gave percentages of the observed Pww and Pdd covered by the downscaled series. The downscaled results could reproduce more parts of Pdd than those of Pww in most of the climatic zones, which might be explained partly by the fact that precipitation events were rare compared with the non-precipitation events. Generally, the downscaled results could reproduce 60 - 90% of the observed Pww in those humid and semi-humid climatic zones, but could only reproduce 30 - 60% of the observed Pww in the arid and semi-arid climatic zones (Fig. 8.9). However, the downscaled results could reproduce most of the observed Pdd (Fig. 8.10). In most of the climatic zones and season, the percentages were all above 90%. Pdd was obviously underestimated in the relatively humid zones compared with other zones in each season, but still above 60%.

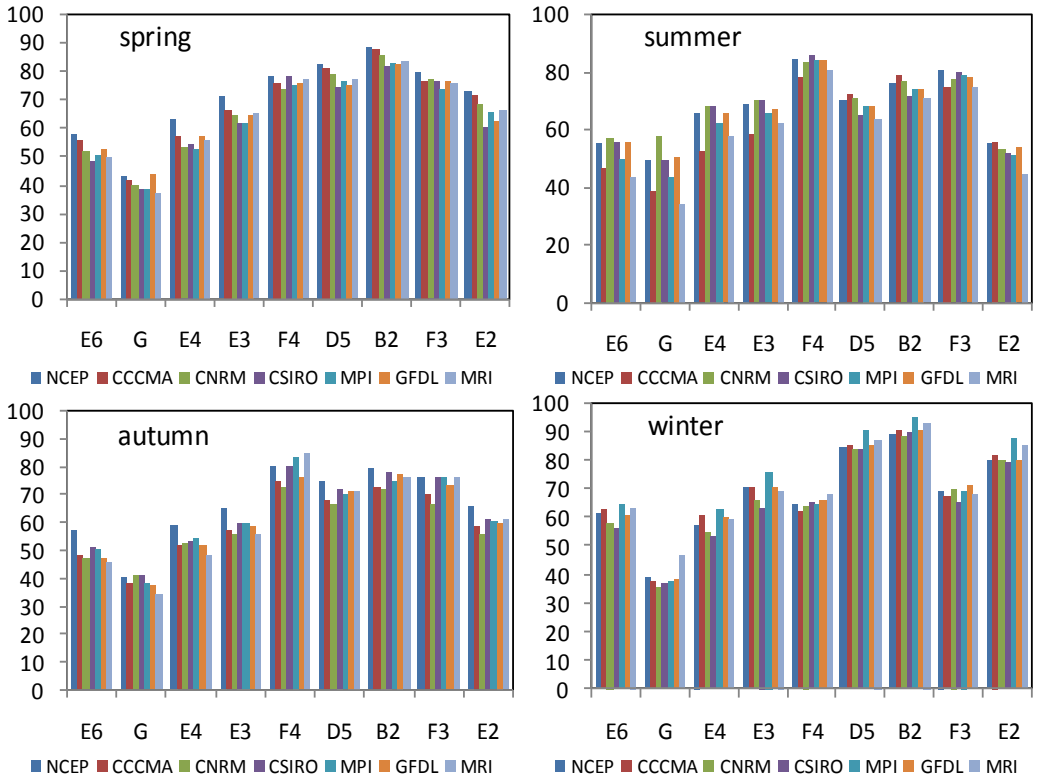

Fig. 8.9. As Fig. 8.3 but for but for the percentage of the observed Pww reproduced by the downscaled series.

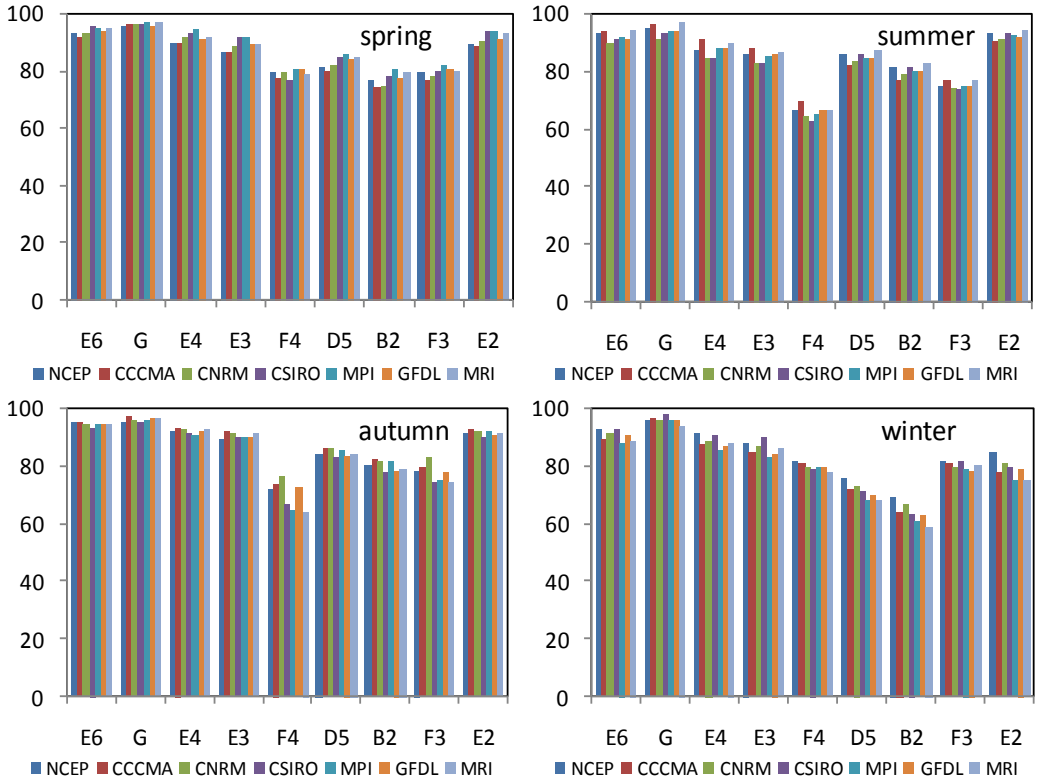

Fig. 8.10. As Fig. 8.3 but for the percentage of the observed Pdd reproduced by the downscaled series.

8.3.3 Projected precipitation changes under Scenario A2

The above evaluation showed that the downscaled results from the GCMs have a similar skill in reproducing the most important characteristics of the observed local precipitation such as rainfall amount (e.g., SDII amd ppSD) and frequencies at different intensities (e.g., nr001, nr020 and nr200), as well as inter-annual variance (e.g., pssnSD). The SOM-SD was then applied without further adjustment to the GCMs for projecting future precipitation change under scenario A2. The projected rainfall changes were represented as the anomalies between the two 20-year future period (i.e., 2046 – 2065 and 2081 - 2100) and the baseline period (1961 - 2000).

8.3.3.1 Future-A (2046－2065)

The projections based on the downscaled GCM data showed a consistent decrease in SDII (-1.0 to 0.0) in winter for all GCMs except for the CCCMA, in which SDII decreased from - 0.5 to 0.0 in the climatic zones of E6, G, E4, E3, F4 and E2 (Fig. 8.11). In spring, a similar consistent decrease trend (-1.0 to 0.0 mm) was also found in all of the climatic zones except for the zone G, where the GCMs of CCCMA, CNRM, MPI and MRI gave a slight increase (below 0.5mm). However, in summer and autumn, most of the GCMs showed an increasing trend in the arid and semi-arid zones (below 1.0mm for summer and below 0.5 for autumn), while they gave an opposite trend in the humid and semi-humid zones (about -0.5mm). As for mean total precipitation days in each season (nr001), almost all GCMs gave a decreasing trend represented by two significant characteristics (Fig. 8.12). The first one was that nr001 decreased faster in spring and winter than in summer and autumn. The second was nr001 would drop down faster in the humid zones (about -8 days for spring and winter) than in arid and semi-arid zones (about -4 days for spring and winter). The projected changes in P95 showed a similar condition to SDII in spring and winter in that most of the GCMs would generate a decrease trend (-4.0mm in spring and -2.0 in winter) (Fig. 8.13). However, the changes became more complicated in autumn and summer. In summer, most of the GCMs would produce an increase in P95 for the humid zones while they would produce an opposite trend in the arid and semi-arid zones. In autumn, there was no consistent trend between the GCMs except for the very humid zones of D5 and B2, where they would give a consistent decrease (about -2.0mm).

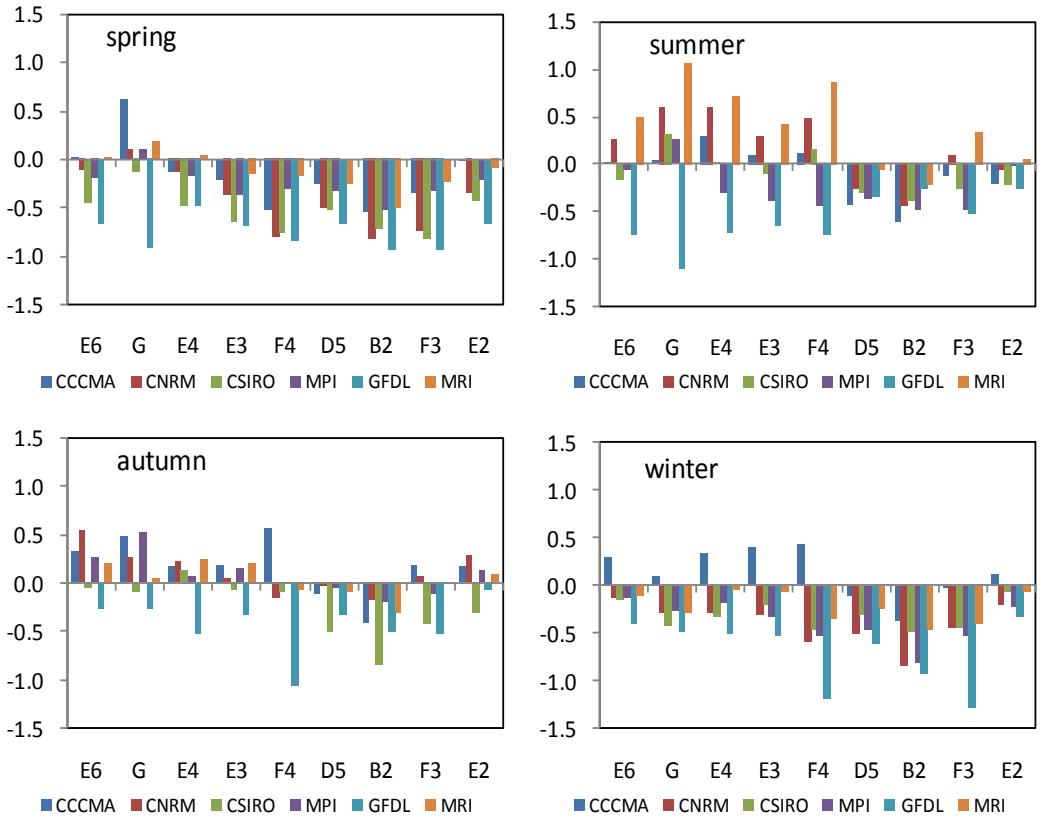

Fig. 8.11 Seasonal anomalies of mean daily precipitation on wet days (SDII) between 2046–2065 and 1961–2000 with the A2 scenarios.

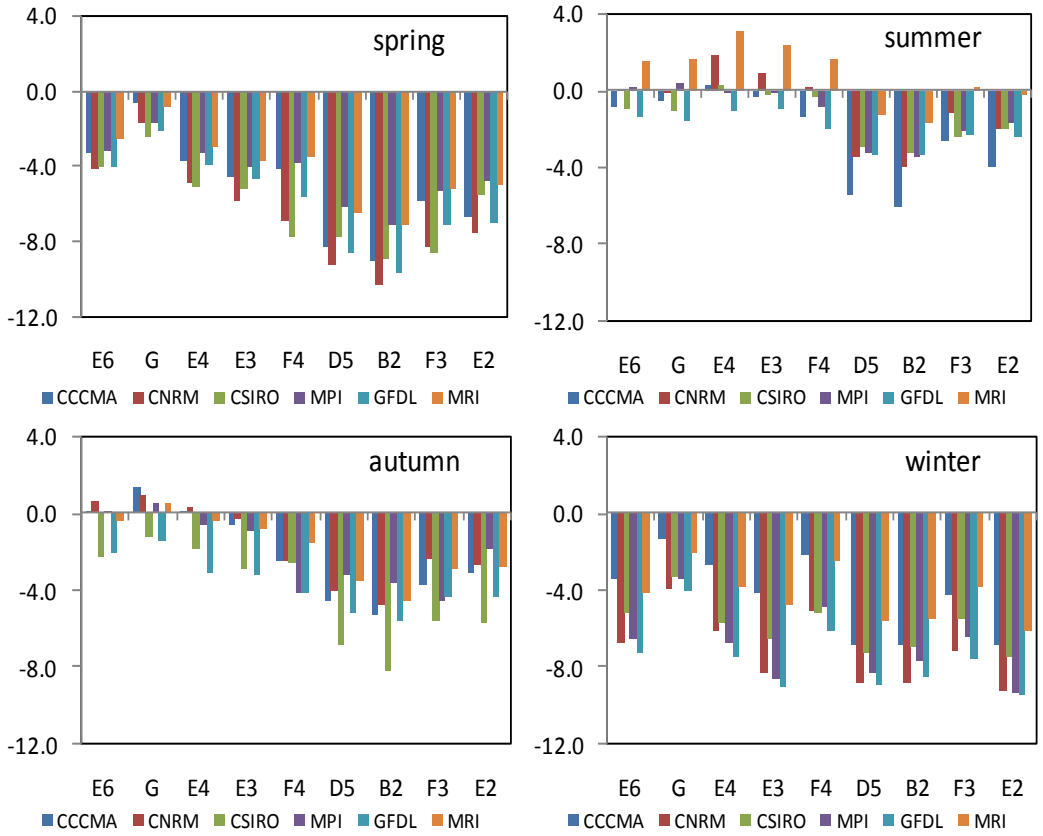

Fig. 8.12. As Fig. 8.11 but nr001.

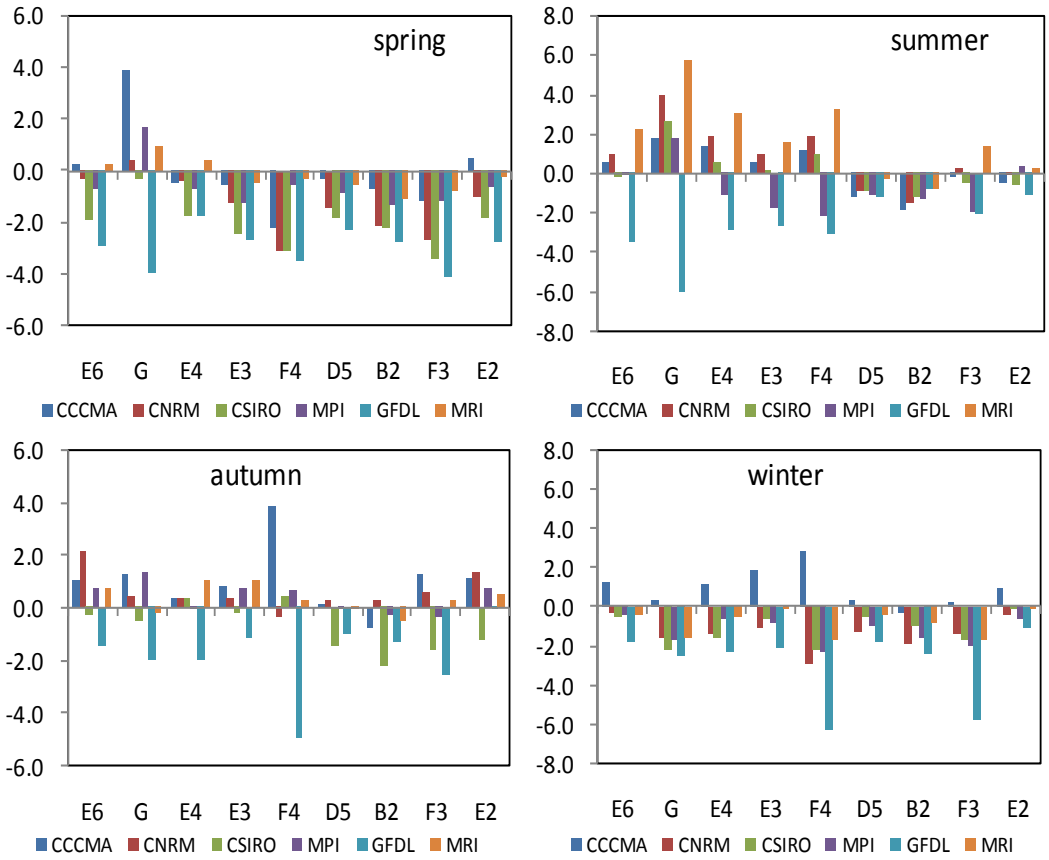

Fig. 8.13. As Fig. 8.11 but for P95.

8.3.3.2 Future-B (2081－2100)

The projections during the future-B are presented in Figs. 14 - 16 for the SDII, nr001 and P95, respectively. Obviously, the GCM models predicted much more significant changes for future- B compared to the Future-A period. In spring and winter, SDII would decrease -1.0 to 0.5mm and -1.5 to 0.5mm (Fig. 14), respectively. It decreased more significantly in the humid climatic zones than that in the arid and semi-arid zones. In summer and autumn, most of the GCMs would produce a consistent decrease of SDII in zones D5 and B2 (about -0.5mm), while the change in other zones would lie between -0.5 and 0.5mm. A more significant decrease in nr001 could be found in winter (-16 to -8 days) and spring (-12 to -4 days) compared with the Future-A projection (Fig. 8.15). Moreover, the GCMs (except CCCMA and CNRM) would also produce a consistent decrease in autumn (-8 to -2 days). In summer, the GCMs would generate an increase in zones of D5, B2, F3 and E2 (about 4 days), while they might generate a decrease in zones of E4, E3 and F4 (about -2days). A relatively consistent decrease in P95 would occur in spring and winter for all of the GCMs except for the CCCMA (-1.0 to 4.0mm; Fig.

8.16). No consistent change could be found for other seasons, with the projected changes being between -2.0 and 4.0 mm.

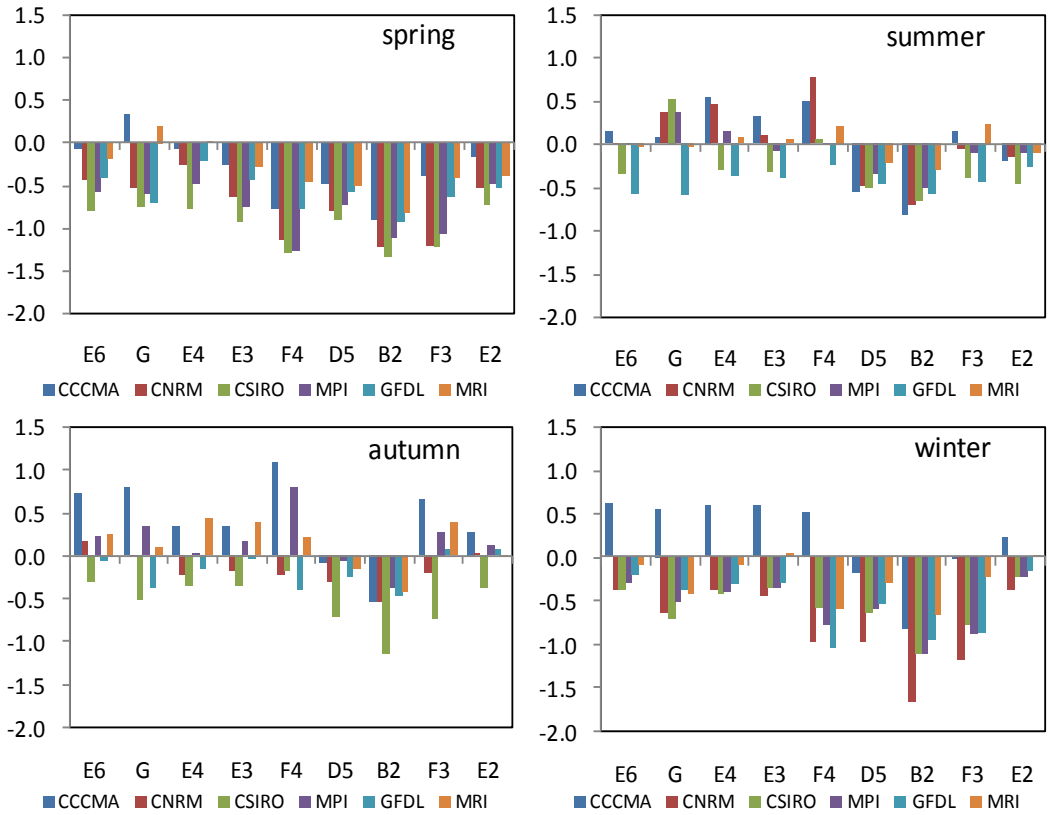

Fig. 8.14 Seasonal anomalies of mean daily precipitation on wet days (SDII) between 2081–2100 and 1961–2000 with the A2 scenarios.

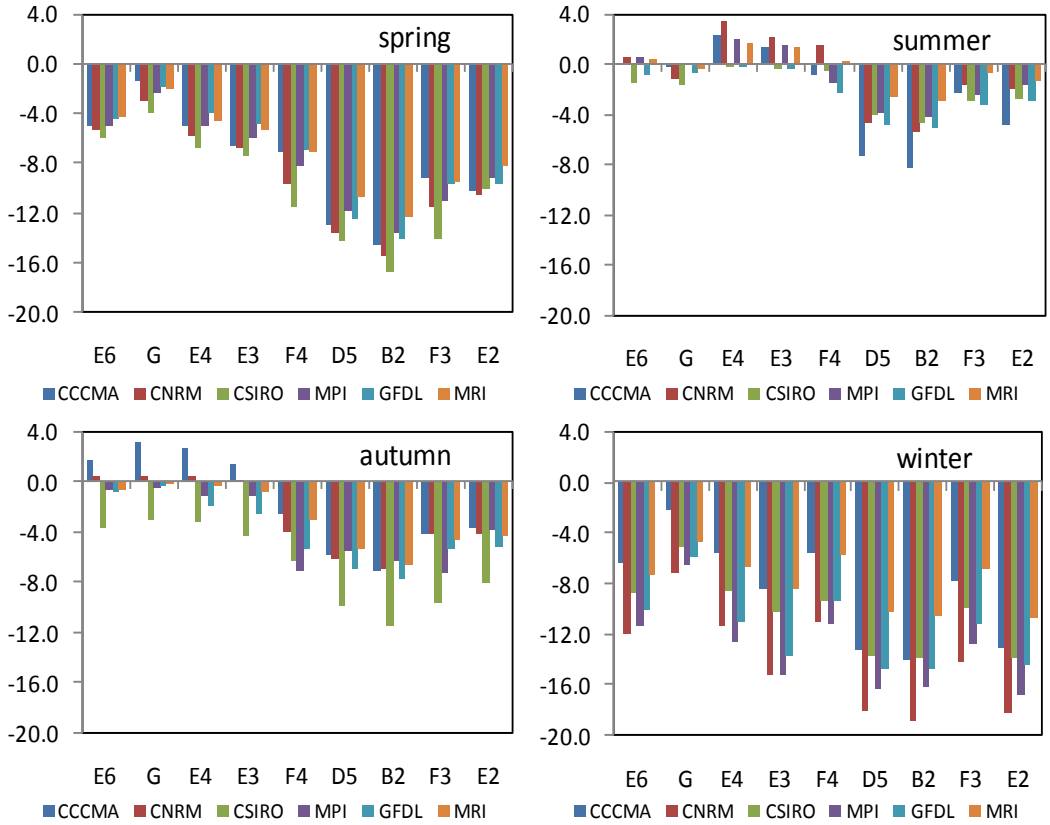

Fig. 8.15. As Fig. 8.14 but for precipitation days (nr001).

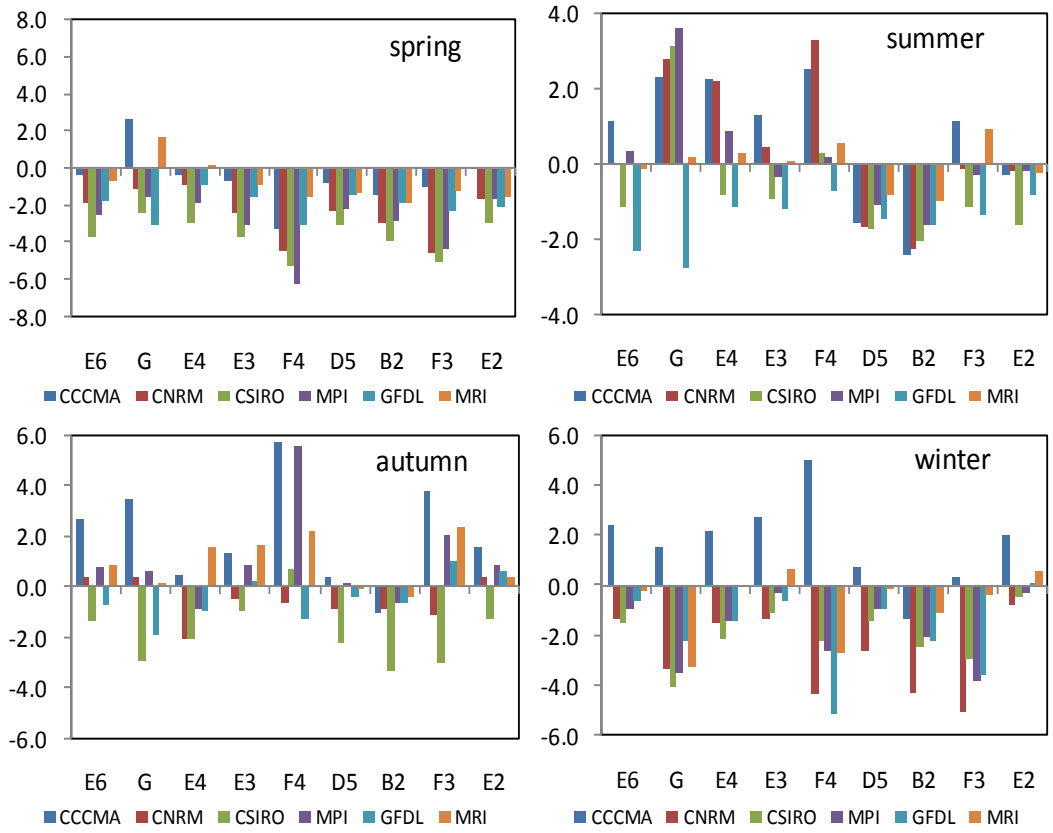

Fig. 8.16. As Fig. 8.14 but for P95.

8.3.4 Compared with raw GCM outputs

The downscaled precipitation was compared with the direct GCM projections. Taking Future-A (2046-2065) as an example, seasonal local precipitation change on wet days (SDII) was averaged over the whole case study area (Fig. 8.17). There were significant differences between the downscaled changes and those from the direct GCM projections in spring and winter as most of GCM produced increase trends, in contrast with the downscaled changes. However, they showed similar changes in autumn although with different amplitudes. In summer, some downscaled changes showed similar results with their corresponding GCMs (CSIRO, GFDL and MRI), while others did not (CCCMA, CNRM and MPI). Taking the case study area as a whole, it was found that the downscaling could not produce a complete convergence of climate change projections for multiple GCMs.

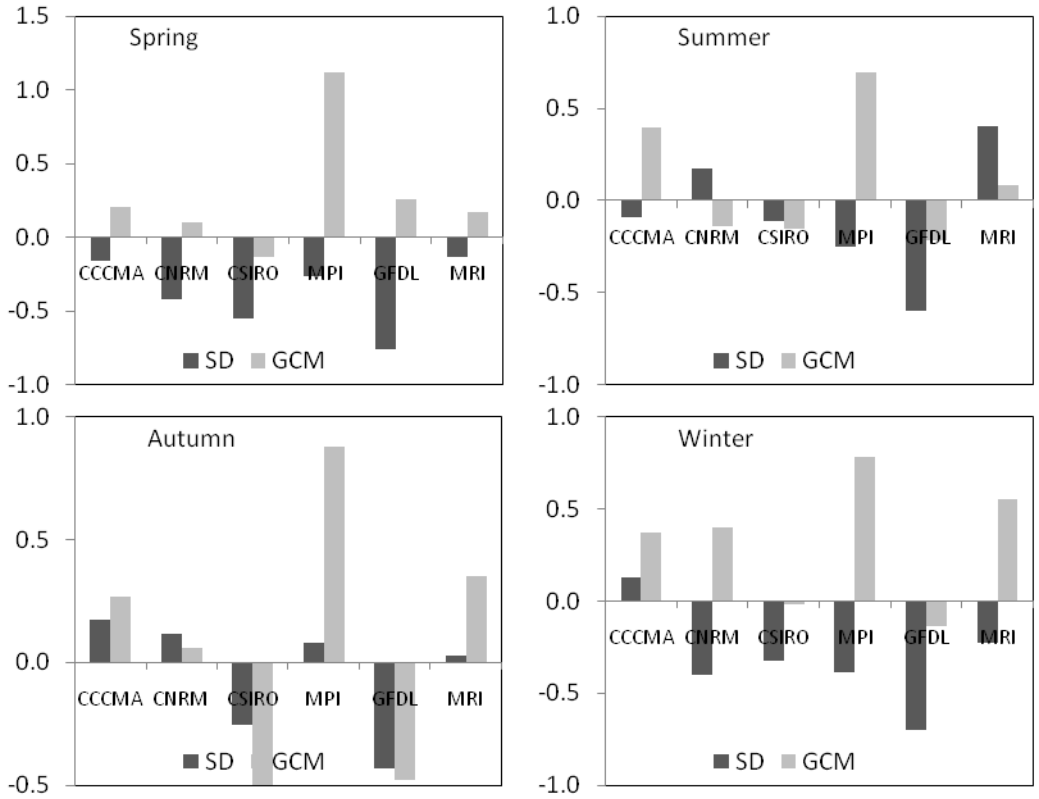

Fig. 8.17. Seasonal precipitation changes in SDII for both the original GCM projections (GCM) and the downscaled projections (SD) during Future-A (2046-2065). The changes are calculated as the difference averaged over the whole case study area between the Future-A and the baseline period (1961-2000).

8.4 Conclusion and discussion

In this chapter, the SOM-SD was applied to downscale the daily precipitation from six GCM models (CCCMA, CRNM, CSIRO, MPI, GFDL and MRI). Before constructing future regional climate change scenarios, the selected predictors were evaluated firstly based on the synoptic climatology. The analysis showed that these GCMs could, to a certain extent, reproduce a similar synoptic climatology depicted by the NNR. The similarity (i.e., correlation between synoptic pattern frequencies) between the NNR and the GCMs was generally above 0.80. These predictors then were assessed further through the SOM-SD with downscaling precipitation during the baseline period (1961-2000). The downscaled results from the GCMs compared well with that from the NNR and the observed data for various aspects of the precipitation characteristics (e.g., mean, standard deviation and frequency), indicating that the SOM-SD and the selected GCMs could be used for climate change projections. Future precipitation projections downscaled from the GCM models showed a consistent decrease in intensity and wet days for

spring and winter. As a consequence the total precipitation amount would decrease in these seasons. Moreover, the decrease in total precipitation amount appeared more significant in the humid zones (about -20% in the Future-A period and about -40% in the Future-B period) than in the arid and semi-arid zones (between -10 -20%). However, in the other two seasons, there was no consistent trend among the GCMs. The main discrepancy occurred in the arid and semi-arid climatic zones. About half of the GCMs would produce a decrease in precipitation intensity and days while others would give an opposite trend. In the humid zones, there was still a relatively consistent decrease trend among the GCMs.

In this study, although the SOM-SD was built using the NNR, the availability of large-scale predictors from the GCMs was taken into consideration at the same time. The results highlight that several issues call for future analysis when applying the SOM-SD to downscale GCM outputs and to construct high-resolution regional climate change scenarios.

Large-scale predictor variables must be carefully selected and assessed systematically. This is very true when a downscaling prototype that was built only on NNR predictors (e.g., in Chapter 4) was employed to GCM outputs. As other studies stated, a further procedure should be carried out to assess whether these predictors from the NNR could be reliably represented by GCMs (e.g., Fowler et al., 2007; Hofer et al., 2010). This study found that the not all GCMs could reproduce a NNR predictor uniformly well. For example, some GCMs can model the Q7 very well, while others cannot. In such a case, if only a GCM and the NNR are considered every time, six different downscaling models would be built for precipitation. Therefore, to find a possibly proper transfer function for all GCMs, a compromise was employed that only those predictors modeled acceptably by all GCMs were used in this study (i.e., SLP, Q5, T7 and Pr). Moreover, it should be noted that the predictors used in Chapter 4 had taken this issue into account.

To some extent, the above compromise to select predictors also demonstrated a fact that building a downscaling method truly depended on the time, data and technical resources available. For example, many studies usually preferred using the variables of geopotential height (Z) and relative humidity (RH) as primary predictors. However, these two variables were not provided at daily scale in the CMIP3 multi-model database. Maybe this is a reasonable explanation why there is

no consensus on the most appropriate selection for different downscaling models in different regions over the world (Fowler et al., 2007; Hofer et al., 2010). This study also found that the SOM-SD was sensitive to the predictor of specific humidity (Q). A trend analysis showed that Q would increase faster than other predictors in the future. Moreover, the SOM learning procedure gave an equal weight for each predictor. These factors led to the inevitable result that the Q became a dominant driver of future precipitation change. Many downscaling studies suggested that both Q and RH or absolute humidity should be included as predictors. This was because the former reflected how close to saturation the atmosphere was, while the latter reflected the total water content (e.g., Hewitson and Crane, 2006). However, the RH data were not available in the CMIP3 database, neither. Although these variables could be derived from other variables, the calculated result does not match the observed data very well. If possible, the SOM-SD will be further evaluated in the future by using the above predictors.

Furthermore, GCM outputs cannot represent the present-day atmospheric circulations as the anticipated accuracy level. Thus it is very difficult to select the predictors that reproduce very similar synoptic characteristics to the reanalysis data (e.g., NNR), which became evident in this study. This was anticipated to have some impact on the downscaled results. Similar to other studies, only the difference in downscaled results between present-day and future period was used to show the possible changes. However, for the impact studies, hydrological and agricultural models, they may need the direct downscaling time series outputs instead of the calculated changes. On the other hand, it was found that the GCMs could not accurately reproduce the seasonality of synoptic patterns (represented from the NNR data). As a consequence, the downscaled precipitation failed to reproduce the precipitation seasonality without using the SPP scheme. This was not the case for the NNR data, since the SOM-SD showed a very similar performance no matter using or not using the SPP scheme (Chapter 5). Thus, the SPP scheme was mainly designed and was also necessary for downscaling GCMs.

To an extent, these issues may be relieved as the new generation GCM outputs are published in CMIP5 (http://cmip-pcmdi.llnl.gov/cmip5/). However, it can be expected that not all problems will be solved for good, due to the complexity in the climate systems and other factors. Thus, the downscaling results still need further improvements before feeding into impact studies. For example, some kind

of statistical-bias-correction methods can be introduced to adjustment of the downscaled results. This is further analyzed in Chapter 9.

CHAPTER NINE

STATISTICAL BIAS CORRECTION ON DOWNSCALED DAILY PRECIPITATION

9.1 Introduction

Downscaling techniques are based on the assumption that the predictors used are realistically simulated. In a broad sense, they belong to the Perfect Prog(nosis) downscaling (e.g., Klein et al., 1959; Kalnay, 2003; Wilks, 2006). However, not all of the predictors used can be realistically simulated by GCMs. They may contain the inevitable model bias due to inadequate knowledge of key physical processes (e.g., cloud physics) and simplification of the natural heterogeneity of the climate system that exist at finer spatial scales. GCMs, therefore, still have difficulties to reproduce the observed atmospheric circulation very well at a large-(larger-) scale (e.g. Mullan et al., 2001), let alone for a smaller spatial domain for downscaling (Randall et al., 2007), despite an increasing ability of GCMs to successfully model present–day climate (Harvey and Wigley, 2003; Nieto et al., 2004; Reichler and Kim, 2008).

The possible lack of reliability at large-scale variable simulations by GCMs must have a negative impact on the quality of downscaling results, and in turn affect the reliability of the projected climate changes. Statistical downscaling models, despite selecting predictors carefully, cannot completely remove systematic biases in models. There are two possible solutions to the problem. Firstly, some techniques can be used to eliminate systematic errors in the simulations of GCMs (e.g., Ghil and Mechos, 1992) and then provide reliable predictors for downscaling. However, it is a big challenge and beyond the scope of this study. Another alternative is to correct the downscaled results using statistical methods so as to make them approximate to the corresponding observed values, as termed as bias correction. There are many methods that can be used to carry out bias correction, such as the pattern scaling (e.g. Mitchell 2000, 2003) and the statistical bias correction (e.g. Wood et al., 2004; Ines and Hansen, 2006; Piani et al., 2010;

Li et al., 2010). The statistical bias correction methods are generally employed for GCM-based precipitation and involve some form of transfer function derived from cumulative distribution functions (CDFs) of observations and model simulations. These approaches are also known as Model Output Statistics (MOS; Maraun et al., 2010). With the increasing skill of regional climate models (RCMs) and the availability of RCM scenarios, MOS methods are becoming popular (Maraun et al., 2010). The scheme of different downscaling approaches and their combinations is represented in Fig. 9.1. The left part of the figure was the traditional usage of MOS (e.g., Themeßl et al., 2010), while the right part is the technical routine proposed by this study. The methods are relatively simple and have been successfully used in hydrologic and many other climate impact studies (e.g., Cayan et al., 2008; Hayhoe et al., 2004; Maurer and Hidalgo, 2008). However, these methods were mainly carried out to correct bias of monthly downscaled precipitation (e.g., Wood et al., 2004) and were seldom applied to correct daily downscaled rainfall.

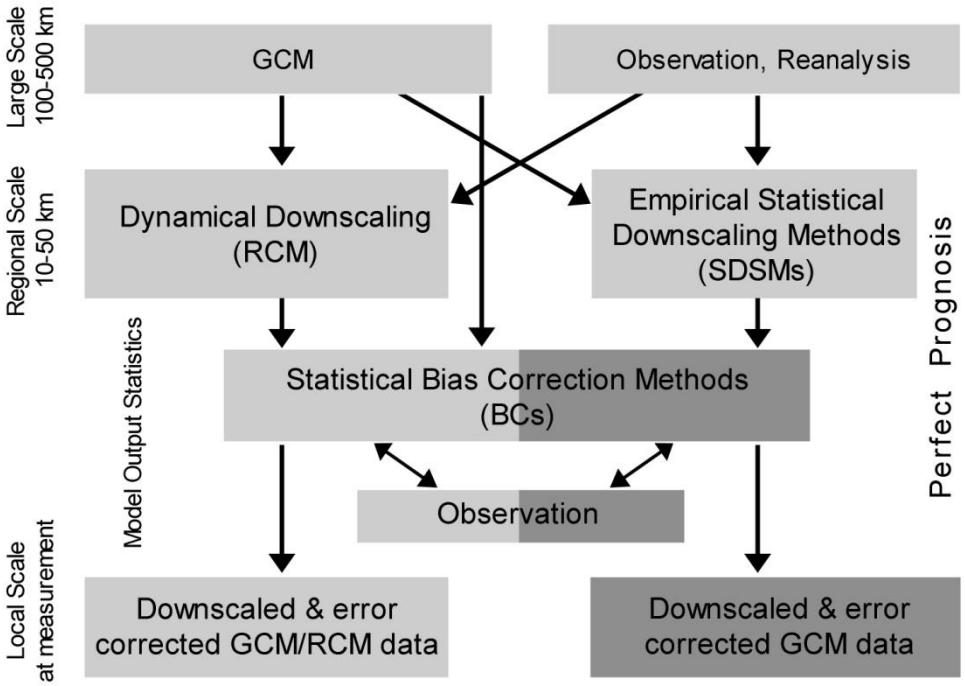

Fig. 9.1. Scheme of different downscaling methods and their combinations. Darker grey color indicates the proposed method presented in this chapter (modified after Themeßl et al., 2010).

This chapter focuses on a method of statistical bias correction (BC) that applies an equal distance-based quantile-to-quantile mapping method to correct the downscaled daily precipitation by the SOM-SD from GCMs. This method,

designated as SOM-BCSD, makes the best use of the advantages of both statistical downscaling and bias corrections: the SOM-SD has a good skill in generating a reasonable CDF of downscaled daily precipitation to make it more adjustable than the direct GCM-based precipitation (noted only similar CDFs are considered to be adjustable, otherwise BC would possibly introduce some large errors); the BC method makes the CDF of the downscaled precipitation more closely approach to the observed CDF.

9.2 Statistical bias correction methods

The basic procedure of bias correction is to establish a statistical relationship or transfer function between the downscaled outputs and observed values during the historical period and then apply the transfer function to future downscaled projections in order to eliminate those possible systematic errors (Ines and Hansen, 2006; Piani et al., 2010; Li et al., 2010). Currently, almost all BC methods are applicable only to a single downscaled time series *versus* a single observed time series. To apply the method to SOM-SD becomes a little complicated because the SOM-SD produces an ensemble of multiple runs. Therefore, the ensemble was considered as a whole to compare with the observed values and perform the BC operation. In addition to the method proposed by this study, other two popular methods also are included in the SOM-SD, and are described in detail below.

9.2.1 Correcting monthly rainfall by rescaling or a multiplicative shift

One of the simple bias correction methods is pattern-scaling (Santer et al., 1990). Various pattern scaling techniques have been used in climate change scenario construction (e.g., Chapter 13 of IPCC, 2001; Hanssen-Bauer et al., 2003; Widmann et al., 2003; Diaz-Nieto and Wilby, 2005). For the simplest pattern scaling method, a rescaling (multiplicative) factor during the baseline period was calculated to correct the bias of the mean monthly downscaled rainfall as follows:

$$x_i' = x_i \frac{\bar{X}_{OBS}}{\bar{X}_{sim}} \qquad (9.1)$$

Where x_i and x_i' refer to the downscaled and corrected rainfall on day *i*, and $\bar{X}_{sim}$ and $\bar{X}_{OBS}$ are the long-term monthly mean rainfall from the downscaled and observations for a given month (it should be noted that $\bar{X}_{OBS}$was an ensemble

mean). The same procedure applies to the downscaled precipitation from the GCM scenarios. It is clear that the sole objective of the scaling procedure is to adjust rainfall amount in order to reproduce the long-term mean observed rainfall for a specific month, without any operation to correct the systematic error in frequency or the intensity distribution (Ines and Hansen, 2006).

9.2.2 Simultaneous frequency and intensity correction

The daily precipitation event is intermittent in nature, especially for dry regions. Consequently, the separation of daily precipitation into frequency (fraction of precipitation days, or wet days) and intensity (rainfall per wet day) in model simulations allows for a more accurate precipitation modeling evaluation. Therefore correcting any bias of the two rainfall components will also correct the monthly total rainfall itself. A two-step BC procedure is therefore proposed to simultaneously adjust the two components of downscaled rainfall to make it approximate the long-term observed distribution at each downscaling target grid. For convenience, and consistency with the convention of updating GCM forecasts monthly, the proposed BC procedure was carried out monthly.

9.2.2.1 Correcting precipitation frequency

To perform a BC operation, the observed precipitation was firstly truncated using the threshold value of 0.1mm ($\bar{x} = 0.1$) to obtain an ideal frequency distribution. Then, the downscaled daily precipitation during the baseline period was fitted into an empirical frequency distribution. By finding a threshold $\bar{x}_{sim}$, this distribution was truncated so as to make sure that its frequency above the threshold would approximate the observed precipitation frequency (Ines and Hansen, 2006). The threshold $\bar{x}_{sim}$ was calculated from the empirical observed and downscaled cumulative precipitation distribution as,

$$\bar{x}_{sim} = F_{sim\_B}^{-1}(F_{obs}(\tilde{x})) \qquad (9.2)$$

Where $F(\cdot)$ and $F^{-1}(\cdot)$ denote a cumulative distribution function (CDF) and its inverse, $\tilde{x}$ represents the truncated observed time series at a threshold $\bar{x} = 0.1$, and the subscripts of *sim* and *obs* indicate downscaled or observed daily precipitation, while the *_B* indicates the baseline period. Moreover, this threshold $\bar{x}_{sim}$ was also used to truncate the downscaled precipitation during the future

period.

The above correction procedure was only applicable to the condition where the SOM-SD overestimated the precipitation frequency, which is more common for the GCM-based precipitation (Ines and Hansen, 2006; Dai, 2006; Sun et al., 2006). When frequency was underestimated, the frequency was not corrected or was offset by adding some artificial precipitation events. Ines and Hansen (2006) suggested that only drizzles (with 0.1 mm rainfall) should be used, but they pointed out that such a procedure might distort the corrected frequency distribution. Therefore, in this present study, precipitation events were randomly selected from the downscaled data and to offset the frequency deficit. Moreover, the corrected percentage of the frequency deficit between downscaled data during the baseline period and observed data was used to correct the downscaled precipitation frequency for the future period.

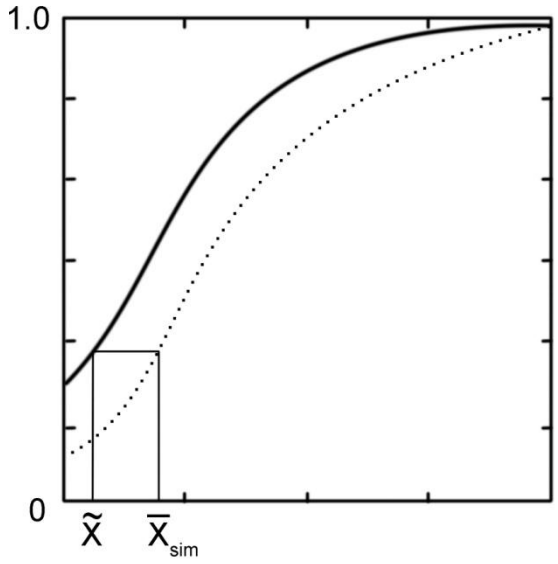

Fig. 9.2. Illustration of how to select a threshold to truncate the CDF of the original downscaled daily precipitation (dashed line). The $\bar{x}_{sim}$ was the selected threshold for the downscaled data, which had a same CDF value as the truncated observed data at $\bar{x} = 0.1$ (thick line).

9.2.2.2 Correction of precipitation intensity

After correcting precipitation frequency, the intensity distribution of the truncated downscaled daily precipitation could be further adjusted by the rescaling method or the quantile-based mapping methods (CDF matching) (Panofsky and Brier, 1968; Law and Kelton, 1982). For the latter, a typical procedure is to map the distribution of downscaled daily precipitation, i.e., the CDF of daily rainfall amounts above the truncated threshold ($\bar{x}_{sim}$)in a particular month onto that of

observed data. The corrected downscaled precipitation x' on day i during the baseline period can be calculated as

$$x_i' = \begin{cases} F_{obs}^{-1}(F_{sim\_B}(x_i)), & x_i \geq \tilde{x}_{sim} \\ 0, & x_i < \tilde{x}_{sim} \end{cases} \quad (9.3)$$

where $F(\bullet)$ and $F^{-1}(\bullet)$ denote the CDF of either the observations (*obs*) or downscaled results (*sim*) and its inverse during the baseline period. To bias correct downscaled values for a future period, the method needs firstly to find the corresponding percentile values for these future (downscaled) values on the CDF of the downscaled values during the baseline period and then search for the observed values on the CDF of the observations at the same found percentile locations. Thus, the original downscaled results were totally replaced by those values found on the CDF of the observations. Because, this BC procedure was based on CDF and replacing, it hereafter was termed as CDFP. Figure 9.3 (A) illustrated how it worked.

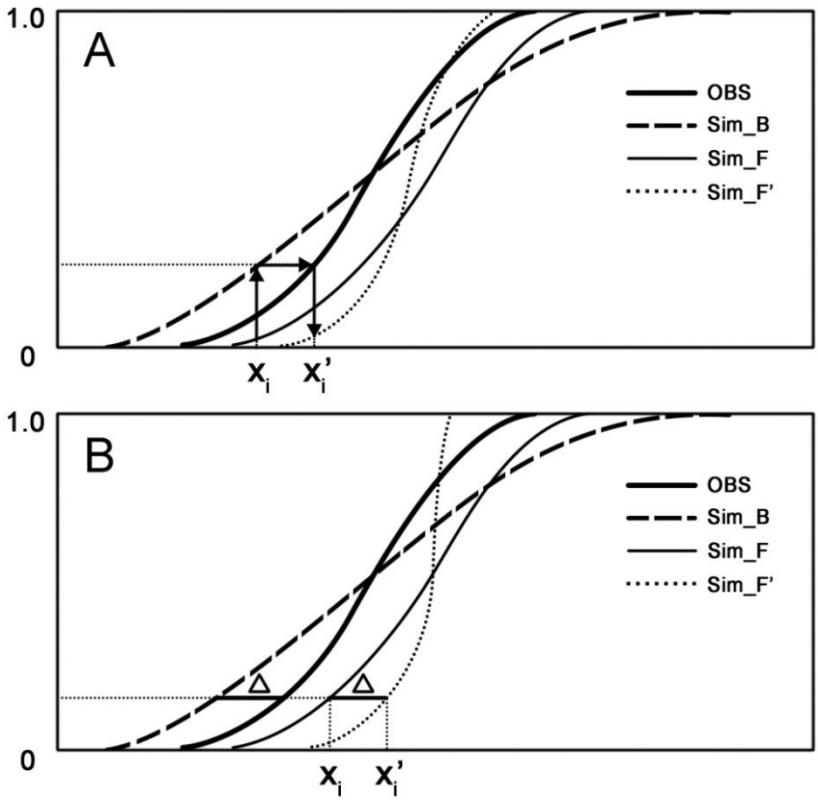

Fig. 9.3. Schematic of methodology of (A) CDFP and (B) EDCDF. Solid black line donated the observations (OBS). Thick dashed line donated the downscaled data during the baseline period (SIM_B). Thin dashed line represented the downscaled data for future period (SIM_F). Dotted-dashed line donated the corrected data as SIM_F' (modified after Li et al., 2011).

The above BC method has been successfully used in hydrologic and crop simulations as well as many other climate impact studies (e.g., Ines and Hansen, 2006; Cayan et al., 2008; Piani et al., 2010). The significant characteristics of the method is that it adjusts all moments (i.e., the entire distribution matches that of the observations for the baseline period), while maintaining the rank correlation between downscaled results and observations. However, the method was based on an important assumption; namely, the precipitation distribution does not change over time. In other words, the future projection will still follow the same statistical characteristics of the observed precipitation (e.g., the variance and skew) during the baseline period and only the mean would change. However, some studies have shown that the precipitation characteristics would change over time (e.g., Benestad et al., 2008; Meehl et al., 2007; Milly et al., 2008). This was also seen from the original downscaled results from the SOM-SD.

In view of these facts, an equal distance-based CDF mapping method (EDCDF) was proposed to correct the downscaled daily precipitation by the SOM-SD from GCMs. This method was different from the above traditional method in that the information from the CDF of the downscaled projection was also incorporated into the BC procedure. For a given percentile, it was assumed that the difference between the downscaled and observed value during the baseline period also applies to the future period. Thus, the corrected downscaled precipitation x' on day i for the future period can be calculated as,

$$x_i' = \begin{cases} x_i + F_{obs}^{-1}(F_{sim\_F}(x_i)) - F_{sim\_B}^{-1}(F_{sim\_F}(x_i)), & x_i \geq \tilde{x}_{sim} \\ 0, & x_i < \tilde{x}_{sim} \end{cases} \quad (9.4)$$

where $F(\bullet)$ and $F^{-1}(\bullet)$ denote the CDF of either the observations (*obs*) or downscaled results (*sim*) and its inverse during the baseline period (*_B*) and future period (*_F*). The Fig. 9.3 (B) illustrated how this BC procedure worked. As can be seen from the figure, the difference between the downscaled and observed values during the baseline period at each percentile was considered as the systematic error to be superimposed upon the CDF of the downscaled values at the corresponding percentile during the future period. This was the reason why the method was termed the equidistant CDF matching method. Compared with CDFP, the difference between the CDFs for the future and baseline periods was also

taken into account in EDCDF. However, the two methods will generate an identical BC result if the distribution for the future climate is the same as that for the baseline period. Moreover, if the changes in variability are small, results from both methods will be close to each other.

The above 2 BC methods are all based on CDF and rely on the statistical relationships between the two CDFs (observed, downscaled for the baseline period) to correct the third one (downscaled for the future period)). Indeed, the differences between the downscaled results of the future and baseline period could also be superimposed onto the observed CDF to construct new projections. The above 2 methods involved the operation of taking the inverse of the CDFs. In practice, the CDFs can be either empirical (i.e., sorted arrays of observations) or fitted to some theoretical distribution such as the gamma distribution (e.g., Ines and Hansen, 2006; Piani et al., 2010; Li et al., 2010), Log-Logistic Distribution (e.g., Shouki et al., 1988) or exponential distribution (e.g., Madi and Raqab, 2007). However, a single theoretical distribution does not always work well for regions with very complicated climate types and orographic features such as the case study area (Vlček and Huth, 2009). Moreover, fitting a distribution often needs long-term observed precipitation data. For simplicity, only the empirical distribution was considered in order to represent observed and downscaled precipitation intensities. Although three methods have been integrated into the SOM-SD, only the BC result from the EDCDF method is presented. This is because the pattern scaling method and CDFP have widely been used in many studies and no further validation is needed here.

9.2.3 Data

To match the GCM simulations for present-day climate, only the period from 1961-2000 was used, which was termed as the baseline period. The downscaled precipitation time series were from six GCMs (i.e., CCCMA, CNRM, CSIRO, GFDL, MPI and MRI) and covered the baseline period and two 20-year periods (2046-2065 and 2081-2100) of future projections under the SRES A2 Scenario. Because the downscaled data were at 0.25°×0.25° spatial resolution, all analyses were carried out at this resolution. Detailed information about these GCMs and the downscaled precipitation data can be found in Chapters 2 and 8, respectively.

9.2.4 Analyses

There are many statistical indices related to precipitation characteristics of both the frequency and intensity of different categories, which are important statistical properties to assess the hydrological or other impacts of climate change. Although the BC method was based on CDF and which simultaneously corrected the precipitation frequency and intensity, total rainy days (nr001; >0.1mm/day) and the first and second moments of daily precipitation (SDII and ppSD) on rainy days were provided. In addition, the Kolmogorov-Smirnov (K-S), test a non-parametric good-of-fit test, was applied to compare the cumulative distribution function (CDF) of observed and corrected downscaled daily precipitation time series. The downscaled daily precipitation data were an ensemble of 500 runs for each precipitation grid, and 90% confidence intervals (5-95%) were provided for these indices through a bootstrapping technique (Khan et al., 2006; Dibike et al., 2008).

9.3 Results

In practice, an iteration process is necessary for the BC process. Generally, a five time's iteration is sufficient. However, it demands a large amount of computing time if there are many grids in an area such as in this study. It was found that the BC result was acceptable with a one-time iteration. Therefore, the BC procedure was carried out once on each grid in the case study area.

9.3.1 Baseline

Although the BC procedure was performed monthly, all evaluations were carried out in a seasonal style. Based on the observed probability distribution functions (PDFs), the skill of the BC method was evaluated the first two moments of the PDFs: the mean (SDII) and the standard deviation (ppSD) on wet days.

The corrected SDII for each season was very accurate (Fig. 9.4). Each point in Fig. 9.4 corresponds to a single one of the 9 climatic zones for a specific GCM, with the X-axis representing the observed mean value across all grids in that zone and the Y-axis the corrected mean. After bias correction, errors in the mean were negligible and there was no bias toward either high or low values, including at the tails of the distribution (large or small observed values). Compared with the

original downscaled values (Fig. 8.1), the differences in SDII among the GCMs almost disappeared as the observed data were used to correct all GCM downscaling outputs.

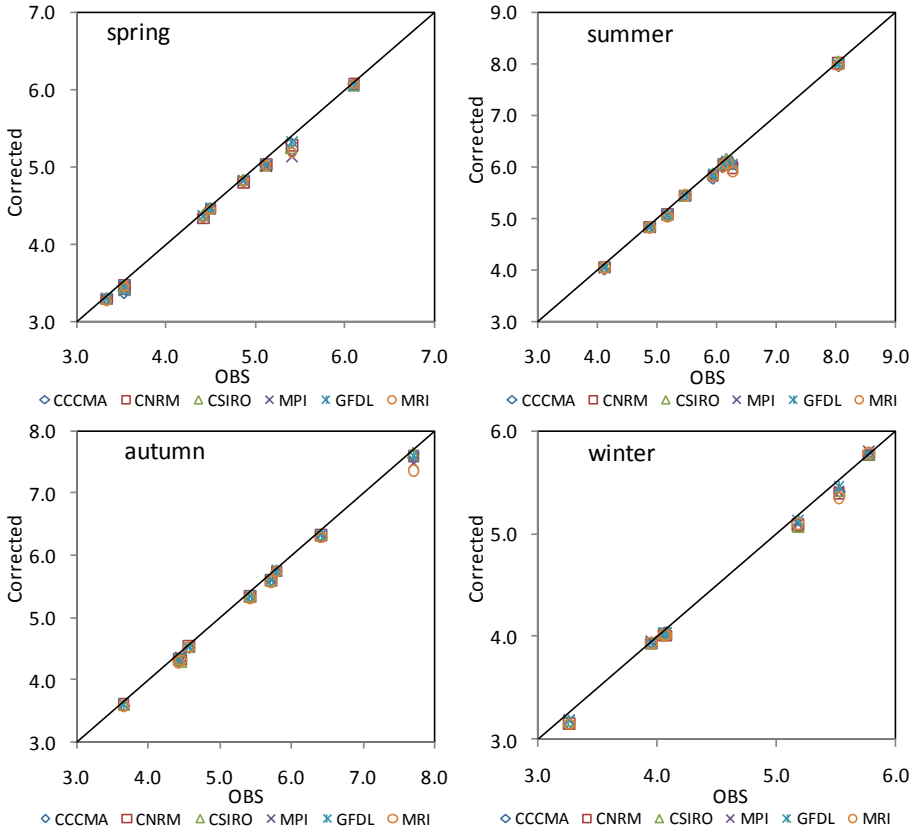

Fig. 9.4. Scatter plots of the corrected *versus* observed mean of daily precipitation on wet days (SDII; mm/day). On each graph, there is one point per climatic zone and per GCM; the total number of points per graph is the number of climatic zones times six named GCMs. The line of perfect fit (the diagonal) is also shown. The downscaled values were computed as ensemble means of the ensemble for 500 runs during the baseline period 1961- 2000.

The BC procedure must have had impacts on the second moment of the PDF daily precipitation - ppSD. These effects for each season are shown in Fig .9.5. All of the corrected ppSDs could almost approximate observed ppSD no matter where they were in the distribution. The better correction appeared in the three seasons other than summer, when the ppSD was underestimated, especially toward the higher values. Compared with the original downscaled values (Fig. 8.2), the differences among the named GCMs became smaller and the corrected ppSD converged more towards the observed values.

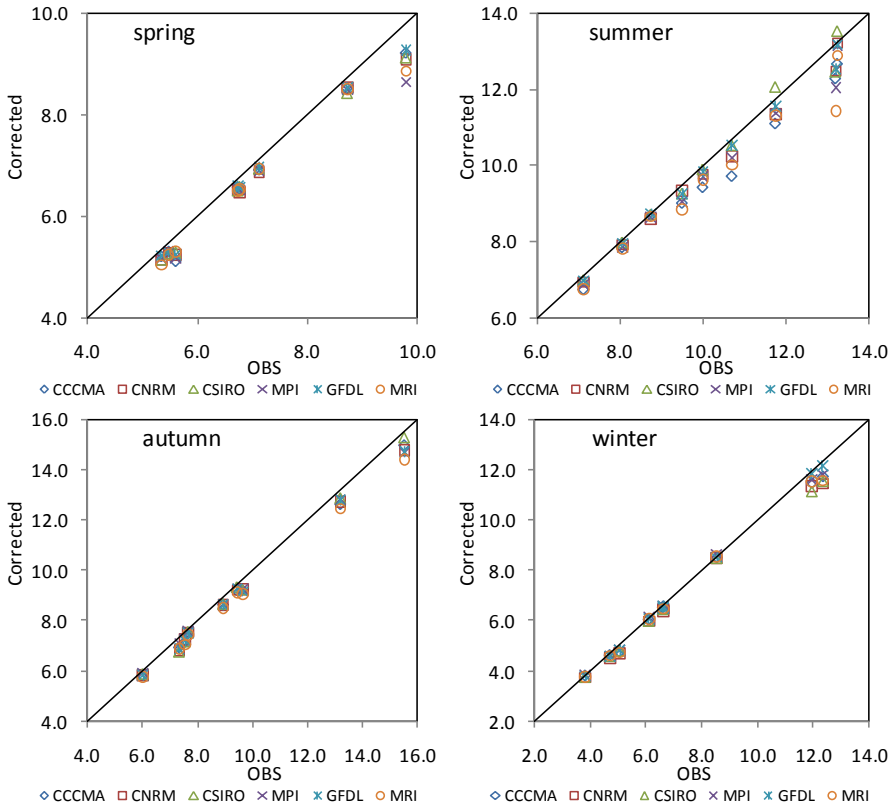

Fig. 9.5. As Fig 9.4 but for standard deviations (ppSD).

Daily precipitation belongs to a type of non-Gaussian distribution in nature, which is especially true for dry regions. Only correctly modeling the first two moments still has the potential to give a biased estimate of the shape of its PDF. Moreover, the BC method was based on CDF. Therefore, the non-parametric Kolmogorov-Smirnov (K-S) goodness-of-fit test was used to assess the CDFs of observed and corrected downscaled daily precipitation on wet days. The null hypothesis of the K-S test is of no CDF difference in paired samples (Press et al., 1992; Lopes et al., 2007; Corder and Foreman, 2009). As also stated previously, the K-S test calculated the test statistic p value and made a choice to either accept or reject the null hypothesis at a given significant level α based on the calculated p value. The p value is the probability of wrongly rejecting the null hypothesis if it is in fact true. In this study, an α value of 0.05 was used. When $p<0.05$, it indicates that the null hypothesis is unlikely to be true and the null hypothesis should be rejected. The test results (p-values) are presented in Table 9.1, where each value is an average across all the grids available for a particular region. The 90% confidence intervals for the 500 runs were also listed in the parentheses. The table shows that he p-values of the goodness-of-fit test were all above 0.05 (α=0.05) even for the low bounds of the 90% confidence intervals, indicating that they all passed the K-

S test. However, this was not the case for the original downscaled values, (See Table 8.3, where some runs in the ensemble would fail to pass the test). This indicated that although the ensemble was bias-corrected as a whole, it still make improvement for each run in the ensemble.

Figure 9.6 shows the corrected yearly mean precipitation days represented as nr001 for each season. The figure shows that the corrected results for the GCMs could reproduce the observed nr001 very well, especially in winter. However, in the other three seasons, nr001 was underestimated slightly. In addition, when compared with the original downscaled values (Fig. 8.6), it was not difficult to find that the BC method performed better when the precipitation days were overestimated, rather than when they were underestimated. This indicated that randomly adding some precipitation events was not a very effective way of offsetting the precipitation frequency deficit and had its own limits. Moreover, adding precipitation events would have distorted the relationship between the synoptic pattern and precipitation events.

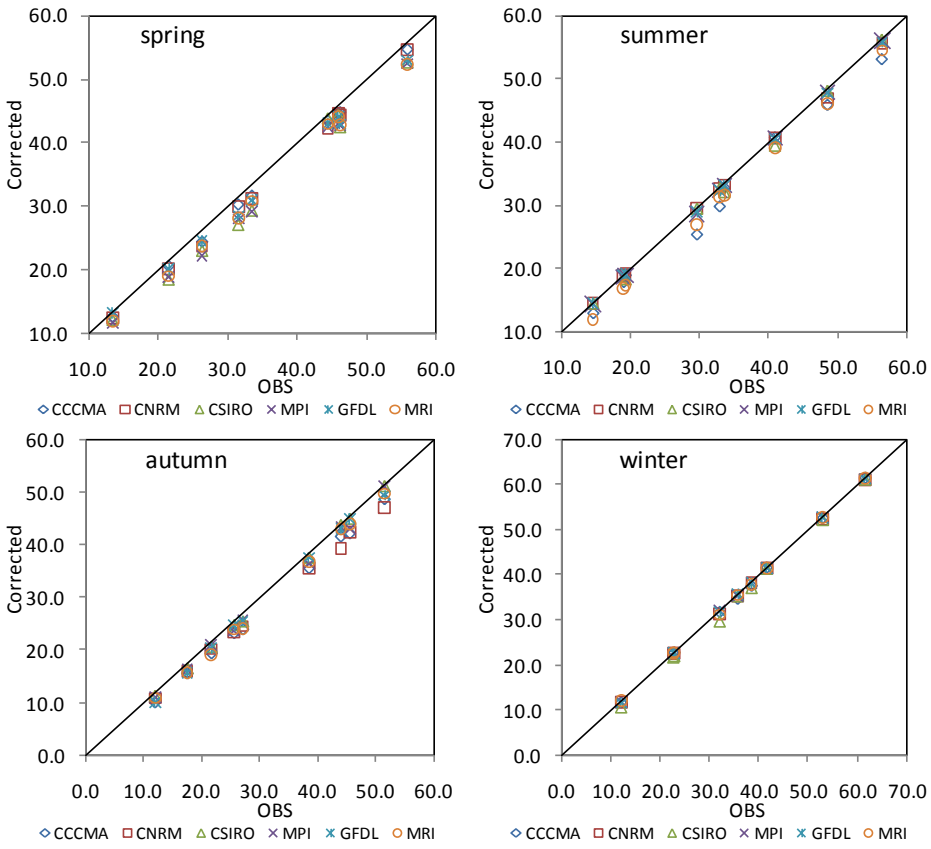

Fig. 9.6. As Fig 9.4 but for the total precipitation days (nr001).

Table 9.1. Mean of non-parametric Goodness-of-fit test results (*p*-values) for comparing the distribution of corrected and observed daily precipitation on wet days in each climatic zone. Each value is an average across all the grids available in a particular zone. These statistics are derived from the ensemble of 500 runs in the baseline period (1961-2000); 90% of confidence intervals are given in parentheses.

spring	CCCMA	CNRM	CSIRO	MPI	GFDL	MRI
E6	0.84(0.32, 0.98)	0.84 (0.31, 0.98)	0.82(0.29, 0.98)	0.83 (0.29, 0.98)	0.84 (0.31, 0.98)	0.83 (0.29, 0.98)
G	0.86 (0.32, 1.00)	0.84 (0.30,0.99)	0.84(0.30, 1.00)	0.80 (0.26, 0.99)	0.85 (0.33, 1.00)	0.83 (0.28, 1.00)
E4	0.82 (0.29, 0.99)	0.81 (0.28, 0.99)	0.82(0.27, 0.99)	0.82 (0.27, 0.99)	0.83 (0.30, 0.99)	0.83 (0.28, 0.99)
E3	0.82 (0.29, 0.99)	0.82 (0.28, 0.99)	0.81(0.28, 0.99)	0.81 (0.27, 0.99)	0.83 (0.30, 0.99)	0.82 (0.29, 0.99)
F4	0.82 (0.29, 0.99)	0.81 (0.28, 0.99)	0.75(0.28, 0.96)	0.59 (0.20, 0.93)	0.82 (0.30, 0.99)	0.70 (0.23, 0.95)
D5	0.81 (0.29,0.99)	0.81 (0.29,0.99)	0.80(0.27, 0.99)	0.81 (0.28, 0.99)	0.81 (0.29, 0.99)	0.80 (0.27, 0.99)
B2	0.83 (0.29, 0.99)	0.81 (0.27, 0.99)	0.79(0.26, 0.99)	0.81 (0.29, 0.99)	0.82 (0.30, 0.99)	0.80 (0.26, 0.99)
F3	0.82 (0.30, 0.99)	0.82 (0.28, 0.99)	0.78(0.26, 0.99)	0.80 (0.29, 0.99)	0.83 (0.30, 0.99)	0.81 (0.29, 0.99)
E2	0.83 (0.30, 0.99)	0.83 (0.29, 0.99)	0.80(0.27, 0.99)	0.81 (0.28, 0.99)	0.83 (0.30, 0.99)	0.81 (0.28, 0.99)
summer	CCCMA	CNRM	CSIRO	MPI	GFDL	MRI
E6	0.82 (0.29, 0.98)	0.84 (0.32, 0.98)	0.83 (0.31, 0.98)	0.84 (0.32, 0.98)	0.84 (0.31, 0.98)	0.82 (0.29, 0.98)
G	0.82 (0.28, 0.99)	0.82 (0.28, 0.99)	0.85 (0.30, 1.00)	0.84 (0.29, 1.00)	0.83 (0.31, 1.00)	0.82 (0.26, 0.99)
E4	0.79 (0.25, 0.99)	0.82 (0.30, 0.99)	0.82 (0.29, 0.99)	0.82 (0.29, 0.99)	0.83 (0.30, 0.99)	0.81 (0.26, 0.99)
E3	0.79 (0.25, 0.99)	0.82 (0.29, 0.99)	0.81 (0.27, 0.99)	0.83 (0.30, 1.00)	0.83 (0.30, 0.99)	0.82 (0.29, 0.99)
F4	0.79 (0.26, 0.99)	0.80 (0.26,0.99)	0.78 (0.27, 0.99)	0.81 (0.29, 0.99)	0.82 (0.29, 0.99)	0.78 (0.24, 0.99)
D5	0.80 (0.27, 0.99)	0.81 (0.28, 0.99)	0.81 (0.27, 0.99)	0.83 (0.30, 0.99)	0.83 (0.30, 0.99)	0.82 (0.28, 0.99)
B2	0.81 (0.30, 0.99)	0.81 (0.28, 0.99)	0.81 (0.27, 0.99)	0.82 (0.31, 0.99)	0.82 (0.30, 0.99)	0.81 (0.29, 0.99)
F3	0.79 (0.27, 0.99)	0.80 (0.29, 0.99)	0.80 (0.28, 0.99)	0.82 (0.30, 0.99)	0.83 (0.30, 0.99)	0.81 (0.28, 0.99)
E2	0.82 (0.29, 0.99)	0.84 (0.30, 1.00)	0.82 (0.29, 0.99)	0.84 (0.30, 1.00)	0.84 (0.29, 1.00)	0.82 (0.28, 1.00)
autumn	CCCMA	CNRM	CSIRO	MPI	GFDL	MRI
E6	0.81 (0.30, 0.98)	0.81 (0.31, 0.98)	0.83 (0.32, 0.98)	0.83 (0.32, 0.98)	0.81 (0.30, 0.98)	0.81 (0.30, 0.98)
G	0.81 (0.25, 0.99)	0.84 (0.29, 0.99)	0.86 (0.29, 1.00)	0.84 (0.31, 1.00)	0.81 (0.26, 1.00)	0.83 (0.28, 1.00)
E4	0.82 (0.29, 0.99)	0.83 (0.29, 0.99)	0.84 (0.31, 1.00)	0.85 (0.33, 1.00)	0.84 (0.30, 1.00)	0.82 (0.28, 0.99)
E3	0.83 (0.30, 0.99)	0.83 (0.29, 0.99)	0.83 (0.30, 0.99)	0.83 (0.31, 0.99)	0.84 (0.30, 1.00)	0.80 (0.27, 0.99)
F4	0.82 (0.30, 0.99)	0.81 (0.29, 0.99)	0.81 (0.29, 0.99)	0.57 (0.19, 0.78)	0.82 (0.30, 0.99)	0.55 (0.18, 0.69)
D5	0.82 (0.29, 0.99)	0.82 (0.29, 0.99)	0.81 (0.29, 0.99)	0.83 (0.30, 0.99)	0.83 (0.30, 0.99)	0.81 (0.29, 0.99)
B2	0.82 (0.30, 0.99)	0.82 (0.30, 0.99)	0.77 (0.25, 0.98)	0.82 (0.30, 0.99)	0.82 (0.30, 0.99)	0.82 (0.28, 0.99)
F3	0.82 (0.29, 0.99)	0.82 (0.29, 0.99)	0.79 (0.26, 0.99)	0.81 (0.29, 0.99)	0.83 (0.31, 0.99)	0.78 (0.27, 0.99)
E2	0.83 (0.29, 0.99)	0.83 (0.30, 0.99)	0.84 (0.31, 1.00)	0.84 (0.30, 1.00)	0.84 (0.30, 1.00)	0.83 (0.30, 0.99)
winter	CCCMA	CNRM	CSIRO	MPI	GFDL	MRI
E6	0.83 (0.31, 0.98)	0.83 (0.30, 0.98)	0.84 (0.30, 0.98)	0.83 (0.30, 0.98)	0.83(0.31, 0.98)	0.83 (0.31, 0.98)
G	0.83 (0.31, 1.00)	0.84 (0.33, 1.00)	0.82 (0.27, 0.99)	0.83 (0.30, 1.00)	0.83 (0.31, 1.00)	0.83 (0.30, 0.99)
E4	0.83 (0.30, 0.99)	0.83 (0.30, 1.00)	0.83 (0.29, 1.00)	0.82 (0.29, 0.99)	0.83 (0.29, 0.99)	0.83 (0.30, 0.99)
E3	0.83 (0.30, 0.99)	0.82 (0.29, 0.99)	0.82 (0.28, 0.99)	0.81 (0.29, 0.99)	0.82 (0.30, 0.99)	0.82 (0.30, 0.99)
F4	0.82 (0.31, 0.99)	0.83 (0.30, 0.99)	0.81 (0.29, 0.99)	0.81 (0.29, 0.99)	0.83 (0.30, 0.99)	0.79 (0.29, 0.99)
D5	0.81 (0.29, 0.99)	0.81 (0.29, 0.99)	0.81 (0.29, 0.99)	0.79 (0.25, 0.99)	0.81 (0.29, 0.99)	0.80 (0.28, 0.99)
B2	0.81 (0.29, 0.99)	0.81 (0.30, 0.99)	0.80 (0.28, 0.99)	0.76 (0.25, 0.99)	0.81 (0.27, 0.99)	0.79 (0.27, 0.99)
F3	0.83 (0.30, 0.99)	0.82 (0.30, 0.99)	0.82 (0.28, 0.99)	0.82 (0.29, 0.99)	0.82 (0.29, 0.99)	0.82 (0.29, 0.99)
E2	0.82 (0.29, 0.99)	0.82 (0.28, 0.99)	0.82 (0.29, 0.99)	0.80 (0.27, 0.99)	0.82 (0.29, 0.99)	0.81 (0.28, 0.99)

9.3.2 Future projections under the A2 Scenario

In this section, the BC method was applied to downscaled results from the 6 GCMs under the A2 scenario. The objective was to see how the bias corrected future projection compared to the original downscaled output. From the above section, it was found that the BC method performed similarly in all seasons, therefore only the corrected results in winter are taken as an example and represented. Moreover, the future period was limited from 2046-2065. The differences in SDII and nr001 between the corrected and original downscaled daily precipitation are displayed in Fig. 9.7. The top panel of the figure shows that the corrected differences in SDII are generally between -0.6 and 0.8mm/day. The larger correction was found in the relatively humid zones of F4, F3 and B2.There was no generic spatial pattern among the GCMs. For nr001, the bias correction method reduced the precipitation days for all GCMs, implying a systematic error among all GCMs to generate more rain-days than observed. Moreover, the deduction appeared more significant in zones D5, B2 and E2 for the GCMs of MPI and MRI, indicating a larger systematic error in nr001 for the two GCMs.

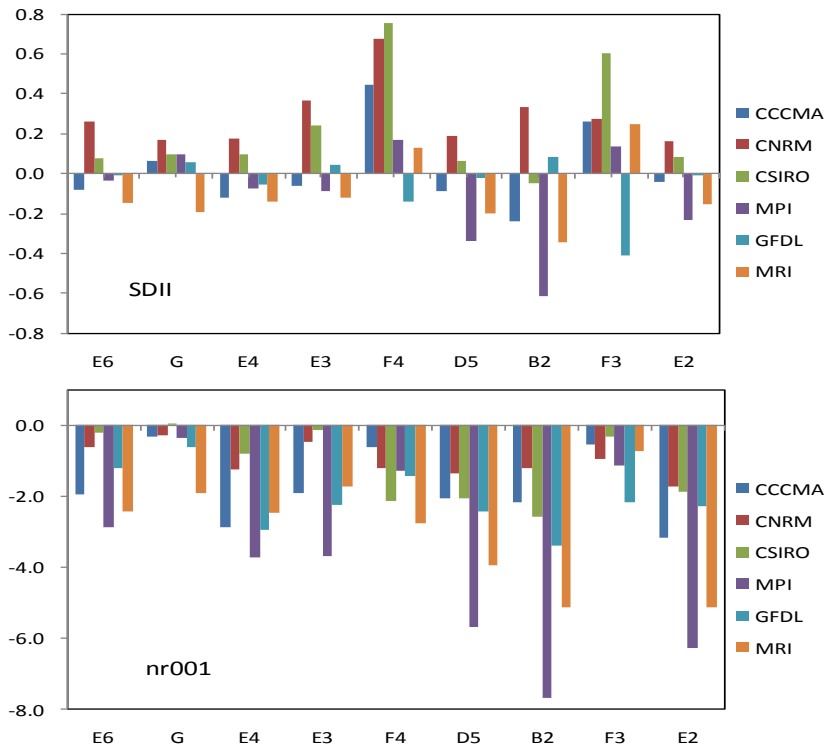

Fig. 9.7. Differences in SDII and nr001 between the corrected and the original downscaled daily precipitation specified by the named GCMs (different colored bars) and the climatic zones (names on the X-axis) for winter during the period from 2046 to 2065. Each value was an average across all the grids available in a particular climatic zone.

9.4 Conclusion and discussion

In this chapter, a CDF-based bias correction method was introduced to correct the systematic error in the downscaled GCM daily precipitation. Different from most others, which only adjust the precipitation intensity, the proposed method took a two-step procedure to correct both the frequency and the intensity distribution of daily rainfall. If the original downscaled precipitation frequency is greater than the observed frequency for a given month, the frequency is corrected by discarding some precipitation events. To correct the intensity distribution, the difference between the observed and downscaled precipitation at each percentile of CDF of the original downscaled precipitation during the baseline period was treated as systematic error and was superimposed onto the corresponding CDF of the original downscaled precipitation for different periods. The method explicitly considers changes in the distribution of the future climate (Eq. 9.4), instead of assuming that historic CDF distribution applies to the future period used in some other statistical bias correction methods (Eq. 9.3). Since the precipitation amount is the product of precipitation intensity and frequency, correcting these two precipitation components also corrects the total precipitation amount.

During the baseline period, the method is able to reduce significantly biases in the original downscaled precipitation. After bias correction, both the frequency and precipitation amount of the downscaled precipitation are more approximated to the observed values. Moreover, the differences among the six GCMs almost disappeared. The method also improved downscaled standard deviations of daily precipitation from different GCMs and made them converge towards the observed values. However, it appeared that the method performed better when the precipitation frequency was overestimated by the SOM-SD. When precipitation frequency was underestimated, the method could, to a certain extent, correct the frequency deficit. The issue could be further relieved by randomly adding more precipitation events to the downscaled data, but at a possible cost of the relationship between the synoptic pattern and precipitation events that was the foundation of the SOM-SD.

For the future scenario projections, the bias correction results showed that there was no generic spatial pattern among the GCMs for SDII. Taking winter as an example, the differences between the corrected and original downscaled daily

precipitation were generally between -0.6 and 0.8 mm/day. For the wet days, the bias correction procedure showed a consensus deduction (about 4 days) among the GCMs. Many other studies only used the difference in downscaled results between present-day and future period to show the possible changes. However, impact studies, such as hydrological and agricultural models, may need the direct downscaling time series outputs instead of the calculated changes. From this point of view, the bias correction presented in this study can be used to transfer the downscaling time series for impact studies.

However, the downscaled series for the baseline and future periods were both offset by the same systematic errors. Therefore, this procedure can not significantly modify the downscaled precipitation changes for each GCM. Thus, the correction method presented in this chapter cannot also reduce the dispersion of the downscaled projections among GCMs, and merely is a tool for making the downscaled precipitation more applicable for impact studies. The SOM-SD's ability to generate convergent downscaling projections largely depends on the performance of the GCMs employed. That is to say, the GCMs should reliably reproduce the temporal evolution of synoptic states in the past. On the other hand, they should generate a convergent response to a same emission scenario.

The bias correction method is also viewed as a statistical downscaling technique itself and is commonly known as Model Output Statistics (MOS; Wood et al., 2004; Ines and Hansen, 2006; Maraun et al., 2010). Generally, MOS was applied to RCM outputs instead of GCM outputs. This is because RCMs could produce more reliable daily precipitation distributions than GCMs. Therefore, this kind of method was also referred as distribution-wise (Maraun et al., 2010). However, it is worth noting that such a method calibrates only distributions but disregards any pair-wise relationships between predictor and predictand. The reliability of future precipitation projections is determined mostly by the precipitation produced by the models such as downscaling models, RCMs and GCMs. Where the simulated precipitation has simply no skill the application of a bias correction method would not be justified, even if corrected and observed precipitation intensity distribution could be brought into perfect agreement.

The SOM-BCSD is, to the author's knowledge, the first trial to make use of the advantages of a statistical downscaling method and a bias correction method. It is

expected that the SOM-SD could give a relatively appropriate estimate of the statistical characteristics for the future precipitation by downscaling the atmospheric circulation variables from GCMs, while the bias correction could further correct the systematic errors. In addition, the bias correction method is used only as an auxiliary tool in the SOM-SD and does not lead to intense changes on the downscaled precipitation by the SOM-SD.

Finally, the proposed method, like other bias correction methods, assumes a time-invariant transfer function, which may not hold in a changing climate but seems reasonable given the current state of climate modeling research.

CHAPTER TEN

CONCLUSIONS AND OUTLOOK

10.1 Introduction

Coupled ocean/atmosphere general circulation models (OA/GCMs) have widely been identified as a powerful tool for showing the need for global action to curb the anthropogenic emissions that cause climate change. However, these models provide less helpful information for adaptation at regional and local scales (Schiermeier, 2007). Over the last decade, the scientific community is developing regional climate downscaling (RCD) techniques to reconcile the scale mismatch between coarse-resolution OA/GCMs and location-specific information needs of adaptation planners (Wilby et al., 2009).

However, many these RCD techniques still dwell on theoretical studies and are not impact-studies oriented. With climate change adaptation/mitigation assessment getting popular and practical, regional downscaling should play an important role in the top-down (also known as 'scenario-led') or the bottom-up climate risk assessment framework. At this point, the main objective of this thesis was the development and application of a statistical downscaling method (SDSM) to local-scale climate change scenario construction for regional water and food security study. A statistical downscaling framework was developed based on a comprehensive literature review. The framework involved selecting predictors corresponding to predictands, building the statistical relationship between the two, calibrating and verifying the relationship and constructing local-scale climate change scenarios, as well as outputting proper indicators.

Southeast Australia was selected as the case study area, due to the complex climatic conditions and highly diverse landscape ranges that make it ideal for downscaling study. In addition, the climate variability and global changes have demonstrated a strong impact on regional ecological and economic fluctuations for Australia (Nicholls, 1997). It was expected that the framework would synthesize the advanced information in the field of statistical downscaling.

10.2 Conclusions

10.2.1 Synoptic climatology and SOM-SD

The statistical downscaling method proposed by this study was based on a non-linear classification technique known as self-organizing maps (SOMs; Kohonen, 2001) and has therefore been named SOM-SD. The SOM algorithm has been widely applied to synoptic climatologic studies all over the world, including Australia (e.g., Cassano et al., 2006, 2007; Hope, 2006; Hope et al., 2006). The synoptic climatology is the theoretical foundation of statistical downscaling (Klein and Glahn 1974; von Storch, 1999). However, a careful evaluation of the feasibility of applying SOM to statistical downscaling was still needed. In this research, the evaluation was conducted based on the daily NCEP/NCAR reanalysis data (NNR; Kalnay et al., 1996; Kistler et al. 2001) and the observed precipitation data across Southeast Australia. The results showed that the derived large-scale synoptic patterns from the NNR data had an excellent relationship with the statistical characteristics of observed precipitation such as frequency and intensity. All of these indicated that the SOM can be used for statistical downscaling.

Based on the above finding, a prototype of the SOM-SD was constructed using the NNR data and the observed data for the case study area. The first step of the prototype SOM-SD development was to select appropriate predictors for the corresponding predictand, which would determine the success or failure of the final SOM-SD (Hofer et al., 2010; Maraun et al., 2010; Wilby et al., 2004). The selected predictors needed to fulfill the following conditions: (1) co-exist in the NNR data and the CMIP3 archives; (2) have a physical relationship to the predictand; (3) be reliably represented by the reanalysis data and GCMs; (4) carry the signal of climate change. Another important factor in constructing a SDSM is to select an appropriate downscaling domain (e.g., Brinkmann, 2002; Wilby et al., 2004). In this study, a 3×3 grid domain was selected with the grid resolution of 2.5º×2.5º. The relationships, or the transfer function, between the large-scale synoptic patterns and observed daily predictands were derived using predictors from NNR. The synoptic patterns depicted the generalized characteristics in the predictors, so that each of them corresponded to a subset of a particular predictand. In other words, many predictand values could map to the same

synoptic pattern. Against this background, a conditional stochastic re-sampling technique was used to generate an ensemble of possible predictand values for a synoptic pattern to be downscaled (Lall and Sharma, 1996), which made the SOM-SD different from other deterministic SDSMs, such as regression-based methods. To strengthen the precipitation seasonality of the downscaled predictands, a so-called 'Seasonal Precipitation Pool (SPP)' scheme was introduced into the SOM-SD.

It should be noted that the SOM-SD only created a single downscaling model for all months or seasons. In this sense, it is in contrast to many other downscaling methods, which use separate models for each month or season (e.g., Timbal et al., 2009; Chu et al., 2010). The advantage of such a singular method is that the annual cycle of precipitation/temperature comes out of the model itself, rather than being externally imposed, with the same "physics" giving rise to both the annual cycle and inter-annual variability. Such a singular model has a potential disadvantage that it may not predict monthly/seasonal anomalies as skillfully as a set of models constructed separately for each month or season. However, it does not seem an issue in this study, as the downscaling skill from such a singular model is comparable to that from those models built seasonally in most of the case study area.

Thus, the SOM-SD builds a relatively simple, transparent and physically meaningful relationship between predictors and predictands. It combines the advantages of synoptic classification methodology and stochastic re-sampling technique, which could be seen as an effective statistical downscaling scheme at present (e.g., Christensen and Hewitson, 2007; Cawley et al., 2007). The synoptic classification provides an accurate and relatively transparent tool for analyzing the controlling regimes for local-scale precipitation, while the stochastic re-sampling can explore the probability of daily precipitation in a Monte Carlo simulation way. With the ability to generate a full range of time series data, the SOM-SD output allows probability and risk analysis which are essential for climate change impact assessment, given the large uncertainty of climate change projections.

10.2.2 SOM-SD calibration and validation

Based on the NNR predictors, the applicability of the SOM-SD was calibrated and

validated by downscaling daily precipitation, minimum and maximum temperature across a variety of different climatic zones over southeast Australia. The accuracy of the method was analyzed in a seasonally stratified style. The results showed that (1) classification of circulation patterns is a powerful tool for capturing the representative local-scale precipitation and temperature regimes, while the SSP re-sampling scheme could, to a certain extent, improve the seasonality modeling of these predictands; (2) the SOM-SD exhibits high skills in the average climatological statistics of the daily precipitation and temperature time series, including mean values, rainy days, wet/dry-day persistence in each season. Furthermore, the model can accurately reproduce the cumulative distribution of frequency (CDF); (3) the method can reconstructs without bias the observed extreme precipitation and temperature characteristics; (4) the method can, to a certain extent, reproduce the inter-annual variability for precipitation and temperature.; (5) the method shows good suitability in that the performance is consistent with historical observations across a variety of climatic zones and seasons. Overall, no particular zone stands out as a climatic entity where the downscaling skill in reproducing all statistical indices is consistently lower or higher across seasons. However, comparatively speaking, the performance in the arid/semi-arid region is inferior to that in other regions. There were fewer precipitation events to train the SOMs in these environments, especially when estimating extreme values. Therefore, the lower skill in these regions could partly be explained by lower information content for model calibration.

The outputs from SDSMs, in most cases, are used to provide a product (in the form of data or information) for impact studies. However, few coordinated efforts have been made to evaluate and compare plethora of downscaling approaches in order to provide information in a way that helps the choice of downscaling method suitable for a given impact assessment. Therefore, a quantitative evaluation is necessary to evaluate the skill of a downscaling approach to ensure that the selected one meets the application and the end user needs. The generic requirements include the correct representation of the predictands for (1) mean and extreme state, (2) temporal variability, (3) spatial variability, and (4) consistency between different local-scale variables, and these are required also for future scenarios (Maraun et al., 2010). In addition, a non-parametric technique known as bootstrap simulation was introduced to perform the uncertainty analysis

(Castrup, 1995; Dibike et al., 2008).

10.2.3 Model comparison

For precipitation, an additional comparison was carried out with two closely related models: the unconditional stochastic model and the Analog model (AM). The three models did not show obvious differences in reproducing the multi-year mean climatological statistics of the observed precipitation time series. However, there were significant differences among them in modeling the inter-annual variability. The AM gave the best performance because the nature of the method was to search the only best analogue from the past observation, while the SOM-SD showed a large improvement compared with the unconditional stochastic model. Furthermore, the best performance from the AM can mostly be covered by the range simulated by the SOM-SD. The unconditional model used in this study just re-samples randomly from all historical data for each target downscaling grid on each season, not using predictors at all. From this point of view, it is not a genuine downscaling method. As expected, it can not reproduce observed inter-annual variability at all. However, it really proves that precipitation can be conditioned on large-scale synoptic patterns, rather than a totally stochastic process.

10.2.4 Application to GCMs

When applied to the GCM baseline data, the SOM-SD showed consistent results for the downscaled temperatures with the observed values. For the downscaled precipitation, however, the SOM-SD did not perform as well as it did for the NNR data. To some extent, it indicated that the GCMs failed to accurately reproduce the observed climate depicted by the NNR. In order to overcome this problem, two statistical bias correction techniques were integrated into the SOM-SD for adjusting downscaled precipitation. The first one was a traditional bias correction method that mapped the distribution of downscaled variables (precipitation and temperature) onto that of gridded observed data (e.g. Wood et al., 2004; Ines and Hansen, 2006; Piani et al., 2010). The second one was proposed by this study, which maps the differences in CDFs between the downscaled and observed values onto the CDF of the downscaled values, which means the differences between the CDFs were considered as systematic errors. When two methods were applied to

the downscaled daily precipitation from six GCMs, they made the downscaled results converge towards the observed values. The two methods were also used to adjust the downscaled results from the future scenarios.

When an SDSM is applied to downscale GCM scenarios, the transfer function between predictors and predictands (found under current climate) is assumed still valid in future climate conditions. The assumption can only be verified after the fact. This implies that many published findings about downscaling derived climate change impacts should be viewed with caution (Charles et al., 1999). In this study, an indirect approach was introduced into the SOM-SD to analyze such a stationarity issue; by checking the frequency change of each synoptic pattern of the large-scale atmospheric circulation under changing climate conditions. This method was also used to analyze the ability of GCMs to replicate synoptic circulation patterns (e.g., Cassano et al., 2006; Hope et al., 2006), and further used to select appropriate predictors for downscaling. If future climate results in intense change, it is very likely for some atmospheric states to converge toward some synoptic patterns resulting in the frequencies of these patterns increasing fast under future climate. Thus, the non-parametric Kolmogorov-Smirnov (K-S) test (Corder and Foreman, 2009) was employed to check the CDF change in terms of the frequencies of the synoptic patterns from both the GCM baseline and scenario data as a whole. The analysis results indicated that the future atmospheric states would really change compared with current climate; however, the changes would not become so strong that they could change the CDF of present synoptic patterns.

When the SOM-SD was applied to the selected GCMs under the A2 scenario, the downscaled results showed a spatially consistent increase for both daily minimum and maximum temperature, with a more significant warming trend in summer than in winter. The increase in maximum temperature appeared larger than that for minimum temperature. However, for both temperatures, the changes varied among the GCMs. Moreover, the warming trend becomes faster in the later period (2081-2100) than in the middle (2046-2065) of 21st century. Future precipitation projections downscaled from the GCMs showed consistent decreases in rainfall intensity and rainfall days for spring and winter. For these two seasons, the decrease in total precipitation appeared more significant in the humid zones (about -20% in the 2046-2065 and about -40% in the 2081-2100) than in the arid and semi-arid zones (between -10% and -20%). However, in the other two seasons,

there was no consistent change trend of precipitation among the GCMs, where the main discrepancy occurred in the arid and semi-arid climatic zones. This was because about half of the GCMs produced a decrease in precipitation intensity and rainfall days, while others gave an opposite trend. In the humid zones, there was a relatively consistent decrease in total precipitation among the GCMs.

10.2.5 Limitations

Although the SOM-SD showed a relatively high skill in downscaling daily precipitation and temperature, it has many similar issues as other SDSMs.

Firstly, the method is incapable of predicting new daily records, because the predicted values are only taken from archives from past observations (Imbert and Benestad, 2005; Hidalgo et al., 2008; Timbal et al., 2009). By fitting the observed data into some theoretical distributions, the problem that SOM-SD is unable to extrapolate of new values can be relieved to an extent. However, this method was not adopted in this study, because no single distribution will be suitable for such a large case study area characterized with complex climate conditions and complicated landscapes.

Secondly, it tends to systematically underestimate the long consecutive spells of wet/dry days. This can be explained partly by the fact that the SOM-SD used an unsupervised learning algorithm to find the relationship between large-scale predictors and precipitation. The learning algorithm classified predictors into synoptic patterns without using any information from precipitation. Therefore, the relationship cannot be expected very strong.

Thirdly, the SOM-SD used the GCM simulated precipitation and temperature fields as predictors. The improved skill was significant, particularly in strengthening the simulation of the inter-annual variability for precipitation and temperature. This result was also identified by other studies (e,g,, Salathe, 2003; Widmann et al., 2003). This may become a limitation of the SOM-SD in that the skill is tied to a specific GCM (Maurer and Hidalgo, 2008). This issue appears more serious for precipitation. Some studies do not recommend using the variables determined completely by the GCM (e.g., surface fluxes, heating rates, or precipitation) as predictors (Wilby et al., 2004; Hofer et al., 2010), because these fields may be depicted less accurately than other potential predictor

variables in the GCM (such as upper air temperature, wind and geopotential height). However, this study found that using GCM precipitation as a predictor for downscaling precipitation could improve significantly the ability in modeling the inter-annual variability. To some extent, this indicates that the GCM precipitation may reflect the complexity of physical processes (as represented in the GCM) in producing precipitation (Robertson et al., 2004; Maurer and Hidalgo, 2008; Hidalgo et al., 2008).

Fourthly, the SOM-SD used different predictor suites for precipitation and temperature downscaling. In another words, downscaled predictand series were constructed independently from one variable to another. This will imply that the covariance of these two predictands might not necessarily be preserved in the resulting time series. This could have consequences for some crop and hydrological modeling which may require realistic interactions between multiple driving variables. Although this issue was not covered as part of this study, it was investigated during the procedure to build downscaling model for precipitation and temperature. The preliminary attempts showed that it was very difficult to find such a common predictor suite for both precipitation and temperature downscaling to provide similar skills as each suite did for each predictand. This issue will be further investigated using the new CMIP5 database where more predictors can be analyzed and assessed.

In addition, the bias correction method was introduced to eliminate the systematic error between GCM and observed data distributions by assuming a time-invariant transfer function. This assumption may not hold in a changing climate.

10.3 Outlook

Not a downscaling method, whether a physical process-based dynamic one or statistically based one, could be perfect and capable of solving all issues in the field of downscaling at present and in the near future. Against this background, there are several promising directions worth noting:

1) Development of probabilistic rather than deterministic downscaling algorithms would be appropriate and robust (Cawley et al., 2007; Christensen and Hewitson, 2007). A probabilistic downscaling method can provide a probabilistic description of the uncertainty of downscaling outputs that can be

further exploited in impact studies, especially where the principal focus lies on the implications of extreme events, which by their very nature are not modeled well by the conditional mean (Cawley et al., 2007). Clearly the distribution of plausible impacts is exactly the information required by such users as government institutions or the insurance industry for well-informed policy-making and forward planning.

2) Introduction of advanced nonlinear techniques into the SDSMs to better depict the correlations among the predictors as well as those between predictors and predictands, such as the Bayesian neural network (Khan and Coulibaly, 2006), the relevance vector machine (Ghosh and Mujumdar, 2008) and the fuzzy rule-based classification scheme (Yang et al., 2010). Moreover, existing downscaling methods need to be updated according to newly available data and information.
3) Development of new downscaling methods that could combine the advantages of current downscaling methods. For example, with the increasing reliability and availability of RCM scenarios, recent work on statistical downscaling has aimed to combine the benefits of these two approaches (e.g., Fuentes and Heimann, 2000; Hellström and Chen, 2003; Boé et al., 2006).
4) Incorporation of information from multiple downscaling algorithms to improve prediction performance and estimate predictive uncertainty, since different models will have different skill for a given task (Burnham and Anderson, 2004). Multi-model ensembles of downscaling have been shown to provide larger improvements on gauging the uncertainty of future climate scenarios at local scales over individual models (e.g., Coelho et al., 2006; Haylock et al., 2006).
5) Evaluation of downscaling techniques by directly linking to climate-change impact studies (e.g., Teutschbein et al., 2011). In practice, the choice of downscaling method not only hinges on the time, data and technical resources available, but also the intended application (Wilby et al., 2009). Moreover, the value of a downscaling method can be reflected only after it is put in a practical impact study to inform climate risk assessment and adaptation options appraisal.

This study is a landmark project, offering downscaled climate change projections across a large part of the southeastern Australian continent. Moreover, the SOM-

SD is following above directions and is still under continuous improvement. Further on-going developments are underway to maximize the benefits from this work. Specifically, the current development has been focusing on the following aspects:

- ***Preprocessing Predictors***. Add methods, such as the principal component analysis (PCA; Wilks, 2006) and the projection pursuit (Jones and Sibson, 1987), to preprocess input data and to reduce random noise among them. At present, the SOM-SD does not have this component, because the downscaling was carried out in a small domain of 3×3 grids. However, preprocess may become an issue if more predictors are added into the method.

- ***Using supervised algorithms***. Use a supervised SOM instead of the originally unsupervised SOM to perform synoptic classification. Current classification procedure in SOM-SD was carried out independently of the predictand information. It is expected that the relationship between predictors and predictand will receive significant improvement using the supervised learning algorithm since predictand will directly take part in the learning procedure.

- ***Model inter-comparison***. Compare with other downscaling methods including SDSMs and dynamic downscaling methods as well as model output statistics (MOS) to further identify its strengths and weaknesses. The weaknesses will be improved according to the latest developments.

- ***Validation with latest datasets.*** Calibrate and validate the method using other available reanalysis data, such as the ERA-40 and the JRA-25. Data quality is always a limitation to all downscaling methods. Moreover, some new predictors will be tested with the newest GCM outputs to be published in CMIP5. The key objective is to find some predictors to depict the precipitation process in the downscaling and to avoid using the GCM simulated precipitation as predictors. The SOM-SD hereby will overcome the dilemma that its skill is GCM-dependent.

- ***Linking with impact models. Evaluate its skill by linking to climate change impact models such as crop yield and hydrological models.*** As stated before, the case study area covers most of the Murray-Darling Basin made up of the catchments of the Murray River, where it is one of the most important

agricultural regions in Australia. It is well known that climate change has direct and indirect impacts on regional water resources and crop production in this region (Beare and Heaney, 2002).

REFERENCES

Aksoy, H. (2000). Use of Gamma distribution in hydrological analysis. Turk Journal of Engineering and Environmental Science, 24, 419–428.

Alexander, L., Hope, P., Collins, D., Trewin, B., Lynch A., & Nicholls, N. (2007). Trends in Australia's climate means and extremes: a global context. Aust. Meteorol. Mag., 56, 1-18.

Allen, M. R., & Ingram, W. J. (2002). Constraints on future changes in climate and the hydrologic cycle. Nature, 419, 224– 232.

Anandhi, A., Srinivas, V., Nanjundiah, R.S., Nagesh Kumar D. (2008). Downscaling precipitation to river basin in India for IPCC SRES scenarios using support vector machine. International Journal of Climatology, 28, 401–420.

Bachner, S., Kapala, A., & Simmer, C. (2008). Evaluation of daily precipitation characteristics in the CLM and their sensitivity to parameterizations. Meteorol. Z., 17, 407–419. doi:10.1127/0941-2948/2008/0300.

Barnett, T., & Preisendorfer, R. (1978). Multifield analog prediction of short-term climate fluctuations using a climate state vector. J. Atmos. Sci., 35, 1771–1787.

Barnes, S. L. (1994a). Applications of the Barnes objective analysis scheme. Part 1: effects of under sampling, wave position and station rnadomness. J. Atmos. Oceanic Tech., 11, 1433-48.

Barnes, S. L. (1994b). Applications of the Barnes objective analysis scheme. Part 2: Improving derivative estimates. Atmos. Oceanic Tech., 11, 1449-58.

Barnes, S. L. (1994c). Applications of the Barnes objective analysis scheme. Part 3: Tunning for minimum error. J. Atmos. Oceanic Tech., 11, 1459-79.

Barry, R. G., & Perry, A. H. (2001). Synoptic climatology and its applications. In Synoptic and Dynamic Climatology, Barry RG, Carleton AM (eds). Routledge: London; 547–603.

Barstad, I., Sorteberg, A., Flatoy, F., & Déqué, M. (2009). Precipitation, temperature and wind in Norway: dynamical downscaling of ERA40. Clim. Dyn., 33, 769-776.

Beare, S., & Heaney, A. (2002). Climate change and water resources in the Murray-Darling Basin, Australia: Impacts and possible adaptation. 2002 World Congress of Environmental and Resource Economists, 24-27 June, Monterey, California, USA.

Beersma, J. J., & Buishand, T. A. (2003). Multi-site simulation of daily precipitation and temperature conditional on the atmospheric circulation. Clim. Res., 25, 121–133.

Bellone, E., Hughes, J., & Guttorp, J.P. (2000). A hidden Markov model for downscaling synoptic atmospheric patterns to precipitation amounts. Clim Res, 15, 1–12.

Benestad, R. E. (2003). What can present climate models tell us about climate change? Climatic Change, 59, 311-332.

Benestad, R. E., Hanssen-Bauer, I., & Deliang, C. (2008). Empirical statistical downscaling. World Sci., Singapore.

Benestad, R. E. (2010). Downscaling precipitation extremes correction of analog models through PDF predictions. Theor Appl Climatol, 100, 1–21.

Bensmail, H., Celeux, G., Raftery, A. E., & Robert, C. P. (1997). Inference in Model-Based Cluster Analysis. Statistics and Computing, 7, 1–10.

Bergant, K., & Kajfez-Bogataj, L. (2005). N-PLS regression as empirical downscaling tool in climate change studies. Theor Appl Climatol, 81, 11–23.

Biau, G., Zorita, E., von Storch, H., & Wackernagel, H. (1999). Estimation of precipitation by kriging in the EOF space of the sea level pressure field. J. Climate, 12, 1070–1085.

Bishop, C. M. (1995). Neural Networks for Pattern Recognition, Oxford: Oxford University Press.

Boé, J., Terray L, Habets, F., & Martin, E. (2006). A simple statistical–dynamical downscaling scheme based on weather types and conditional resampling. J Geophys Res, 111, D23106.

Brinkmann, W. A. R. (2002). Local versus remote grid points in climate downscaling, Clim. Res., 21(1), 27–42.

Bronstert, A., Niehoff, D., & B¨urger G. (2002). Effects of climate and land-use change on storm runoff generation: present knowledge and modeling capabilities. HYDROL PROCESS 16(2), 509–529.

Brown, J. R., Jakob, C., & Haynes, J. (2010). Rainfall frequency and intensity over Australia and their association with the atmospheric circulation in a global climate model. Journal of Climate, 23(24), 6504-6525.

Buonomo, E., Jones, R. G., Huntingford, C., & Hannaford, J. (2007). On the robustness of changes in extreme precipitation over Europe from two high resolution climate change simulations. Q. J. R. Meteorol. Soc., 133, 65–81.

Burnham, K. P., & Anderson, D. R. (2004). Multimodel inference: understanding AIC and BIC in model selection. Sociological Methods and Research, 33 (2), 261–304.

Busuioc, A., Tomozeiu, R., & Cacciamani, C. (2008). Statistical downscaling model based on canonical correlation analysis for winter extreme precipitation events in the Emilia-Romagna region. Int. J. Climatol., 28, 449-464.

Cannon, A. J., & McKendry, I. G., (2002). A graphical sensitivity analysis for statistical climate models: Application to Indian monsoon rainfall prediction by artificial neural networks and multiple linear regression models. International Journal of Climatology, 22, 1687–1708.

Cavazos, T., & Hewitson, B. C. (2005). Performance of NCEP-NCAR reanalysis variables in statistical downscaling of daily precipitation. Clim. Res., 28, 95–107.

Cassano, E. N., Lynch, A. H., Cassano, J. J., & Koslow, M. R. (2006). Classification of synoptic patterns in the western Arctic associated with extreme events at Barrow, Alaska, USA, Clim. Res, 30, 83– 97.

Cassano, J. J., Uotila, P., & Lynch, A. H. (2006). Changes in synoptic weather patterns in the polar regions in the twentieth and twenty-first centuries, part 1: Arctic. Int. J. Climatol., 26, 1027-1049.

Cassano, J. J., Uotila, P., Lynch, A. H., & Cassano, E. N. (2007). Predicted changes in synoptic forcing of net precipitation in large Arctic river basins during the 21st century. J. Geophys. Res., 112, G04S49. doi:10.1029/2006JG000332.

Cassano, E. N., & Cassano, J. J. (2010). Synoptic forcing of precipitation in the Mackenzie and Yukon River basins. Int. J. Clim., 30, 658-674.

Castellvi, F., & Stockle, C.O. (2001). Comparing the performance of Climgen and Wgen in the generation of temperature and solar radiation. Trans. ASAE 44 (5), 1683–1687.

Castrup, H. (1995), Analyzing Uncertainty for Risk Management, Proc. 49th ASQC Annual Quality Congress, Cincinnati.

Cawley, G. C., Janacek, G. J., Haylock, M. R., & Dorling, S. R. (2007). Predictive uncertainty in environmental modeling. Neural Networks, 20, 537–549.

Cayan, D. R., Maurer, E. P., Dettinger, M. D., Tyree, M., & Hayhoe, K. (2008). Climate change scenarios for the California region, Clim. Change, 87, Suppl. 1, 21–42. doi: 10.1007/s10584-007-9377-6.

Charles, S., Bates, B., Whetton, P., & Hughes, J. (1999). Validation of downscaling models for changed climate conditions: case study of southwestern Australia. Climate Research, 12, 1-14.

Charles, S., Bates, B., Viney, N. (2003). Linking atmospheric circulation to daily rainfall patterns across the Murrumbidgee River Basin. Water Sci. Technol. 48 (7), 233–240.

Charles, S., Bates, B., Smith, I., & Hughes, J. (2004). Statistical downscaling of daily precipitation from observed and modeled atmospheric fields. Hydrol. Processes, 18, 1373–1394.

Chen, D., Achberger, C., Räisänen, J., & Hellström, C. (2006). Using statistical downscaling to quantify the GCM-related uncertainty in regional climate change scenarios: a case study of Swedish precipitation. Advances in Atmospheric Sciences, 23(1), 54–60.

Christensen, J. H., & Christensen, O. B. (2007). A summary of the PRUDENCE model projections of changes in European climate by the end of this century, Clim. Change, 81, 7–30.

Christensen, J. H., Hewitson, B., Busuioc A., et al. (2007). Regional Climate Projections. In: Climate Change (2007). The Physical Science Basis. Contribution of Working Group I to the Fourth Assessment Report of the Intergovernmental Panel on Climate Change [Solomon, S., D. Qin, M. Manning, Z. Chen, M. Marquis, K.B. Averyt, M. Tignor and H.L. Miller (eds.)]. Cambridge University Press, Cambridge, United Kingdom and New York, NY, USA.

Chu, J. T., Xia, J., Xu, C. Y., & Singh, V. P. (2010). Statistical downscaling of daily mean temperature, pan evaporation and precipitation for climate change scenarios in Haihe River, China. Theor Appl Climatol., 99, 149–161. DOI: 10.1007/s00704-009-0129-6.

Coelho, C. A. S., Stephenson, D. B., Doblas-Reyes, F. J., Balmaseda, M., Guetter, A., & G. van Oldenborgh, J. (2006). A Bayesian approach for multi-model downscaling: Seasonal forecasting of regional rainfall and river flows in South America. Meteorological Applications, 13, 73–82.

Corder, G.W., & Foreman, D.I. (2009). Nonparametric Statistics for Non-Statisticians: A Step-by-Step Approach. Wiley, ISBN 9780470454619.

Corte-Real, J., Zhang, X., & Wang, X. (1995). Downscaling GCM information to regional scales: A non-parametric multivariate regression approach. Climate Dyn., 11, 413–424.

Crabb, P. (1997). Murray Darling Basin Resources. Murray Darling Basin Commission, Canberra.

Crane, R. G., & Hewitson, B. C. (1998). Doubled CO2 precipitation changes for the Susquehanna Basin: down-scaling from the genesis general circulation model. Int J. Climatol., 18, 6576.

Crane, R. G., & Hewitson, B. C. (2003). Clustering and upscaling of station precipitation records to regional patterns using self-organizing maps (SOMs). Climate Research, 25, 95–107.

Cubasch, U., et al. (1995). Regional climate changes as simulated by time-slice experiments. Climatic Change, 31, 273-304.

Cubasch, U., von Storch, H., Waszkewitz, J., & Zorita, E. (1996). Estimates of climate changes in southern Europe using different downscaling techniques. Climate Res., 7, 129–149.

Dai, A. (2006). Precipitation characteristics in eighteen coupled climate models. Journal of Climate, 19, 4605–4630.

Daley, R. (1991). Atmospheric Data Assimilation. Cambridge University Press, Cambridge, 457pp.

Davison, A. C., & Hinkley, D. (2006). Bootstrap Methods and their Application (8th Ed.). Cambridge: Cambridge Series in Statistical and Probabilistic Mathematics.

Dawson, R. J., et al. (2009). Integrated analysis of risks of coastal flooding and cliff erosion under scenarios of long term change. Climatic Change, 95(1-2), 249-288.

Dessai, S., Lu, X. & Resbey, J.S.(2005). On the role of climate scenarios for adaptation planning. Global Environmental Change., 15, 87-97.

Díez, E., Primo, C., García-Moya, J. A., Gutiérrez, J. M., & Orfila, B. (2005). Statistical and dynamical downscaling of precipitation over Spain from DEMETER seasonal forecasts. Tellus, 57A, 409–423.

Déqué, M., & Piedelievre, J. P. (1995). High resolution climate simulation over Europe. Climate Dynamics, 11, 321-339.

Diaz-Nieto, J., & Wilby, R.L. (2005). A comparison of statistical downscaling and climate change factor methods: impacts on low flows in the River Thames, United Kingdom. Clim. Change, 69, 245–268.

Dibike, Y. B., Gachon, P., St-Hilair,e A., Ouarda T.B.M.J., Nguyen T. V. (2008). Uncertainty analysis of statistically downscaled temperature and precipitation regimes in Northern Canada. Theoretical and Applied Climatology, 91, 149–170.

Dickinson, R. E., Errico, R. M., Giorgi, F., & Bates, G. T. (1989). A Regional Climate Model for the Western United States. Climatic Change, 15(3) 383-422.

Donaldson, R. J., Dyer, R. M. & Kraus, M. J. (1975). An objective evaluation of techniques for predicting severe weather events, Preprints, 9th Conference on Severe Local Storms, American Meteorol. Soc, Boston, MA, 321–326.

Efron, B., & Tibshirani, R. J. (1993). An introduction to the bootstrap. New York: Chapman & Hall.

El-Nahry, A. H. (2010). Climate change and its impacts on the coastal zone of the Nile Delta, Egypt. Environmental Earth Sciences, 59(7) 1497-1506.

El Kadi, A. K. A. & Smithson, P. A. (1992). Atmospheric classifications and synoptic climatology. Progress in Physical Geography, 16, 432–55.

Enke, W., Schneider, F., & Deutschländer, T. (2005a). A novel scheme to derive optimized circulation pattern classifications for downscaling and forecast purposes. Theoretical and Applied Climatology, 82, 51-63.

Everitt, B. S. (2002). Cambridge Dictionary of Statistics. CUP. ISBN 0-521-81099-x

Faucher, M., Burrows, W.R., & Pandolfo, L. (1999). Empirical-statistical reconstruction of surface marine winds along the western coast of Canada. Climate Research, 11 (3), 173–190.

Fernández, J. & Sáenz, J. (2003). Improved field reconstruction with the analog method: searching the CCA space. Clim. Res., 24, 199-213.

Fernández, J. (2004). Statistical and dynamical downscaling models applied to winter precipitation on the Cantabrian coast, Ph. D. Thesis, University of the Basque Country.

Finnis, J., Cassano, J., Holland, M., Serreze, M., & Uotila, P. (2009). Synoptically forced hydroclimatology of major Arctic watersheds in general circulation models; Part 1: the Mackenzie River Basin. International Journal of Climatology, 29, 1226–43.

Fischer, M. M., & Leung, Y. (2001). Geocomputational Modeling: Techniques and Applications, Advances in Spatial Science. Berlin, New York: Springer-Verlag.

Fischer, M., Dewitte, B., & Maîtrepierre, L. (2004). A non-linear statistical downscaling model: El Niño/Southern Oscillation impact on precipitation over New Caledonia, Geophys. Res. Lett., 31, L16204. Doi: 10.1029/2004GL020112.

Fowler, H. J., Blenkinsop, S., & Tebaldi, C. (2007). Linking climate change modeling to impact studies: Recent advances in downscaling techniques for hydrological modelling, Int. J.Climatol., 27, 1547–1578.

Fox-Rabinovitz, M., Takacs, L. L., Govindaraju, R. C., & Suarez, M. J. (2001). A variable-resolution stretched-grid general circulation model: regional climate simulation. Mon. Weather. Rev., 129, 453-469.

Fox-Rabinovitz, M., Côté, J., Dugas, B., Déqué, M., & McGregor, J. L. (2006). Variable resolution general circulation models: Stretched-grid model intercomparison project (SGMIP). J. Geophys. Res, 111, D16104. Doi: 10.1029/2005JD006520.

Frias, M. D., Zorita, E., Femandez, J., & Rodriguez-Puebla, C. (2006). Testing statistical downscaling methods in simulated climates. Geophys Res Lett., 33, L19807. Doi: 10.1029/2006GL027453.

Fu, C. B., Wang, S., Xiong, Z., Gutowski, W.J., Lee, D. K., McGregor, J. L., Sato, H., Kato , H., Kim, J. W., & Suh, M. S. (2005). Regional climate model intercomparison project for Asia, Am. Meteorol. Soc., pp. 257–266.

Fuentes, U., & Heimann, D. (2000). An improved statistical–dynamical downscaling scheme and its application to the Alpine precipitation climatology. Theoretical and Applied Climatology, 65, 119–135.

Fuhrer, J., Beniston, M., Fischlin, A., Frei, C., Goyette, S., Jasper, K. & Pfister, C. (2006). Climate risks and their impact on agriculture and forests in Switzerland. Clim. Change, 79, 79–102.

Furrer, R., & Naveau, P. (2007). Probability weighted moments properties for small samples, Stat. Probabil. Lett., 77 (2), 190-195.

Gabriel, K. R., & Neumann, J. (1962). A Markov chain model for daily rainfall occurrence at Tel Aviv. J. R. Meteorol. Soc., 88, 90–95.

Gao, X., Shi, Y., Song, R. Y., Giorgi, F., Wang, Y. G., et al., (2008). Reduction of future monsoon precipitation over China: Comparison between a high resolution RCM simulation and the driving GCM. Meteor. Atmosp. Phys., 99, 73-86.

Geng, S, Penning de Vries F. W. T., & Supit, I. (1986). A simple method for generating daily rainfall data. Agric. For. Meteorol., 36, 363–376.

Geng S., Auburn, J., Brandstetter, E., Li, B. (1988). A Program to Simulate Meteorological Variables. Documentation for SIMMETEO. (Agronomy Report No. 204). University of California, Davis Crop Extension, Davis, California.

Ghil, M., & Mechos, C. R. (1992). Data assimilation and predictability studies for the coupled ocean-atmosphere system. Oceanography, 5, 19-24.

Ghosh, S., Mujumdar, P. P. (2007).Statistical downscaling of GCM simulations to streamtlow using relevance vector machine. Advances in Water Resources.

Gibelin, A. L., & Déqué, M. (2003). Anthropogenic climate change over the mediterranean region simulated by a global variable resolution model. Clim. Dyn., 20, 327–339.

Giorgi, F., Marinucci, M. R., & Visconti, G. (1990). Use of a Limited-Area Model Nested in a General-Circulation Model for Regional Climate Simulation over Europe. Journal of Geophysical Research-Atmospheres, 95(D11), 18413-18431.

Giorgi, F., & Mearns, L. O. (1991). Approaches to regional climate change simulation: A review, Rev. of Geophys., 29, 191-216.

Giorgi, F., Hewitson, B., Christensen, J., Hulme, M., von Storch, H., Whetton, P., Jones, R., Mearns, L., & Fu, C. (2001). Regional climate information – evaluation and projections. In: J.T. Houghton, Y. Ding, D.J. Griggs, M. Noguer, P.J. van der Linden, X. Dai, K. Maskell and C.A. Johnson (eds.). pp. 583–638. Climate Change 2001: The Scientific Basis. Contribution of Working Group I to the Third Assessment Report of the Intergovernmental Panel on Climate Change. Cambridge University Press.

Giorgi, F., Bi, X., & Pal, J. S. (2004). Mean, interannual variability and trends in a regional climate change experiment over Europe. I. Present-day climate (1961-1990). Clim. Dyn., 22, 733-756.

Giorgi, F. (2008). Regionalization of climate change information for impact assessment and adaptation. WMO Bulletion, 57(2), 86-92.

Goodess, C. M., et al. (2010). An intercomparison of statistical downscaling methods for Europe and European regions: Assessing their performance with respect to extreme weather events and the implications for climate change applications, CRU Res. Rep., Clim. Res. Unit, Univ. of East Anglia, Norwich, U. K., in press.

Goubanova, K., & Li, L. (2007). Extremes in temperature and precipitation around the Mediterranean basin in an ensemble of future climate scenario simulations. Global and Planetary Change, 57, 27-42.

Goyal, M. k., & Ojha, C. S. P. (2010). Application of PLS-Regression as Downscaling Tool for Pichola Lake Basin in India. International Journal of Geosciences, 1, 51-57.

Gutiérrez, J. M., Cano, R., Cofiño, A. S., & Sordo, C. (2005). Analysis and downscaling multi-model seasonal forecasts in Peru using self-organizing maps. Tellus A, 57(3), 435-447.

Guttorp, P. (1995). Stochastic Modelling of Scientific Data. Chapman & Hall, London, Chapter 2.

Hannachi, A., Jolliffe, I. T., & Stephenson, D. (2007). Empirical orthogonal functions and related techniques in atmospheric science: A review, Int. J. Climatol, 27, 1119-1152.

Hanson, C. E., Palutikof, J. P., & Davis, T. D. (2004). Objective cyclone climatologies of the North Atlantic: A comparison between the ECMWF and NCEP reanalysis. Clim. Dyn., 22, 757–769.

Hanssen-Bauer, I., Achberger, C., Benestad, R., Chen, D., & Forland, E. (2005). Statistical downscaling of climate scenarios over Scandinavia. Clim. Res., 29(3), 255–268.

Harpham, C., & Wilby, R. L. (2005). Multi-site downscaling of heavy daily precipitation occurrence and amounts. Journal of Hydrology, 312, 235–255.

Harman, J. R., & Winkler, J. A. (1991). Synoptic climatology: themes, applications and prospects. Phys. Geogr., 12, 220–30.

Harvey, L. D. D., & Wigley. T. M. L. (2003). Characterizing and comparing control-run variability of eight coupled AOGCMs and of observations. Part 1: Temperature. Climate Dyn, 21, 619–646.

Hay, L.E., Wilby, R.J.L., & Leavesley, G.H. (2000). A comparison of delta change and downscaled GCM scenarios for three mountainous basins in the United States. Journal of the American Water Resources Association 36: 387–397.

Hay, L. E., & Clark, M. P. (2003). Use of statistically and dynamically downscaled atmospheric model output for hydrologic simulations in three mountainous basins in the western United States, J. Hydrol., 282, 56– 75.

Hayhoe, K. A. (2010). A standardized framework for evaluating the skill of regional climate downscaling techniques. Ph. D Thesis, University of Illinois at Urbana-Champaign.

Haylock, M. R., Cawley, G. C., Harpham, C., Wilby, R. L., & Goodess, C. M. (2006). Downscaling heavy precipitation over the UK: a comparison of dynamical and statistical methods and their future scenarios, Int. J. Climatol., 26: 1397–1415.

Haykin, S., (1994). Neural Networks: A Comprehensive Foundation. IEEE Press, New York.

Hellström, C., Chen, D., Achberger, C., & Räisänen, J. (2001). A comparison of climate change scenarios for Sweden based on statistical and dynamical downscaling of monthly precipitation. Clim Res 19:45–55.

Hellström, C., & Chen, D. (2003). Statistical downscaling based on dynamically downscaled predictors: application to monthly precipitation in Sweden. Adv Atmos Sci 20, 951–958.

Hewitson, B. C., & Crane, R. G. (1996). Climate downscaling: Techniques and application, Clim. Res., 7, 85–95.

Hewitson, B. C., & Crane, R. G. (2002). Self-organizing maps: applications to synoptic climatology. Climate Research, 22, 13–26.

Hewitson, B. C., & Crane, R. G. (2005). Gridded area-averaged daily precipitation via conditional interpolation. J. Clim., 18: 41–57.

Hewitson, B. C., & Crane, R. G. (2006). Consensus between GCM climate change projections with empirical downscaling: precipitation downscaling over South Africa. Int J Climatol 26: 1315–1337.

Hidalgo, H. G., Dettinger, M. D., & Cayan, D. R. (2008). Downscaling with Constructed Analogs: Daily Precipitation and Temperature Fields Over the United States. California Energy Commission, PIER Energy-Related Environmental Research. EC-500-2007-123.

Hofer, M., Mölg, T., Marzeion, B., & Kaser, G. (2010). Empirical-statistical downscaling of reanalysis data to high resolution air temperature and specific humidity above a glacier surface (Cordillera Blanca, Peru), J. Geophys. Res., 115, D12120. Doi: 10.1029/2009JD012556.

Holland, G. J., Lynch, A. H., & Leslie, L. M. (1987). Australian east-coast cyclones. Part I: Synoptic overview and case study. Monthly Weather Review 115, 3024-3046.

Hope, P. K. (2006). Projected future changes in synoptic systems influencing southwest Western Australia. Climate Dynamics, 26, 765–80.

Hope, P. K., Drosdowsky, W., & Nicholls, N. (2006). Shifts in the synoptic systems influencing southwest Western Australia. Climate Dynamics, 26, 751–64.

Hopkins, L. C., & Holland, G. J. (1997). Australian Heavy-Rain Days and Associated East Coast Cyclones: 1958–92. Journal of Climate 10, 621–635.

Hughes. J., Guttorp, P., & Charles ,S. P. (1999). A non-homogeneous hidden Markov model for precipitation occurrence. Appl. Stat., 48, 15–30

Hutchinson, M. F., McIntyre, S., Hobbs, R. J., Steinm J. L., Garnett, S., & Kinloch, J. (2005). Integrating a global agro-climatic classification with bioregional boundaries in Australia. Global Ecology and Biogeography, 14, 197–212.

Huth, R. (1999). Statistical downscaling in central Europe: Evaluation of methods and potential predictors, Clim. Res., 13, 91–103

Huth, .R, & Kysely, J. (2000). Constructing site-specific climate change scenarios on a monthly scale using statistical downscaling. Theor. Appl. Climatol., 66, 13–27.

Huth, R., Beck, C., Philipp, A., Demuzere, M., Ustrnul, Z., Cahynova´, M., Kysely´, J., & Tveito, O.E. (2008). Classifications of atmospheric circulation patterns: recent advances and applications. Annals of the New York Academy of Sciences, 1146, 105–52.

Imbert, A., & Benestad, R. E. (2005). An improvement of analog model strategy for more reliable local climate change scenarios. Theor. Appl. Climatol., 82, 245–255. DOI: 10.1007/s00704-005-0133-4.

Ines, A. V. M., & Hansen, J.W. (2006). Bias correction of daily GCM rainfall for crop simulation studies. Agricultural and Forest Meteorology, 138, 44-53.

IPCC. (2001). Climate change 2001: impacts, adaptation, and vulnerability. Contribution of Working Group II to the Third Assessment Report of the Intergovernmental Panel on Climate Change. Cambridge University Press: Cambridge, New York.

IPCC. (2007a). Climate Change 2007: Impacts, Adaptation and Vulnerability. Contribution of Working Group II to the Fourth Assessment Report of the Intergovernmental Panel on Climate Change, Cambridge, Cambridge University Press, UK.

IPCC. (2007b). Climate Change 2007: The Physical Science Basis. Contribution of Working Group I to the Fourth Assessment Report of the Intergovernmental Panel on Climate Change Cambridge, United Kingdom and New York, NY, USA. Cambridge University Press.

IPCC. (2007c). Summary for Policymakers. In: Climate Change 2007: The Physical Science Basis. Contribution of Working Group I to the Fourth Assessment Report of the Intergovernmental Panel on Climate Change. Cambridge, United Kingdom and New York, NY, USA, Cambridge University Press.

Johansson, B., & Chen, D. (2003). The influence of wind and topography on precipitation distribution in Sweden: Statistical analysis and modeling. Int J Climatol, 23, 1523-1535.

Jones, M. C., & Sibson, R. (1987). "What is Projection Pursuit?". Journal of the Royal Statistical Society, Series A (General) 150 (1): 1–37. Doi: 10.2307/2981662.

Jones, P. G., & Thornton, P. K. (2000). Marksim: Software to generate daily weather data for Latin America and Africa. Agronomy J. 92, 445–453.

Jones, R. G., Nogure, M., Hassell, D. C., Hudson, D., Wlson, S. S., Jenkins, G. J., & Mitchell, J. F. B. (2004). Generating high resolution climate change scenarios using PRECIS. Met Office Hadley Centre, Exeter, UK, 40pp.

Kalnay, E., Kanamitsu, M., Kistler, R., Collins, W., Deaven, D., Derber, J., Gandin, L., Iredell, M., Saha, S., White, G., Woollen, J., Zhu, Y., Chelliah, M., Ebisuzaki, W., Higgins, W., Janowiak, J., Mo, K., Ropelewski, C., Wang, J., Leetma, A., Reynolds, R., Jenne, R., & Joseph, D. (1996). The NCEP/NCAR 40-year reanalysis project. Bull Am Meteorol Soc. 77, 437–471.

Kalnay, E. (2003). Atmospheric Modeling, Data Assimilation, and Predictability. Cambridge Univ. Press, New York. 341 pp.

Kalteh, A. M., & Berndtsson, R. (2007). Interpolating monthly precipitation by self-organizing map (SOM) and multilayer perceptron (MLP). J. Hydrol Sci., 52, 305e317.

Katz, R.W. (1996). Use of conditional stochastic models to generate climate change scenarios. Climatic Change, 32, 237-255.

Katz, R.W. and Parlange, M.B. (1996). Mixture of stochastic processes: adaptation to stochastic downscaling. Climate Research, 7, 185-193.

Katz, R. W., Parlange, M. B., & Naveau, P. (2002). Statistics of extremes in hydrology. Adv. Water Resour., 25, 1287–1304.

Khalili, M., Brissette, F., Leconte, R. (2009). Stochastic multi-site generation of daily weather data. Stoch Environ Res Risk Assess. 23, 837–849.

Khan, M., Coulibaly, P., & Dibike, Y. (2006). Uncertainty analysis of statistical downscaling methods. Journal of Hydrology, 319, 357–382.

Kidson, J. W., & Watterson, I. G. (1995). A synoptic climatological evaluation of the changes in the CSIRO nine-level model with doubled CO2 in the New Zealand region. Int. J. Climatol. 15, 1179–1194.

Kilsby, C. G., Jones, P. D., Burton, A., Ford, A. C., Fowler, H. J., Harpham, C., James, P., Smith, A., & Wilby, R. L. (2007). A daily weather generator for use in climate change studies. Environ. Modell. Software, 22(12), 1705–1719.

Kistler, R., Kalnay. E., Collins, W., Saha, S., White, G., Woollen, J., Chelliah, M., Ebisuzaki, W., Kanmitsu, M., Kousky, V., van den Dool, H., Jenne, R., Fiorino, M. (2001). The NCEP/NCAR 50-year reanalysis: monthly means CD-ROM and documentation. Bull Am Meteorol Soc 82,247–267.

Klein, W. H., Lewis, B. M., & Enger, I. (1959). Objective prediction of 5-day means temperatures during winter. J. Meteorol., 16, 672–682.

Kohonen, T. (1982). Self-organized formation of topologically correct feature maps. Biological Cybernetics 43, 59–69.

Kohonen, T. (1990). The self-organizing map. Proceedings of the Institute of Electrical and Electronics Engineers 78 (9), 1464–1480.

Kohonen, T. (2001) .Self-Organizing Maps. Springer: Berlin 501.

Kruizinga, S., & Murphy, A. (1983). Use of an analog procedure to formulate objective probabilistic temperature forecasts in the Netherlands. Mon. Wea. Rev., 111, 2244–2254.

Jones, P.D., Hulme, M., & Briffa, K.R. (1993). A comparison of Lamb circulation types with an objective classification scheme. International Journal of Climatology, 13, 655-663.

Jones, R. G., Murphy, J. M., & Noguer, M. (1995). Simulation of climate change over Europe using a nested regional-climate model. I: Assessment of control climate, including sensitivity to location of lateral boundaries, Q. J. R. Meteorol. Soc., 121, 1413–1449.

Jolliffe, I.T. (2002). Principal Component Analysis, 2nd Ed. Springer, 487 pp.

Lall, U., & Sharma, A. (1996). A nearest neighbor bootstrap for resampling of hydrologic time series. Water Resour. Res., 32(3), 679– 693.

Lamb, H. (1972). British Isles weather types and a register of daily sequence of circulation patterns. Geophys Mem 116, HMSO, London.

Law, A.M., & Kelton, W.D. (1982). Simulation Modeling and Analysis. McGraw-Hill Book Co., USA, p. 400.

Leung, L. R., & Wigmosta, M. S. (1999). Potential climate chance impacts on mountain watersheds in the Pacific Northwest. J AM WATER RESOUR AS. 35,1463–1471.

Li, Y., & Ian Smith (2009). A statistical downscaling model for southern Australia winter rainfall. Journal of Climate, 22(5), 1142-1158.

Liang, X. Z., Li, L., Dai, A., & Kunkel, K. E. (2004a). Regional climate model simulation of summer precipitation diurnal cycle over the United States. Geophys. Res. Lett., 31, L24208. doi: 10.1029/2004GL021054.

Liang, X. Z., Li, L., Kunkel, K. E., Ting, M. F., & Wang J. X. L. (2004b). Regional climate model simulation of U.S. precipitation during 1982-2002. Part I: Annual cycle. J. Climate, 17, 3510-3529.

Liang, X. Z., Xu, M., Kunkel, K. E., Grell, G. A., & Kain, J. S. (2007). Regional climate model simulation of U.S.-Mexico summer precipitation using the optimal ensemble of two cumulus parameterizations. J. Climate, 20, 5201-5207.

Lim, Y. K., Shin, D. W., Cocke, S., LaRow, T. E., Schoof, J. T., O'Brien, J. J., & Chassignet, E. P. (2007). Dynamically and statistically downscaled seasonal simulations of maximum surface air temperature over the southeastern United States. J. Geophys. Res., 112, D24102, doi: 10.1029/2007JD008764.

Lin, G. F., & Chen, L. H. (2006). Identification of homogeneous regions for regional frequency analysis using the self-organising map. J Hydrol, 324, 1–9.

Little, M. A., Rodda, H. J. E., & McSharry, P. E. (2008). Bayesian objective classification of extreme UK daily rainfall for flood risk applications. Hydrol. Earth Syst. Sci. Discuss., 5, 3033-3060, doi: 10.5194/hessd-5-3033-2008.

Lobell, D. B. (2007). Global scale climate - crop yield relationships and the impacts of recent warming, Environmental Research Letters, 2(1).

Lobell, D. B. (2008). Why are agricultural impacts of climate change so uncertain? The importance of temperature relative to precipitation, Environmental Research Letters, 3(3).

Lopes, R. H. C., Reid, I., & Hobson, P. R. (2007). The two-dimensional Kolmogorov-Smirnov test. XI International Workshop on Advanced Computing and Analysis Techniques in Physics Research (April 23–27, 2007) Amsterdam, the Netherlands.

Lorenz, E.N. (1956). Empirical orthogonal functions and statistical weather prediction. Science Report 1, Statistical Forecasting Project, Department of Meteorology, MIT (NTIS AD 110268), 49 pp.

Lorenz, P., & Jacob, D. (2005). Influence of regional scale information on the global circulation: a two-way nesting climate simulation. Geophysical Research Letters, 32, L14826.

Lynch, A. H., Uotila, P., & Cassano, J. J. (2006). Changes in synoptic weather patterns in the polar regions in the twentieth and twenty-first centuries, part 2: Antarctic. Int J Climatol. 26, 1181– 1199.

MacCracken, M. C., Barron, E. J., Easterling, D. R., Felzer, B. S., & Karl, T. R. (2003). Climate change scenarios for the U.S. national assessment. Bull. Am. Met. Soc., 84, 1711–1723. Doi: 1710.1175/BAMS-1784-1712-1711.

MacQueen, J. B. (1967). Some Methods for classification and Analysis of Multivariate Observations. 1. Proceedings of 5th Berkeley Symposium on Mathematical Statistics and Probability. University of California Press. pp. 281–297.

Madi M.T., & Raqab M. Z. (2007). Bayesian prediction of rainfall records using the generalized exponential distribution. Environmetrics, 18, 541–549.

Main, J. P. L. (1997). Seasonality of circulation in southern Africa using the Kohonen self organizing map. MS thesis, Department of Environmental and Geographical Science, University of Cape Town, 84 pp.

Maraun, D., et al. (2010). Precipitation downscaling under climate change: Recent developments to bridge the gap between dynamical models and the end user, Rev. Geophys., 48, RG3003, doi:10.1029/2009RG000314.

Maurer, E.P. (2007). Uncertainty in hydrologic impacts of climate change in the Sierra Nevada, California under two emissions scenarios. Climatic Change, Vol. 82, No. 3-4, 309-325. doi: 10.1007/s10584-006-9180-9.

Maurer, E.P. & Hidalgo, H. G. (2008). Utility of daily vs. monthly large-scale climate data: an intercomparison of two statistical downscaling methods. Hydrology and Earth System Sciences, 12, 551-563.

Mearns, L. O., et al. (2009). A regional climate change assessment program for North America. Eos Trans. AGU, 90(36), 311.

McGregor, J. L. (2005). C-CAM: Geometric aspects and dynamical formulation [electronic publication]. CSIRO Atmospheric Research Tech. Paper No. 70, 43 pp.

Meehl, G. A., Covey, C., McAvaney, B., Latif, M., & Stouffer, R. J. (2005). Overview of the Coupled Model Intercomparison Project. Bulletin of the American Meteorological Society, 86, 89–93.

Mehrotra, R., Srikanthan, R., & Sharma, A. (2006). A comparison of three stochastic multi-site precipitation occurrence generators. Journal of Hydrology, 331, 280–292.

Milly, P. C. D., Betancourt, J., Falkenmark, M., Hirsch, R. M., Kundzewicz, Z. W., Lettenmaier, D. P., & Stouffer, R. J. (2008). Stationarity is dead: Whither water management? Science, 319, 573–574. doi:10.1126/ science.1151915.

Mitchell, T. D. (2000). An investigation of the pattern scaling technique for describing future climates. PhD thesis, University of East Anglia, Norwich.

Mitchell, T. D. (2003). Pattern scaling: an examination of the accuracy of the technique for describing future climates. Climatic Change 60, 217–242.

Morioka, K., Tomoki, T., & Yamagata, T. (2010). Climate variability in the southern Indian Ocean as revealed by self-organizing maps, Clim. Dynam (in press). doi:10.1007/s00382-010-0843-x, 2010.

Mullan, A. B., Wratt, D. S., & Renwick, J. A. (2001). Transient Model Scenarios of Climate Change for New Zealand. Weather and Climate. 21, 3-34.

Murphy, B. F., & Timbal, B. (2008). A review of recent climate variability and climate change in southeastern Australia. Int J Climatol., 28, 859–879.

Naveau, P., Nogaj, M., Ammann, C., Yiou, P., Cooley, D., & Jomelli, V. (2005). Statistical methods for the analysis of climate extremes. C. R. Geosci., 337(10–11), 1013–1022.

Neitsch, S. L., Aronld, J. G., & Williams, J. R. (1999). Soil and Water Assessment Tool, Uer's Manual.

Newton, G. (2009). Australia's environmental climate change challenge: overview with reference to water resources. Australasian Journal of Environmental Management, 16(3) 130-139.

Nicholls, N. (1997). Increased Australian wheat yield due to recent climate trends. Nature. 387, 484-485.

Nicholls, N. (2005). Climate variability, climate change and the Australian snow season. Aust. Meteorol. Mag., 54, 177-185.

Nicholls, N., Uotila, P., & Alexander, L. (2009). Synoptic influences on seasonal, interannual and decadal temperature variations in Melbourne, Australia. International Journal of Climatology. doi: 10.1002/joc.1965.

Nieto, S., Frias, M. D., & Puebla, R. (2004). Assessing two different climatic models and the NCEP-NCAR reanalysis data for the description of winter precipitation in the Iberian Peninsula. International Journal of Climatology, 24,361–376.

Nishiyama, K., Endo, S., Jinno, K., Uvo, C. B., Olsson, J., & Berndtsson, R. (2007). Identification of typical synoptic patterns causing heavy rainfall in the rainy season in Japan by a self-organizing map. Atmospheric research, 83, 185-200.

Norena, J. E. O. (2009). Vulnerability of water resources in the face of potential climate change: generation of hydroelectric power in Colombia. Atmosfera, 22(3) 229-252.

Obled, C., Bontron, G., Garcon, R. (2002). Quantitative precipitation forecasts: a statistical adaptation of model outputs through an analogs sorting approach. Atmos Res, 63, 303–324.

Opitz-Stapleton, S., & Gangopadhyay, S. (2010). A non-parametric, statistical downscaling algorithm applied to the rohini river basin, nepal. Theoretical and Applied Climatology. DOI 10.1007/s00704-010-0301-z.

Osborn, T.J., & Hulme, M. (1997). Development of a relationship between station and grid-box rainday frequencies for climate model evaluation. Journal of Climate, 10, 1885–1908.

Panofsky, H. A., &. Brier, G. W. (1968). Some Application of Statistics to Meteorology, 224 pp., Pa. State Univ., University Park, Pa.

Piani, C., Haerter, J. O., & Coppola, E. (2009). Statistical bias correction for daily precipitation in regional climate models over Europe, Theor. Appl. Climatol., 99, 187–192.

Pielke R.A., Adegoke J., Beltran-Przekurat A., Hiemstra C.A., Lin J., Nair U.S., Niyogi D., & Nobis T.E. (2007). An overview of regional land-use change and land-cover impacts on rainfall. Tellus B Chem. Phys. Meteorol. 59, 587–601. doi:10.1111/j.1600-0889.2007.00251.x.

Pijanowski, B. C., Brown, D. G., Shellito, B. A., & Manik, G. A. (2002). Using neural networks and GIS to forecast land use changes: a land transformation model. Computers, Environment and Urban Systems, 26(6), 553–576.

Pinto, J. G., Neuhaus, C. P., Leckebusch, G. C., Reyers, M., & Kerschgens, M. (2010). Estimation of wind storm impacts over Western Germany under future climate conditions using a statistical-dynamical downscaling approach. Tellus Series A-Dynamic Meteorology and Oceanography, 62A (2), 188-201.

Pook M. J., McIntosh, P. C., & Meyers, G. A. (2006). The synoptic decomposition of cool-season rainfall in the southeastern Australian cropping region. Journal of Applied Meteorology and Climatology, 45, 1156–1170.

Pook, M., Lisson, S., Risbey, J., Ummenhofer, C. C., McIntosh, P., & Rebbeck, M. (2009). The autumn break for cropping in southeast Australia: trends, synoptic influences and impacts on wheat yield. International Journal of Climatology, 29, 2012-2026. *DOI: 10.1002/joc.1833.*

Preisendorfer, R. W. (1988). Principal Component Analysis in Meteorology and Oceanography, Elsevier, Amsterdam.

Press, W. H., Flannery, B. P., Teukolsky, S. A., & Vetterling, W. T. (1992). Kolmogorov-Smirnov Test. In Numerical Recipes in FORTRAN: The Art of Scientific Computing, 2nd ed. Cambridge, England: Cambridge University Press, pp. 617-620.

Qi, L., Leslie, L. M., & Speer, M. S. (2006). Climatology of cyclones over the southwest Pacific. Meteorology and Atmospheric Physics 91, 201-209.

Racsko, P., Szeidl, L., & Semenov, M. (1991). A serial approach to local stochastic weather models. Ecol. Model. 57, 27–41.

Randall, D.A., Wood, R.A., Bony, S., Colman, R., Fichefet, T., Fyfe, J., Kattsov, V., Pitman, A., Shukla, J., Srinivasan, J., Stouffer, R.J., Sumi, A., & Taylor, K.E. (2007). Cilmate Models and Their Evaluation. In: Climate Change 2007: The Physical Science Basis. Contribution of Working Group I to the Fourth Assessment Report of the Intergovernmental Panel on Climate Change [Solomon, S., D. Qin, M. Manning, Z. Chen, M. Marquis, K.B. Averyt, M.Tignor and H.L. Miller (eds.)]. Cambridge University Press, Cambridge.

Reichler, T., & Kim, J. (2008). How well do coupled models simulate today's climate? Bull. Am. Meteorol. Soc., 89, 303–311. doi: 10.1175/ BAMS-89-3-303.

Reusch, D.B., Alley, R.B., & Hewitson, B.C. (2005). Relative performance of Self-Organizing Maps and Principal Component Analysis in pattern extraction from synthetic climatological data. Polar Geogr., 29(3), 188–212.

Richardson, C. W. (1981). stochastic simulation of daily precipitation, temperature, and solar radiation, Water Resour. Res., 17(1), 182–190.

Richardson, C., & Wright, D. A. (1984). WGEN: A model for generating daily weather variables, Rep. 8, 83 pp., Agric. Res. Serv., U.S. Dep. of Agric., Washington, D. C.

Risbey, James S., Michael J. Pook, Peter C. McIntosh, Matthew C. Wheeler, Harry H. Hendon, 2009: On the Remote Drivers of Rainfall Variability in Australia. Mon. Wea. Rev., 137, 3233–3253. doi: 10.1175/2009MWR2861.1.

Robertson, A., Kirshner, S., Smyth, P. (2004). Downscaling of daily rainfall occurrence over Northeast Brazil using a hidden Markov model. J. Clim. 17, 4407–4424.

Robinson, P.J. & Finkelstein, P.L. (1991) The Development of Impact-Oriented Climate Scenarios. Bull. Amer. Met. Soc, 72, 481-490.

Rummukainen, M. (1997). Methods of statistical downscaling of GCM simulations, Rep. Meteorol. Climatol., 80, Swed. Meteorol. and Hydrol. Inst., Norrköping.

Salathé, E.P. (2003). Comparison of various precipitation downscaling methods for the simulation of streamflow in a rainshadow river basin. International Journal of Climatology, 23, 887-901.

Sammon, J. W. (1969). A nonlinear mapping for data structure analysis. IEEE Transactions on Computers 18: 401–409.

Santer, B.D., Wigley, T. M. L., Schlesinger, M.E., & Mitchell, J. F. B. (1990). Developing Climate Scenarios from Equilibrium GCM results. Report No. 47, Max-Planck-Institut-für-Meteorologie, Hamburg, 29 pp.

Saunders, I.R., & Byrne, J. M. (1996). Generating regional precipitation from observed and GCM synoptic-scale pressure fields, southern Alberta, Canada. Climate Research 6, 237–249.

Saunders, I.R., & Byrne, J. M. (1999). Analysis of blocking events from observations and ECHAM model simulations. International Journal of Climatology 19, 1165–1176.

Schmidli, J., Goodess, C., Frei, C., Haylock, M., Hundecha, Y., Ribalaygua, J. et al. (2007). Statistical and dynamical downscaling of precipitation: an evaluation and comparison of scenarios for the European Alps. J. Geophys. Res., 112, D04105.1–D04105.20.

Schuenemann, K., Cassano, J., & Finnis, J. (2009), Forcing of precipitation over Greenland: Synoptic Climatology for 1961–99. J. Hydrometeorol. 10, 60–78. doi:10.1175/2008JHM1014.1.

Semenov, M. A., & Barrow, E. M. (1997). Use of a stochastic weather generator in the development of climate change scenarios. Climatic change, 35, 397-414.

Semenov, M.A., & Barrow, E. M. (2002). LARS-WG: A Stochastic Weather Generator for Use in Climate Impact Studies, Version 3.0, User Manual.

Schmidli, J., Goodess, C. M., Frei, C., Haylock, M. R., Hundecha, Y., Ribalaygua, J., & Schmith, T. (2007). Statistical and dynamical downscaling of precipitation: An evaluation and comparison of scenarios for the European Alps. J. Geophys. Res., 112. D04105, doi: 10.1029/2005JD007026.

Schiermeier Q. (2007). Get practical, urge climatologists. Nature, 448, 234–235.

Schneider, S., & Steinacker, R. (2009). Utilization of radar information to refine precipitation fields by a variational approach, Meteorology and Atmospheric Physics, 103(1-4) 137-144.

Sharma, D., Das Gupta, A., & Babel M. S. (2007). Spatial disaggregation of bias-corrected GCM precipitation for improved hydrologic simulation: Ping river basin, Thailand. Hydrol Earth Sys Sci., 11(4), 1373–390.

Sheridan, S. C., & Lee, C. C. (2010). Synoptic climatology and the general circulation model, Progress in Physical Geography, 34(1): 101-109.

Shi, H., Yu, R., Li, J., Zhou, T. (2009). Development of a regional climate model (CREM) and evaluation on its simulation of summer climate over eastern China. J. Meteor. Soc. Japan, 87(3), 381-401.

Shi, Z. G., Yan, X. D., Yin, C. H., & Wang, Z. M. (2007). Effects of historical land cover changes on climate. Chinese Science Bulletin, 52(18), 2575–2583.

Shouki, M. M., Mian, I. U. H., & Tracy, D.S. (1988). Sampling properties of estimators of the log-logistic distribution with application to Canadian precipitation data. Can. J. Statistics, 16, 223–236.

Solomon, S., Qin, D., Manning, M., Chen, Z., Marquis, M., Averyt, K., Tignor, M.,Miller, H.L. (Eds.), (2007). Climate Change 2007: the Physical Science Basis.Contribution of Working Group I to the Fourth Assessment Report of the Intergovernmental Panel on Climate Change, Chap. IPCC, 2007: Summary for Policymakers. Cambridge University Press, Cambridge, United Kingdom and New York, NY.

Speer, M. S., & Geerts, B. (1994). A synoptic-mesoalpha scale climatology of flash floods in the Sydney metropolitan area. Australian Meteorological Magazine, 43, 87-103.

Speer, M. S., & Leslie, L.M. (1997). A climatology of coastal ridging over south-eastern Australia. International Journal of Climatology, 17, 831-845.

Steinacker, R., Ratheiser, M., Bica, B., Chimani, B., Dorninger, M., Gepp, W., Lotteraner ,C., Schneider, S., & Tschannett, S. (2006). A mesoscale data analysis and downscaling method over complex terrain. Mon. Wea. Rev., 134(10), 2758–2771.

STARDEX. (2001). Statistical and regional dynamical downscaling of extremes for European regions, description of work (PDF). Accessed 2004-02-17.

Stocker, T. F., Clarke, G. K. C., Le Treut, H., Lindzen, R. S., Meleshko, V. P., Mugara, R. K., Palmer, T. N., Pierrehumbert, R. T., Sellers, P. J., Trenberth, K. E., & Willebrand, J. (2001). Physical climate processes and feedbacks, in: Climate Change 2001: The Scientific Basis, edited by: Houghton, J. T., Ding, Y., Griggs, D. G., et al., Cambridge University Press, Cambridge, 417–470.

Sturman, A., & Tapper, N. (2004). The Weather and Climate of Australia and New Zealand. Oxford University Press, Melbourne (Victoria, Australia).

Sun, Y., Solomon, S., Dai, A., & Portmann, R. (2006). How often does it rain? Journal of Climate, 19, 916–934.

Suppiah, R., Preston, B., Whetton, P.H., McInnes, K.L., Jones, R.N., Macadam, I., Bathols, J., & Kirono, D. (2006). Climate change under enhanced greenhouse conditions in South Australia (http://www.sapo.org.au/pub/pub6923.html)

Tapper, N., & Hurry, L. (1996). Australia's Weather Patterns – An Introductory Guide, Dellasta Pty Ltd, Mount Waverly, Victoria.

Teutschbein, C., Wetterhall, F., & Seibert, J. (2011). Evaluation of different downscaling techniques for hydrological climate-change impact studies at the catchment scale. Clim Dyn. DOI 10.1007/s00382-010-0979-8.

Themeßl, M., Gobiet, A., & Leuprecht, A. (2010). Empirical-statistical downscaling and error correction of daily precipitation from regional climate models. Int J Clim, DOI: 10.1002/joc.2168.

Thornton, P.K., Hoogenboom, G., Wilkens, P.W., & Jones, J.W. (1994). Seasonal analysis. In: G.Y. Tsuji, G. Uehara and S. Bolas, Editors, DSSAT Version 3. Vol. 3, University of Hawaii, Honolulu, Hawaii, pp. 1–61.

Timbal, B., & McAvaney, B. (2001). An analog-based method to downscale surface air temperature: application for Australia. Clim. Dyn., 17, 947–963.

Timbal, B., Dufour, A., & McAvaney, B. (2003). An estimate of future climate change for western France using a statistical downscaling technique. Climate Dynamics, 20, 807–823. DOI 10.1007/s00382-002-0298-9.

Timbal, B., Fernandez, E., Li Z. (2009). Generalization of a statistical downscaling model to provide local climate change projections for Australia. Environ Soft Model. doi:10.1016/j.envsoft. 24: 341-358.

Toch, Z. (1991). Intercomparison of circulation similarity measures. Mon Wea Rev. 119, 55-64.

Trenberth, K. E., Dai, A., Rasmussen, R. M., & Parsons, D. B. (2003). The changing character of precipitation. Bulletin of the American Meteorological Society, 84, 1205–1217.

Trigo, R. M., & Palutikof, J. P. (1999). Simulation of daily temperatures for climate change scenarios over Portugal: a neural network model approach. Climate Research 13 (1), 45–59.

Trigo R. M., & Palutikof J. P. (2001). Precipitation scenarios over Iberia: a comparison between direct GCM output and different downscaling techniques. J. Clim. 14 (23), 4422–4446.

Tripathi, S., Srinivas, V. V., & Nanjundiah, R. S. (2006). Downscaling of precipitation for climate change scenarios: a support vector machine approach. J Hydrol., 330, 621–40.

Tumbo, S.D., Mpeta, E., Tadross, M., Kahimba, F. C., Mbillinyi, B. P., & Mahoo, H. F. (2010). Application of self-organizing maps technique in downscaling GCMs climate change projections for Same, Tanzania. J. Phys. Chem. Earth, 35: 608-617. doi:10.1016/j.pce.2010.07.023.

Uppala, S. M., llberg, K. A°., Simmons, P. W., Andrae, A. J., et al. (2005). The ERA-40 reanalysis. Quarterly Journal of the Royal Meteorological Society 131, 2961–3012.

van der Linden, P., & Mitchell, J. F. B. (2009). ENSEMBLES: Climate change and its impacts: Summary of research and results from the ENSEMBLES project, technical report, Met Off. Hadley Cent., Exeter, U. K.

Vlček, O., & Huth R. (2009). Is daily precipitation Gamma-distributed? Adverse effects of an incorrect application of the Kolmogorov-Smirnov test. Atmos. Res., 93, 759-766.

van den Dool, H. (1994). Searching for analogs, how long must we wait? Tellus, 46A, 314–324.

von Storch, H. (1999a). On the use of "inflation" in statistical downscaling. J. Clim., 12(12), 3505–3506.

von STORCH, H. (1999b). The global and regional climate system. In H von Storch and G Fl¨oser, editors, Anthropogenic Climate Change, GKSS School of Environmental Research, pages 3–36. Springer–Verlag, Berlin.

von Storch, H., Hewitson, B., & Mearns, L. (2000). Review of empirical downscaling techniques. In: T, Iversen, and BAK, Høiskar (eds), Regional Climate Development Under Global Warming. General Technical Report 4. http://regclim.met.no/rapport 4/presentation02/presentation02.htm.

Vrac, M., Stein, M., & Hayhoe, K. (2007). Statistical downscaling of precipitation through nonhomogeneous stochastic weather typing. Clim. Res., 34, 169–184.

Wang, Y., Leung, L. R., McGregor, J. L., Lee, D. K., Wang, W. C., & et al., (2004). Regional climate modeling: Progress, challenges, and prospects. J. Meteor. Soc. Japan, 82, 1599-1628.

Wang, X. L., Swail, V. R., & Cox, A. (2010). Dynamical versus statistical downscaling methods for ocean wave heights. Int J Climatol 30, 317–332.

Ward Systems Group, (1996). NeuroShell 2.0. Ward Systems Group, Inc., Executive Park West, 5 Hillcrest Drive, Frederick, MD.

Wetterhall, F., Halldin, S., & Xu, C. Y. (2005). Statistical precipitation downscaling in central Sweden with the analog method. J Hydrol 306:174–190.

Wetterhall, F., Halldin S., & Xu, C.Y. (2007). Seasonality properties of four statistical-downscaling methods in central Sweden, Theor. Appl. Climatol., 87 (1), 123-137.

Wetterhall, F., Bárdossy, A., Chen, D., Halldin, S., & Xu, C. Y. (2009). Statistical downscaling of daily precipitation over Sweden using GCM output. Theoretical and Applied Climatology 96, 95-103.

Widmann, M., Bretherton, C.S., & Salathé E.P., (2003). Statistical precipitation downscaling over the Northwestern United States using numerically simulated precipitation as a predictor. J. Clim., 16, 799–816.

Wilbanks, T. J., Romero Lankao, P., Bao, M., Berkhout, F., Cairncross, S., Ceron, J. P., Kapshe, M., Muir-Wood, R., & Zapata-Marti, R. (2007). Industry, settlement and society. Climate Change 2007: Impacts, Adaptation and Vulnerability. Contribution of Working Group II to the Fourth Assessment Report of the Intergovernmental Panel on Climate Change. Parry, M. L., Canziani, O. F., Palutikof, J. P., van der Linden, P. J., & Hanson, C. E., Eds., Cambridge University Press, Cambridge, UK, 357-390.

Wilks, D.S. (1992). Adapting stochastic weather generation algorithms for climate change studies. Climatic Change, 22, 67-84.

Wilks, D. S., & Wilby, R. L. (1999). The weather generation game: A review of stochastic weather models, Prog. Phys. Geogr., 23(3), 329–357.

Wilks, D. S. (2006). Statistical Methods in the Atmospheric Sciences, 2nd ed., 627 pp., Academic, Amsterdam.

Wilby, R. L., & Wigley, T. M. L. (1997). Downscaling general circulation model output: A review of methods and limitations, Prog. Phys. Geogr., 21, 530–548.

Wilby, R. L., & Wigley T. M. L. (2000). Precipitation predictors for downscaling: observed and general circulation model relationships. International Journal of Climatology, 20(6), 641–661.

Wilby, R. L., Conway, D., & Jones, P. D. (2002). Prospects for downscaling seasonal precipitation variability using conditioned weather generator parameters. Hydrological Processes, 16, 1215–1234.

Wilby, R. L., Charles, S. P., Zorita, E., Timbal, B., Whetton, P., Mearns, L.O. (2004). Guidelines for use of climate scenarios developed from statistical downscaling methods, supporting material of the Intergovernmental Panel on Climate Change, available from the DDC of IPCC TGCIA, 27.

Wilby, R. L. & Harris, I. (2006). A framework for assessing uncertainties in climate change impacts: low-flow scenarios for the River Thames, UK, Water Resour. Res., 42, W02419, doi: 10.1029/2005WR004065.

Wilby, R. L., Troni, J., Biot, Y., et al. (2009). A review of climate risk information for adaptation and development planning. International Journal of Climatology, 29, 1193-1215.

Wilby, R.L., & Dessai, S. *(*2010*).* Robust Adaptation to Climate Change. Weather, *65, 7, 180-185.*

Wolfe, D. W., Ziska, L., Petzoldt, C., Seaman, A., Chase, L., & Hayhoe, K. (2008). Climate Change Impacts on Northeastern U.S. Agriculture, Mitigation and Adaptation Strategies for Global Change, 13, 555-575.

Wood, A. W., Leung, L. R., Sridhar, V., & Lettenmaier, D. P. (2004). Hydrologic implications of dynamical and statistical approaches to downscaling climate model outputs. Climatic Change, 62, 189-216.

Xiong, Z., Fu, F. C., & Yan, X. D. (2009). Regional integrated environmental model system and its simulation of East Asia summer monsoon. Chinese Science Bulletin, 54(22), 4253-4261. DOI: 10.1007/s11434-009-0669-2.

Yang, C., Chandler, R. E., Isham, V. S., & Wheater, H. S. (2005). Spatial-temporal rainfall simulation using generalized linear models, Water Resour. Res., 41, W11415. doi: 10.1029/2004WR003739.

Yang, W, Bárdossy, A., & Caspary, H. J. (2010). Downscaling daily precipitation time series using a combined circulation- and regression-based approach. Theor Appl Climatol. DOI 10.1007/s00704-010-0272-0.

Yarnal, B. (1993). Synoptic climatology in environmental analysis. London: Belhaven Press, 195 pp.

Yates, D., Gangopadhyay, S., Rajagopalan, B., & Strzepek, K. (2003). A technique for generating regional climate scenarios using a nearest-neighbor algorithm, Water Resour. Res., 39(7), 1199, doi: 10.1029/2002WR001769.

Yin C.H., Li Y.P, Ye W., Bornman J., & Yan, X. D. (2010). Statistical downscaling of regional daily precipitation over southeast Australia based on self-organizing maps. Theor Appl Climatol (in press). DOI: 10.1007/s00704-010-0371-y.

Young, K. (1994). A multivariate chain model for simulating climatic parameters from daily data, J. Appl. Meteorol., 33(6), 661–671.

Zangl, G. (2004). The sensitivity of simulated orographic precipitation to model components other than cloud microphysics. Quart J Roy Meteor Soc., 130, 1857–1875.

Zhu, J., & Liang X. Z. (2005). Regional climate model simulation of U.S. soil temperature and moisture during 1982-2002. J. Geophys. Res., 110, D24110. doi: 10.1029/2005JD006472.

Zhu, J., & Liang, X. Z. (2007). Regional climate model simulations of U.S. precipitation and surface air temperature during 1982-2002: Interannual variation. J. Climate, 20, 218-232.

Zorita, E., Hughes, J. P., Lettenmaier, D. P., & von Storch, H. (1995). Stochastic characterization of regional circulation patterns for climate model diagnosis and estimation of local precipitation. J Clim 13, 223–234

Zorita, E., & von Storch, H. (1999). The analog method as a simple downscaling technique: comparison with more complicated methods. Journal of Climate, 12, 2474–2489.

Zou, L., Zhou, T., Li, L. Z. X., Zhang, J. (2010). East China Summer Rainfall Variability of 1958-2000: Dynamical Downscaling with a Variable-Resolution AGCM. Journal of Climate (Accepted and In Press).